ENVIRONMENTAL RESEARCH MONOGRAPH 1979-4

A Public Service of

Syncrude Canada Ltd.

CONCENTRATION FLUCTUATIONS IN PLUMES

D. D. J. Netterville
Syncrude Canada Ltd.

CONCENTRATION FLUCTUATIONS IN PLUMES

D. D. J. Netterville
Syncrude Canada Ltd.

F O R E W O R D

Syncrude Canada Ltd. is producing synthetic crude oil from a surface mine in the Athabasca Tar Sands area of north-eastern Alberta. The present report describes research on a statistical method for determining air quality around industrial sites. The study results will be especially useful for atmospheric dispersion modellers concerned with short-term pollution episodes.

Syncrude's Environmental Research Monographs are published verbatim from the final reports of professional environmental consultants or in-house staff. Only proprietary technical or budget-related information is withheld. Because we do not necessarily base our decisions on just one opinion, recommendations found in the text should not be construed as commitments to action by Syncrude.

Syncrude Canada Ltd. welcomes public and scientific interest in its environmental activities. Please address any questions or comments to Syncrude Environmental affairs, 10030 - 107 Street, Edmonton, Alberta, T5J 3E5.

This report may be referred to as:

CONCENTRATION FLUCTUATIONS

IN PLUMES

Syncrude Canada Ltd.
Environmental Affairs Department

by

D. D. J. Netterville
Atmospheric Research Coordinator
Syncrude Canada Ltd.

ABSTRACT

The random fluctuation of concentration levels in a
plume is studied using a wind tunnel simulation of dispersion
in the neutrally stable atmospheric boundary layer. A fast
response hot-film probe is developed and used to measure
high frequency fluctuations of helium tracer concentration in
the wind tunnel. Plume intermittency is well described by a
Gaussian error function model originally developed for turbu-
lence intermittency in round free jets. The classic reflected
Gaussian model for mean concentrations successfully reproduces
the spatial distribution of mean concentration in the elevated
tracer plume. An expression for the mean field eddy diffus-
ivity is obtained from the reflected Gaussian model, and
compares favorably with experimentally-derived values. For
non-uniform winds, the vertical eddy diffusivity has a complex
variation with height above ground, becoming discontinuous
near the source height. Measurements show that local pro-
duction and dissipation of concentration variance $\overline{c'^2}$ are not
in balance. In fact, as the plume moves downwind, production
becomes negligible compared with dissipation of $\overline{c'^2}$ within
the plume. A new dissipated Gaussian model for $\overline{c'^2}$ is derived
from the variance balance equation for the special case of
negligible production and fluctuations which decay at two-
thirds the rate of those in isotropic grid turbulence. This

model provides a good description of the spatial distribution
of concentration variance within the plume. Support is pro-
vided for assumptions made in earlier work on concentration fluctuations,
in that the rate of variance dissipation is observed to be proportional
to local concentration variance, with the proportionality
factor being the reciprocal of a decay time scale which is
constant across the plume and which increases linearly with
distance from the source. A statistical intermittent log-
normal concentration model is developed and successfully
compared with measured peak-to-mean ratios and complete
probability density functions of the concentration fluctu-
ations; the model parameters are concentration mean, variance
and intermittency. The highest peak concentrations are
observed to occur about two thirds of the distance out to the
point of maximum mean concentration.

ACKNOWLEDGEMENTS

DEDICATION

This study is dedicated to the memory of
my brother John Arthur Netterville, whose
own Ph. D. research was ended by a drunk
driver on February 16, 1977.

TABLE OF CONTENTS

vii

LIST OF TABLES

LIST OF FIGURES

LIST OF SYMBOLS

Units

Symbol	Description	Units
a	constant in plume spread power law $\sigma_y = ax^p$	m^{1-p}
a	constant in decay time relation (5.55)	sec
A	cross-sectional area of streamtube ingested by probe	m^2
A	absorption coefficient in Eq. (5.55)	-
A_1	constant relating $\bar{c}$, U_T and Q in Eq. (3.4)	ppm/m^2
A_2	constant relating $\sqrt{\overline{c'^2}}$, U_T and Q in Eq. (3.5)	ppm/m^2
A_3	constant relating measured $\sqrt{\overline{(\frac{\partial c'}{\partial t})^2}}$, U_T and Q in Eq. (3.7)	$ppm/m^{5/2}sec^{1/2}$
A_4	constant relating undisturbed $\sqrt{\overline{(\frac{\partial c'}{\partial t})^2}}$, U_T and Q in Eq. (3.10)	$ppm.sec^{1/2}/m^{7/2}$
A_5	constant relating undisturbed $\sqrt{\overline{(\frac{\partial c'}{\partial t})^2}}$ to measured $\sqrt{\overline{(\frac{\partial c'}{\partial t})^2}}$ in Eq. (3.11)	sec/m
b	constant in plume spread power law $\sigma_z = bx^q$	m^{1-q}
b	constant in decay time relation (5.55)	sec/m
B	proportionality constant in Eq. (4.16)	-
c	instantaneous species concentration	ppm

		Units
$\bar{c}$	mean species concentration	ppm
c'	instantaneous deviation from the mean concentration ($= c - \bar{c}$)	ppm
c_{cal}	calibration concentration for probe transient response	ppm
c_o	median value of non-zero concentrations	ppm
c_o	centerline concentration in axisymmetric plume	ppm
c_p	'peak' concentration which is exceeded a fraction P of the time	ppm
C_p	specific heat at constant pressure	cal/g·°K
$\overline{c'^2}$	concentration variance about the mean	ppm^2
$\sqrt{\overline{c'^2}}$	root-mean-square (rms) concentration	ppm
$\overline{(\frac{\partial c'}{\partial t})^2}$	concentration time derivative variance	ppm^2/sec^2
d	dissipation coefficient in Eq. (5.17)	-
d_s	source diameter	m
D	diameter of ingested streamtube in Fig. (3.10)	m
D	molecular concentration diffusivity	m^2/sec
D	dilution parameter defined by Eq. (6.19)	-

$\overline{E}$ mean probe output voltage   volts

f   radial mean concentration profile function   -

f   frequency of concentration fluctuations   cycles/sec

f_n natural frequency of fast response probe   cycles/sec

F   normalized signal frequency in Eq. (2.3)   -

g   radial concentration variance profile function   -

h   convection heat transfer coefficient for hot-film   -

H   source height   m

i   fluctuation intensity, rms/mean   -

I_1, I_2 integrals defined by Eqs. (5.25) and (5.26) respectively   m

k   thermal conductivity   cal/m·sec·°K

K   radial concentration eddy diffusivity in axisymmetric plumes m^2/sec

K_m momentum diffusivity m^2/sec

K_y lateral eddy diffusivity of mean concentration m^2/sec

K_y' lateral eddy diffusivity of concentration variance m^2/sec

K_z vertical eddy diffusivity of mean concentration m^2/sec

K_z' vertical eddy diffusivity of concentration variance m^2/sec

m mass of ingested eddy   g

$\dot{m}$ mass flux through probe   g/sec

n boundary layer wind profile exponent in power law representation $U \sim z^n$ -

n noise signal from fast response sensor   ppm

p probability density function (pdf)   -

p exponent in plume spread power law $\sigma_y = ax^p$ -

ppm   parts per million, by volume   -

ppth   parts per thousand, by volume   -

P probability that concentration c_p is exceeded   -

$\mathbb{P}$ cumulative probability distribution function (cdf)   -

Pr Prandtl Number ν/k -

P_v production of concentration variance, Eq. (5.30) ppm^2/sec

q exponent in plume spread power law $\sigma_z = bx^q$ -

Q pollutant emission rate m^3/sec

r radial coordinate in axisymmetric plume   m

$r_{1/2}$ radial distance to intermittency half-point ($\gamma = 1/2$) in axisymmetric jets or plumes   m

r^2 coefficient of determination in Eq. (6.16)   -

R autocorrelation function, e.g. Eq. (4.6)   -

RC time constant for an R-C circuit   sec

Re Reynolds Number for wind tunnel flow, $\nu\delta/U_\delta$ -

s signal obtained from fast response probe   ppm

S short notation for concentration variance $\overline{c'^2}$ ppm^2

Sc Schmidt Number ν/D -

s_o 'source variance' parameter in Eq. (5.13)   -

t time   sec

t_o, t_d constants in dissipation relation (5.31)   sec, sec/m

T_d decay time scale for concentration fluctuations   sec

u'	fluctuating wind speed component in mean wind direction	m/sec
$-\overline{u'c'}$	vertical Reynolds mass flux of mean concentration	ppm·m/sec
$-\overline{u'w'}$	vertical Reynolds stress	m^2/sec^2
$-\overline{u'c'^2}$	vertical Reynolds flux of concentration variance	ppm^2·m/sec
U	wind speed in boundary layer	m/sec
U_d	probe 'dissipation velocity', the reciprocal of A_5; defined by Eq. (3.15)	m/sec
U_o	uniform wind speed, independant of height above ground	m/sec
v'	fluctuating lateral wind speed component	m/sec
V	mean lateral wind speed in boundary layer	m/sec
V_{exit}	velocity of helium leaving the source	m/sec
V_{in}, V_{out}	probe signal voltage before and after attenuation	volts
w'	fluctuating vertical wind speed component	m/sec
W	mean vertical wind speed in boundary layer	m/sec
x, x_s	distance downwind from source	m
$x_{1/2}$	distance along plume centerline to intermittency half-point	m

		Units
x_0	distance downwind from effective origin	m
y	lateral distance off plume centerline	m
$y_{1/2}$	crosswind distance from plume centerline to intermittency half-point	m
z	height above ground	m
z_0	boundary layer roughness height	m
$Z_{1/2} - H$	vertical distance from plume centerline up to intermittency half-point	m
α	dissipation parameter in Eq. (5.45)	-
α	normalizing parameter in Weibull distribution	ppm^{β}
β	exponent in Weibull distribution	-
β	approximate proportionality factor between Lagrangian and Eulerian integral time scales	-
γ	intermittency factor	-
γ_T	concentration intermittency due to atmospheric turbulence	-
γ_θ	concentration intermittency due to slow shifts in wind direction	-
δ	boundary layer thickness	m
δ	background parameter in Weibull distribution	ppm

δ delta function in Eq. (6.4)

ζ critical damping ratio of probe response   -
curve, Eq. (2.3)

η dimensionless radial coordinate, Eq. (5.37)   -

λ Taylor microscale of a fluctuating variable,   m
e.g. Eq. (3.13)

Λ integral length scale of a fluctuating   m
variable

μ absolute viscosity   g/m·sec

ν kinematic viscosity of air m^2/sec

ρ density g/m^3

σ standard deviation of a fluctuating variable   -

σ_B standard deviation of plume radius   m
fluctuations about $r_{1/2}$

σ_L logarithmic standard deviation of non-   -
zero concentrations

σ_n standard deviation of probe noise signal   ppm

σ_y standard deviation of lateral Gaussian   m
mean concentration profile

σ_y' standard deviation of lateral Gaussian   m
concentration variance profile

σ_z standard deviation of vertical reflected   m
Gaussian mean concentration profile

σ_z' standard deviation of vertical dissipated   m
Gaussian concentration variance profile

$\left.\begin{array}{l} \sigma_{x\gamma} \\[1em] \sigma_{y\gamma} \\[1em] \sigma_{z\gamma} \end{array}\right\}$ shape parameters for plume intermittency   m
profile Eq. (4.20); similar to σ_B

τ time variable in autocorrelation function   sec

τ_1, τ_2 time constants in probe response Eq. (2.1)   sec

T integral time scale   sec

ϕ_c dissipation rate of concentration fluctuations ppm^2/sec

ϕ_N net dissipation $\phi_c - P_v$ ppm^2/sec

ω_n natural frequency of fast response probe   rad/sec

Subscripts

c   for concentration

E   Eulerian

E   property of tracer-containing turbulent eddy

H   evaluated at source height

L   Lagrangian

P   evaluated within the probe inlet

s   evaluated at the source

S   evaluated within probe, at hot-film sensing element

T   evaluated in the tunnel, just upwind of probe location

u   for alongwind velocity

v   for lateral velocity

δ evaluated at top of boundary layer

CHAPTER I

THE SIGNIFICANCE OF CONCENTRATION FLUCTUATIONS

1.0 Introduction

The most serious consequence of high energy consumption
by industrial societies is the rapid depletion of fossil fuels.
As the high quality liquid and gaseous hydrocarbon fuels
become exhausted, a return to the use of coal becomes more
attractive. However, one reason for the reduced use of coal
was that it is a dirty fuel which releases sulfur and parti-
culate matter as byproducts of combustion. Industries that
propose to burn coal for energy must satisfy the appropriate
government agencies that the surrounding environment will not
be adversely affected by atmospheric emissions of sulfur and
particulates. Coal-fired plants attract attention because
they are increasing in number and are among the most visible
sources of atmospheric emissions; in fact, any plant using a
chimney will also be subject to the same rules.

The constraint most often imposed on industry by
government is that plant operations must not lead to ground
level concentrations of sulfur dioxide in excess of a specified
level. The most noticeable problem with such constraints is
that even the most modern, clean-operating plants are occasion-
ally in violation of air quality standards, usually because
meteorological conditions have temporarily prevented adequate

atmospheric dispersion of emissions. In fact it is not practical to specify a constant plant emission rate which will never under any circumstances lead to violations of existing air quality standards.

Public disapproval of industrial emissions, if focussed on such unavoidable violations of the air quality standards, can place both government and industry in a difficult position. For this reason there is growing pressure for more realistic constraints which require that specified ground level concentrations never be exceeded <u>more than a small fraction of the time</u>. This crucial change is practicable only if there is adequate understanding of the factors which influence the frequency of occurrence of a specified concentration. This occurrence frequency is called the probability density function (pdf) of concentration fluctuations, and a study of its properties and the factors influencing its form is the purpose of this report.

1.1 Concentration Fluctuation Probabilities

It is well known that air pollution levels near industrial plants vary with time, and a series of pollution measurements will most likely show short-term peak values which are much higher than the mean. These peaks may produce the illegal pollutant concentrations referred to previously. A measure of this tendency is the 'peak-to-mean' concentration ratio, where the peak concentration c_p is defined as that value

which is not exceeded more than a fraction P of the time
(or equivalently, that the specified concentration has a
probability P of being exceeded).

Revision of short-term air quality standards can only
be done if P is established for every peak concentration of
interest. Long term statistics of full scale peak-to-mean
concentration ratios [e.g. Shruaikar & Patel (1977)] provide
useful information on the relationship between P and c_p.
Because concentration fluctuations are a random variable, P
can be computed for a specified peak concentration C_p from

$$P(c_p) = 1 - \int_0^{c_p} p(c)dc = \int_{c_p}^{\infty} p(c)dc , \qquad (1.1)$$

where p(c) is the probability density function of the concen-
tration fluctuations. Current knowledge about the form of
the pdf has been obtained from two approaches:

- measurements of actual concentration time series
  provide specific examples of the pdf, to which
  empirical equations are fitted.

- physical arguments are used to derive heuristic models
  for the pdf, which are then compared with observed
  values.

The empirical approach is guaranteed to provide a good descrip-
tion of observed pdf forms, and the observations can provide

physical insight to the processes causing concentration fluctuations. Because the <u>input</u> of physical insight is minimal, the method is weak in establishing in advance how the pdf values should vary as meteorological conditions change. The heuristic approach is stronger in this regard because the physical processes causing concentration fluctuations are usually linked in some way with local meteorology. It is difficult, however, to include all the relevant physics in a heuristic model of the concentration pdf.

A good example of the pdf curve-fitting approach is that of Apt (1976) who fitted a Weibull three-parameter distribution to two-week averages of atmospheric radioactivity data taken over periods of one year. The Weibull curve gives a zero probability that concentration zeros occur, which means that the observed phenomenon of pollutant concentrations which are intermittently zero cannot be incorporated by this model. This disadvantage is removed in the three-parameter lognormal curve successfully fitted to full scale data by Ott and Mage (1976).

Examples of heuristic pdf models include the exponential distribution function favored by Barry (1974) and the two-parameter lognormal model proposed by Csanady (1969, 1973 p. 228). Rather than determining the model parameters by curve-fitting to observed probability distributions, as required by empirical models, the exponential model parameters are simply the local concentration mean and intermittency, while the

lognormal model parameters are local concentration mean and variance. If the concentration mean, variance and inter- mittency are known for a given meteorological condition, then the heuristic models allow a direct calculation of the concentration pdf. Typical distribution shapes for some empirical and heuristically-derived pdf models are sketched in Fig. 1.1.

The various probability models discussed above will be described in detail in Chapter VI, and a new heuristic three-parameter lognormal model will be developed and tested. This intermittent lognormal model is an extension of the two- parameter lognormal pdf model developed by Csanady (1969, 1973 p. 228), and incorporates eddy dilution and concentration inter- mittency in a physically reasonable way. The model input parameters are the local values of mean concentration $\bar{c}$, concentration variance $\overline{c'^2}$, and concentration intermittency γ.

1.2 Mean Concentration

The spatial distribution of mean concentration in an elevated plume is usually considered to be well known. The most widely used model for this distribution is the reflected Gaussian,

$$\bar{c} = (\frac{Q}{2\pi U_H \sigma_y \sigma_z}) \exp(\frac{-y^2}{2\sigma_y^2})\{\exp\left[\frac{-(z-H)^2}{2\sigma_z^2}\right] + \exp\left[\frac{-(z+H)^2}{2\sigma_z^2}\right]\} ,$$

(1.2)

the application of which is considered in Chapter V. This
equation, originally an empirical extention of the Gaussian
solution to the one-dimensional Fickian (constant eddy
diffusivity K) diffusion equation

$$\frac{d\bar{c}}{dt} = K \frac{\partial^2 \bar{c}}{\partial x^2} \ ,$$

has recently been derived for dispersion in bounded flows
by Veigele and Head (1978). Vertical and lateral profiles
of mean concentration in an elevated plume have been measured
in the present study, and in Chapter V are fitted to Eq.
(1.2). It is shown that, in order for Eq. (1.2) to satisfy
the diffusion equation under non-uniform wind conditions,
the concentration eddy diffusivity must vary through the plume
in a specific way. The results verify that the simple reflec-
ted Gaussian model adequately describes the spatial distribu-
tion of mean concentration in elevated plumes.

1.3 Concentration Variance

Expressions for the spatial distribution of concentra-
tion variance $\overline{c'^2}$ inside elevated plumes are rare, due mainly
to lack of appropriate data. The meandering plume model of
Gifford (1959) requires that the concentration variance be
zero at a fixed distance from the moving plume centerline,
while the exponential pdf model of Barry (1974) requires that the
standard deviation $\sqrt{\overline{c'^2}}$ be directly proportional to the mean concentration $\bar{c}$

within the plume. The concentration variance predicted by these models is due not to atmospheric turbulence within the plume, but rather to large scale bodily motions (meandering) of the plume centerline. The models cannot account for the observations of concentration variance reported by Becker, Rosensweig and Gwozdz (1966) for pipe flows in which plume meander was negligible. The observations show concentration fluctuation intensities $i_c \equiv \sqrt{\overline{c'^2}}/\bar{c}$ in excess of unity at the plume centerline, and increasing without limit toward the plume edges.

To explain such observations, Csanady (1967) has derived from the equation of continuity a conservation law for the concentration variance in turbulent diffusion. The components of the conservation equation are similar to those found in the energy balance of a turbulent mixing layer or boundary layer. The conservation equation is, with $S \equiv \overline{c'^2}$,

$$\underbrace{U \frac{\partial S}{\partial x}}_{\text{advection}} = \underbrace{K(\frac{\partial^2 S}{\partial y^2} + \frac{\partial^2 S}{\partial z^2})}_{\substack{\text{gradient} \\ \text{flux}}} + \underbrace{2K\left[(\frac{\partial \bar{c}}{\partial y})^2 + (\frac{\partial \bar{c}}{\partial z})^2\right]}_{\text{production}} - \underbrace{\frac{S}{T_d}}_{\text{dissipation}} , \quad (1.3)$$

where U is the mean wind speed, K the constant eddy diffusivity of concentration mean and variance, and T_d the dissipation time scale. Csanady obtains a closed form solution for the spatial distribution of concentration variance by assuming that both $\bar{c}$ and $\overline{c'^2}$ diffuse with constant diffusivity K at equal rates. This assumption leads to axially symmetric

profiles of $\overline{c'^2}$, and restricts the solution to regions of uniform wind velocity far from solid flow boundaries. The derivation, solution and necessary assumptions for Eq. (1.3) are discussed in more detail in Chapter V.

An approximate solution to the conservation equation derived by Csanady (1967) can be obtained by assuming that the rate of production of concentration fluctuations is exactly equal to the rate at which the concentration fluctuations are dissipated. In that case Eq. (1.3) reduces immediately to a solution for the concentration variance,

$$\overline{c'^2} = 2KT_d \left[\left(\frac{\partial \overline{c}}{\partial y}\right)^2 + \left(\frac{\partial \overline{c}}{\partial z}\right)^2 \right] , \qquad (1.4)$$

where $\overline{c'^2}$ is expressed in terms of the mean field. This relation has been used by Kewley (1978) in a study of fast chemical reactions in a turbulent plume. The solution Eq. (1.4) for $\overline{c'^2}$ is unrealistic because it predicts zero variance on the plume centerline. Thus, Kewley recommends an empirical correction to the solution, as sketched on the next page.

The region of most interest for atmospheric dispersion lies close to the ground, where plumes are influenced by the nearby solid boundary. The solution to Eq. (1.3) for $\overline{c'^2}$ obtained by Csanady (1967) is therefore an approximation to the actual distribution of $\overline{c'^2}$ in plumes moving in this region of the atmospheric boundary layer, because the solid boundary presented by the ground is not included in the analysis.

$$\overline{c'^2}$$

empirical correction

Eq. (1.4)

0
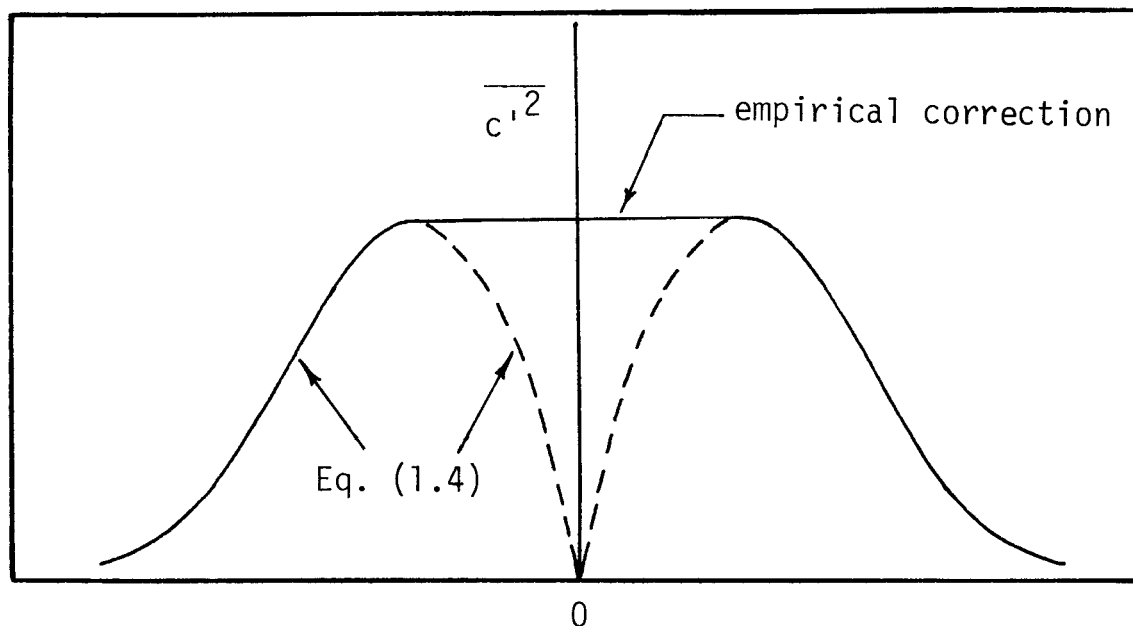
Radial Distance Off Plume Centerline

However, without additional data there is little hope of
developing a more exact model. For this reason, the present
study provides new measurements of vertical and lateral pro-
files of concentration variance in plumes emitted near the
ground. Using these measurements as a basis, Chapter V shows that local
production and dissipation of concentration fluctuations are not in balance.
As the plume moves downwind, production becomes negligible compared with
dissipation of $\overline{c'^2}$. Then, for plumes in uniform winds far above
the ground, concentration variance can be calculated from the
simplified equation

$$U \frac{\partial S}{\partial x} = K\left(\frac{\partial^2 S}{\partial y^2} + \frac{\partial^2 S}{\partial z^2}\right) - \frac{S}{T_d} , \qquad (1.5)$$

$$\underbrace{\hphantom{U \frac{\partial S}{\partial x}}}_{\text{advection}} \qquad \underbrace{\hphantom{K\left(\frac{\partial^2 S}{\partial y^2} + \frac{\partial^2 S}{\partial z^2}\right)}}_{\text{gradient flux}} \qquad \underbrace{\hphantom{\frac{S}{T_d}}}_{\text{dissipation}}$$

which, for $T_d = \sigma^2/2K$, predicts a Gaussian lateral and vertical distribution for $S = \overline{c'^2}$, identical to that found for mean concentration $\bar{c}$. This observation leads in Chapter V to a new dissipated Gaussian model for the spatial distribution of concentration variance $\overline{c'^2}$ in plumes carried close to the ground.

1.4 Concentration Intermittency

Only scanty information is available on the spatial distribution of concentration intermittency in elevated chimney plumes. Barry (1970) discusses field measurements of plume intermittency, and relates these to long-term wind direction fluctuations. This approach is reasonable when the plume centerline is seldom above the receptor location, but does not provide information on internal plume intermittency caused by atmospheric turbulence. Intermittency γ can be described by two components,

$$\gamma = \gamma_\theta \cdot \gamma_T ,$$

where γ_θ is caused by large scale meandering movements of the plume; the contribution γ_T is due to smaller scale atmospheric turbulence which transports uncontaminated eddies at random

across the receptor location. The turbulent fluctuations producing γ_T are normally assumed to have periods of one hour or less in the atmosphere.

The phenomenon of plume meander occurs over periods of from 1 to 3 hours, and is caused by wind direction changes at the high frequency end of the fluctuation range included in γ_θ (the low frequency components of γ_θ are due to wind direction changes by weather systems). As mentioned previously, Gifford (1959) developed a theory which predicts concentration fluctuation probabilities due to meandering alone, with no contribution from the randomness of atmospheric turbulence. The turbulent contribution to intermittency has not previously been measured in elevated plumes, but some guidance is available from the work of Becker, Hottel and Williams (1965), who examined scalar intermittency in round free jets. They found that in self-generated jet turbulence, the radial position of the jet boundaries fluctuated in a Gaussian manner, so the intermittency factor γ_T could be well described by the Gaussian error function. New measurements of plume intermittency caused by boundary layer turbulence have been made in the present study, and Chapter IV shows that the Gaussian error function accurately describes the spatial distribution of concentration intermittency inside elevated plumes.

1.5   Measuring Concentration Fluctuations

In this experimental investigation, concentration fluctuations were measured in a laboratory simulation of a neutrally stable (adiabatic) atmospheric boundary layer. Chapter III will discuss the rationale for, and the methods used to provide this simulation. Briefly, the main reason for this choice is that the inability to model all atmospheric phenomena simultaneously in the laboratory is far outweighed by the ability to provide adjustable, reproducible steady flow conditions in which reasonable averaging times give statistically reliable results.

The laboratory measurement of high-frequency scalar fluctuations in turbulent flows has attracted little attention during the last several decades. The most recent reviews of current work appear to be those of Csanady (1973, Ch. 7) and Hinze (1975, Ch. 3&6). Scalar properties of interest have usually been the fluid temperature or species concentration. The present lack of fluctuation data is due in large part to the experimental difficulties encountered in making the measurements. The experimental problems generally include: low signal-to-noise ratios (often less than unity), detector sensitivity to extraneous noise sources (environmental or electronic), insufficient frequency response, inability to obtain dynamic calibration, cumbersome or expensive design, and toxic, explosive or messy tracer materials.

In spite of these problems which are, after all, not unique to the measurement of turbulent scalar fluctuations, several measuring systems have been developed which have given satisfactory results; a survey of the available techniques is presented in Appendix A. These devices fall into one of three groups:

- light-scattering probes, in which the amount of light scattered into a photo-receptor is proportional to the number of tracer particles in a sample volume.

- heated element probes, in which the voltage required to maintain a hot wire or film at a constant temperature is proportional to the temperature and composition of the gas flowing over the element.

- conductivity detectors, in which the electrical conductivity of an aqueous electrolytic solution is proportional to the concentration of electrolyte flowing over the sensor.

An assessment of the potential usefulness of various fluctuation detectors is presented in the review by Fackrell (1976). The advantages and disadvantages of the various probe types are compared in Table 1.1, from which it is apparent that no single measurement technique works well under all circumstances. The development and testing of a new hot-film

fast response concentration sensor designed specifically
for the present study is described in Chapter II.

1.6 Summary

The purpose of this study is to provide new informa-
tion on the behavior of the probability distribution of
concentration fluctuations inside an elevated plume. The
intermittent lognormal model developed for the pdf can be
used only if the spatial distributions of mean concentration
$\bar{c}$, concentration variance $\overline{c'^2}$ and concentration intermittency
γ are known inside the plume.

A new fast response concentration sensor was developed
and used to measure these parameters in a wind tunnel simula-
tion of the atmospheric boundary layer. An existing model
for the spatial distribution of mean concentration in plumes
is verified, and a model for intermittency in jets is shown
to work well in elevated plumes. In addition, a new 'dissipated
Gaussian' model is shown to successfully describe the spatial
distribution of concentration variance inside elevated plumes.

TABLE 1.1

SCALAR FLUCTUATION DETECTORS

DETECTOR TYPE	ADVANTAGES	DISADVANTAGES
LASER - DOPPLER LIGHT- SCATTERING PROBE [Yang & Meroney (1975)]	- good for dispersion of particulates and gases. - no flow distortion of sample volume. - provides real-time data measurements. - good frequency response, adequate spatial resolution. - simultaneous fluctuating velocity measurements - point, sheet or volume sampling - dual system measures spatial correlations - robust probe design - simple probe construction	- slow molecular diffusion of oil fog tracer ($S_c \approx 4 \times 10^4$) limits accurate observation of dissipative eddies. - large probe precludes use in small spaces. - difficult to measure overall frequency response. - special device needed for tracer generation; tracer can be messy or toxic. - tracer may adhere to solid boundaries. - cannot take measurements flush to solid boundaries.
INFRA-RED LIGHT- SCATTERING PROBE [Motycka & Leutheusser (1972)]	- good for dispersion of particulates and gases. - wider applicability due to small probe size. - provides real-time measurements. - adequate frequency response. - small amount of flow distortion in sample volume. - robust probe design. - simple probe construction.	- slow molecular diffusion of oil fog tracer ($S_c \approx 4 \times 10^4$) limits accurate observation of dissipative eddies. - relatively poor spatial resolution. - cannot measure velocity fluctuations. - difficult to measure overall frequency response. - special device needed for tracer generation; tracer can be messy or toxic. - tracer may adhere to solid boundaries. - cannot measure flush to solid boundaries.
DUAL - ELEMENT HOT WIRE/FILM PROBE [Way & Libby (1971)]	- good for disperion of gases - Helium tracer ($S_c \approx .25$) is clean and easy to use. - wide applicability due to small probe size. - good frequency response and spatial resolution. - accurate observation of dissipative eddies. - simultaneous fluctuating velocity measurements. - negligible flow distortion in sample volume. - can measure close to solid boundaries	- requires very accurate calibration, careful use and complicated off-line data processing. - optimum design difficult to establish. - difficult to measure overall frequency response. - delicate probe design and construction.
FLUCTUATING TEMPERATURE PROBE [Fiedler (1974)]	- good for dispersion of gases. - temperature tracer ($Pr = .7$) is clean and easy to use. - wide applicability due to small probe size. - good frequency response and spatial resolution. - accurate observation of dissipative eddies. - negligible flow distortion in sample volume. - simple probe construction. - provides real-time measurements. - can measure close to solid boundaries.	- may be sensitive to velocity fluctuations. - adequate signal-to-noise ratios may be difficult to obtain. - solid flow boundaries act as heat sinks. - delicate probe design. - difficult to measure overall frequency response.
SINGLE - ELECTRODE CONDUCTIVITY PROBE [Gibson & Schwartz (1963)]	- good for disperion of liquids. - salt tracer is clean and easy to use. - can detect species concentration or temperature fluctuations. - good frequency response and adequate spatial resolution. - small amount of flow distortion in sample volume. - robust probe design. - provides real-time measurements.	- slow molecular diffusion of salt tracer ($S_c \approx 700$) limits accurate observation of dissipative eddies. - delicate probe construction. - difficult to measure overall frequency response. - limited to dispersion in liquids. - needs redesign to measure flush to solid boundaries.

PARAMETERS: obtained via curvefit to cumulative distribution

pdf(c)

$1-\gamma$

3-PARAMETER LOGNORMAL Ott & Mage (1976)

area = $1-\gamma$

0   c   Concentration

PARAMETERS: $\bar{c}$, $\overline{c'^2}$

pdf(c)

LOGNORMAL Csanady (1973)

$\sqrt{\overline{c'^2}}$

0     $\bar{c}$ c   Concentration

$1-\gamma$

$\gamma^2/\bar{c}$

PARAMETERS: $\bar{c}$, γ

pdf(c)

EXPONENTIAL Barry (1970)

0     $\bar{c}$ c   Concentration

$1-\gamma$

PARAMETERS: $\bar{c}$, $\overline{c'^2}$, γ

pdf(c)

INTERMITTENT LOGNORMAL Present Study

$\sqrt{\overline{c'^2}}$
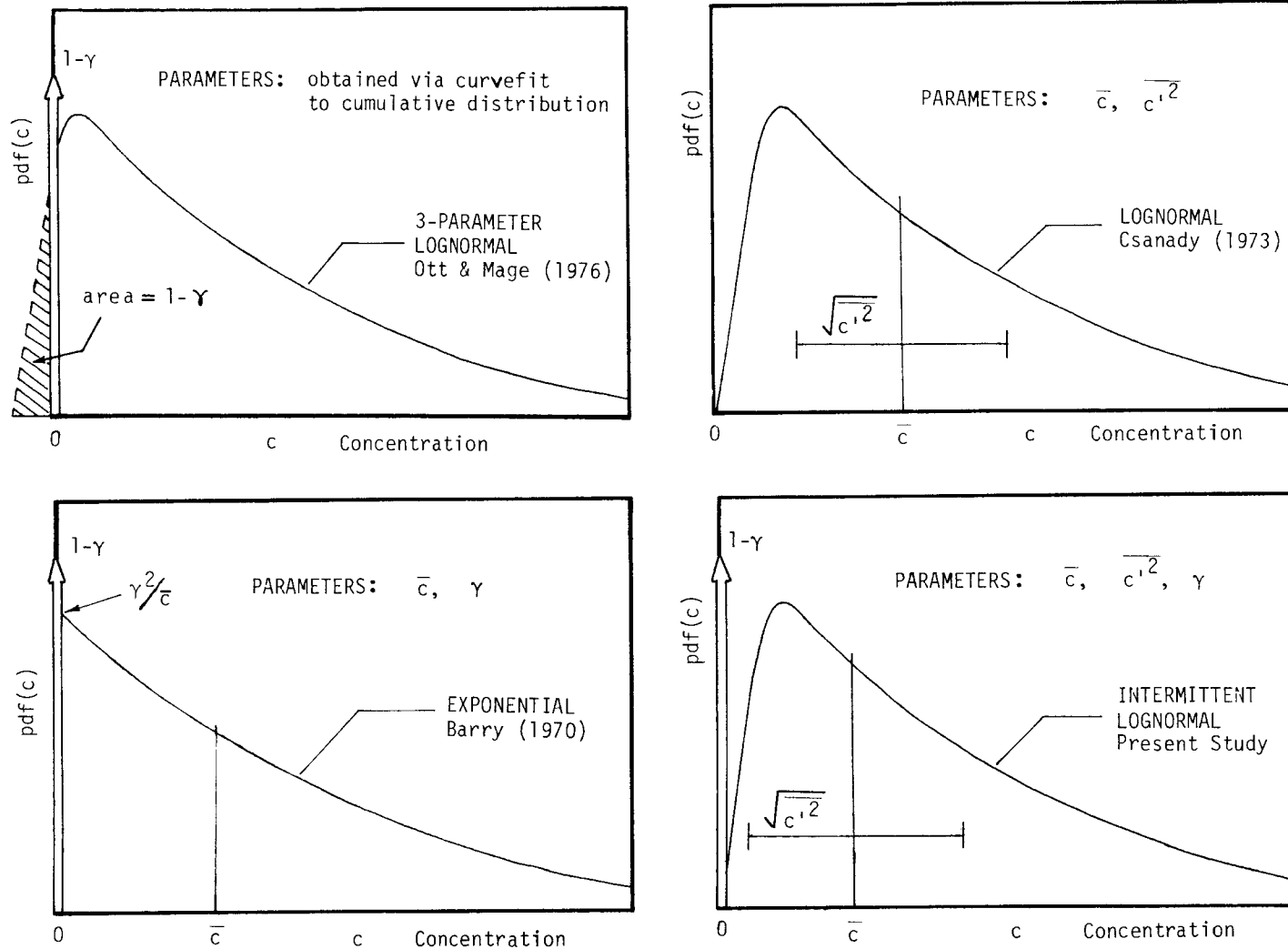
0     $\bar{c}$ c   Concentration

FIG. I.I   Typical Distribution Shapes for Some Concentration PDF Models

CHAPTER II

THE HOT-FILM CONCENTRATION DETECTOR

2.0 Introduction

The fast-response sensors currently available for detecting high frequency scalar fluctuations in laboratory or industrial-scale turbulent flow were discussed in Chapter I. None of the sensors are perfect, and selection of an optimum probe type is at best a compromise because sensor limitations make some goals, such as small probe size, real-time data analysis, high signal-to-noise ratio and good spatial resolution, difficult to obtain from one system. The purpose of this chapter is to describe the design and calibration of a new helium concentration detector which uses a single hot-film sensor as the active element. This new design provides a useful alternative to other available fast-response scalar detectors.

2.1 Probe Design

One of the objectives was to develop a fast response concentration detector that would be small enough for use in a wind tunnel of cross-section 30 cm x 30 cm. An anemometer-driven hot-film was selected for the sensing element because it combined robustness with good frequency response. In order to detect concentration, the user must exploit the sensitivity

of hot-film temperature to the thermal conductance of the gas flowing past the element. The classic theory of convection heat transfer in Holman (1968, p. 134) shows that heat lost from the film is related to the gas properties by

$$h \sim \mu^{-1/6} C_p^{1/3} k^{2/3} \rho^{1/2} U^{1/2} \; .$$

Helium was chosen as the tracer material because its properties are much different from those of air, and it is therefore easily detected. Also, it has the desireable attributes of being clean, non-toxic, non-flammable and low in cost.

The details of the probe design and construction are given in Appendix B. In brief, the fast response concentration sensor (FRCS) is an aspirated probe in which the velocity is held constant by means of a choked orifice downstream of the hot film sensing element. This configuration is similar to that used by Blackshear and Fingerson (1962) and Kuretsky (1967) for detecting scalar fluctuations in a turbulent flow. A short fiber filter in the probe inlet reduces sensitivity to wind tunnel turbulence. The aspiration velocity is not adjustable, so the probe usually samples anisokinetically. This means that external flow streamlines must either draw together or move apart while entering the probe, depending on whether the aspiration velocity is faster or slower than the local tunnel speed. Isokinetic sampling was not practical because it requires that the suction speed be adjusted to local tunnel speed at every probe location, and changing the suction speed causes the probe calibration to vary. It will be shown in Chapter III that corrections to the measured concentration time derivative

are necessary to compensate for signal dissipation caused by the probe

inlet filter.

Following the format of Table 1.1, some attributes

of the new probe are given in Table 2.1, and an axial

probe cross-section is shown in Fig. 2.1 along with a close-up

photograph of the probe.

TABLE 2.1

CHARACTERISTICS OF NEW FAST RESPONSE CONCENTRATION DETECTOR

DETECTOR TYPE	ADVANTAGES	DISADVANTAGES
SINGLE HOT-FILM FLUCTUATING CONCENTRATION DETECTOR	- good for dispersion of gases. - Helium tracer ($S_c \simeq$ .25) is clean and easy to use. - small probe size. - good frequency response and spatial resolution. - provides real-time measurements. - overall frequency response can be measured. - robust probe design. - inexpensive and easy to construct.	- anisokinetic sampling. - unknown flow distortion of sample volume. - care required to eliminate sensitivity to velocity and pressure fluctuations. - probe can diffuse or distort small eddies. - needs redesign for measurements close to solid boundaries.

2.2 Calibration of Steady-State Response

Before the concentration fluctuation detector could be

used in the laboratory, its steady state and transient

response to helium concentration had to be determined. Steady-

state calibration of the concentration detector required helium-

air mixtures of accurately known composition, in a reproducible,

inexpensive form. The mixtures were obtained by using rotameters
to meter the flow of separate streams of helium and air into a
mixing chamber. The helium was of research grade and was
purchased in standard high pressure bottles from a commercial
gas supplier. The air was obtained from the laboratory
compressed air supply, and was filtered and dried prior to use.
Five glass-tube rotameters were used to cover a flow range of
20 cm^3/min. to 20,000 cm^3/min. The flow meters were
calibrated to an accuracy of ± 2% of reading for flows of air,
helium or Refrigerant R-12 (molecular weight 122). Calibration
at low flow rates used a soap-bubble flowmeter, and at higher
rates positive displacement of water in an inverted graduated
cylinder.

The Thermo-Systems 1276-10A hot-film sensor was driven
by a DISA 55D05 battery-powered constant temperature anemometer,
chosen because of its low noise characteristics. In order to
ensure operation with the proper hot-film overheat ratio of
1.5, the cold probe resistance was measured with a high-resolu-
tion digital ohmmeter. The corresponding operating resistance
was then calculated and an external decade resistance box was
adjusted to properly balance the circuit. A battery voltage
supply, voltage offset box and nulling volt-meter were connected
to the output of the anemometer so that the zero-helium out-
put voltage could be set at any desired value. This flexibility
was useful for later signal processing, especially when measur-
ing voltages which fluctuated about zero. The Hewlett-Packard

5326B DVM could not correctly average a signal of varying polarity, so a stable, adjustable voltage offset capability was necessary. Low noise input was obtained by using batteries to provide the diode-stabilized offset voltage. Circuit diagrams for the voltage offset devices are presented in Appendix B.

A schematic of the calibration setup is shown in Fig. 2.2. Early attempts at steady-state calibration were complicated by drift in the zero-helium voltage from the probe. The drift was traced to small amplitude, low frequency, random temperature fluctuations in the calibration gas mixture and in the laboratory. Drift of this sort occurs in anemometer systems where there is no temperature compensating arm in the bridge. The problem was overcome by passing the mixture first through copper coils immersed in water at room temperature, and then blowing the mixture over the probe inside the wind tunnel. The tunnel was operated at low speed to provide ventilation past the probe and to aid in stirring the air-conditioned laboratory air thoroughly for temperature uniformity. In addition, the effects of zero drift were corrected for by switching the helium on and off every 10 seconds during calibration at a fixed helium level, and subtracting this zero reading from adjacent helium readings. Three groups of ten "helium on" readings were averaged to obtain the resulting probe output voltage. The continuous signal sketched (next page) on the left was therefore "chopped" as at the right, so that the

zero drift caused no problem. A strip chart was used to monitor the probe output; quantitative readings were obtained using a Hewlett-Packard 5623B voltage-to-frequency counting DVM connected to a line printer.
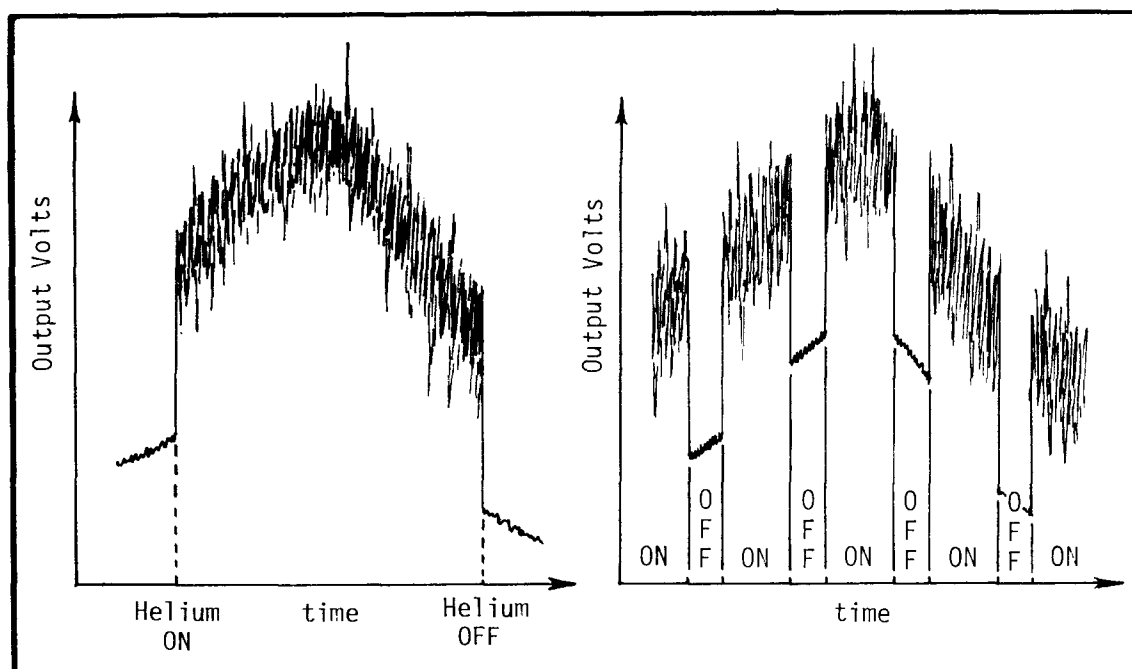
The calibration curves obtained for the probe showed a linear relationship between output voltage and helium concentrations of up to 1% (10 ppth) by volume. The concentrations observed during the experimental phase of the work were

usually much less than this 10 ppth linear limit. A typical
calibration curve for helium is shown in Fig. 2.3. Six hot-
film sensors were calibrated during the experiments; the
calibration constants ranged from 1.5 to 2.0 ppth/mv. One
sensor was also calibrated for Refrigerant R-12/air mixtures
so the effect of tracer density and molecular diffusivity
could be studied. The R-12 calibration curve obtained is also
shown in Fig. 2.3. Note that the probe output voltage decreases
with increasing concentration for the R-12 tracer, and in-
creases with increasing helium tracer concentration. This
occurs because the heat conductance of R-12 is lower than that
of air, while that of helium is higher. The curves also show
that the probe is about five times more sensitive to helium
than to R-12 concentrations, and for this reason helium was
used exclusively during the experiments.

2.3 Calibration of Transient Response

The calibration procedure described in the previous
section showed that the probe output voltage varies linearly
with the steady-state tracer concentration. The next step
was to investigate the probe response to a rapidly changing
tracer concentration. Ideally, one would wish for a concen-
tration which fluctuated sinusoidally between zero and some
known value. The frequency of oscillation would then be
slowly increased until the probe was no longer capable of
fully responding to the input. This would be indicated by a

decrease in the amplitude of the fluctuating probe output voltage. Unfortunately, this ideal calibrating concentration signal is impracticable because of the difficulties in accurately modulating the concentration. A more practical calibrating signal is a step-change in concentration.

Diffusion acts to smear the boundary between volumes containing different tracer concentrations, so that sharp gradients are difficult to maintain. Therefore, the key to calibration of transients is to expose the probe to high temporal, not spatial, concentration gradients. This was done in the present study by swinging the probe on a pendulum rapidly across the outlet of a 10 ppth helium/air jet. It was felt that the combination of sharp jet boundary and moving probe would provide the required concentration gradient. The alternative of moving the jet was rejected because of the distorted and smeared jet boundaries that would result from the forced entrainment of still air into the upwind face of the jet. A schematic of the configuration is shown in Fig. 2.4.

A stand was used to anchor a simple hinge device, into which the 0.5 m long probe support stem was inserted. This resulted in a pendulum-like configuration, with the sensor swinging through a vertical plane on an arc of 0.5 m radius. The pendulum pivot friction was adjusted so that at the bottom of its arc the probe swung through the jet at between 5 and 7 m/s. This speed was close to the probe aspiration velocity, which was in turn close to the wind speed in the tunnel during

the experiments. The probe output voltage was monitored on a storage oscilloscope which was set to trigger just before the probe passed into the helium jet.

A typical oscilloscope trace is also presented in Fig. 2.4. Note that the probe output reaches the steady value about 1 - 2 ms after it first begins to rise. The probe velocity across the helium jet was about 5 mm/ms. This means the probe moved 5 - 10 mm while the output voltage was rising. It is possible that turbulent mixing at the jet boundary smeared the step change across a region this thick, but 2 - 4 mm is more likely for the gradient region. Probably only the first 0.5 ms of voltage rise was affected by concentration gradients at the jet boundary. The 3% overshoot of the final steady-state voltage is caused by the electronic feedback circuitry in the DISA 55D05 constant temperature anemometer. This small amount of electronically induced signal overshoot improves the probe frequency response.

2.4 Probe-Induced Signal Attenuation

It is not possible to separate the effect of finite jet concentration gradients from the effect of finite probe frequency response. Therefore, a conservative estimate of the probe frequency response is obtained by assuming that the observed concentration-time curve of Fig. 2.4 is due entirely to non-instantaneous response of the probe to a step change in concentration. The frequency response is determined by examining

the behavior of an electric circuit which responds as in Fig. 2.4 to a step change in voltage input. A simple R-C circuit analog, which gives a frequency bandwidth of 800 Hz (see Fig. 2.6), is inadequate because it does not exhibit the initially sluggish response or the subsequent voltage overshoot apparent in Fig. 2.4. Later work by Wilson and Netterville (1979) shows this behavior to be more characteristic of a third-order low pass filter circuit which includes a damped harmonic oscillator in addition to the R-C components. Such a circuit is an approximate electric analog to two processes occuring in the probe-anemometer system, shown schematically in Fig. 2.5:

- Inside the FRCS, the square concentration wave-front is diffused by the fiber filter, and acquires an S-shaped Gaussian error function distribution according to the solution for dispersion in tubes formulated by G. I. Taylor (1953). The error function is approximated by the exponential response of an R-C circuit element having a natural frequency $\omega_{n_1} = 1/RC = 1/\tau_1 = 2\pi f_{n_1}$.

- The electronic feedback circuitry of the DISA 55D05 constant temperature anemometer drives the probe voltage as a damped harmonic oscillator, which causes the initially sluggish probe response and the subsequent signal overshoot. The harmonic oscillator has a natural frequency $\omega_{n_2} = 1/\tau_2$ and operates with a critical damping ratio ζ.

It has been shown by Wilson and Netterville (1979) that such a system has the impulse response

$$\frac{V_{out}}{V_{in}} = 1 - \frac{(\tau_1/\tau_2)^2 \exp(-t/\tau_1)}{1-2\zeta(\tau_1/\tau_2)+(\tau_1/\tau_2)^2} +$$

$$+ \frac{\exp(-\zeta t/\tau_2)\sin(\sqrt{1-\zeta^2}t/\tau_2 - \Phi)}{\{(1-\zeta^2)[1-2\zeta(\tau_1/\tau_2) + (\tau_1/\tau_2)^2]\}^{1/2}} , \qquad (2.1)$$

where

$$\Phi = \tan^{-1}(-\sqrt{1-\zeta^2}/\zeta) + \tan^{-1}(\frac{\sqrt{1-\zeta^2}\tau_1/\tau_2}{1-\zeta\tau_1/\tau_2}) . \qquad (2.2)$$

The time constants τ_1 and τ_2 and the damping ratio ζ were determined from a least-squares fit of Eq. (2.1) to the experimental response curve of Fig. 2.4. The optimum values were τ_1 = 0.42 ms, τ_2 = 0.30 ms and ζ = 0.49. The theoretical system response Eq. (2.1) has been plotted in Fig. 2.4 using these values; the fit between theory and experiment is seen to be good. Note that for the special case of $\tau_1 = \tau_2 = \tau$ and ζ = 1/2, the impulse response (2.1) would reduce to that of a third-order Butterworth filter.

The probe's attenuation of a steady unit sine wave input of frequency f is (Wilson and Netterville (1979))

$$\frac{V_{out}}{V_{in}} = \{[1-(1+2\zeta\tau_1/\tau_2)F^2]^2 + [F\{2\zeta+(1-F^2)\tau_1/\tau_2\}]^2\}^{-\frac{1}{2}},$$
$$(2.3)$$

with $F = f/f_n$, where $f_n = 1/2\pi\tau_2$ = 530 Hz. The attenuation curve Eq. (2.3) has been plotted in Fig. 2.6 along with a

typical experimental concentration fluctuation spectrum.
The fast response sensor attenuates the concentration signal
by 10% at 300 Hz, and the signal is attenuated by a factor
of two (3 db down) at about 600 Hz. Concentration fluctuations
above 450 Hz were not observed in the wind tunnel; the energy-
containing eddies which produce virtually all of the concen-
tration variance occur in the range 0 - 150 Hz, and are
attenuated by a negligible amount. When the tunnel speed was
systematically varied (this is discussed in Chapter III),
the measured concentration variance $\overline{c'^2}$ proved to be insensitive
to the presence or absence of high frequency signal components.
Thus, it is concluded that the probe's frequency response is
adequate for measuring $\overline{c'^2}$.

The sensor does not appear to work as well when measure-
ments of concentration dissipation are desired. The natural
dissipation of concentration fluctuations occurs mainly at the
high frequency end of the spectrum, typically peaking at fre-
quencies 3 to 5 times higher than $\overline{c'^2}$, where Eq. (2.3) predicts
the most probe-induced signal attenuation. An increasing
wind speed, such as occurs vertically through the wind tunnel
boundary layer, shifts the concentration spectrum towards higher
frequencies, thereby exposing more of the eddies producing time-
derivatives to probe-induced attenuation. Chapter III will
show that there is considerable probe-induced dissipation of
the high frequency fluctuations, more than is indicated by the
theoretical attenuation of Eq. (2.3). Specifically, a velocity-

dependant signal attenuation appeared in measurements of con-
centration time derivative variance $\overline{(\frac{\partial c'}{\partial t})^2}$ needed for
estimating natural dissipation rates. The question of success-
fully applying the fast response sensor to concentration
measurements in the wind tunnel is discussed in more detail
in the next chapter.
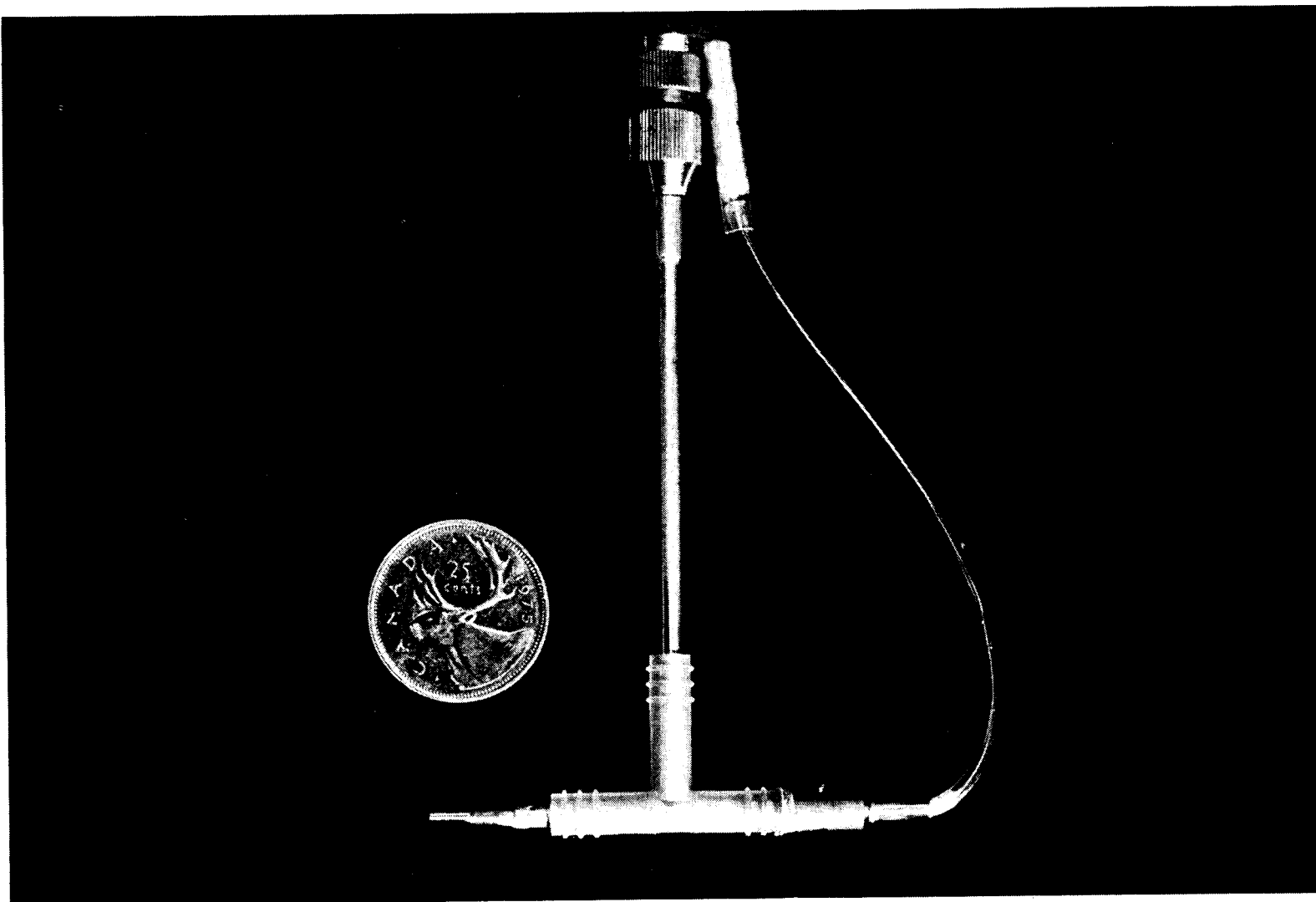
FIG. 2.1a   The Fast Response Concentration Detector

TO VACUUM PUMP

$Q = 14.85$ cm^3/sec at ROOM CONDITIONS

PLASTIC TUBE TEE

SCALE
|←——1 cm——→|

TO BRIDGE

PROBE
SUPPORT

CHOKED ORIFICE
0.60 mm DIA.

INLET TUBE
2.38 mm OD

0.165 O.D.

SAMPLE VELOCITY
$U_i = 6.94$ m/sec

EPOXY

QUARTZ HOT FILM SENSOR
0.025 mm DIA.

SPACER AND
STIFFENER

FIBER FILTER AND
FLUCTUATION DAMPER
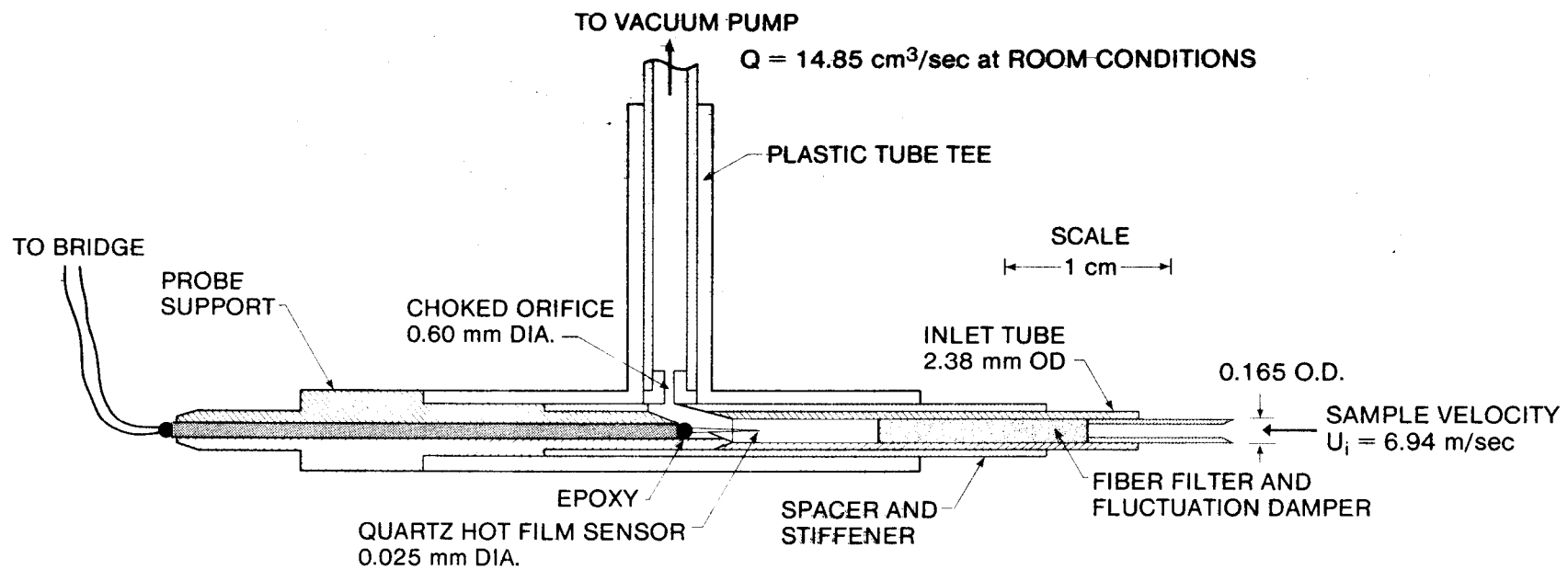
FIG. 2.1b The Fast Response Concentration Detector
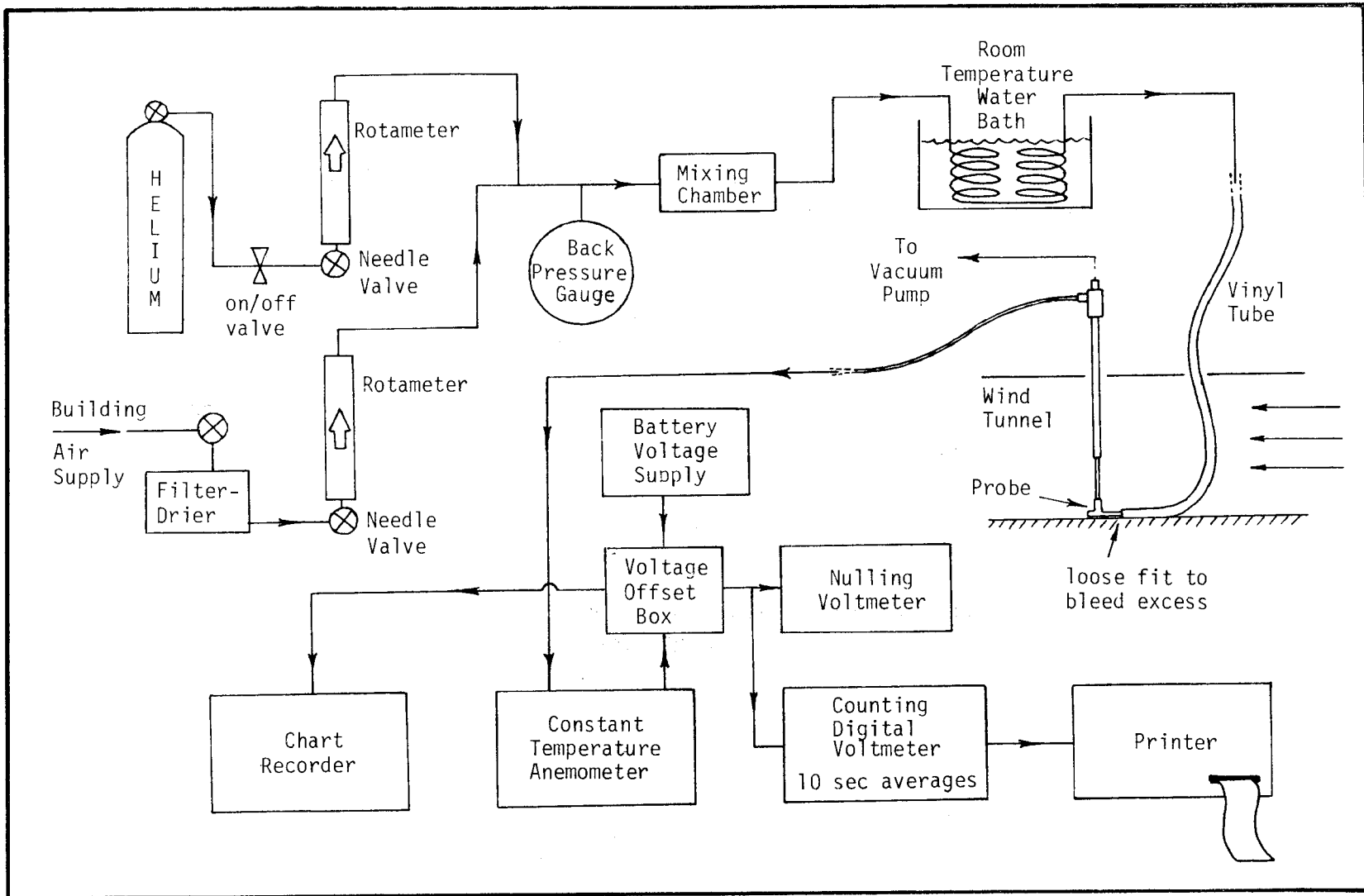
FIG. 2.2   Steady State Calibration Equipment
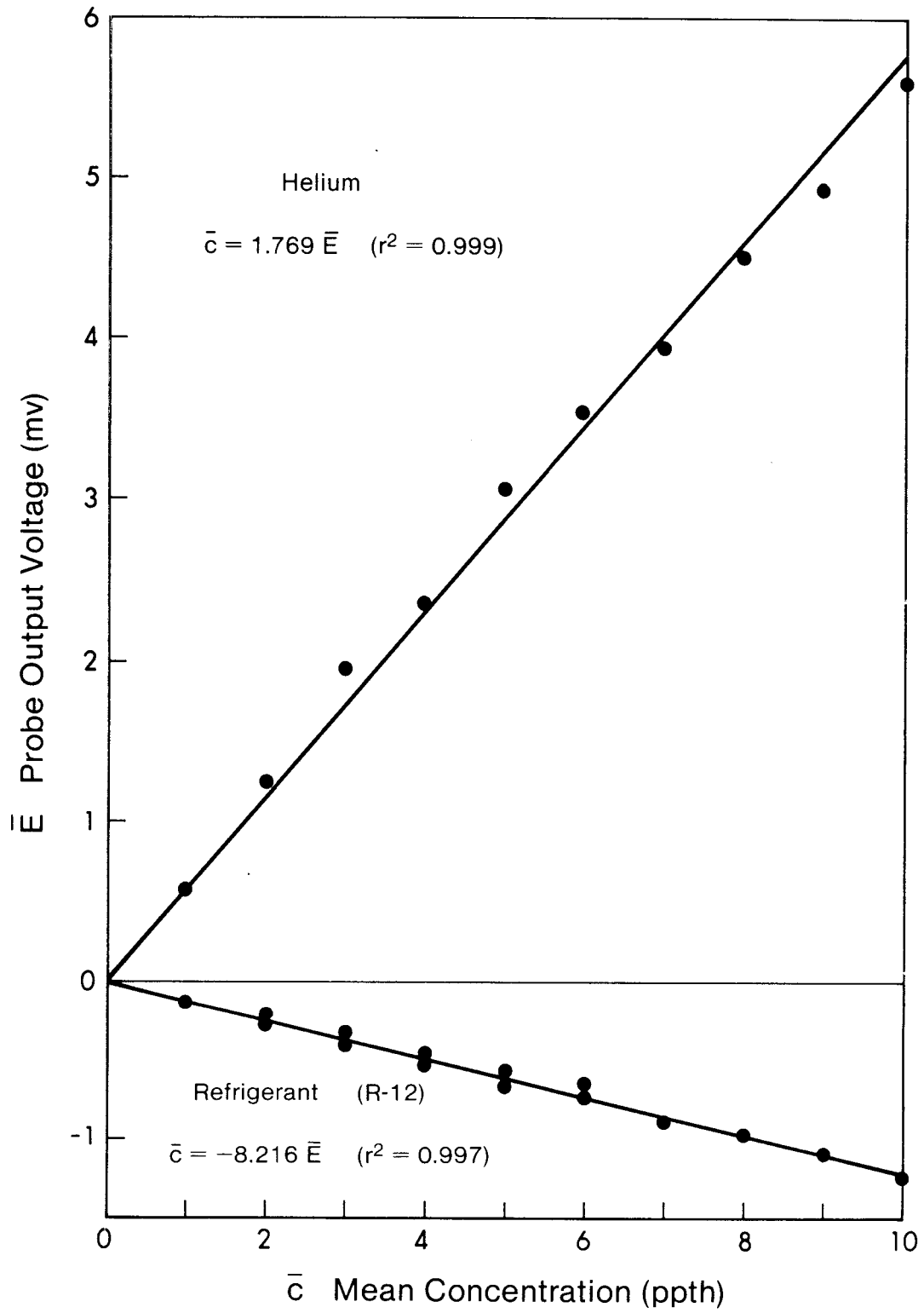
FIG. 2.3   Calibration Curves for
Steady Concentrations
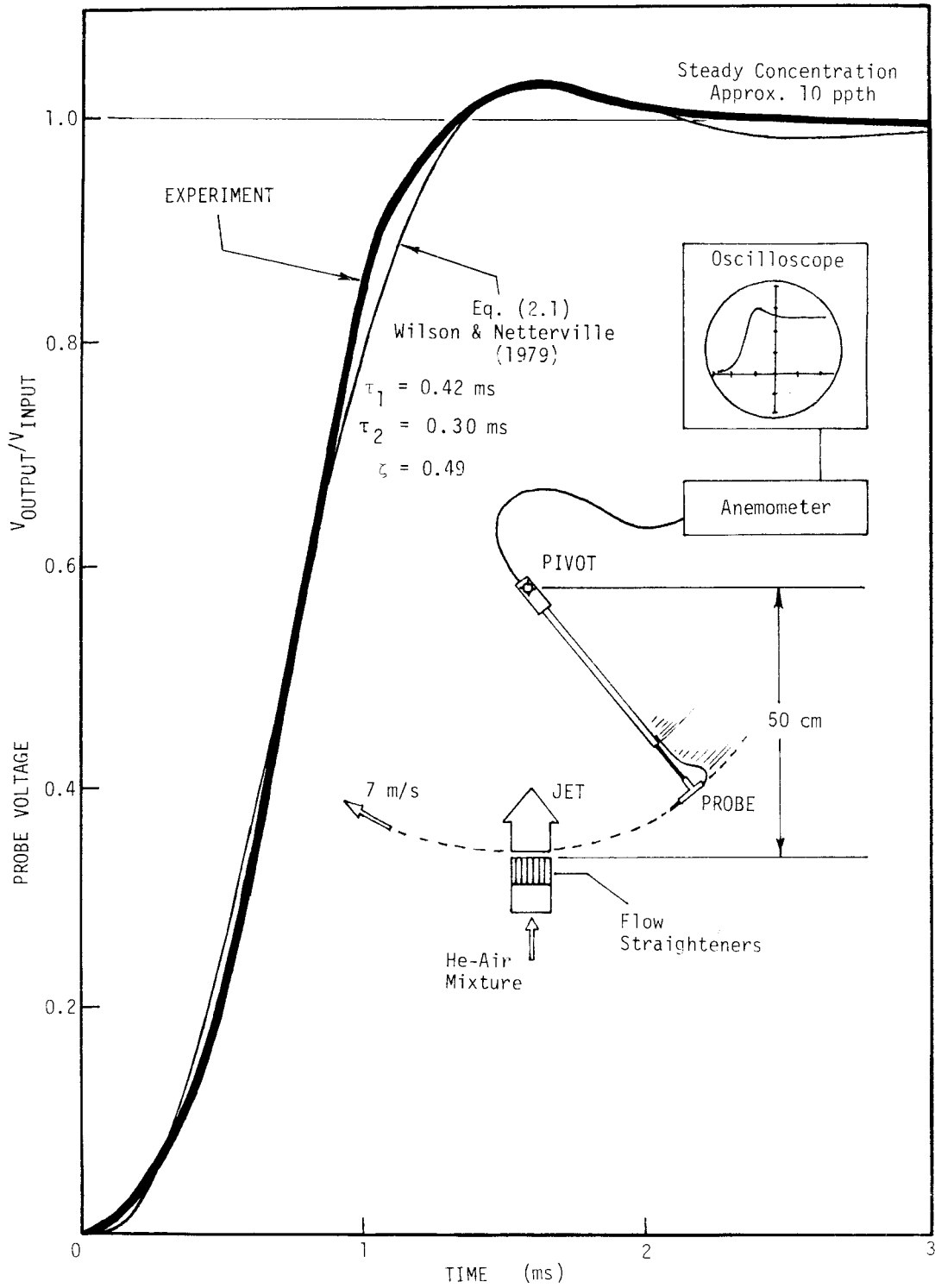
FIG. 2.4   Probe Response to a
Concentration Step-Change
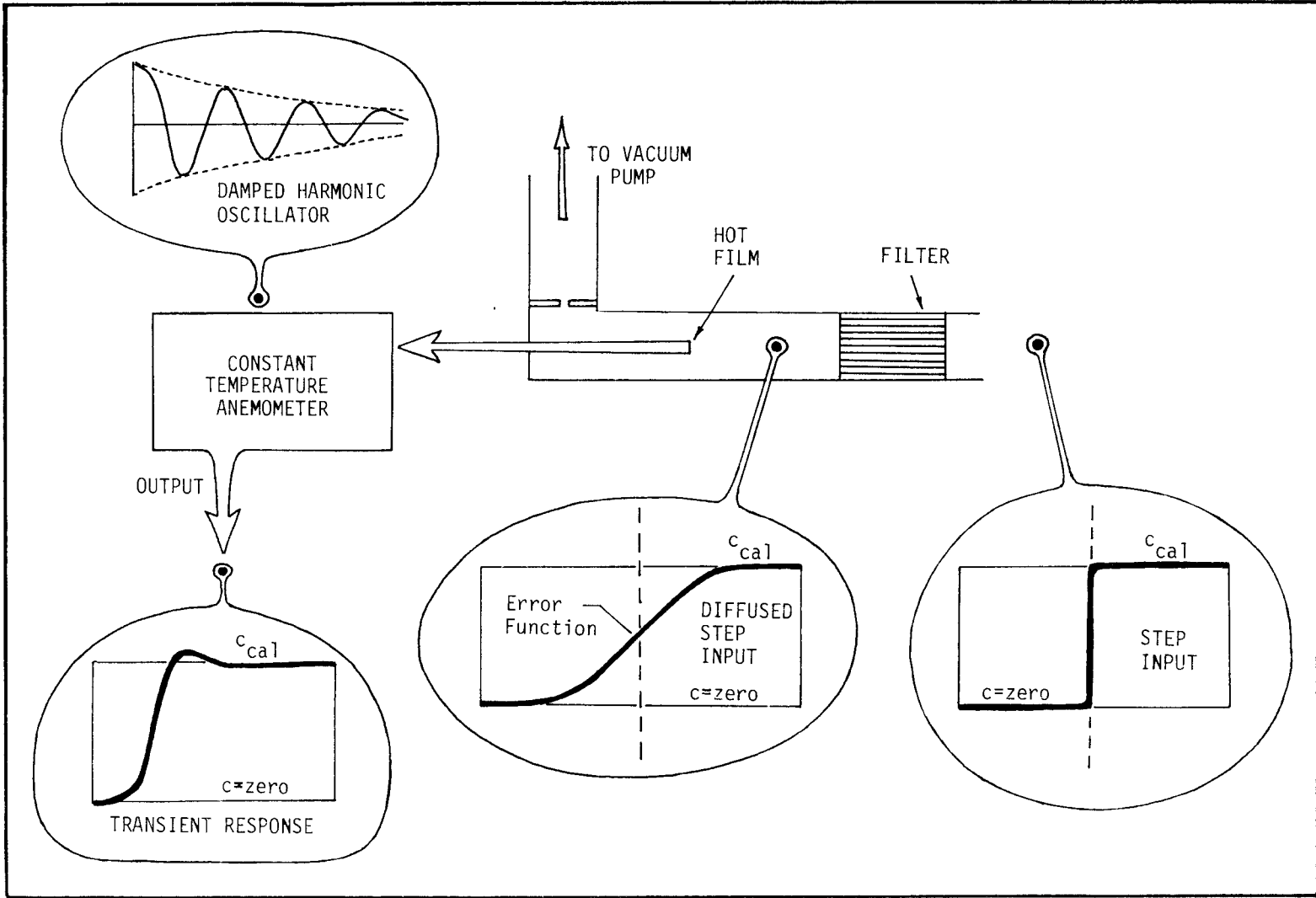
FIG. 2.5   Distortion of Step Input by Aspirated Probe

Concentration Signal
Attenuation Eq. (2.3)

Simple RC
Approximation

$$\frac{V_{out}}{V_{in}} = [1 + \left(\frac{f}{455}\right)^2]^{-\frac{1}{2}}$$

Probe Located Under Plume Centerline

Downwind Distance = 12.5 Source Heights

Height Above Ground = 0.2 Source Heights

Wind Speed at Probe Height = 5.7 m/s

Probe Suction Velocity = 7 m/s

f·S(f)
Corrected
for Attenuation

V_{out}/V_{in} Concentration Signal Attenuation

fS(f) Concentration Spectrum (Hz · ppth²)

Observed Frequency f (Hz)

FIG. 2.6 Probe-Induced Attenuation

of Concentration Spectrum

CHAPTER III

WIND TUNNEL MODELLING AND CONCENTRATION

MEASUREMENT TECHNIQUES

3.0 Introduction

Atmospheric dispersion can be studied by making full-scale measurements in the field, or alternatively, the study can approximate real conditions by laboratory simulation of the atmospheric boundary layer. This latter approach provides control over flow parameters such as wind speed and direction, and measurements in the laboratory can be repeated until statistically reliable quantities are obtained, without concern for the vagaries of the weather. One disadvantage of laboratory simulations is that some atmospheric flow properties, such as vertical gradients of temperature and wind direction, are difficult to simulate. Also, the constraining roof and side walls of the tunnel can cause flow features which are absent in most atmospheric flows. An example of this is the flow acceleration and turbulence inhomogeneity in the downwind direction which was observed in the present wind tunnel flow. However, for a great many interesting dispersion problems the advantages of adjustable, reproducible steady flow conditions far outweigh the disadvantages of laboratory simulation. Because stable $\overline{c'^2}$ values required about 10^4 integral scales of turbulence to be sampled, it is unlikely that the present

wind tunnel concentration measurements could have been obtained in the field with sufficient accuracy and detail to provide successful verification of the theoretical models developed in Chapters IV, V and VI.

3.1   Simulation of the Atmospheric Boundary Layer

Atmospheric boundary layers are generated by the natural interaction between rough ground and the wind. For neutrally stable flows of sufficiently high Reynolds number, all naturally grown turbulent boundary layers are similar in structure, so that relatively thin laboratory boundary layers reflect in reduced scale the structure of the thick atmospheric boundary layer. The difficulty with laboratory flows is that naturally developed turbulent boundary layers must pass over a very long fetch of roughness elements before they grow thick enough for model testing.

Artificial stimulation of turbulent mixing can be used to create thick turbulent boundary layers within the confines of short wind tunnel test sections. Photographs of the wind tunnel are shown in Figs. 3.1 and 3.2; the components are shown schematically in Fig. 3.3. This wind tunnel configuration generates an artificially thickened boundary layer with vortex generators (spires) and barrier used to stimulate upwind mixing. The method is similar to that used by Counihan (1969, 1970), and reduces the required boundary layer generation length from about 80

boundary layer heights to about 8.

The technique of stimulating rapid boundary layer growth has certain practical obstacles that must be overcome. One of the most serious problems was poor lateral (crosswind) uniformity of the flow field. The non-uniformity was traced to a wake instability behind the spires causing the main air flow to become attached to one or the other of the tunnel walls. Uniform flow was obtained by slightly rotating each spire around its vertical axis, just enough to prevent the wall flow attachment. To do this effectively required a quick measure of the resulting lateral wind profile; this was obtained with a streamlined pitot tube rake which connected to an inclined multitube manometer. The effect of slight changes to the spire angles of attack could thus be observed immediately, making the trial and error adjustment of the lateral wind profile a relatively simple task. The final profiles of wind speed and turbulence were measured with DISA hot wires; they are shown in Fig. 3.4, in which it is seen that the lateral uniformity is within ± 3% throughout the central 90% of the test section width.

The simulated atmospheric boundary layer employed for this study has also been used by Wilson (1977) to model boundary layer flow over two-dimensional ridges. By comparing mean wind and turbulence parameters with full scale data reported by Counihan (1975), Wilson found that the model scale factor for the present simulated atmospheric boundary

TABLE 3.1

COMPARISON OF WIND TUNNEL BOUNDARY LAYER WITH FULL SCALE

ATMOSPHERIC BOUNDARY LAYER CHARACTERISTICS COMPILED BY COUNIHAN (1975)[*]

Parameter	Length Scale 2000:1		Length Scale 4000:1	
	Wind Tunnel	Neutral Stability Atmos. B.L. with same Z_o	Wind Tunnel	Neutral Stability Atmos. B.L. with same Z_o
Roughness Height Z_o	0.09 m	-	0.18 m	-
Wind Profile Power Law n	0.168	$0.123 + 0.03$	0.168	0.157 ± 0.03
Boundary Layer Thickness δ	250 m	600 m $\pm$?	500 m	600 m $\pm$?
$\sqrt{\overline{u'^2}}/U$ @ 30 m	0.15	0.12 ± 0.02	0.18	0.15 ± 0.02
$\sqrt{\overline{v'^2}}/\sqrt{\overline{u'^2}}$ @ 30 m	0.85	0.75 ± 0.15	0.80	0.75 ± 0.15
$\sqrt{\overline{w'^2}}/\sqrt{\overline{u'^2}}$ @ 30 m	0.62	0.50 ± 0.1	0.55	0.50 ± 0.1
$\overline{u'w'}/U_\delta^2$ @ 30 m	0.0024	0.0021 ± 0.0005	0.00236	0.0023 ± 0.0005
Integral Length Scale Λ_x @40m	75 m	180 m $\pm$ 40	150 m	150 m $\pm$ 30

[*]adapted from Wilson (1977)

layer is approximately 4000:1. Table 3.1 shows the various turbulence parameters measured in the present study.

The model scale factor relating the simulated atmospheric boundary layer to the full scale is not as important for the present experiments as it is for problems dealing with dispersion around obstacles. The plume concentration measurements described in later chapters are used to derive models of the spatial and statistical distribution of concentration fluctuations within an elevated plume. Most conclusions are drawn from examinations of the internal plume structure, and the theoretical predictions should apply over a wide range of scale factors. The single source height can represent both tall industrial stacks and low sources emitting close to the ground.

3.2   The Turbulent Wind Field

Hot-wire anemometers (DISA 55D30) were used to measure the mean and turbulent wind field in the tunnel, with a 0.3 mm diameter pitot-static tube and inclined manometer providing occasional wind profiles for comparison. A pitot-static reference tube upstream of the spires was used daily for setting the wind tunnel speed to a constant, repeatable value. This convenient upwind location meant that the reference tube never had to be moved during the experiments. The hot wire probes were calibrated for mean velocity in a small wind tunnel using dynamic head pressure taps as a standard. Day-to-day calibration adjustments in the experimental wind tunnel were

accomplished by:

1. using a pitot-static tube to measure wind speed in the test section at a point 20 cm above the tunnel floor, where turbulence was low.

2. replacing the pitot-static tube with the hot wire probe.

3. making fine adjustments to the probe overheat ratio so the measured velocity agreed with that from the pitot-static tube.

Mean velocity was obtained by passing the linearized hot wire anemometer output voltage to a voltage-to-frequency counting digital voltmeter (Hewlett Packard 5326B) set for 100 sec averages. The turbulent velocity components were measured by first filtering the linearized signal to remove noise components above 20,000 Hz, then passing the signal to an electronic signal processor. The processing included:

1. removal of low frequency mean and noise components (< 0.1 Hz) by A.C. capacitive coupling of the processor input.

2. signal amplification, addition and subtraction to obtain the fluctuating velocity components u', v' and w'.

3. signal differentiation to obtain the velocity time derivative $\frac{\partial u'}{\partial t}$.

4. signal multiplication to obtain the variance

   components u'^2, v'^2, w'^2, $(\frac{\partial u'}{\partial t})^2$ and the Reynolds

   stresses $u'w'$, $u'v'$ and $v'w'$.

The processed signals were then averaged for 100 seconds on the V-to-F counting DVM. Single DISA 55P11 hotwire probes (1.25 mm filament) gave good spatial resolution for detailed mean wind measurements. DISA 55P61 X-wire probes with a sample volume of about one cubic mm were used for rms turbulence and Reynolds stress measurements.

The wind tunnel reference speed of 10 m/s was chosen high enough to avoid Reynolds number dependance in the turbulence and concentration measurements. The criteria for selecting this speed are discussed in Section 3.5. Vertical profiles of the mean and turbulent velocities are shown in Fig. 3.5; these values were maintained for all dispersion measurements. The vertical profiles are given for $x/H = 12.5$, midway along the wind tunnel test section. Measurements upstream or downstream of this position exhibited the same profile shapes, but varied systematically in magnitude. These gradients in the flow direction are shown in Fig. 3.6.

There are two separate effects which produce the observed alongwind gradients. First, boundary layers growing on the tunnel sides and roof gradually reduced the effective tunnel cross-sectional area so that the mean velocity increased slightly in the downwind direction. Also, the surface roughness was not able to generate enough turbulence to balance the

decaying turbulence from the spires and barrier. The result was the observed gradual decrease in turbulence levels down the tunnel. In later chapters it will be seen that the effect of the axially nonhomogeneous flow field is observed only in the rate of plume growth, and can be effectively removed by correction techniques.

The profiles of root mean square (rms) turbulence components in Fig. 3.5 have the desired vertical uniformity through the plume dispersion layer $0 \leq z/H \leq 3$, and the boundary layer comparison in Table 3.1 shows very good agreement with full scale data for a wind tunnel scale factor of 4000:1. This indicates that the method of artificially stimulating the upstream turbulent mixing process can produce a realistic laboratory simulation of the full scale atmospheric boundary layer.

3.3 Measuring the Concentration Field

The fast response concentration sensor described in Chapter II was used for measuring the concentration fluctuations reported in subsequent chapters. However, the slow but random zero drift from the hot film anemometer made accurate mean concentration measurements with the fast response detector very cumbersome. The mean concentration field was determined with a slow response, high accuracy heated element conductivity detector developed by Wilson (1977), shown schematically in Fig. 3.3. A continuous sample was drawn from the tunnel

test section through a 1 mm OD moveable probe, into the detector, where it passed over a thermal conductivity bridge of the same type used in gas chromatographs. A reference sample drawn simultaneously from upwind of the spires was passed over the opposite arm of the bridge to compensate for fluctuations in background helium concentration; zero drift was monitored by systematically turning the helium tracer off and on. The helium-induced bridge imbalance, directly proportional to helium concentration, was amplified prior to measurement on a voltage-to-frequency counting digital volt-meter set for 100 sec averages, and was continuously displayed on a chart recorder. The concentration readings from the system were reproducible within ± 2% on a month-to-month basis, a performance which matched the accuracy of concentration fluctuations determined with the fast response sensor.

The signal from the fluctuation detector was processed by analog electronic circuits to measure concentration variance, time derivatives and intermittency. The basic sequence of signal processors and monitors is shown schematically in Fig. 3.7. The signal processing steps were to:

1. Apply an offset voltage to remove the pure-air component of the hot wire signal.

2. Use a low-pass filter to remove the high-frequency noise component (> 1500 Hz) from the signal.

3. Use capacitive AC coupling (basically a high-pass filter) to remove the very low frequency zero drift component (< 0.1 Hz).

4. Amplify the signal as necessary and send to correlator and spectrum display for analysis of autocorrelations, probability density functions and spectra.

5. Pass the signal through a differentiator circuit to obtain concentration time derivative $\frac{\partial c'}{\partial t}$.

6. Square the signal (c' or $\frac{\partial c'}{\partial t}$ as required) with a multiplier circuit to obtain c'^2 or $(\frac{\partial c'}{\partial t})^2$.

7. Use a low pass filter to remove the high frequency noise (> 5000 Hz) introduced by the signal processing circuits.

8. Use a voltage-to-frequency counting digital voltmeter to take 100 second averages of $\overline{c'^2}$ and $\overline{(\frac{\partial c'}{\partial t})^2}$.

3.4 Measuring Concentration Intermittency

Near the fringes of the plume, the concentration signal spent an appreciable length of time at the level corresponding to pure air. A typical signal trace is sketched on the next page, and shows detectable levels of helium tracer to be present only about 80% of the time. This time fraction is called the concentration intermittency γ, and varies from near unity in the plume core to zero in the uncontaminated air outside the plume. It is obvious that the concentration intermittency must be known in order to describe the statistical properties of the concentration fluctuations. The method used to measure signal intermittency was similar in concept to that used by
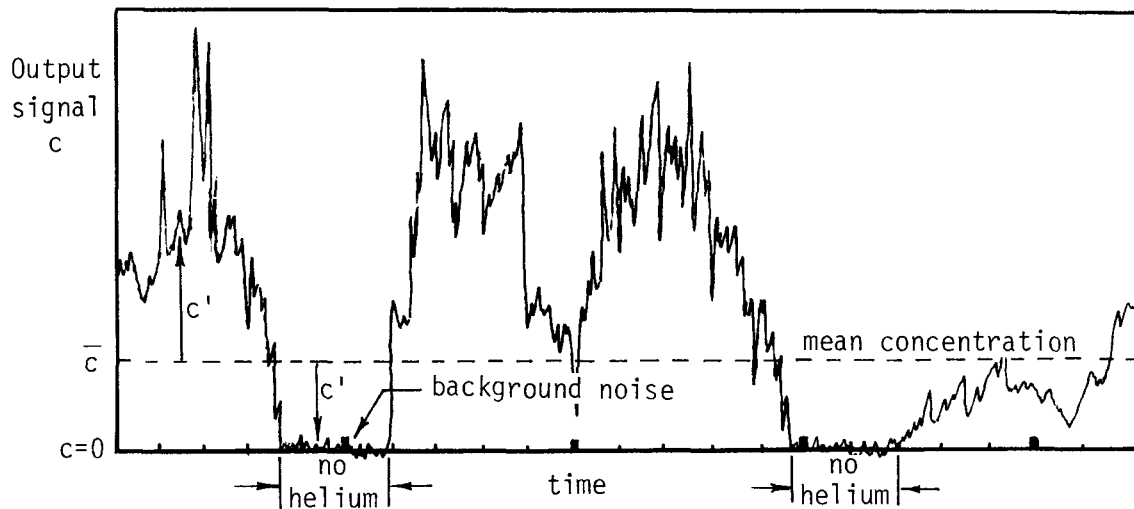
Becker, Hottel and Williams (1965), and consisted of alter-
nately amplifying the concentration signal by a factor of 10
and then clipping the signal at 0.8 volts. After three such
stages, a nonlinear amplification step was obtained by squaring
the signal. This improved the signal-to-noise ratio, because
the low level noise components were amplified less than the
larger signal components. After two more amplification-
clipping stages, a low amplitude 500 kHz sine wave was added
to the signal to provide regularly spaced time steps for a
frequency counter. Zero drift was rough-trimmed with a voltage
offset and nulling voltmeter prior to the first amplification-
clipping stages, and was fine-trimmed with a voltage offset
and oscilloscope before input to the frequency counter. To

reduce sensitivity to the amplified air noise over the probe
and the electronic system noise, the sine wave amplitude and
the frequency counter trigger level were set so that the
counter was triggered only about 20% of the time. This
resulted in a count of about 100 kHz with the helium off. The
counting procedure is shown schematically in the sketch below.

HELIUM OFF ⟵ ⟶ HELIUM ON

Counting ∿ 100 kHz   Counting <100 kHz

clipping
level
0.8V

500
kHz

concentration
spike

Voltage
Output
From
Amplifier

This would be incorrectly
counted if 500 kHz
amplitude was too high

trigger
level

noise

noise

zero

counting here   time
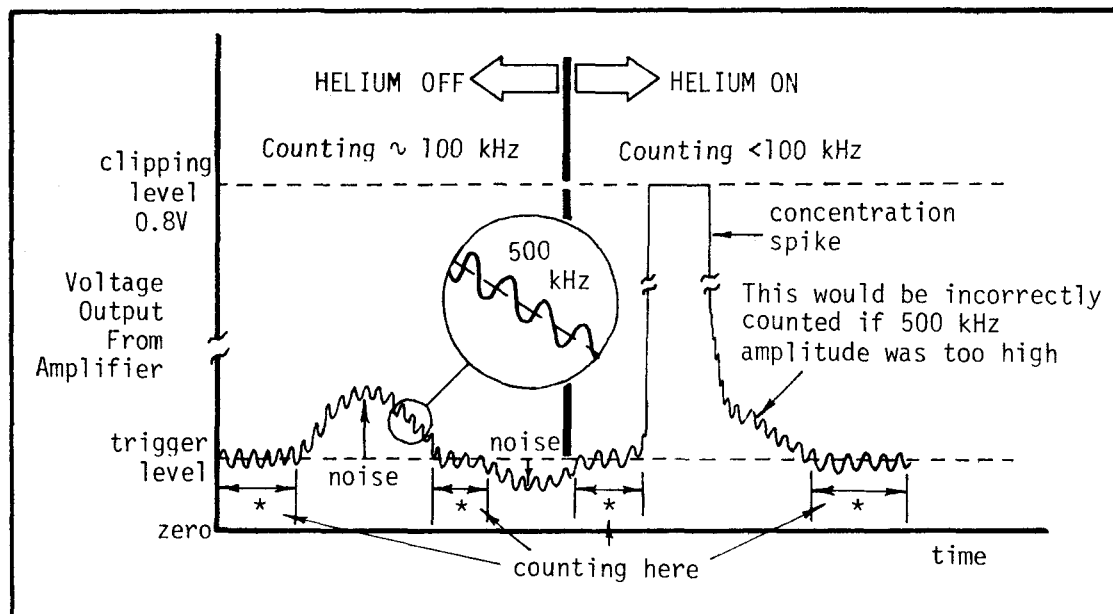
A low sine wave amplitude is used because, if the noise was
submerged within a high amplitude sine wave, so that 500 kHz
was counted with the helium off, any low level tracer gas
signals would also trigger the counting process and falsely
indicate that no tracer gas was present. The portion of time

that tracer gas is present is defined as the intermittency γ, calculated from

$$\gamma = 1 - \frac{\text{frequency with tracer on } (\leq 100 \text{ kHz})}{\text{frequency with tracer off } (\simeq 100 \text{ kHz})}.$$

A schematic of the intermittency circuit is given in Fig. 3.8, and results of the intermittency measurements are discussed in Chapter IV.

3.5 Reynolds Number Effects on Mass Diffusion

The Reynolds number of the flow in full-scale atmospheric boundary layers is on the order of 10^8, whereas the Reynolds number of the flow in the wind tunnel simulation was only about 10^5. Turbulent dispersion in the wind tunnel must therefore be independant of Reynolds number if the simulation is to provide information applicable to the full scale.

The wind tunnel speed had to be set high enough to avoid Reynolds number effects. However, to keep the signal-to-noise ratio of the fast response concentration sensor as high as possible, slow wind tunnel speeds giving low dilution and low noise from impact pressure fluctuations were desireable. Therefore, the tunnel was operated at the lowest wind speed which was still high enough for Reynolds number independance. For a tunnel reference speed of 10 m/s, signal-to-noise ratios for rms concentration were usually greater than 5. Typical

noise levels corresponded to an rms concentration fluctuation of 0.2 ppth. The variation of mean concentration and Reynolds stress $-\overline{u'w'}$ with tunnel speed is shown in Fig. 3.9, along with the effect of changing the ratio of source exit velocity to wind speed at source height. The ratio $\overline{c}\, U_T/Q$ was independant of tunnel speed wherever Reynolds number effects were absent. This region corresponded to tunnel speeds greater than about 10 m/s, and this speed was used for all the experiments. The ratio of source velocity to local tunnel speed was fixed at unity to ensure that plume spread characteristics resulted entirely from atmospheric (as opposed to self-generated) turbulence.

3.6 Correction for Anisokinetic Sampling

Anisokinetic sampling occurs when the fast response sensor aspirates samples at a velocity U_p different from the local tunnel speed U_T. The wind speed increased vertically through the tunnel boundary layer, so there was only one height at which the sampling occurred isokinetically (in this case, at $z = 1$ cm, where $U_T = U_p = 7$ m/s). Fig. 3.10 illustrates the ingested streamline pattern for the case where $U_p < U_T$.

The mass of an eddy cannot change while moving through the probe, so

$$m_{eddy} = (\rho A U t)_T = (\rho A U t)_p = (\rho A U t)_S = constant \, ,$$

$$(3.1)$$

where ρ is density, A the cross-sectional area of the ingested stream tube, U the eddy velocity, and t the transit time for an eddy to pass a point in space. The subscript T indicates conditions in the tunnel, P indicates conditions just inside the probe inlet, and S indicates conditions at the hot-film sensor, after the eddy has passed through the filter at the probe inlet.

The mass flow per unit time must be the same at any point along the ingested stream tube, so that

$$\dot{m} = \frac{m_{eddy}}{t_{transit}} = \rho_T A_T U_T = \rho_P A_P U_P = \rho_S A_S U_S = constant.$$

$$(3.2)$$

Combining Eqs. (3.1) and (3.2) gives $t_S = t_P = t_T$, which means the time for an eddy to pass a fixed point in space is unchanged by anisokinetic sampling, so that fluctuation frequencies inside the fast response sensor are the same as in the tunnel,

$$f_S = f_P = f_T.$$

$$(3.3)$$

The fluctuation frequency f_T within the tunnel must be directly proportional to tunnel speed; a series of concentration spectrum observations at different tunnel speeds showed the expected proportional relationship between spectral peaks and tunnel speed, confirming Eq. (3.3).

Fig. 3.9 verified that for sufficiently high tunnel speeds the mean concentration $\bar{c}$ is related to tunnel speed U_T and emission rate Q by

$$\frac{\bar{c} \, U_T}{Q} = A_1(x,y,z), \qquad (3.4)$$

where A_1 is a function only of x, y and z, independant of Q and U_T. The rms concentration should also vary with Q/U_T,

$$\frac{\sqrt{\overline{c'^2}} \, U_T}{Q} = A_2(x,y,z). \qquad (3.5)$$

Measurements of $\overline{c'^2}$ were made at various values of Q and U_T; the observed linear relationship between $\sqrt{\overline{c'^2}} \, U_T$ and Q shown in Fig. 3.11 verifies Eq. (3.5). Thus no anisokinetic sampling correction is necessary for concentration variance $\overline{c'^2}$.

The dissipation ϕ_c of concentration fluctuations can be related to the variance of the concentration time derivative by

$$\phi_c = \frac{6D}{U_T^2} \left. \overline{\left(\frac{\partial c'}{\partial t}\right)^2} \right|_{tunnel}, \qquad (3.6)$$

as shown in Chapter V. Measurements of dissipation rate were required, so the dependance of time derivative variance on tunnel speed (or Reynolds number) was investigated. The measurements plotted in Fig. 3.11 show a relation between $\frac{\partial c'}{\partial t}$, Q and U_T

given by

$$\frac{U_T}{Q}^{1/2} \sqrt{\overline{\left(\frac{\partial c'}{\partial t}\right)^2}} \Bigg|_{\text{measured}} = A_3(x,y,z) , \qquad (3.7)$$

which was quite startling considering that variations of $\bar{c}$ and $\sqrt{\overline{c'^2}}$ given by (3.4) and (3.5) were inversely proportional to U_T rather than its root. A clue to the unravelling of this mystery is found in Chapter V , where it is shown that concentration time derivatives can be related to other properties of the concentration field by a diffusion equation, so that

$$\overline{\left(\frac{\partial c'}{\partial t}\right)^2} = \frac{U_T^2}{6D}\left[2K_y\left(\frac{\partial \bar{c}}{\partial y}\right)^2 + 2K_z\left(\frac{\partial \bar{c}}{\partial z}\right)^2 + K_y'\frac{\partial^2 S}{\partial y^2} + \right.$$

$$\left. + \frac{\partial}{\partial z}\left(K_z'\frac{\partial S}{\partial z}\right) - U\frac{\partial S}{\partial x}\right] , \qquad (3.8)$$

where all the K's are proportional to U_T, and $S \equiv \overline{c'^2}$. Then, using Eqs. (3.4) and (3.5),

$$\overline{\left(\frac{\partial c'}{\partial t}\right)^2} \sim \Sigma[\text{terms of } O(U_T Q^2)] . \qquad (3.9)$$

The concentration time derivative variance is proportional to $U_T Q^2$, so that

$$\frac{1}{U_T^{1/2} Q} \sqrt{\overline{\left(\frac{\partial c'}{\partial t}\right)^2}}\Bigg|_{tunnel} = A_4(x,y,z) . \qquad (3.10)$$

Combination with Eq. (3.7) gives a relation between actual and observed rms time derivatives,

$$\sqrt{\overline{\left(\frac{\partial c'}{\partial t}\right)^2}}\Bigg|_{tunnel} = A_5 U_T \sqrt{\overline{\left(\frac{\partial c'}{\partial t}\right)^2}}\Bigg|_{measured} . \qquad (3.11)$$

The explanation for this behavior must lie in the sensor response characteristics. According to Eq. (3.11), the measured rms time derivative shows an unexpected inverse dependance on tunnel speed. However, from Eq. (3.3), eddy timescales are not distorted by anisokinetic sampling. Thus the observed behavior implies that high frequency c' fluctuations (responsible for most of the time derivative variance) lose amplitude while passing through the probe, probably due to dissipation of small eddies within the filter at the probe inlet. The observed inverse relationship between measured rms time derivative and tunnel speed means that the probe's dissipative effect on the high frequency portion of the concentration spectrum is directly proportional to the fluctuation frequency, as sketched on the next page. The specific relation between probe-induced dissipation and signal frequency (or equivalently,

tunnel speed) probably depends on the shapes of the concentration spectrum and the attenuation curve for the probe; a physical reason for the apparently linear relationship is not obvious.
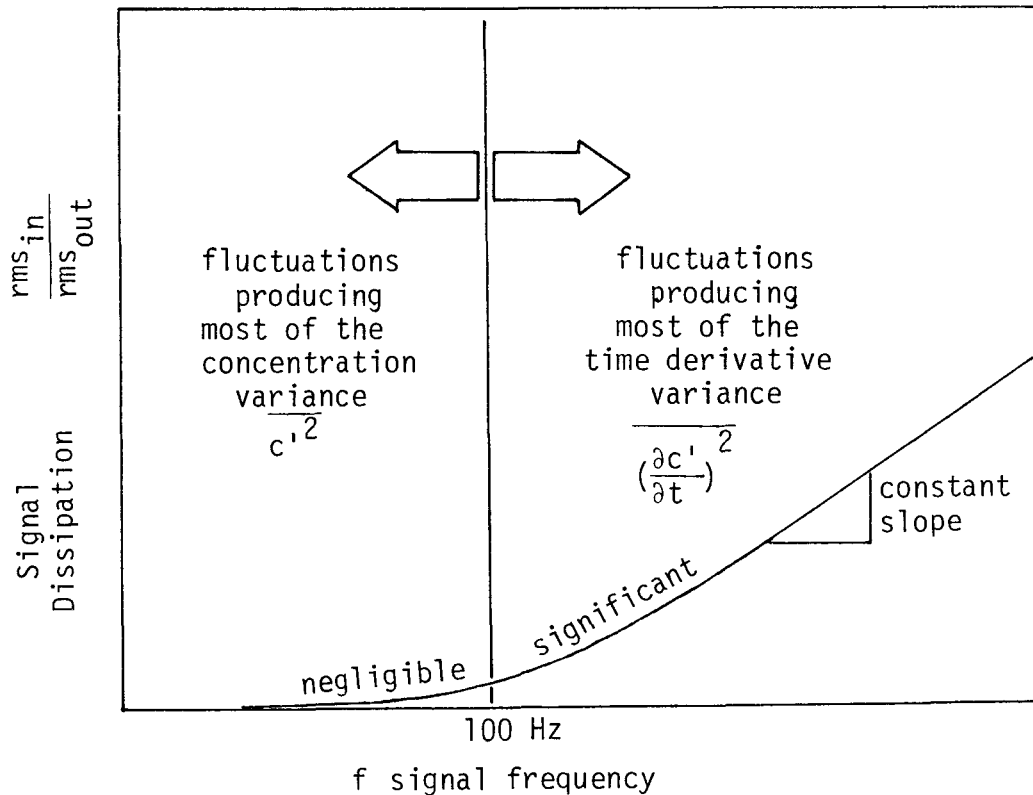
An estimate for the magnitude of the proportionality constant A_5 appearing in Eq. (3.11) can be obtained from an expression derived by Hinze (1975, p. 290) relating the concentration and velocity fluctuation microscales,

$$\frac{\lambda_u}{\lambda_c} = \sqrt{Sc} \ . \qquad\qquad (3.12)$$

Here $Sc \equiv \nu/D$ is the Schmidt number (0.25 for dilute helium into air), and λ_u and λ_c are the Taylor microscales of along-wind velocity and concentration respectively, calculated from

$$\lambda_u^2 = 2 \ U_T^2 \ \overline{u'^2} \ / \ \overline{\left(\frac{\partial u'}{\partial t}\right)^2} \tag{3.13}$$

and

$$\lambda_c^2 = 2 \ U_T^2 \ \overline{c'^2} \ / \ \overline{\left(\frac{\partial c'}{\partial t}\right)^2}\bigg|_{tunnel} . \tag{3.14}$$

These expressions are combined with Eq. (3.11) to give a probe 'dissipation velocity' U_d,

$$U_d \equiv \frac{1}{A_5} = U_T Sc^{-\frac{1}{2}} \sqrt{\frac{\overline{u'^2}}{\overline{c'^2}}} \sqrt{\frac{\overline{\left(\frac{\partial c'}{\partial t}\right)^2}}{\overline{\left(\frac{\partial u'}{\partial t}\right)^2}}}\bigg|_{measured} , \tag{3.15}$$

which is used to correct the measured time derivative variance according to

$$\overline{\left(\frac{\partial c'}{\partial t}\right)^2}\bigg|_{tunnel} = \left(\frac{U_T}{U_d}\right)^2 \overline{\left(\frac{\partial c'}{\partial t}\right)^2}\bigg|_{measured} . \tag{3.16}$$

Measurements of velocity and concentration time derivative variance were made in a vertical plane through the plume centerline at $x/H = 12.5$; the resulting estimates for U_d are presented in Table 3.2.

TABLE 3.2

PROBE DISSIPATION VELOCITY FOR CONCENTRATION

TIME DERIVATIVE VARIANCE

Z/H	U_d(m/s)
0.5	6.8
1.0	7.2
1.5	7.3
2.0	7.2

Within experimental accuracy the fast response probe's dissipation velocity is U_d = 7 m/s — remarkably close to the probe's aspiration velocity U_p = 6.94 m/s, although this may be coincidence. Thus, the concentration time derivatives measured in this study were corrected for dissipation in the anisokinetic fast response sensor according to Eq. (3.16) with U_d = 7 m/s.

It is interesting to substitute (3.16) back into the relation (3.6) between dissipation and time derivative. Then

$$\phi_c = \frac{6D}{U_d{}^2} \left. \overline{\left(\frac{\partial c'}{\partial t}\right)^2} \right|_{measured} ,$$

which means that the measured profiles of concentration time

derivative variance are directly proportional to the <u>actual</u> dissipation rate of concentration fluctuations. As a result, the anisokinetic fast response sensor can be used to measure local concentration dissipation rates without the need for knowledge of the local wind field.
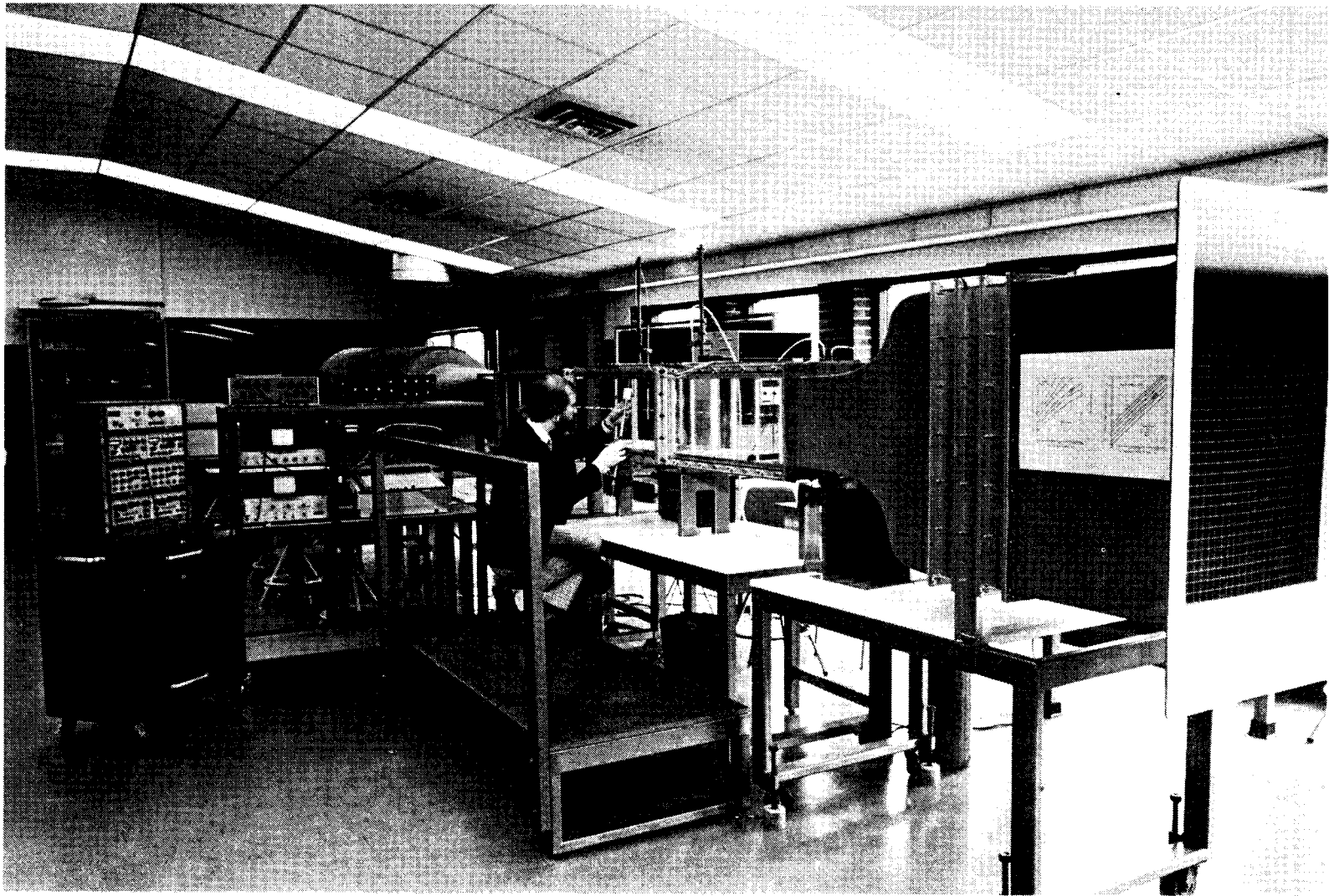
FIG. 3.1   The Wind Tunnel Laboratory
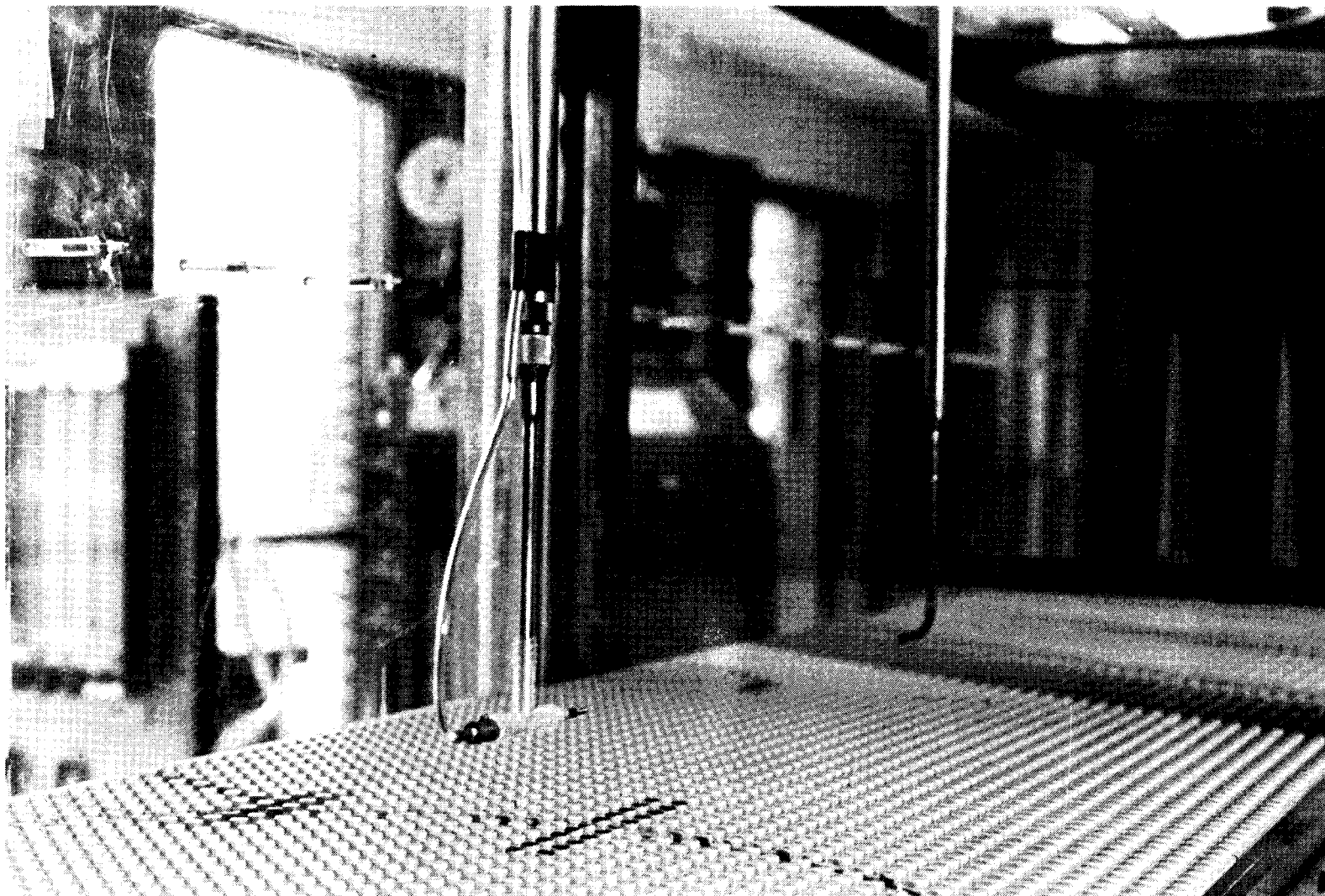
FIG. 3.2   The Tunnel Test Section
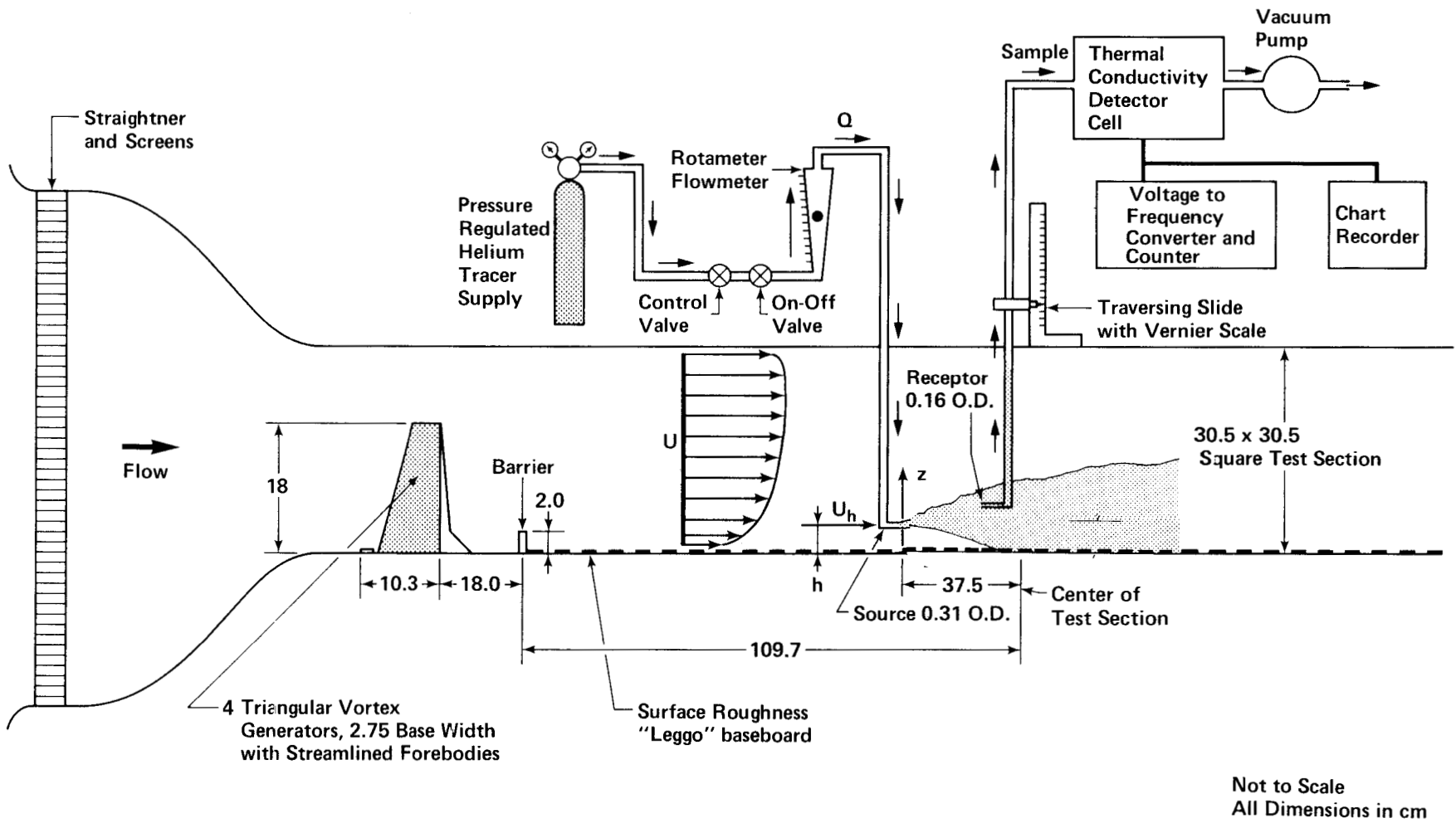
FIG. 3.3 Wind Tunnel System for Plume Simulation
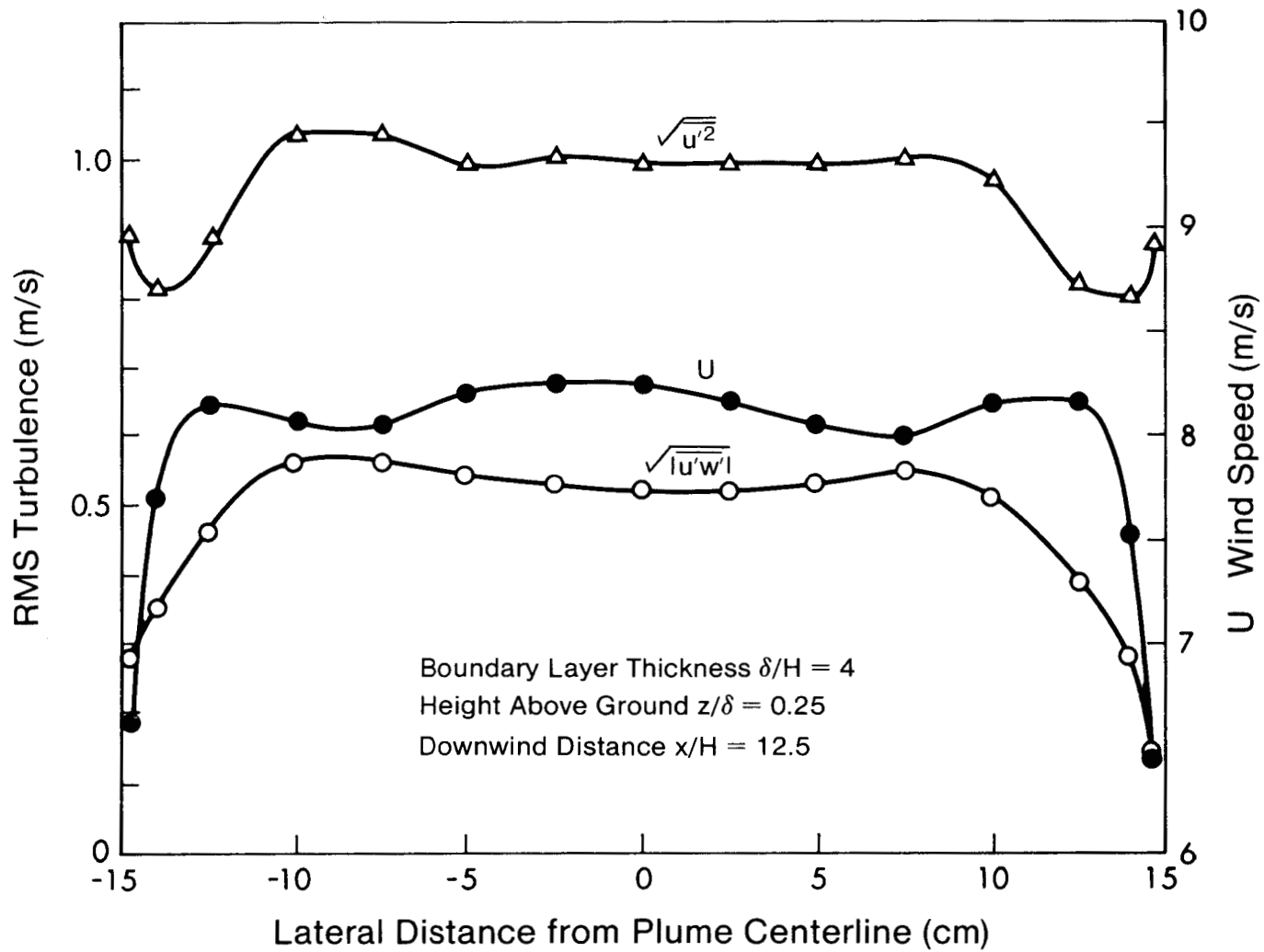
FIG. 3.4   Lateral Profiles of Mean Wind
and Turbulence at Source Height

U   Wind Speed (m/s)
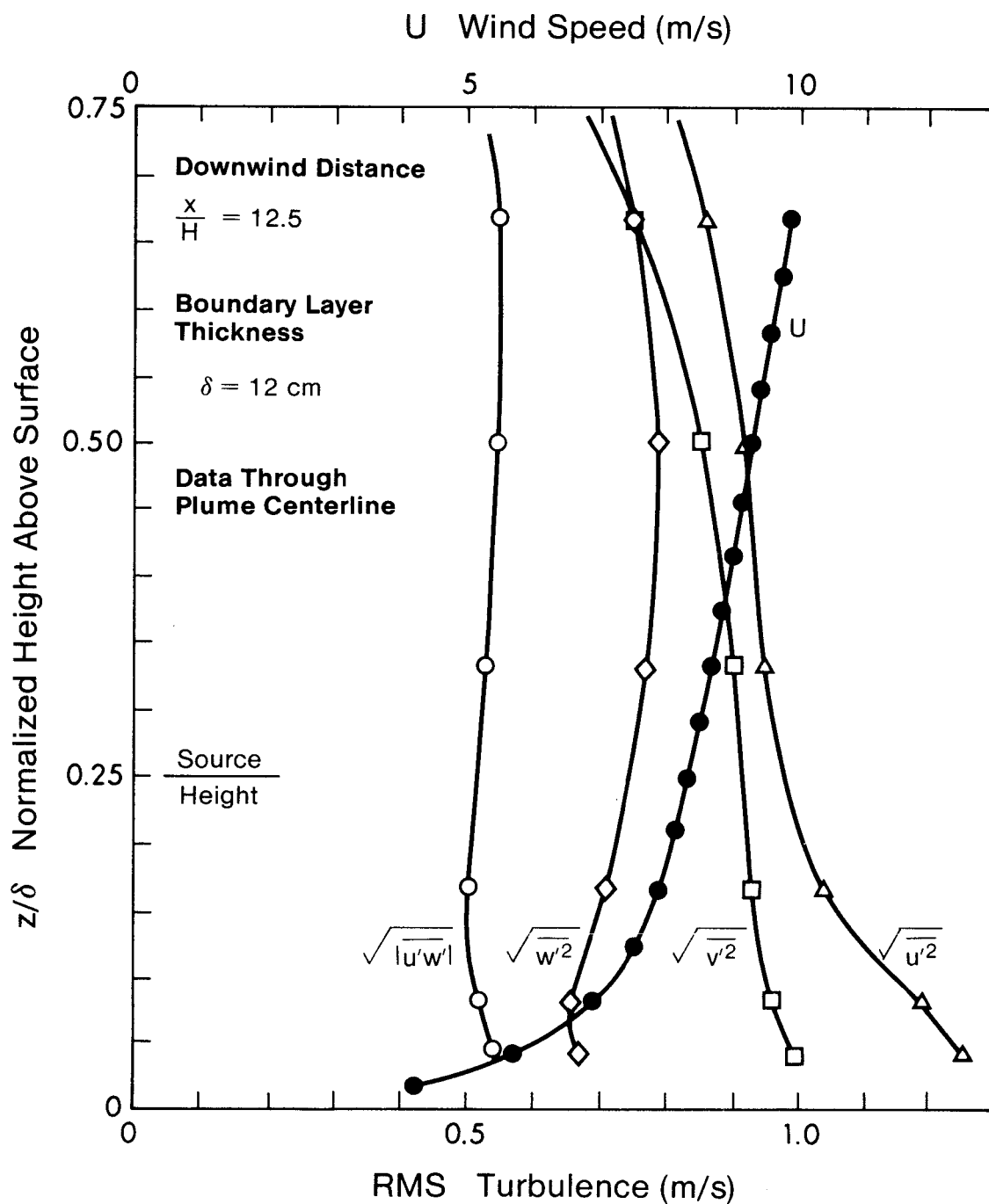
FIG. 3.5 Vertical Profiles of Mean Wind and
Turbulence on Plume Centerline
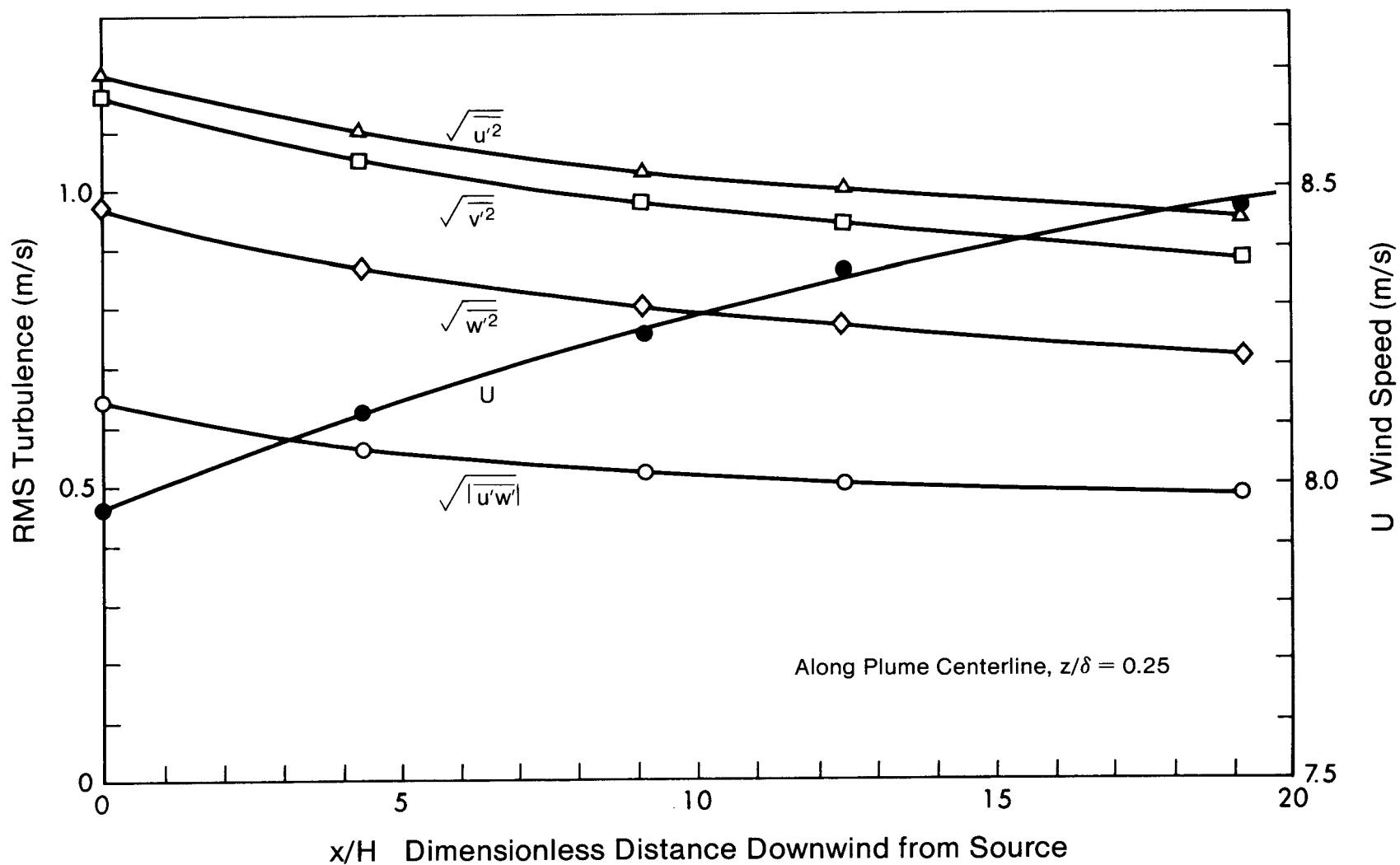
FIG. 3.6 Axial Profiles of Mean Wind and Turbulence at Source Height on Plume Centerline
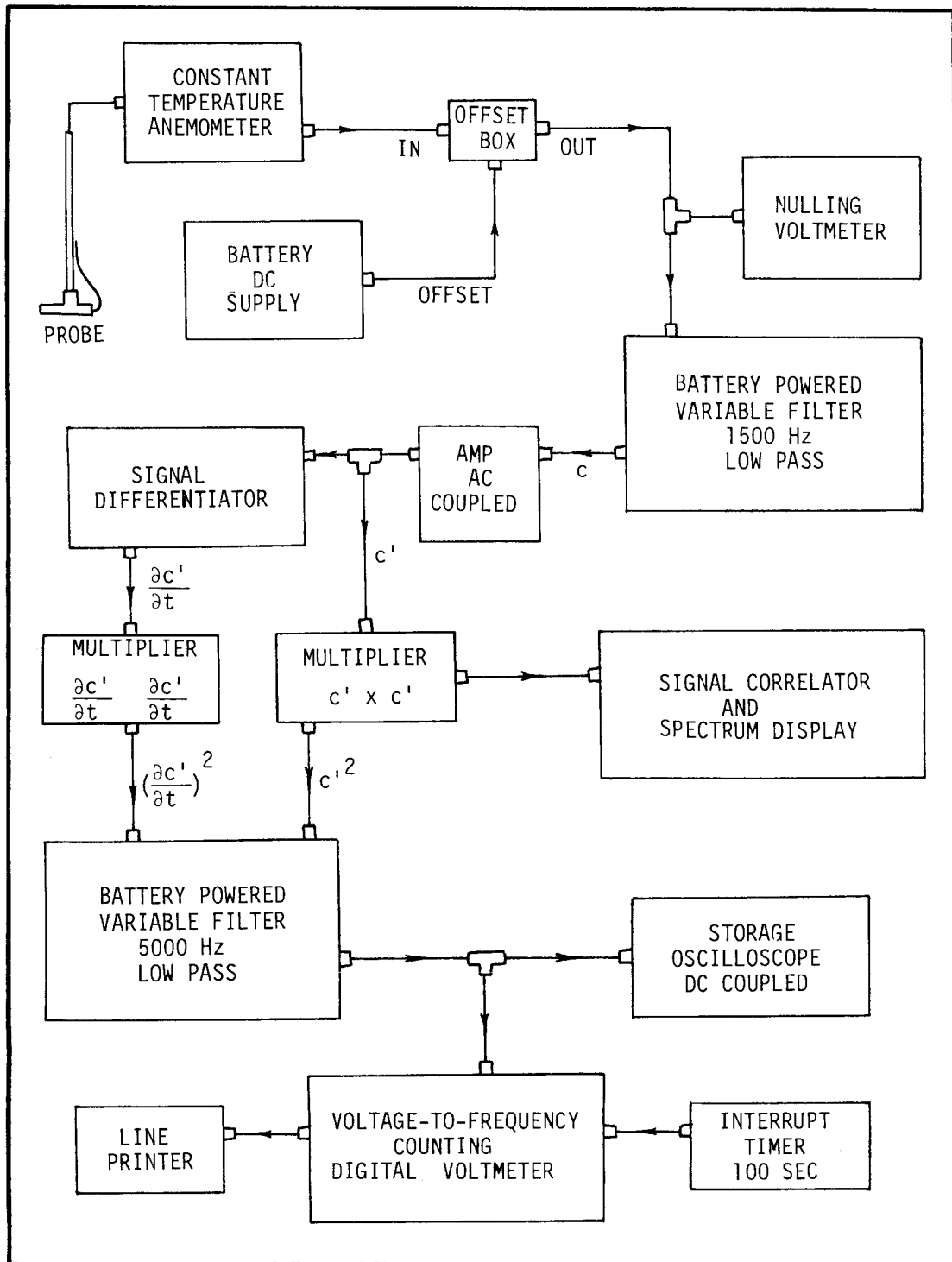
FIG. 3.7 Equipment for Measuring
Concentration Fluctuations
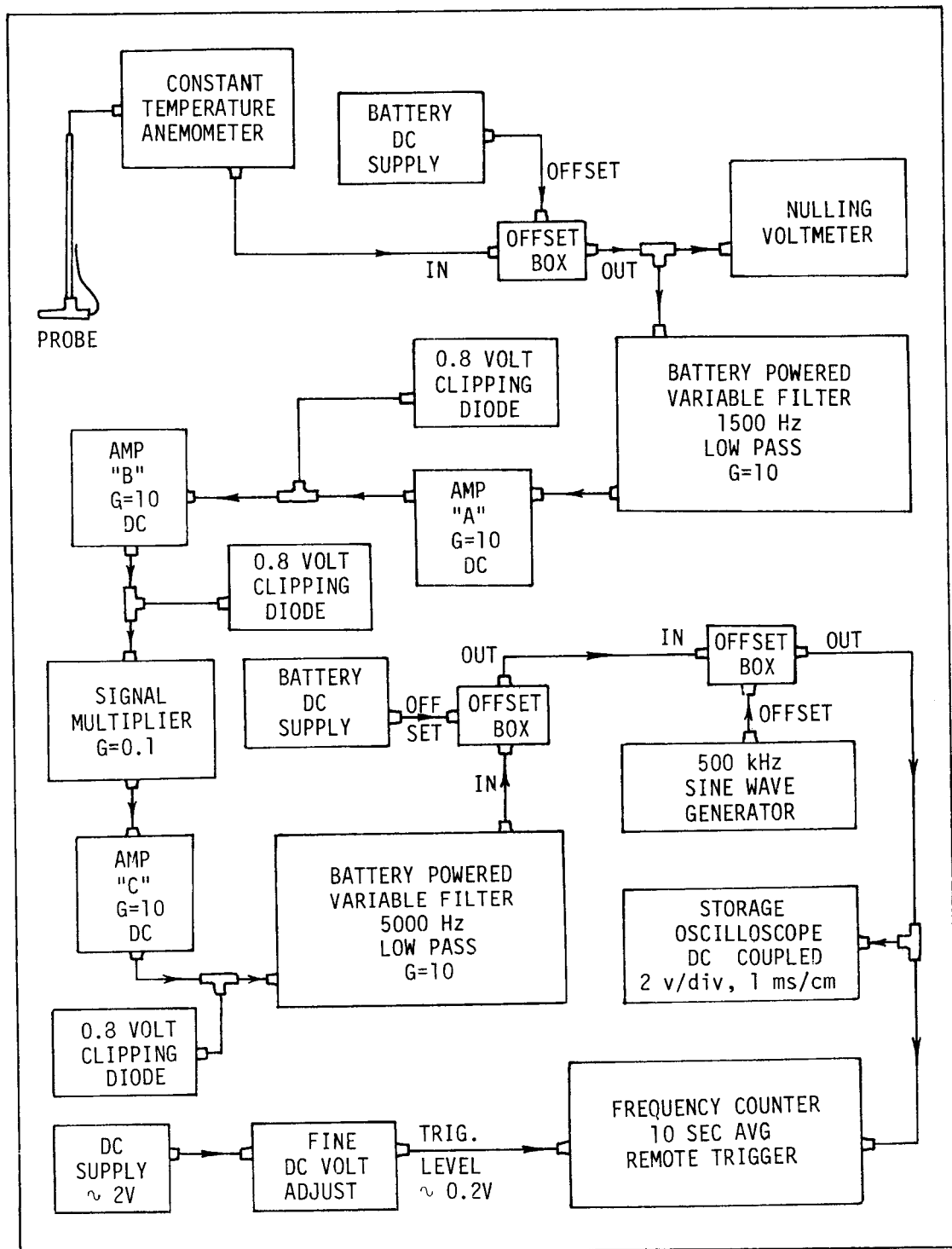
FIG. 3.8   Equipment for Intermittency
Measurements

$$Re = \frac{U_T\delta}{\nu} \quad \text{Reynolds Number}$$
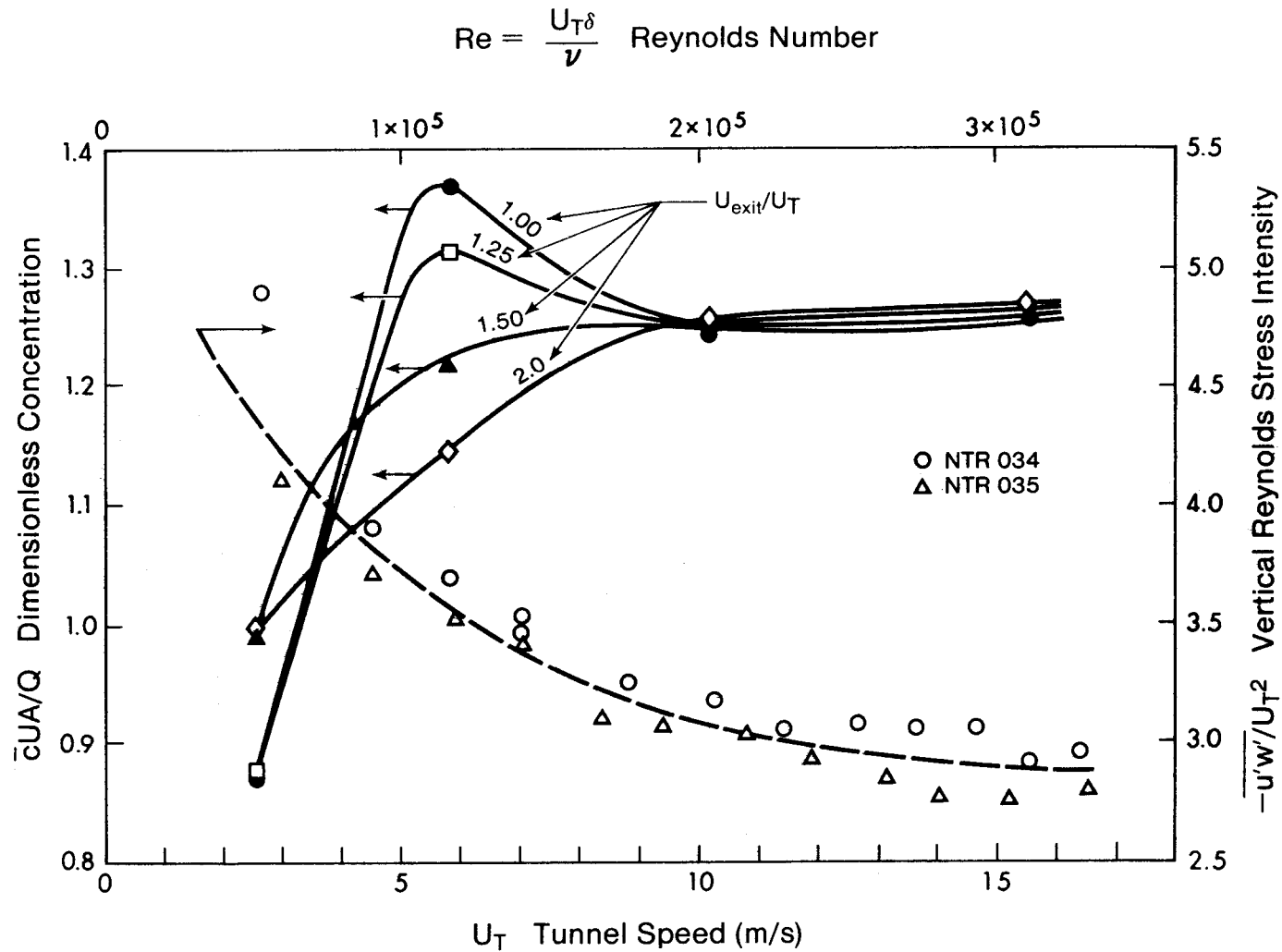
FIG. 3.9 Variation of Mean Concentration and Reynolds Stress with Tunnel Speed and Source Exit Velocity Ratio

NOT TO SCALE
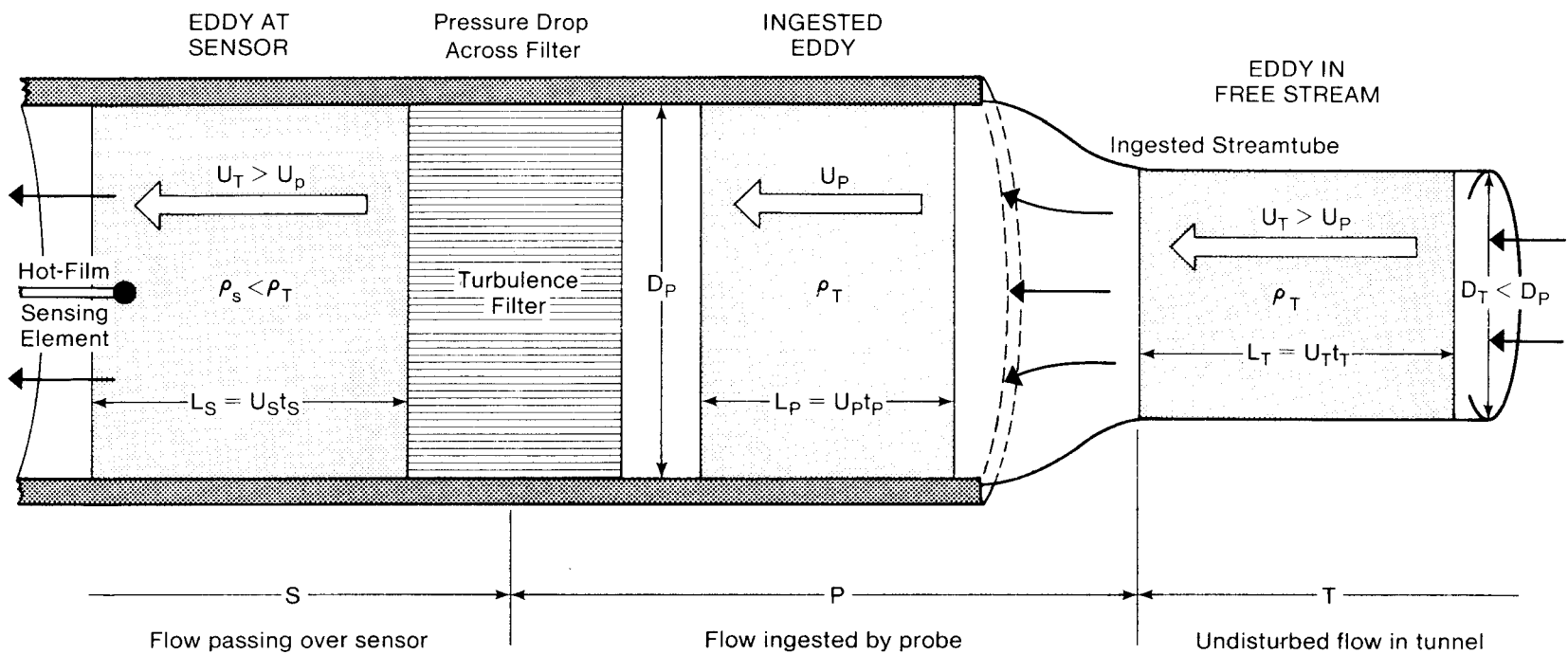
FIG. 3.10   Anisokinetic Sampling by Aspirated Probe
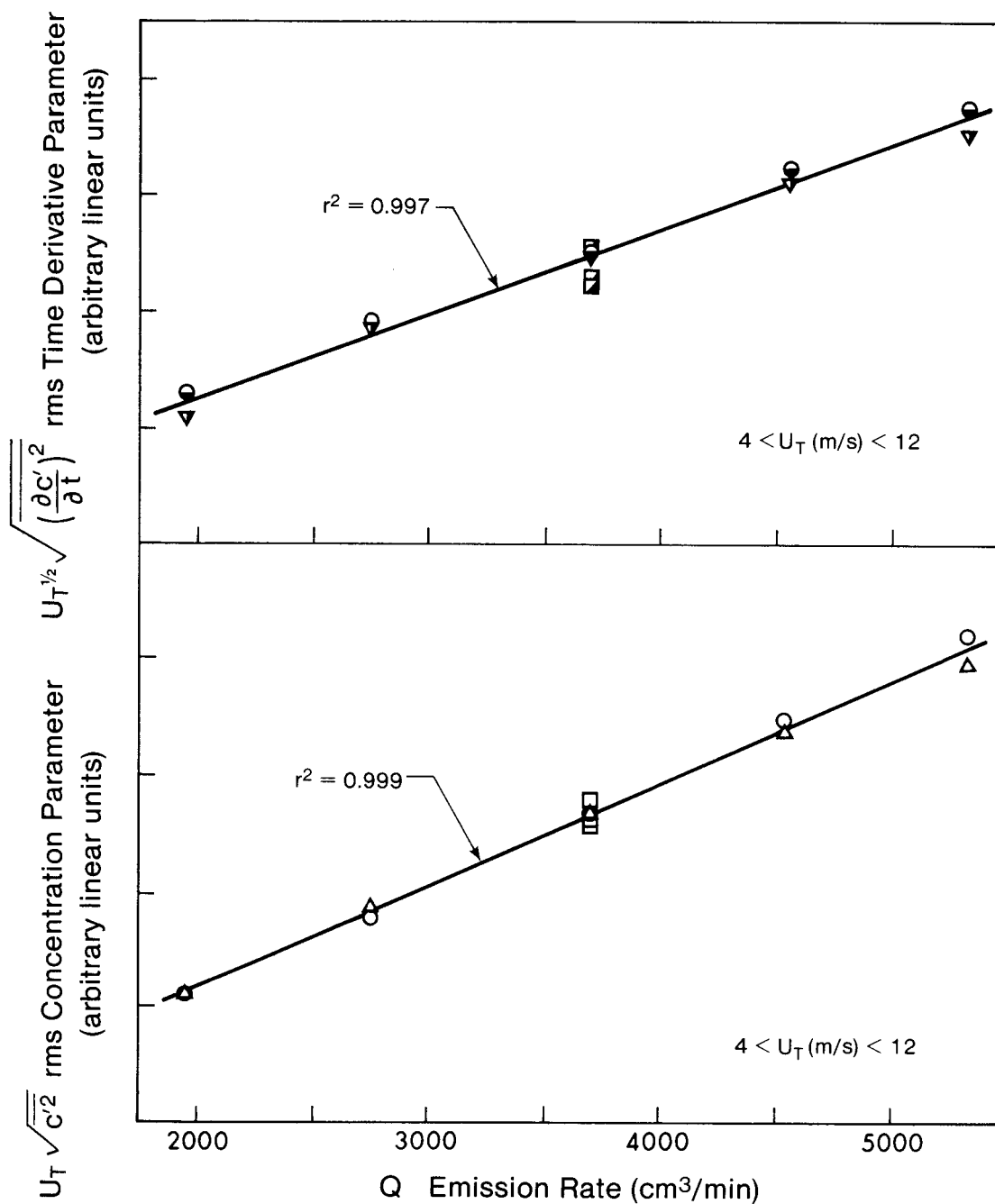
FIG. 3.11 Dependance of Concentration and
Time Derivative Variances on
Emission Rate and Wind Speed

CHAPTER IV

CONCENTRATION INTERMITTENCY AND RATES OF PLUME GROWTH

4.0 Introduction

One object of this study is to construct a simple but flexible statistical model for concentration probabilities in elevated plumes. The statistical model developed in Chapter VI achieves simplicity through pdf shape parameters written in terms of the local values for mean concentration $\bar{c}$, concentration variance $\overline{c'^2}$ and concentration intermittency γ. Model flexibility results from the implicit inclusion of atmospheric physical processes through the spatial distributions of these parameters; predicted values for $\bar{c}$, $\overline{c'^2}$ and γ can be used in the statistical model to forecast concentration probabilities.

This chapter deals with the downwind spread of the mean concentration field, and relates this rate of plume growth to the velocity autocorrelation function. Then, the spatial distribution of concentration intermittency in elevated plumes is shown to follow a Gaussian error curve similar to that for turbulence intermittency in free jets. The width of plume intermittency profiles appears to be proportional to the width of the mean concentration field.

4.1 Measurements of Plume Spread

Simple, reliable models for predicting $\overline{c'^2}$ and γ in chimney plumes have not yet appeared in the literature. However, the spatial distribution of mean concentration $\overline{c}$ in plumes has been widely studied, and a number of predictive techniques for $\overline{c}$ are available. The simple reflected Gaussian model introduced in Chapter I is shown in Chapter V to provide a good fit to mean concentration profiles obtained in the present study. The reflected Gaussian model Eq. (1.1) has the form

$$\overline{c} = \left(\frac{Q}{2\pi U_H \sigma_y \sigma_z}\right) \exp\left(\frac{-y^2}{2\sigma_y^2}\right) \left\{ \exp\left[\frac{-(z-H)^2}{2\sigma_z^2}\right] + \exp\left[\frac{-(z+H)^2}{2\sigma_z^2}\right] \right\} ,$$

with Q the source emission rate and U_H the wind speed at source height H; y and z are the lateral distance from plume centerline and height above ground, respectively. The plume geometry parameters σ_y and σ_z, functions of downwind distance x, are the lateral and vertical standard deviations of the plume concentration profiles. They describe the rate at which the plume grows as it moves downwind.

The literature contains literally hundreds of reports on full scale measurements of σ_y and σ_z in elevated plumes. One example is that of Singer and Smith (1966), which has been recommended by the ASME (1973). Values of σ_y and σ_z observed

in wind tunnel simulations of plume dispersion must agree with these full scale data before a successful simulation can be claimed. Profiles of mean concentration measured for the present study were compared with values calculated from the reflected Gaussian Eq. (1.1). A least-squares error technique was used to obtain values for σ_y and σ_z. The location of plume cross-sections measured in the wind tunnel is shown in Fig. 4.1; the best-fit values of σ_y and σ_z are given in dimensionless form in Table 4.1.

TABLE 4.1

DIMENSIONLESS STANDARD DEVIATION FOR

PROFILES OF MEAN CONCENTRATION

x/Λ_{Lu}	σ_y/Λ_{Lu}	σ_z/Λ_{Lu}
0.8	0.077	0.062
1.2	0.107	0.088
1.7	0.145	0.123
2.3	0.186	0.147
3.6	0.255	0.182

The measurements used to obtain the velocity integral length scale $\Lambda_{Lu} = \beta U T_{Eu}$ will be discussed in Section 4.2.

Taylor's (1922) statistical theory of turbulent diffusion predicts that sigma increases linearly with x close to the source, and approaches a square-root dependance on x at large distances from the source. Large distances are defined as $x \gg \Lambda_{Lu}$, where $\Lambda_{Lu} = UT_{Lu}$ is the Lagrangian integral length scale of velocity fluctuations, discussed in the next section. In either case, sigma should depend linearly on the (constant) turbulence intensities $i_v = \sqrt{\overline{v'^2}}/U$ and $i_w = \sqrt{\overline{w'^2}}/U$ respectively.

The generalized x-dependant form $\sigma = ax^b$ includes both theoretical extremes of linear and square-root variation and, when fitted to the data using least-squares error techniques, gives (with σ and x in cm),

$$\sigma_y = .159 \ x^{.806} \qquad (r^2 = .999) \qquad (4.2)$$

and

$$\sigma_z = .165 \ x^{.724} \qquad (r^2 = .979) . \qquad (4.3)$$

The observed axial variation lies between the two theoretical extremes, with more tendency to linearity than to a square-root dependance. However, Chapter III described how the mean flow along the tunnel centerline accelerated due to boundary layer growth on the tunnel walls, and turbulence decayed because the roughness elements could not maintain the high

levels of turbulence generated by the upwind spires and barrier. As a result the turbulence intensities decreased with x (in cm) at the rate

$$i_v = .145 - .003 \, x^{.63}$$

and (4.4)

$$i_w = .122 - .003 \, x^{.62} .$$

This non-homogeneous turbulence field means that statistical properties of homogeneous turbulence are just approximations to the wind tunnel flow properties. For homogeneous turbulence, the rate of lateral plume spread is proportional to the (constant) turbulence intensity according to

$$\sigma_y^2 = 2 \int_0^t \overline{v'^2} \, (t-\tau) R_v(\tau) d\tau = 2\overline{v'^2} \int_0^t (t-\tau) R_v(\tau) d\tau ,$$

(4.5)

where the autocorrelation coefficient $R_v(\tau)$ is defined as

$$R_v(\tau) \equiv \frac{\overline{v'(t)v'(t-\tau)}}{\overline{v'^2}} .$$

(4.6)

An expression similar to Eq. (4.5) can be written for σ_z.

A first approximation to the value of σ_y in non-homogeneous turbulence is calculated by replacing $\overline{v'^2}$ in Eq. (4.6) by its spatial average value over the range $0 \leq x \leq Ut$. This approximation is obtained by noting that the fluctuating velocity is strongly self-correlated $(R_v > 0)$ for about one integral length scale, a short distance within which the turbulence levels remain almost constant (i.e. locally homogeneous flow). This permits the velocity variance to be defined as the spatial average value, which can be removed from the integrand of Eq. (4.5). These average turbulence values are, from Eq. (4.4),

$$\overline{i}_v(x) = .145 - .002 \, x^{.63}$$

and   (4.7)

$$\overline{i}_w(x) = .122 - .002 \, x^{.62}.$$

Then combining Eqs. (4.2), (4.3) and (4.7) in the form $\sigma = \text{const} \cdot \overline{i} \, x^p$ gives

$$\sigma_y = .95 \, \overline{i}_v \, x^{.88}$$

and   (4.8)

$$\sigma_w = 1.13 \, \overline{i}_w \, x^{.81}.$$

Using the model scale factor of 4000:1, these expressions for σ_y and σ_z in cm can be transformed to meters in the full scale by

$$\sigma_y = 1.46 \, \overline{i_v} \, x^{.88}$$

and   (4.9)

$$\sigma_z = 2.25 \, \overline{i_w} \, x^{.81}.$$

The average value for $\overline{i_v}$ through the test section is $\overline{(i_v)} = 0.129$. Similarly the average value for $\overline{i_w}$ is $\overline{(i_w)} = 0.107$. Using these average values in the above equations gives the simulated full scale power laws (in meters)

$$\sigma_y = 0.19 \, x^{.88}$$

and   (4.10)

$$\sigma_z = 0.24 \, x^{.81},$$

which are compared in Fig. 4.2 with Singer and Smith's (1966) full scale one-hour average values for σ_y and σ_z measured at Brookhaven National Laboratory.

Values of σ_y and σ_z for the simulated plume were derived from concentration field measurements obtained using 100 sec averages. A direct application of the 4000:1 model

scale factor would indicate that these plume spreading rates
correspond to approximately 4-day averages of sigma in the
full scale, rather than the 1-hour averages shown in Fig. 4.2.
However, measurements showed the wind tunnel turbulence spectra to
peak around 30 Hz, with little energy below about 1 Hz;
this lower frequency corresponds to approximately 1-hour
fluctuations in the full scale. Because the wind tunnel does
not simulate the slow velocity fluctuations which cause full
scale sigma values to continuously increase as averaging time
is extended beyond one hour, the wind tunnel sigma values were
essentially independant of averaging time after just a few
seconds; the long 100 sec averages were necessary to smooth
out random fluctuations in the measured concentration variance
$\overline{c'^2}$. The conclusion to be drawn from Fig. 4.2 is that, out to
the farthest modelled distance of 2.5 km, and for averaging
times up to one hour full scale, the simulated atmospheric
boundary layer disperses material at the same rate as a neutral
to slightly unstable full scale boundary layer.

4.2 Velocity and Concentration Autocorrelations

The rate of plume growth is related to the turbulent
velocity fluctuations through equations (4.5) and (4.6). It
should be possible to predetermine plume spread rates solely
from a time series of the lateral and vertical wind components.
The plume spreading rate has asymptotic limits which depend
on the length of time diffusion has been taking place. For

short times ($\tau \rightarrow 0$, $R(\tau) \rightarrow 1$) equation (4.5) reduces to the linear ($\sigma \sim t$) form

$$\sigma_i^2 = \overline{u_i'^2} \, t^2 , \qquad (4.11)$$

and for long diffusion times ($\tau \rightarrow \infty$, $R(\tau) \rightarrow 0$) equation (4.5) can be written as

$$\sigma_y^2 = 2\overline{v'^2} \, T_{Lv} \, (t - T_{Lv}) , \qquad (4.12)$$

where T_{Lv} is the Lagrangian integral time scale obtained from integrating the autocorrelation function for long diffusion times,

$$T_{Lv} \simeq \beta T_{Ev} = \beta \int_0^\infty R_{Ev}(\tau) d\tau . \qquad (4.13)$$

Following Hay and Pasquill (1961), the empirical constant β is a rescaling factor for the time axis which approximates the relation between Lagrangian and Eulerian time series of turbulent variables. Full scale observed values of β vary with turbulence intensity i_v [Pasquill (1975)], going from about 1 to 10 as the atmosphere changes from strongly unstable to strongly stable (Nappo, 1979). The values group around $\beta \simeq 4$ for neutrally stable flows such as occur in the wind tunnel.

The Lagrangian integral time scale of velocity
fluctuations is an important parameter because it character-
izes the persistence of the largest eddies contained in the
plume, and can be used to calculate the final asymptotic
rates of plume spread. A similar Lagrangian integral time
scale can be defined for the scalar concentration fluctuations,

$$T_{Lc} \simeq \beta T_{Ec} = \beta \int_0^\infty R_{Ec}(\tau) d\tau , \qquad (4.14)$$

where

$$R_{Ec}(\tau) \equiv \frac{\overline{c'(t)c'(t+\tau)}}{\overline{c'^2}} . \qquad (4.15)$$

Hinze (1975, p. 290) shows that the ratio of the integral
scale of vector velocity fluctuations to that for scalar
concentration fluctuations should be proportional to the square
root of the Schmidt number when diffusion times are large
$(t \to \infty)$,

$$\frac{T_{Lu}}{T_{Lc}} = B \sqrt{Sc} . \qquad (4.16)$$

The constant of proportionality B is approximately unity.

The autocorrelations of concentration and alongwind
velocity were measured in the wind tunnel on the plume center-
line at $x/H = 12.5$, and the integrations (4.13) (with u in

place of v) and (4.14) were performed graphically; several
observed autocorrelations are reproduced in Fig. 4.3. The
proportionality constant was (with Sc = 0.25 for dilute
helium into air)

$$B = \frac{1}{\sqrt{Sc}} \frac{T_{Lu}}{T_{Lc}} \simeq 2 \qquad (z/H = 0.2)$$

and   (4.17)

$$B \simeq 5 \qquad (z/H = 1) \ .$$

These values for B are quite a bit larger than unity, and
are believed to be due to younger 'ages' for the observed
concentration fluctuations as compared to velocity fluctu-
ations. At the measurement location $x/H = 12.5$, the concen-
tration fluctuations had been diffusing for only $t_c = x_c/U$
$\simeq 46$ ms, whereas the velocity fluctuations generated at the
spires and barrier had been diffusing for $t_u = x_u/U \simeq 140$ ms,
and were effectively three times older. The relation (4.16),
which links the integral scales of velocity and concentration
computed from Eqs. (4.13) and (4.14), is strictly valid only
for large diffusion times $t_u = t_c = t \rightarrow \infty$. The observed large
values of B, possibly resulting from low values of T_{Lc} because
t_c was only one-third of t_u, are not surprizing in light of
the difference in diffusion times for concentration and velocity
fluctuations.

4.3 Plume Intermittency

Concentration measurements near the boundary of a turbulent plume include time periods during which no concentrations are observed. If all such segments of the time series are removed, the remaining portions account for a fraction "γ" of the original concentration record. The parameter γ, the fraction of time during which the plume concentrations are non-zero, is called the concentration intermittency factor, and is similar in concept to that used for turbulence.

The intermittency factor approaches zero at the edges of a plume, where uncontaminated eddies are entrained from the surrounding atmosphere and the contaminated eddies spread outward. On the plume centerline γ often, but not always, approaches unity. In this chapter and Chapter VI, frequent reference will be made to the intermittency of concentration fluctuations, as simply 'intermittency'. References to intermittency of turbulent velocity will be plainly stated as such.

Hinze (1975, Ch. 6) reviews previous studies of the eddy exchange processes which cause turbulence intermittency. Measurements of the instantaneous boundary of turbulent flows show a highly contorted surface of bulges and valleys which appear and disappear at random. Hinze reports that Corrsin and Kistler (1954) have found from work on a round free jet and a plane wake flow that the statistical variations in the

height of the bulges follow a Gaussian distribution. Then the integrated bulge position gives an expression for the turbulence intermittency factor in terms of the Gaussian error function,

$$\gamma = \frac{1}{2} \ \text{erfc} \left[\frac{r_{1/2}}{\sqrt{2} \ \sigma_B} \left(\frac{r}{r_{1/2}} - 1 \right) \right] , \qquad (4.18)$$

where $r_{1/2}$ is the radial position at which the turbulence intermittency has dropped to $\gamma = \frac{1}{2}$, and σ_B is the standard deviation of the turbulent boundary bulges around this position. The measurements of Corrsin and Kistler indicate that both $r_{1/2}$ and σ_B increase linearly with downwind distance x, although at different rates and apparently from different virtual origins. More recent work by Becker, Hottel and Williams (1965, 1966) on free and ducted round jets shows scalar intermittency distributions are also well reproduced by Eq. (4.18). However, they found that the ratio $r_{1/2}/\sigma_B$ varied so slowly with x that all the radial intermittency profiles could be represented by a single average value for $r_{1/2}/\sigma_B$. The elevated plume intermittency profiles measured as part of the present study also show this convenient behavior.

The electronic circuit used for the measurement of vertical, lateral and axial profiles of intermittency in an elevated plume is described in Chapter III. The measured intermittency profiles are shown in Figs. 4.4 to 4.6 along with

fitted Gaussian error function curves of the form given in Eq. (4.18). The spatial distribution of intermittency in the elevated plume was well reproduced by the product of three complementary error functions,

$$\gamma = \frac{1}{8}\text{erfc}\left[\frac{x_{1/2}}{\sqrt{2}\,\sigma_{x\gamma}}\left(\frac{x}{x_{1/2}}-1\right)\right]\text{erfc}\left[\frac{y_{1/2}}{\sqrt{2}\,\sigma_{y\gamma}}\left(\frac{y}{y_{1/2}}-1\right)\right]\text{erfc}\left[\frac{z_{1/2}-H}{\sqrt{2}\,\sigma_{z\gamma}}\left(\frac{z-H}{z_{1/2}-H}-1\right)\right],$$

$$(4.19)$$

with the empirical values

$$\frac{x_{1/2}}{\sigma_{x\gamma}} \simeq 2\sqrt{2}\ ,$$

$$\frac{y_{1/2}}{\sigma_{y\gamma}} \simeq 5.3\sqrt{2}\ , \qquad\qquad (4.20)$$

$$\frac{z_{1/2}-H}{\sigma_{z\gamma}} \simeq 4.6\sqrt{2}\ .$$

Within experimental accuracy these ratios were independant of the downwind distance x, a behavior observed by Becker, Hottel and Williams (1965) for intermittency within an axi-symmetric free jet. Their intermittency profiles were best represented by the shape factor $r_{1/2}/\sigma_B \simeq 4\sqrt{2}$.

The variation of $y_{1/2}$ and $z_{1/2}-H$ with x is tabulated
in Figs. 4.4 and 4.5. It is reasonable to expect that the
magnitudes of $y_{1/2}$ and $z_{1/2}$ are related to the atmospheric
turbulence intensities i_v and i_w as well as downwind distance.
This dependance is conveniently included by relating variations
in $y_{1/2}$ and $z_{1/2}$ to the values of σ_y and σ_z. Two possible
relations are the power law fits

$$y_{1/2} = 3.2\ \sigma_y^{.7},$$

$$ \text{(4.21)} $$

$$z_{1/2}-H = 3.6\ \sigma_z^{.7},$$

and the linear fits

$$y_{1/2} = 1.7\ (\sigma_y + 3d_s),$$

$$ \text{(4.22)} $$

$$z_{1/2}-H = 1.9\ (\sigma_z + 3d_s),$$

where d_s is the source diameter. There is no theoretical
guidance for choosing between the linear or power law forms.
Within experimental accuracy, both fit the data equally well.
Both contain three different constants, with the leading
constants in the ratio

$$3.6/3.2 = 1.9/1.7 = 1.12\ .$$

It is not known what external factors affect the values of the constants, or the ratios between them. The studies reported by Hinze (1975, Ch. 6) are of little help in this regard because they refer almost entirely to velocity intermittency in the self-generated turbulence of wakes and jets in quiescent or laminar flows. The most significant difference between such flows and the present case is the effect of boundary layer turbulence which governs the growth rates σ_y and σ_z (and hence $y_{1/2}$ and $z_{1/2}$ of the passive tracer plume.

Becker, Hottel and Williams (1965) present equations for calculating the concentration mean and variance of the contaminated eddies alone, based on knowledge of the intermittency factor and the overall concentration mean and variance. Using the subscript E to indicate the property of a tracer-containing eddy, the mean eddy concentration is

$$\bar{c}_E = \bar{c}/\gamma \; . \tag{4.23}$$

During a fraction γ of the time, the instantaneous excursion from $\bar{c}$ is $c_E - \bar{c}$, and during $(1-\gamma)$ it is simply $-\bar{c}$. Thus

$$\overline{c'^2} = \gamma \overline{(c_E - \bar{c})^2} + (1-\gamma)\bar{c}^2 \; ,$$

into which is substituted $c_E \equiv \bar{c}_E + c_E'$ to obtain

$$\overline{c_E'^2} = [\overline{c'^2} - (1-\gamma)\overline{c}^2]/\gamma . \qquad (4.24)$$

These equations are useful for combustion problems and flows
incorporating fast chemical reactions, applications in which
the eddy concentrations are important.

Example profiles of measured concentration mean $\overline{c}$
and variance $\overline{c'^2}$ have been abstracted from Chapter V and are
shown in Fig. 4.7. Also shown are the corresponding profiles
of $\overline{c}_E$ and $\overline{c_E'^2}$ obtained from Eqs. (4.23) and (4.24). As the
plume boundaries are approached, the eddy concentration fluctu-
ations achieve a uniform distribution of concentration mean
and variance, with the fluctuation intensity becoming
$i_{c_E} \equiv \sqrt{\overline{c_E'^2}}/\overline{c}_E = 4.3$. This uniform fringe region, in which
concentration variance is due almost entirely to intermittency,
is similar to that observed by Becker, Hottel and Williams
(1966), who measured a smaller asymptotic value of $i_{c_E} = 0.73$.
The different fluctuation intensity may be due to lower turbu-
lence levels within their axisymmetric jet/quiescent fluid
configuration, as compared with the laterally uniform boundary
layer turbulence at plume level in the present study.

Returning our attention to Eq. (4.19) and Fig. 4.5,
it is apparent that the Gaussian error function which fits
data above the plume centerline does not work so well near the
ground. This is probably because the plume boundary fluctuations
near the ground are constrained, so their motions do not follow

a Gaussian distribution. Near the ground, observed variation of γ with x and z is the result of complex interactions. More detailed experiments are needed before the intermittency model (4.19) can be further refined by, for example, the use of a truncated Gaussian position distribution for the lower plume boundary.
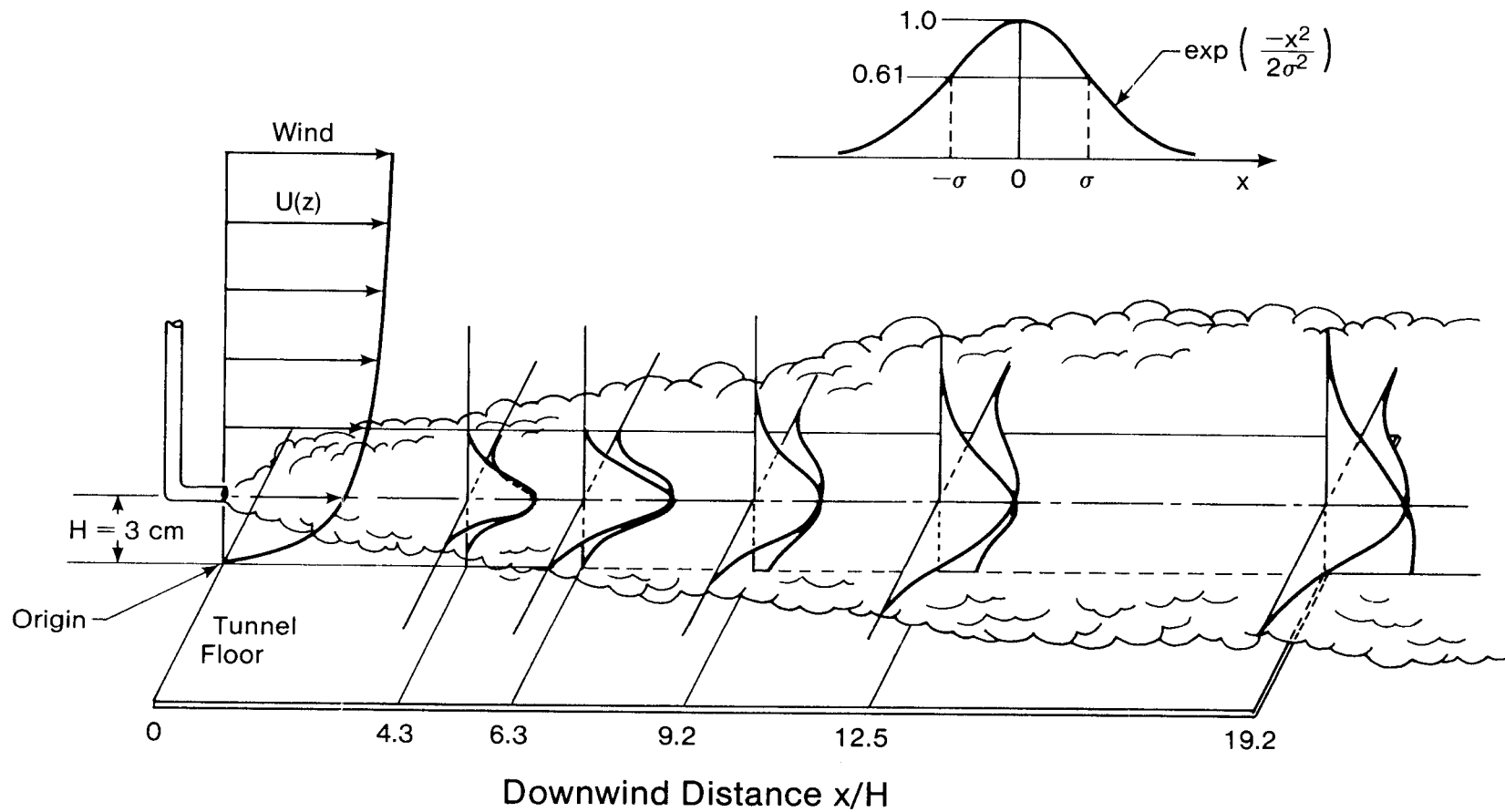
FIG. 4.1 Measurement Locations and Typical
Concentration Profiles
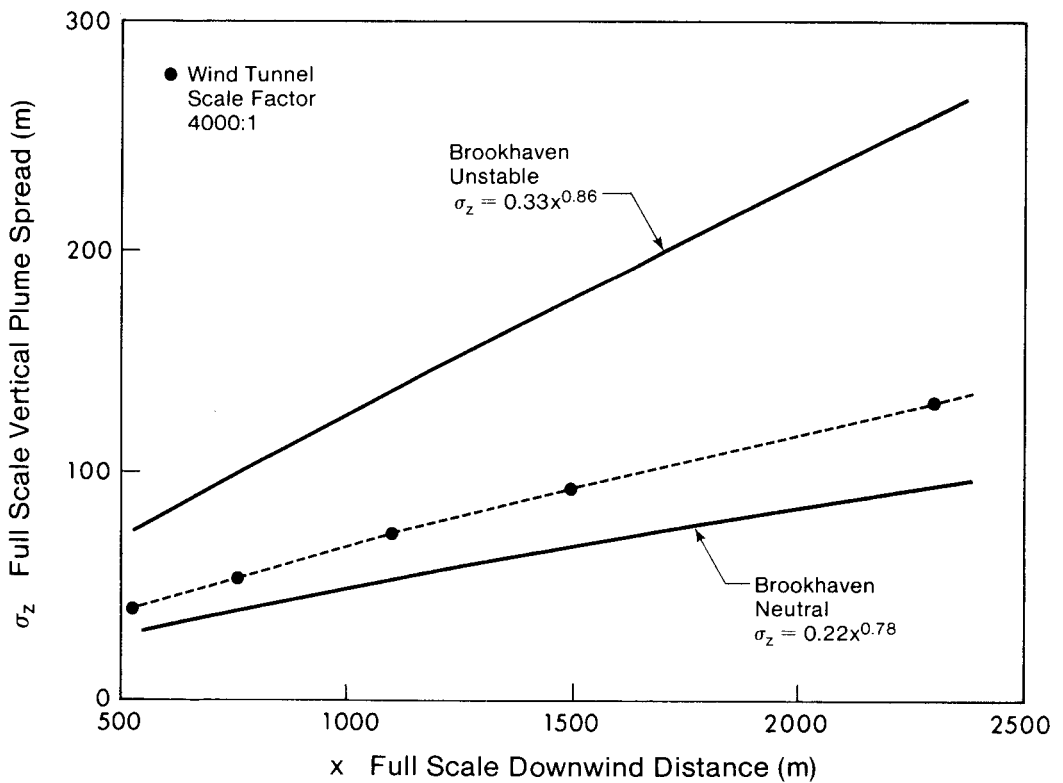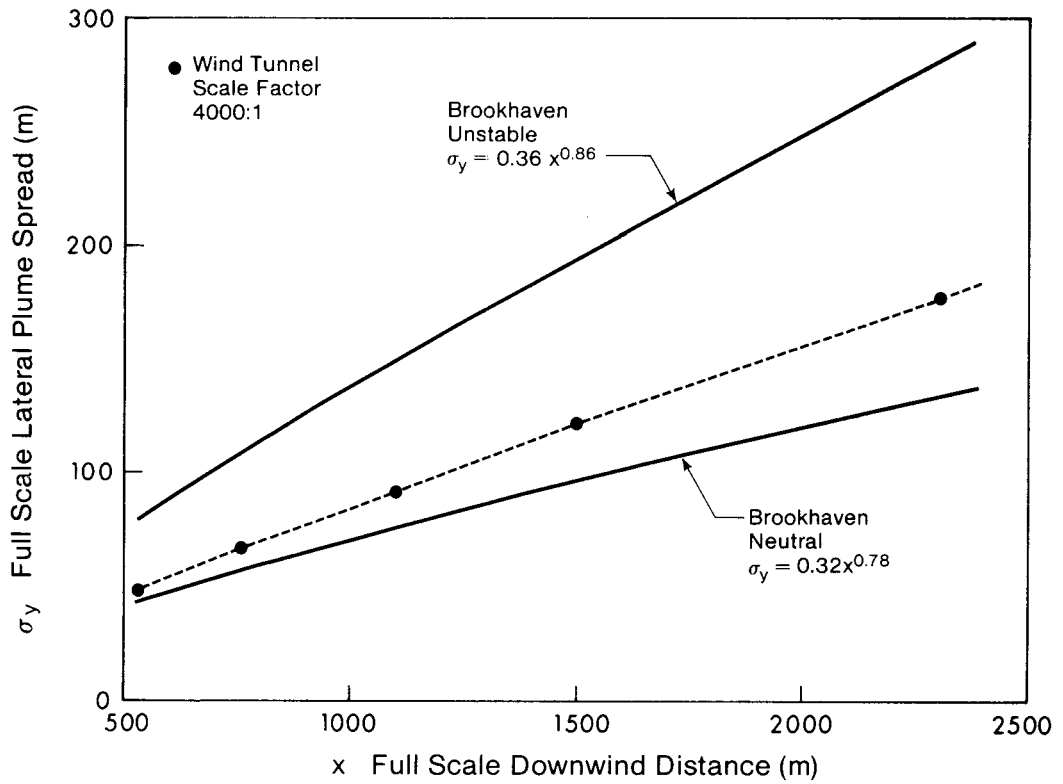
FIG. 4.2 Variation of Plume Spread with Distance from Source, for 4000:1 Scale Factor
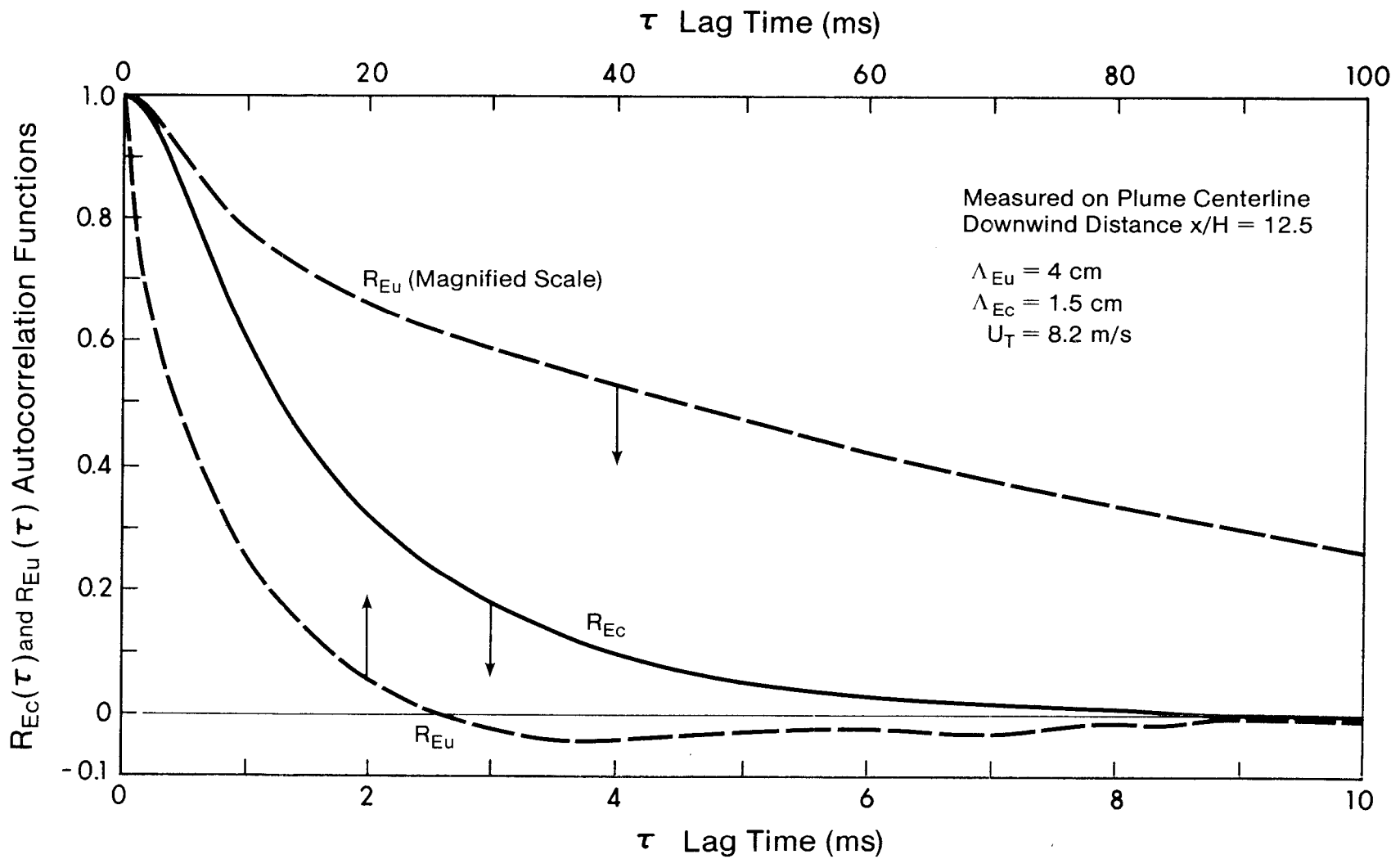
FIG. 4.3 Measured Autocorrelations of Velocity and
Concentration on Plume Centerline

At Source Height

$$\frac{\gamma}{\gamma_H} = \tfrac{1}{2}\, \text{erfc}\left[5.3\left(\frac{y}{y_{1/2}} - 1\right)\right]$$

Dimensionless Lateral Distance $y/y_{1/2}$

γ/γ_H Normalized Intermittency

	x/H	$y_{1/2}/\sigma_y$
○	4.3	3.00
□	6.3	2.79
△	9.2	2.59
◓	12.5	2.34
◪	19.2	2.15
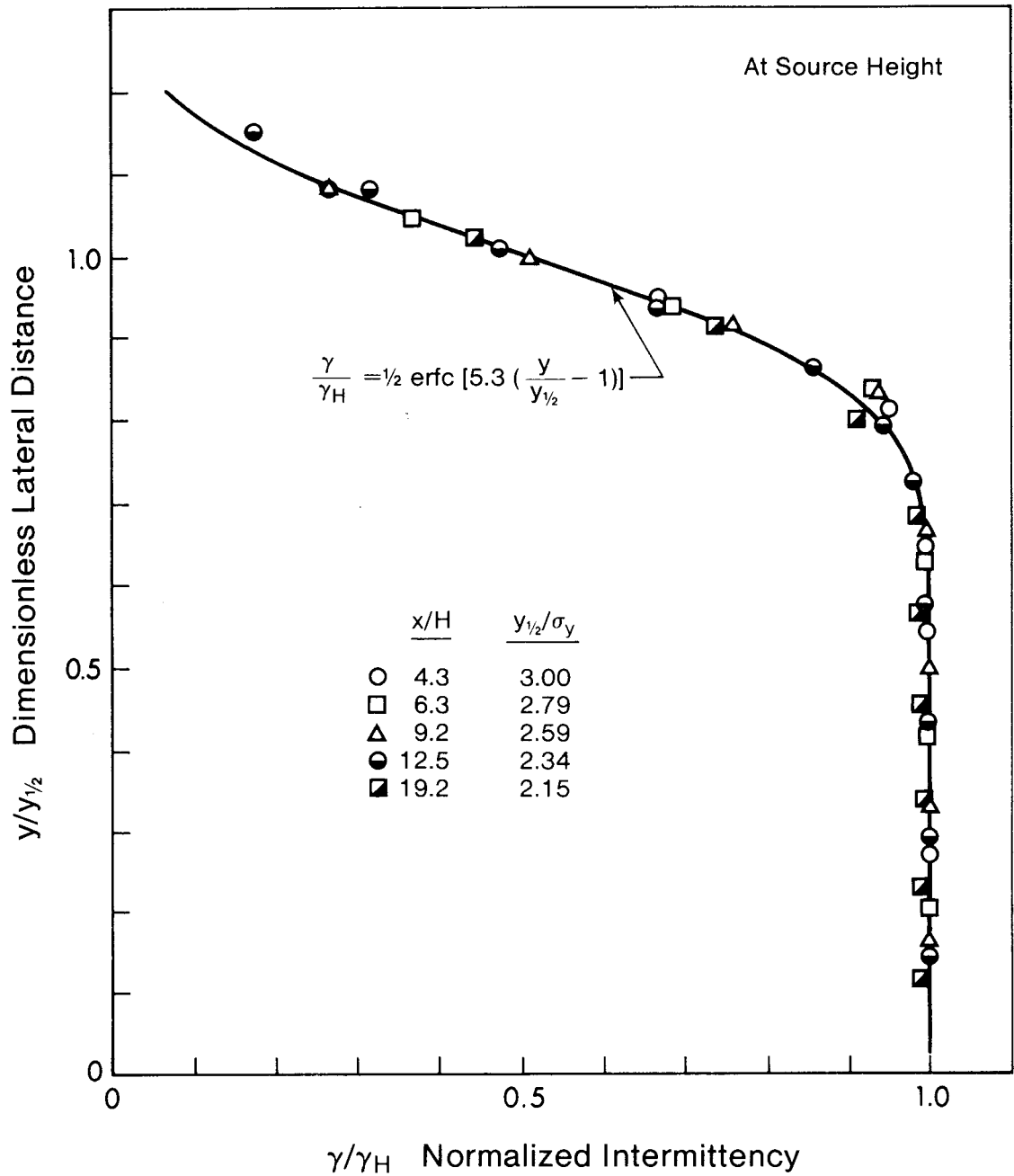
FIG. 4.4 Lateral Concentration Intermittency
Profiles at Plume Height
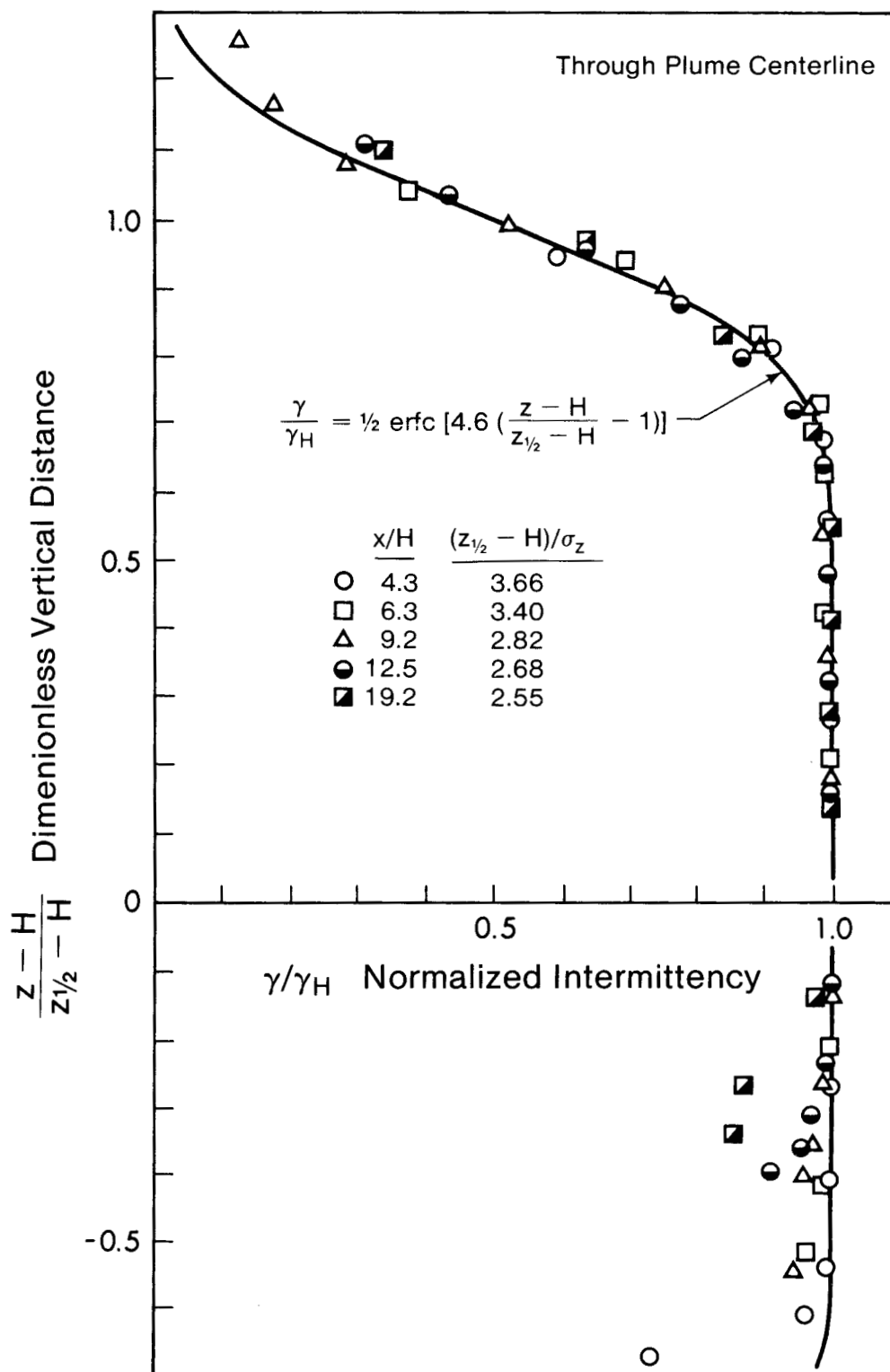
FIG. 4.5 Vertical Concentration Intermittency
Profiles Through Plume Centerline
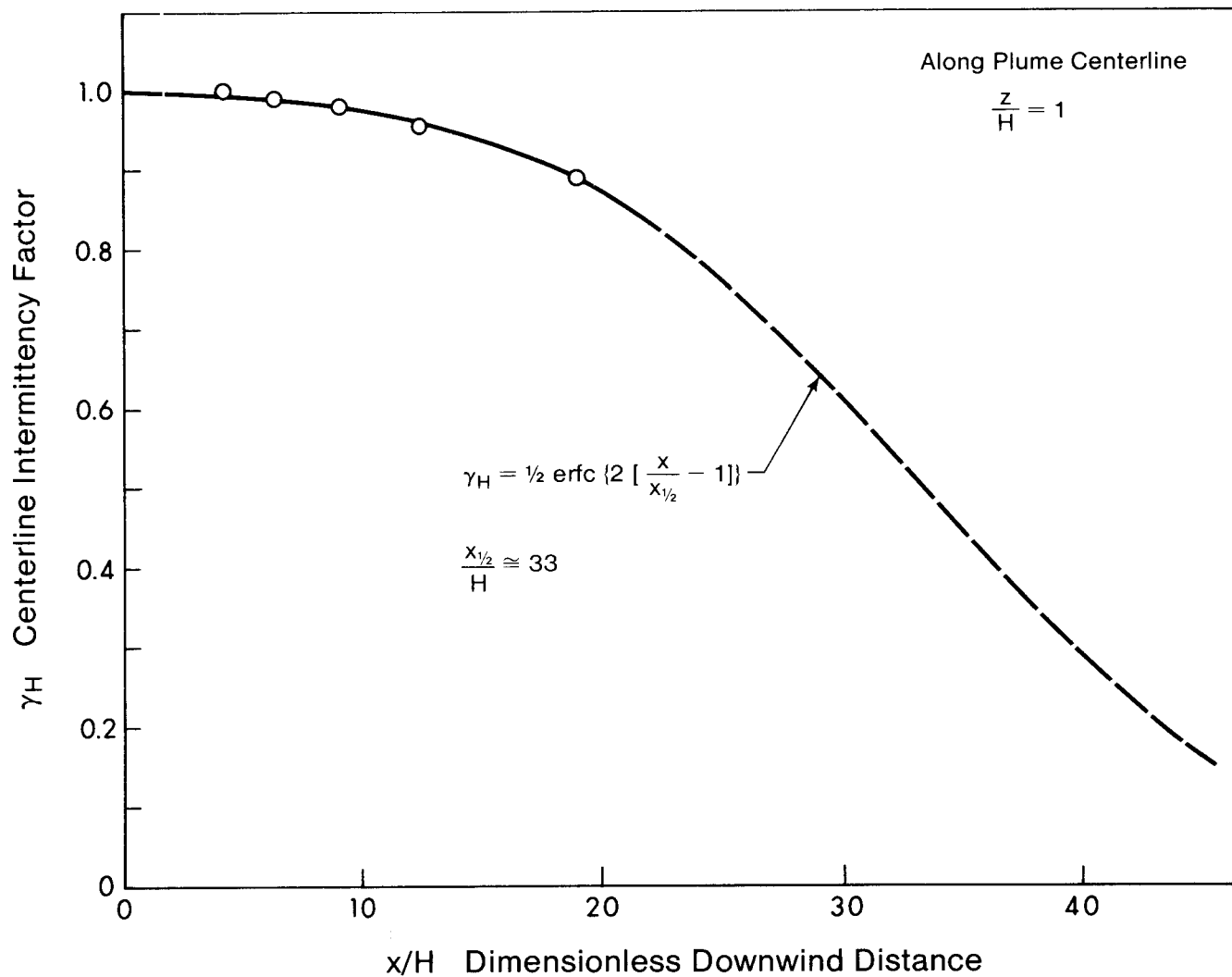
FIG. 4.6 Axial Decrease of Centerline Concentration Intermittency
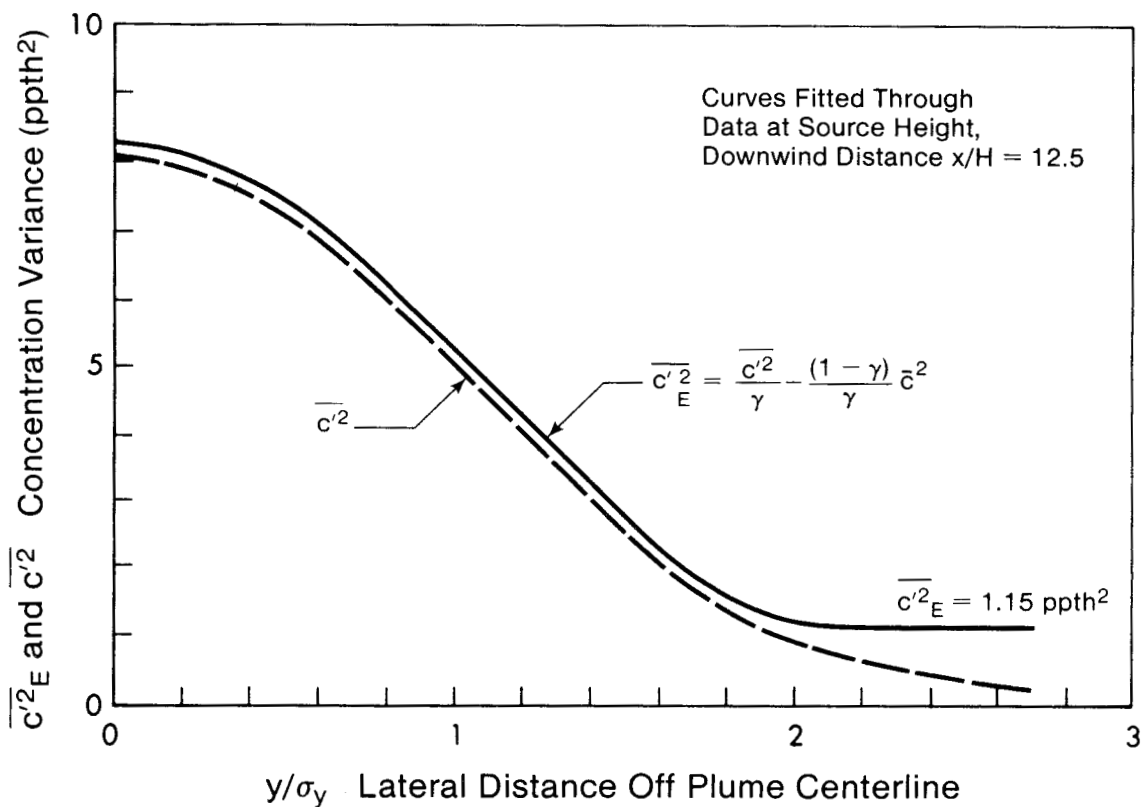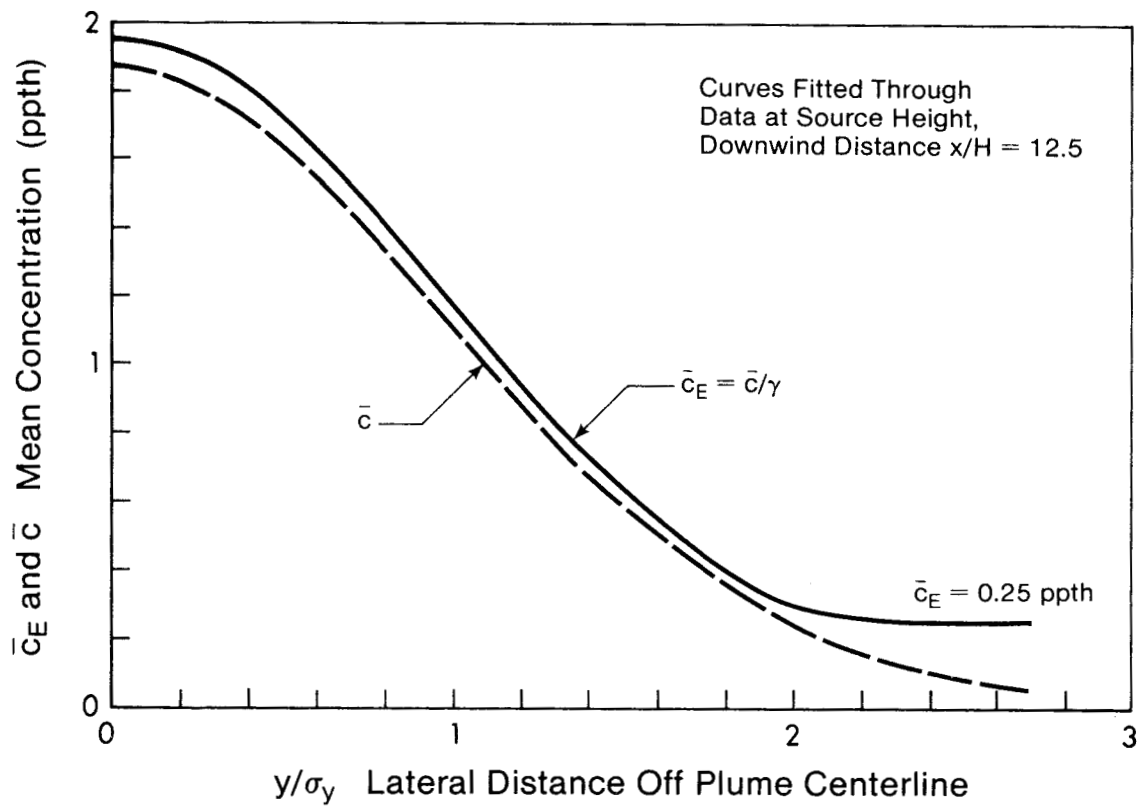
FIG. 4.7 Concentration Mean and Variance
in Dilute Helium Eddies

CHAPTER V

DETERMINISTIC PROPERTIES OF THE

CONCENTRATION FLUCTUATIONS

5.0 Introduction

A dynamically neutral material released continuously
into the turbulent atmospheric boundary layer is transported
by random gusts and eddies, so that the instantaneous material
concentration c(x,t) downwind of the source also becomes a
random variable. A full statistical description of the random
concentration fluctuations is necessary to identify possibly
hazardous peak concentrations, and this requires information
about the concentration probability density function (pdf).
The intermittent lognormal pdf model to be developed in Chapter
VI is expressed in terms of concentration intermittency γ,
time-mean concentration $\bar{c}$, and concentration variance $\overline{c'^2}$.
The intermittency, mean concentration and concentration variance
are statistical rather than physical quantities. However, the
instantaneous concentration c, even though a random variable,
is actually transported and dispersed physically by the turbu-
lent winds, and must be constrained instantaneously by the
equation of species mass conservation,

$$\frac{\partial c}{\partial t} = -\nabla \cdot (\underline{u}c - D\nabla c) \qquad (5.1)$$

where c is the concentration, $\underline{u}$ the random wind vector and D the molecular diffusivity. This equation is useful for dispersion in a turbulent wind field because, as will be shown, it leads to a deterministic description for the spatial distribution of concentration mean $\bar{c}$ and variance $\overline{c'^2}$.

This chapter compares experimental data with predictions from the well-known reflected Gaussian solution for the mean concentration profile. Then, a new deterministic model for concentration variance is developed which compares well with wind tunnel data. This concentration variance is needed as input to the complete statistical model of concentration fluctuations developed in Chapter VI. Finally, key assumptions made in previous work on concentration fluctuations are tested against new wind tunnel data, and their regions of applicability are defined.

5.1 Present State of Knowledge

One recent theoretical work on concentration fluctuations is that of Csanady (1967, 1973) who developed an analytic expression for the variance field downwind of a continuous point or line source in a uniform, unbounded flow containing isotropic turbulence. Both references provide a good review of earlier research which led to Csanady's model. A key element provided by Batchelor, Townsend and Howells (1959) was the observation that concentration variance is a transportable quantity, and can be transferred and dissipated in the same way as turbulence kinetic energy. Hinze (1975, p. 279)

contributed the concept of a concentration microscale, and showed that self-similar correlation coefficients require fluctuation decay rates that vary inversely with travel time. This type of decay was observed experimentally by Gibson and Schwarz (1963).

Csanady's solution, which is based on the mass conservation Eq. (5.1), requires self-similarity of variance profiles, and contains the following assumptions:

- the flux of both mean concentration and concentration variance may be expressed as the product of an eddy diffusivity times gradient;
- the eddy diffusivities in the vertical and crosswind directions are equal and constant for a given cross section of the plume, although they vary with distance from the source;
- the dissipation rate of concentration variance is proportional to the local concentration variance;
- the reciprocal of this proportionality factor is a 'decay time scale' T_d which is constant for a given section but which increases linearly with distance from the source.

New wind tunnel experiments are used in this chapter to test the last two of these assumptions, which are found to be valid in the wind tunnel's simulated atmospheric boundary layer. The measured decay time scale T_d increases with x at a rate which indicates that concentration fluctuations in the tracer

plume are dissipated more slowly than fluctuations in isotropic grid turbulence.

The work of Kewley (1978), mentioned in Chapter I, is an example of the recent application of fluctuation theory to the analysis of fast chemical reactions in a turbulent plume. Kewley makes the same assumptions as Csanady, with the added restriction that the decay time scale of fluctuations be independant of distance. In order to simplify the solution for $\overline{c'^2}$, the advection and gradient flux terms appearing in the variance Eq. (1.3) are neglected on the assumption that they are small compared with the local rates of production and dissipation of fluctuations. Then the local production and dissipation must be in balance, and for $K_y \neq K_z$, $\overline{c'^2}$ is given by

$$\overline{c'^2} = 2T_d[K_y(\frac{\partial \overline{c}}{\partial y})^2 + K_z(\frac{\partial \overline{c}}{\partial z})^2] . \qquad (5.2)$$

Kewley acknowledges that (5.2) can lead to unrealistic profiles, and proposes an empirical adjustment (sketched in Chapter I) that produces flat variance profiles on the plume centerline.

The present experiments show that production and dissipation are not in balance, and in fact that with increasing distance from the source, production of $\overline{c'^2}$ becomes negligible compared with dissipation. It then follows from the variance balance equation (1.3) that the advection and gradient flux terms must be of the same order

as the dissipation term, and cannot be neglected as Kewley suggests.

In summary, existing solutions for the variance field apply only to concentration fluctuations in a homogeneous, isotropically turbulent flow with uniform mean velocity, far from solid boundaries such as the ground. No published theoretical solutions are available for the variance field under more general conditions.

5.2   The Governing Equations

The diffusion equation (5.1) is used as the starting point in the analysis of concentration fluctuations. Separating the turbulent velocity vector and concentration scalar into mean and fluctuating components $\underline{u}=\overline{\underline{u}}+\underline{u}'$ and $c=\overline{c}+c'$, then taking ensemble averages of both sides of Eq. (5.1), gives a balance equation for the mean concentration,

$$\frac{\partial \overline{c}}{\partial t} + \underline{u} \cdot \nabla \overline{c} = -\nabla \cdot \overline{\underline{u}'c'} + D\nabla^2 \overline{c} \ . \qquad (5.3)$$

Subtracting this averaged equation from the original equation provides a relationship for the fluctuating part of the c-field,

$$\frac{\partial c'}{\partial t} + u_i' \frac{\partial \overline{c}}{\partial x_i} + \overline{u}_i \frac{\partial c'}{\partial x_i} + \left(u_i' \frac{\partial c'}{\partial x_i} - \overline{u_i' \frac{\partial c'}{\partial x_i}} \right) = D\nabla^2 c' \ . \quad (5.4)$$

Multiplying this equation by 2c', then taking means and

simplifying by use of the continuity equation $\nabla \cdot \underline{u} = 0$ results in a balance equation for the concentration variance $\overline{c'^2}$,

$$\underbrace{\frac{\partial \overline{c'^2}}{\partial t}}_{\text{transient}} + \underbrace{\overline{u}_i \frac{\partial \overline{c'^2}}{\partial x_i}}_{\text{advection}} = \underbrace{-2\overline{u_i' c'} \frac{\partial \overline{c}}{\partial x_i}}_{\text{production}} + \underbrace{\frac{\partial}{\partial x_i} (D \frac{\partial \overline{c'^2}}{\partial x_i} - \overline{u_i' c'^2})}_{\text{spatial flux}} - \underbrace{\phi_c}_{\text{dissipation}} , \quad (5.5)$$

where ϕ_c is a dissipation function,

$$\phi_c = 2D \overline{(\frac{\partial c'}{\partial x_i})^2} . \quad (5.6)$$

Eq. (5.3) for the mean concentration field is simplified by neglecting axial diffusion (the 'slender plume' approximation) and molecular diffusion. Furthermore, we assume that the Reynolds flux $\overline{-u'c'}$ is proportional to the mean concentration gradient, i.e.

$$-\overline{u_i' c'} = K_i \frac{\partial \overline{c}}{\partial x_i} , \quad (5.7)$$

where the proportionality factor K_i (the 'eddy diffusivity') is a function of x, y and z. Then, for steady state ($\frac{\partial}{\partial t} \to 0$) and a unidirectional mean wind ($\overline{u}_1 = U$, $\overline{u}_2 = \overline{u}_3 = 0$), Eq. (5.3) can be written in the familiar form

$$\underbrace{U \frac{\partial \overline{c}}{\partial x}}_{\text{advection}} = \underbrace{K_y \frac{\partial^2 \overline{c}}{\partial y^2} + \frac{\partial}{\partial z} (K_z \frac{\partial \overline{c}}{\partial z})}_{\text{gradient flux}} , \quad (5.8)$$

where

$$U = U(z),$$

$$K_y = K_y(x,z),$$

$$K_z = K_z(x,y,z),$$

$$c = c(x,y,z).$$

The advection term on the left-hand side of (5.8) is balanced by the gradient flux terms on the right-hand side. The wind field is assumed to be laterally homogeneous, so that K_y is constant in the crosswind direction.

If the same simplifying assumptions are applied to the balance equation for concentration variance $\overline{c'^2}$, the result is (with $S \equiv \overline{c'^2}$ for notational simplicity),

$$\underbrace{U\frac{\partial S}{\partial x}}_{\text{advection}} = \underbrace{K_y'\frac{\partial^2 S}{\partial y^2} + \frac{\partial}{\partial z}(K_z'\frac{\partial S}{\partial z})}_{\text{gradient flux}} + \underbrace{2K_y(\frac{\partial \overline{c}}{\partial y})^2 + 2K_z(\frac{\partial \overline{c}}{\partial z})^2}_{\text{production}} - \underbrace{\frac{6D}{U^2}\overline{(\frac{\partial c'}{\partial t})^2}}_{\text{dissipation}}, \qquad (5.9)$$

where the eddy diffusivities for S are defined by

$$-\overline{u_i'c'^2} = K_i'\frac{\partial S}{\partial x_i} \quad . \qquad (5.10)$$

The dissipation term

$$\phi_c = 2D[\overline{(\frac{\partial c'}{\partial x})^2} + \overline{(\frac{\partial c'}{\partial y})^2} + \overline{(\frac{\partial c'}{\partial z})^2}] = \frac{6D}{U^2}\overline{(\frac{\partial c'}{\partial t})^2} \qquad (5.11)$$

has been simplified by assuming locally isotropic concentra-
tion fluctuations, with Taylor's hypothesis $\frac{\partial}{\partial x} = \frac{1}{U} \frac{\partial}{\partial t}$ replacing
the spatial derivative. The functional dependencies are

$$D = \text{constant},$$

$$U = U(z),$$

$$K_y = K_y(x,z),$$

$$K_y' = K_y'(x,z),$$

$$\bar{c} = \bar{c}(x,y,z),$$

$$\overline{c'^2} \equiv S = S(x,y,z),$$

$$K_z = K_z(x,y,z),$$

$$K_z' = K_z'(x,y,z),$$

$$\overline{\left(\frac{\partial c'}{\partial t}\right)^2} = \overline{\left(\frac{\partial c'}{\partial t}\right)^2}(x,y,z).$$

Equation (5.9), rewritten in polar coordinates, has been
solved by Csanady (1967) for the case of $K_y=K_z=K_y'=K_z'=K(x)$ and
ϕ_c proportional to S, where the proportionality factor T_d
grows linearly with downwind distance x. Later in this
chapter, new experimental data is used to show that this
proportionality assumption on ϕ_c is a very good one, even
with complicated boundary conditions on Eq. (5.9) such as occur
for plumes with ground level reflection of the mean concentration

profile and surface dissipation of the concentration fluctuations.

Eq. (5.9) governs the spatial distribution of concentration variance $\overline{c'^2}$ downwind of a point or line source in a turbulent atmospheric boundary layer. The terms of Eq. (5.9) can be interpreted in the same way as for the turbulence kinetic energy equation: the advection of $\overline{c'^2}$ on the left is balanced on the right by the gradient flux terms, plus the difference between local production and dissipation rates of $\overline{c'^2}$. If it were not for this last difference term, the governing equation (5.9) for concentration variance would have the same form as Eq. (5.8) which governs the spatial distribution of mean concentration. For the case of similar boundary conditions, any differences between the spatial distribution of concentration variance and that of mean concentration must result from the inclusion of this net dissipation term. The present measurements will show that, for an elevated point source emitting a passive contaminant continuously into a turbulent atmospheric boundary layer, production of $\overline{c'^2}$ becomes negligible compared with dissipation as the plume moves downwind. The resulting simplification of the variance equation (5.9), combined with a judicious choice (see Sec. 5.7) for the x-gradient of decay time scale T_d, produces an equation having the same form as that for mean concentration. With different boundary conditions on S, this leads to a theoretical expression for the spatial distribution of concentration variance that agrees very well with the measured profiles of $\overline{c'^2}$.

104

5.3 Wind Tunnel Measurements

Vertical and lateral profiles of mean concentration $\bar{c}$, concentration variance $\overline{c'^2}$ and time derivative variance $\overline{(\frac{\partial c'}{\partial t})^2}$ were obtained at various distances $4.3 \leq x/H \leq 19.2$ downwind of an elevated 'point' source in a simulated atmospheric boundary layer. Details of the measurement methods are given in Chapters II, III and IV. This data was analysed in several ways, and led to the formulation of a theoretical model for the spatial distribution of concentration variance.

5.3.1 Mean Concentration

The first step was to see if the reflected Gaussian model for $\bar{c}$ provided a good description of the observations. The equation

$$\bar{c} = \left(\frac{Q}{2\pi U_H \sigma_y \sigma_z}\right) \exp\left(\frac{-y^2}{2\sigma_y^2}\right) \left\{ \exp\left[\frac{-(z-H)^2}{2\sigma_z^2}\right] + \exp\left[\frac{-(z+H)^2}{2\sigma_z^2}\right] \right\}$$

(5.12)

is widely used to calculate mean concentrations downwind of an elevated point source emitting continuously into an atmospheric boundary layer. In this equation, Q is the pollutant emission rate, U_H is the wind speed at source height H, y and z are the lateral distance from plume centerline and height above ground, respectively, and σ_y and σ_z are x-dependant standard deviations of the (assumed Gaussian) lateral and vertical plume concentration profiles. Veigele and Head (1978) have solved the governing mean field equation (5.8) for bounded flows, and Eq. (5.12)

is the result. Prior to their derivation, justification for the widespread use of Eq. (5.12) rested solely on its good performance in predicting measured values of $\bar{c}$, plus the knowledge that the reflected Gaussian is a solution of the mean field equation for the simplified boundary conditions of uniform flow over an impermeable surface.

A least-squares error fit of Eq. (5.12) to normalized wind tunnel measurements of $\bar{c}$ yielded the values of σ_y and σ_z (discussed in Chapter IV) which appear in brackets in Table 5.1. These best-fit values have been used to generate the theoretical solution (5.12) for $\bar{c}$ at the downwind locations where measurements were taken, and the theory and observations are compared in Figs. 5.1 through 5.7. Fig. 5.1 shows that the observed centerline decrease in mean concentration is well reproduced by the reflected Gaussian model. The observed lateral distribution of $\bar{c}$ is also well represented by the Gaussian model, as shown by Fig. 5.2. Theoretical vertical profiles of mean concentration are compared with observations in Figs. 5.3 to 5.7. The agreement is quite good over the vertical profile as a whole, but near the ground, differences as large as 40% are seen. The reflected Gaussian theory appears to first overestimate and then underestimate the ground level concentrations as the downwind distance increases. Note, however, that the prediction error is not nearly as large as the deviations of 200 to 300 percent often quoted in the literature (e.g. Weil and Jepsen (1977)) as the best performance

to be expected of the Gaussian model. These large error

estimates occur in full-scale field studies, where the input

parameters Q, U_H, σ_y and σ_z are often not accurately known,

and factors such as slow wind direction shifts play an

important role. Wind tunnel experiments, because of their

more accurately measured and steadier conditions, provide a

good indication of what to expect from the Gaussian model

under ideal field conditions: the relative error in mean

concentration predictions is less than 10% of the local con-

centration except at the plume edges and near the ground,

where errors of 20-40% are sometimes observed.

5.3.2 Concentration Variance

One important goal of the wind tunnel experiments

was to measure the spatial distribution of concentration

variance in an elevated plume. The observed axial, lateral

and vertical variations of $\overline{c'^2}$, the root-mean-square (rms)

concentration, are plotted in Figs. 5.1 through 5.7. The

most noticeable difference between the rms and mean con-

centration fields is that the rms concentration decreases

much faster near the ground than does the mean concentration.

This is a very important observation, because it supports the

idea that not only the vector fluctuations of turbulence,

but also the scalar fluctuations undergo a net dissipation

near solid boundaries. The removal of scalar fluctuations

near a solid surface is physically reasonable because in the

thin, highly sheared surface layer, any concentration gradients

tend to be smoothed out by molecular diffusion. In the absence of mean concentration gradients, there is no production of new fluctuations to replace those which are dissipated, so net dissipation is large. However, the extent to which this surface-induced dissipation takes place is difficult to measure. For example, all full-scale concentration field studies show time-varying concentrations at heights only one or two meters above the ground, which indicates that surface dissipation of fluctuations cannot be total. On the other hand, concentration intermittency is an important component of observed full-scale concentration time-series, and Eq. (4.24) shows that, in the presence of intermittency, a minimum concentration variance of $\overline{c'^2} = \gamma^2(1-\gamma)\overline{c}_E^2$ will always be observed, even when fluctuations $\overline{c'^2}_E$ in the non-zero concentration are reduced to zero.

With the fast response sensor used in this study, it was not possible to extend the measurements closer than 0.5 cm (.17 source heights) to the surface, so the dissipative surface layer could not be observed directly. The presence of high dissipation at the surface was deduced from the observed decrease of scalar fluctuations as the surface was approached. In the theoretical analysis, the simplest assumption of complete surface dissipation (zero fluctuations) was used. The conclusions drawn from the subsequent data analysis are not sensitive to this assumption.

The effect of surface-induced dissipation can be thought of as opposite to the solid boundary reflection experienced by the mean concentrations. The following sketch

illustrates the concept of surface-induced dissipation; it
is similar to the "absorption" boundary condition used by
Csanady (1973, p.40) to describe deposition of aerosols on a
vertical wall. An obvious question derives from the observed
$\overline{c'^2}$ profiles:

> How well can the observed distribution of $\overline{c'^2}$
> be reproduced by a Gaussian plume model with
> dissipation rather than reflection at the wall?
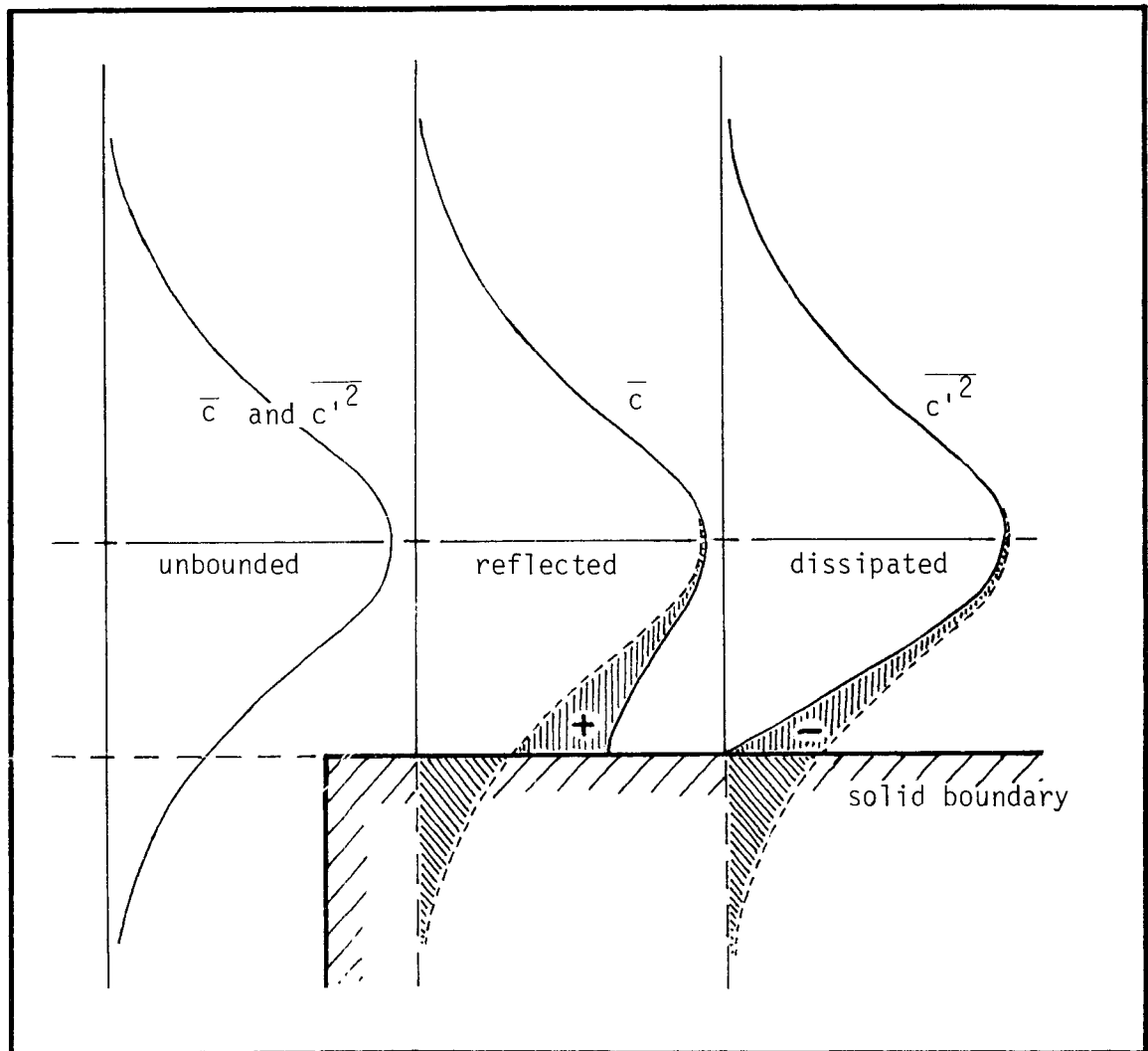
The rms concentration (instead of $\overline{c'^2}$) was selected for plotting in Figs. 5.1 through 5.7 in order to have the same physical units for the mean and fluctuating concentration fields. The plots do not show that lateral distributions of $\overline{c'^2}$ appear to be as Gaussian as the mean concentration. Combining this fact with the observations from Chapter III showing $\overline{c'^2}$ proportional to $(Q/U)^2$ (which was assumed by Csanady (1967)), the following form is suggested for the variance field:

$$S \equiv \overline{c'^2} = s_0 \left(\frac{Q}{2\pi U_H \sigma'_y \sigma'_z}\right)^2 \exp\left(\frac{-y^2}{2\sigma'^2_y}\right) \left\{ \exp\left[\frac{-(z-H)^2}{2\sigma'^2_z}\right] - \exp\left[\frac{-(z+H)^2}{2\sigma'^2_z}\right] \right\},$$

$$(5.13)$$

where s_0 is a 'source variance' parameter whose spatial variation must be determined from experiment. The parameter s_0 is analogous to the normalized concentration source variance $g(0)$ which appears in Csanady's (1967) solution for concentration fluctuations. The last exponential term in Eq. (5.13) is the surface dissipation component; the leading negative sign serves to differentiate it from the positive reflection term in Eq. (5.12) for mean concentration. The dissipation term is the result of a <u>negative</u> image source underground, and in effect creates a distributed surface 'sink' which exactly cancels all fluctuations reaching the surface. This surface sink represents the dissipation of fluctuations taking place in a

very thin layer near the surface. Surface dissipation of fluctuations is consistent with the reflected Gaussian prediction of $\frac{\partial \overline{c}}{\partial z} \to 0$ as $z \to 0$, so that the surface smooths out concentration gradients, at least in the vertical.

Note that total dissipation is assumed in Eq. (5.13), so that concentration fluctuations are forced to zero at the ground. This assumption is probably too restrictive, but the observations with which the dissipated Gaussian model is compared do not provide sufficient detail to distinguish between total and partial dissipation. A way to incorporate partial dissipation into the model will be suggested in the next section.

A least-squares error fit of this dissipated Gaussian model to the normalized wind tunnel measurements of $\overline{c'^2}$ yielded the values of σ_y' and σ_z' given in Table 5.1 (the corresponding values of σ_y and σ_z for the mean field are in brackets).

TABLE 5.1

STANDARD DEVIATIONS FOR CONCENTRATION PROFILES

OF (MEAN) AND VARIANCE

x (cm)	σ_y' (cm)	(σ_y)	σ_z' (cm)	(σ_z)
13.0	1.22	(1.23)	0.92	(1.00)
19.0	1.67	(1.72)	1.39	(1.41)
27.5	2.29	(2.32)	1.98	(1.97)
37.5	2.89	(2.97)	2.34	(2.35)
57.5	4.21	(4.08)	2.70	(2.91)

The first point to note is that Eq. (5.13) is in fact able to reproduce the observed distribution of concentration variance and, as seen from Figs. 5.1 through 5.7, it fits the $\overline{c'^2}$ data at least as well as the reflected Gaussian model (5.12) fits the $\overline{c}$ measurements. The second observation is that, within experimental accuracy, the lateral and vertical standard deviations appearing in the dissipated Gaussian model for $\overline{c'^2}$ are the same as those in the reflected Gaussian model for $\overline{c}$. This is remarkably fortunate, because it means that the large body of literature dealing with the spreading rates of mean concentration fields can also be applied to calculations of the fluctuating concentration field.

After the dissipated Gaussian model (5.13) was proposed and tested against the $\overline{c'^2}$ data, it was discovered that the model could be derived theoretically from the balance equation (5.9). The theoretical derivation, presented in Section 5.7, is based in part on the assumption that $K'_y = K_y$, $K'_z = K_z$, from which it follows that $\sigma'_y = \sigma_y$, $\sigma'_z = \sigma_z$ must be satisfied.

The 'source variance' parameter s_o was determined by dividing Eq. (5.13) by the square of Eq. (5.12) and rearranging to obtain

$$s_o = i_c^2 \cdot \exp\left(\frac{-y^2}{2\sigma_y^2}\right) \frac{\{\exp[-(z-H)^2/2\sigma_z^2] + \exp[-(z+H)^2/2\sigma_z^2]\}^2}{\{\exp[-(z-H)^2/2\sigma_z^2] - \exp[-(z+H)^2/2\sigma_y^2]\}} ,$$

$$(5.14)$$

where $\sigma_y' = \sigma_y$ and $\sigma_z' = \sigma_z$ based on the data in Table 5.1. Here i_c is the intensity of concentration fluctuations, defined by

$$i_c \equiv \frac{\sqrt{\overline{c'^2}}}{\overline{c}} \, . \tag{5.15}$$

Measured values of i_c at 128 receptor points in the wind tunnel were used to determine s_0 from Eq. (5.14); 60% of the data came from the five vertical profiles, and the remaining 40% from the five corresponding lateral profiles. The calculated values of s_0 showed some scatter ($\sim$ 15%) but no significant spatial dependence trends were observed. The average value of s_0 was

$$s_0 = 2.6 \pm 0.4 \, .$$

The results of computing s_0 using observed values of i_c were very gratifying: the value of s_0 was found to be <u>independant</u> of receptor position within the plume. This supports the interpretation of s_0 as a measure of the 'source variance' strength which, for a passive tracer released at the mean wind speed, is most likely proportional to the level of atmospheric turbulence near the source. Recent work by Robins and Fackrell (1979) suggests that the magnitude of s_0 may depend on the ratio of source diameter d_s to the integral scale of turbulence Λ near the source. Further experimental work is needed to quantify the dependance of s_0 on atmospheric turbulence and source characteristics.

5.3.3   Concentration Fluctuation Intensity

The most useful application of the dissipated Gaussian model is to generate the values of concentration fluctuation intensity i_c required as input by the statistical concentration model developed in Chapter VI. This statistical model uses local values of concentration intermittency factor γ and intensity of fluctuations i_c to predict the peak-to-mean concentration ratios at any point downwind of an air pollution source. The fluctuation intensity has been previously defined as $i_c \equiv \sqrt{\overline{c'^2}}/\bar{c}$.

Fig. 5.1 and Figs. 5.8 through 5.13 illustrate the ability of the dissipated Gaussian model for $\overline{c'^2}$ to generate accurate values of i_c when combined with the reflected Gaussian model for $\bar{c}$. The agreement between Eq. (5.16), obtained by dividing Eq. (5.13) by the square of Eq. (5.12),

$$i_c^2 = s_o \exp\left(\frac{y^2}{2\sigma_y^2}\right)\frac{\{\exp[-(z-H)^2/2\sigma_z^2] - \exp[-(z+H)^2/2\sigma_z^2]\}}{\{\exp[-(z-H)^2/2\sigma_z^2] + \exp[-(z+H)^2/2\sigma_z^2]\}^2} ,$$

$$(5.16)$$

and experiment is excellent. In fact, the agreement between (5.16) and experiment is better than the separate agreement of either of its components $\overline{c'^2}$ and $\bar{c}$. This may be due in part to systematic theory-induced errors in calculating $\overline{c'^2}$ with (5.13) being partially cancelled by similar systematic

errors in the calculation of $\bar{c}$ using (5.12). Systematic experimental error is unlikely because measurements of $\overline{c'^2}$ were obtained with an instrument different from that used for mean concentration $\bar{c}$.

One aspect of the suggested Gaussian model for $\overline{c'^2}$ is that it predicts a complete absence of concentration fluctuations at ground level. For purposes of hazard assessment, it is useless to estimate surface fluctuation intensity by placing $z=0$ in Eq. (5.16). This may not be a serious deficiency, because it is unclear if any receptors of practical interest occur exactly at $z = 0$. Fig. 5.9 shows extremely high gradients of i_c near the ground, which indicates that receptors just above ground level can be exposed to significant concentration fluctuations. However, it may be that an empirical dissipation coefficient "d" should be introduced in the dissipated Gaussian model, i.e.

$$S = s_0 \left(\frac{Q}{2\pi U_H \sigma_y \sigma_z}\right)^2 \exp\left(\frac{-y^2}{2\sigma_y^2}\right)\{\exp[-(z-H)^2/2\sigma_z^2] - d \cdot \exp[-(z+H)^2/2\sigma_z^2]\} ,$$

$$(5.17)$$

where d is a number less than unity. Additional wind tunnel measurements of $\overline{c'^2}$ at and near ground level are needed to determine d.

5.4 Mean Field Diffusivity

It is possible to derive values for K_y and K_z from the experimental data. In addition, one can substitute the reflected Gaussian model into the mean field equation (5.8). This allows determination of the vertical concentration diffusivity K_z which, if used in the mean field equation (5.8), would give the same concentration profiles as the reflected Gaussian equation (5.12). The form of this eddy diffusivity profile is of interest, because it may help to define the link between 'K-Theory' and 'Gaussian Model' approaches to the solution of plume dispersion problems under non-uniform wind conditions.

In calculating plume dispersion, a K-theory solution for the mean concentration field is usually obtained by numerically integrating Eq. (5.8) for a given eddy diffusivity field. A general specification of the diffusivity field is not possible, because K_y and K_z are not true properties of the turbulent fluid. They depend on the complete source/flow/boundary configuration, so their values are quite problem-specific. Because of the resulting lack of data on species diffusivity, a common approximation is to replace the unknown species eddy diffusivity K_z with the momentum diffusivity K_m determined from the turbulent velocity field. This approach ignores the fact that K_z depends on the source/boundary configuration, a behavior which appears explicitly in the 'reflected Gaussian' eddy diffusivity derived in this section.

Values for the vertical and lateral eddy diffusivity were derived from the present measurements as follows: First, interpolation and numerical differentiation of data were used to obtain values for U, $\bar{c}$, $\frac{\partial \bar{c}}{\partial x}$ and $\frac{\partial \bar{c}}{\partial z}$ at 2 mm height increments for each of the five vertical profiles through the plume center-line. Then, to simplify the data analysis, and because measurements of lateral flux $-\overline{v'c'}$ were not available, the lateral eddy diffusivities and derivatives of $\bar{c}$ were calculated using a Gaussian distribution for the lateral profiles, so that

$$K_y = \frac{U_{av}}{2} \frac{d\sigma_y^2}{dx} \quad ,$$

$$\left. \begin{aligned} \frac{\partial \bar{c}}{\partial y} &= - \bar{c} \frac{y}{\sigma_y^2} = 0 \quad , \\[2em] \frac{\partial^2 \bar{c}}{\partial y^2} &= \frac{\bar{c}}{\sigma_y^2} \left(\frac{y^2}{\sigma_y^2} - 1 \right) = - \frac{\bar{c}}{\sigma_y^2} \end{aligned} \right\} \text{ on plume centerline .} \qquad (5.18)$$

The vertical eddy diffusivities were derived from experimental measurements by numerical integration of the terms in Eq. (5.8) to obtain

$$K_z = \frac{1}{\partial \bar{c}/\partial x} \int_0^z \left(U \frac{\partial \bar{c}}{\partial x} - K_y \frac{\partial^2 \bar{c}}{\partial y^2} \right) dz . \qquad (5.19)$$

The experimentally derived value of vertical Reynolds flux is provided by (5.19) in combination with (5.7),

$$-\overline{w'c'} = \int_0^z \left(U \frac{\partial \overline{c}}{\partial x} - K_y \frac{\partial^2 \overline{c}}{\partial y^2}\right) dz. \qquad (5.20)$$

Examples of the eddy diffusivities and Reynolds fluxes derived from experiment are shown in Figs. 5.14 through 5.18.

Using the reflected Gaussian model for mean concentration, the expressions required for insertion in Eqs. (5.19) and (5.20) are, for the power laws $\sigma_y = ax^p$ and $\sigma_z = bx^q$ shown to be valid in Chapter IV, numbers (5.12) and (5.18) plus the alongwind gradient for a reflected Gaussian,

$$\frac{\partial \overline{c}}{\partial x} = \frac{\overline{c}}{x}\left[p\left(\frac{y^2}{\sigma_y^2} - 1\right) + \frac{q}{\sigma_z^2}\left\{\frac{[(z-H)^2 - \sigma_z^2]\exp[-(z-H)^2/2\sigma_z^2]}{\exp[-(z-H)^2/2\sigma_z^2] + \exp[-(z+H)^2/2\sigma_z^2]} + \right.\right.$$

$$\left.\left. + \frac{[(z+H)^2 - \sigma_z^2]\exp[-(z+H)^2/2\sigma_z^2]}{\exp[-(z-H)^2/2\sigma_z^2] + \exp[-(z+H)^2/2\sigma_z^2]}\right\}\right], \qquad (5.21)$$

and the vertical gradient of the reflected Gaussian,

$$\frac{\partial \overline{c}}{\partial z} = \frac{\overline{c}}{\sigma_z^2}\left\{\frac{-(z-H)\exp[-(z-H)^2/2\sigma_z^2]}{\exp[-(z-H)^2/2\sigma_z^2] + \exp[-(z+H)^2/2\sigma_z^2]} - \right.$$

$$\left. - \frac{(z+H)\exp[-(z+H)^2/2\sigma_z^2]}{\exp[-(z-H)^2/2\sigma_z^2] + \exp[-(z+H)^2/2\sigma_z^2]}\right\}. \qquad (5.22)$$

Substituting these expressions into Eq. (5.19) and rearranging gives the 'reflected Gaussian' eddy diffusivity of mean concentration

$$K_z = \frac{U_H}{2} \frac{d\sigma_z^2}{dx} \{ \frac{I_1 + I_2}{-(z-H)\exp[-(z-H)^2/2\sigma_z^2] - (z+H)\exp[-(z+H)^2/2\sigma_z^2]} \} \cdot$$

(5.23)

A similar operation on Eq. (5.20) gives the vertical Reynolds mass flux for a reflected Gaussian concentration field,

$$-\overline{w'c'} = \frac{Q \; d\sigma_z/dx}{2\pi\sigma_y\sigma_z^2} (I_1 + I_2)\exp(-y^2/2\sigma_y^2) , \qquad (5.24)$$

where the integrals I_1 and I_2 are given by

$$I_1 = \int_0^z \frac{U}{U_H}\exp[-(z-H)^2/2\sigma_z^2][(z-H)^2/\sigma_z^2 - 1 - (1-y^2/\sigma_y^2)\frac{p}{2q}(1-\frac{U_H}{U})]dz$$

(5.25)

and

$$I_2 = \int_0^z \frac{U}{U_H}\exp[-(z+H)^2/2\sigma_z^2][(z+H)^2/\sigma_z^2 - 1 - (1-y^2/\sigma_y^2)\frac{p}{2q}(1-\frac{U_H}{U})]dz .$$

(5.26)

For uniform wind conditions $U = U_H = U_o$, I_1 and I_2 can be integrated in closed form to yield

$$K_z = \frac{U_o}{2} \frac{d\sigma_z^2}{dx} \qquad\qquad (5.27)$$

and

$$-\overline{w'c'} = -\frac{U_o}{2\sigma_z^2} \frac{d\sigma_z^2}{dx} \, \overline{c} \, z \, , \qquad\qquad (5.28)$$

where $z = 0$ on the plume centerline. Note that (5.27), derived originally by Batchelor (1949), is valid for a bounded or unbounded flow in a uniform wind.

The theoretical expressions (5.23) for K_z and (5.24) for Reynolds flux $-\overline{w'c'}$ are compared with experimental values in Figs. 5.14 through 5.18. The experimental values were obtained by numerical integration of Eqs. (5.19) and (5.20), with experimental measurements used to compute the integrand terms. The agreement between the Gaussian-derived K_z theory and the experiments is qualitatively quite good, with the theoretical eddy diffusivity showing the observed transition from $\subset$-shaped to $\sim$-shaped curves, but requiring a slightly longer travel time before the centerline discontinuity changes character to match observations farther downwind. The good fit between experimental and theoretical profiles of mean concentration (Figs. 5.1 to 5.7) is evidence that the solution of equation (5.8) is relatively insensitive to the values used for K_z. The mathematical reason for this insensitivity is that the mean concentration depends on the spatial integral of eddy diffusivity, i.e. $\overline{c}$ at any receptor depends on the

entire upstream K_z field, and the effect of details in the K_z field is obscured. Thus the distance at which the eddy diffusivity 'flips' from $\subset$-shaped to $\diagup$-shaped curves is not of major importance. This insensitivity to K_z profiles helps to explain why reasonable $\bar{c}$ profiles can be obtained even for diffusivities which are independant of source height (Kumar, 1978).

A surprizing aspect of the diffusivity curves in Figs. 5.14 to 5.17 is that both experimental and theoretical profiles show a discontinuity near the source height. It is probable that the discontinuity is nothing more than an artifact produced by accumulated experimental and numerical errors. However, this discontinuity vanishes from the theoretical profile (5.23) when the wind field becomes uniform, because then the z-gradient denominator in Eq. (5.23) goes to zero at the same point that the numerator becomes zero; at that point, the ratio 0/0 has the value unity and, as expected, K_z takes the constant value given in Eq. (5.27). The discontinuous theoretical solution for K_z occurs only under non-uniform wind conditions, in which case the vertical concentration gradient (denominator of K_z) inconveniently goes to zero while the Reynolds flux (numerator of K_z) is still different from zero. This theoretical non-uniform wind phenomenon is an alternative, but less plausible, explanation for the discontinuity found in the experimental eddy diffusivities.

The theoretical eddy diffusivity equation (5.23) has limited practical application, since it provides no more infor- mation about the mean field than is already contained in the more convenient reflected Gaussian model for $\bar{c}$. The theory's

main feature is that it illustrates how the eddy diffusivity
of concentration in non-uniform winds should depend on the
source location within the wind field as well as the effective
diffusion length scales σ_y and σ_z. The momentum diffusivity
is often used in place of the scalar eddy diffusivity, but
depends on the integral turbulence length scale Λ_u, which was
shown in Chapter IV to be larger than the observed Λ_c for
scalar concentrations. The difference is due to unequal 'ages'
for velocity and scalar fluctuations; most of the vertical
plume spread is complete before the scalar fluctuations are
old enough to be influenced by the low frequency turbulence
contributing to Λ_u. This fact is not widely appreciated and
is often ignored, especially when the Reynolds analogy is
used to equate scalar diffusivity with momentum diffusivity.
Because the momentum diffusivity does not depend on any source
location characteristics, whereas K_z explicitly does, the
analogy is valid only in the asymptotic stage ($\sigma^2 \sim x$,
K independent of x) of plume dispersion in uniform winds.

5.5 Variance Production and Dissipation

The variance equation (5.9) is similar to the mean
field equation (5.8) in that advection and gradient flux terms
are common to both equations. However, Eq. (5.9) contains two
additional terms which describe the local production and
dissipation of concentration fluctuations. The importance of
these extra terms is examined in this section.

Csanady's (1967) solution for $\overline{c'^2}$ produces lateral profiles which have a saddle at the plume centerline if the ratio of dissipation ϕ_c to diffusion SK_y/σ_y^2 is large. High diffusion and low dissipation smooths out the off-centerline peaks which occur at the production maxima, and results in single-peaked distributions much like those observed in the present experiments. The relative importance of production and dissipation in the simulated plume was established by calculating their values from measurements of $\overline{c}$ and $\overline{(\frac{\partial c'}{\partial t})^2}$. Interpolation and numerical differentiation of data from the 76 vertical profile receptor locations were used to derive values for U, $\frac{\partial \overline{c}}{\partial z}$ and $\overline{(\frac{\partial c'}{\partial t})^2}$ at 2 mm height increments for each of the five vertical profiles. The experimental mean field diffusivities derived in Section 5.4 were used for K_z.

Section 5.2 has shown that the eddy dissipation function ϕ_c can be related to the concentration time derivative variance if local isotropy is assumed and Taylor's hypothesis is used. The result was

$$\phi_c = \frac{6D}{U^2} \overline{(\frac{\partial c'}{\partial t})^2} . \tag{5.29}$$

In this case D is the molecular diffusivity of helium in air, equal to 0.65 cm^2/sec. An averaging time of 100 seconds was used to obtain $\sim$ 3% repeatability for measurements of the time derivative variance; the observed values were corrected for probe-induced dissipation as described in Chapter III.

The variance production term is, from Section 5.2,

$$P_V = 2K_y \left(\frac{\partial \bar{c}}{\partial y}\right)^2 + 2K_z \left(\frac{\partial \bar{c}}{\partial z}\right)^2.$$

In the vertical (x,z) plane through the plume centerline, the lateral derivative $\frac{\partial \bar{c}}{\partial y}$ is zero, so that production in the vertical centerline plane is calculated from

$$P_V (y=0) = 2K_z \left(\frac{\partial \bar{c}}{\partial z}\right)^2. \qquad (5.30)$$

The variance dissipation ϕ_c and variance production P_V in this vertical plane, plus net dissipation $\phi_N = \phi_c - P_V$, have been calculated from the measurements, and are plotted against height in Figs. 5.19 through 5.23. To a large extent, the curves behave as expected:

- Production is low at the plume centerline and plume fringes, where concentration gradients are small. The largest production occurs where mean concentration gradients are maximum, in a region defined by a conical surface increasing in diameter downwind, with apex at the source. At larger distances, where the plume has impinged on the ground, this surface becomes semi-conical.

• Dissipation is smallest at the plume fringes and greatest
on the plume centerline. The off-centerline spatial
distribution of variance dissipation is similar to the
distribution of variance itself. In fact, Csanady (1967)
proposes that the dissipation of concentration fluctua-
tions is <u>proportional</u> to the fluctuation intensity, since
the dissipation mechanism should not depend on the
amplitude of fluctuations. The expected proportional
relationship is verified in the next section of this
chapter.

By far the most interesting behavior exhibited by the
measured production and dissipation profiles in Figs. 5.19
through 5.23 is that, as the plume moves downwind, production
decreases and eventually becomes <u>negligible</u> compared with the
dissipation of $\overline{c'^2}$. Then, <u>net</u> dissipation can be approximated
by the dissipation term itself, as suggested by Fig. 5.23,
where the triangles (ϕ_c) and the dotted curve (ϕ_N) are seen to
lie close together. The downwind decrease of production is a
natural consequence of plume growth, during which the plume
material is spread more and more thinly over the plume cross-
section, thereby reducing local concentration gradients. This
assumption of negligible variance production will play a major
role in the theoretical derivation of the dissipated Gaussian
model for $\overline{c'^2}$.

One last point should be made regarding the production
curves, particularly the one shown in Fig. 5.23. Evaluation

of production using Eq. (5.30) requires the experimental eddy diffusivity calculated from Eq. (5.19). This in turn requires the x-gradient of concentration, which is used in the advection term $U\frac{\partial \overline{c}}{\partial x}$. This derivative was calculated from constant-x curves of $\frac{\partial \overline{c}}{\partial x}$ (z) fitted through x-derivatives of $\overline{c}(x)$ curves fitted through constant-z values of $\overline{c}(x,z)$ measured at the five downwind locations. Because the data of Fig. 5.23 was obtained at the last downwind location, the x-derivative there is an extrapolated value, and is subject to more error than x-derivatives at the interior points. This error propagates through the eddy diffusivities to appear as error in the production curve. The error bar on production (and hence on net dissipation) shown in Fig. 5.23 corresponds to an error of ± 25% in the value of $\frac{\partial \overline{c}}{\partial x}$ at this last downwind location.

5.6 Concentration Microscale and Decay-Time Scale

The results of this chapter permit the testing of two assumptions made by Csanady (1967) in formulating his model for concentration fluctuations. The first and most important assumption was that the dissipation rate ϕ_c of concentration fluctuations is directly proportional to the local concentration variance $\overline{c'^2}$. The second assumption was that the proportionality factor can be written as $1/T_d$, where the dissipation time scale T_d increases linearly with travel time t (i.e. using Taylor's hypothesis, a linear increase with

distance x from the source). These assumptions were essential to Csanady's solution because they led to self-similarity of variance profiles, and permitted the unknown dissipation function ϕ_c to be expressed in terms of the unknown concentration variance S, in the form

$$\phi_c = \frac{S}{T_d} = \frac{S}{t_o + t_d x} \,.$$

(5.31)

Csanady states that the constants t_o and t_d depend on the relative 'age' difference between the atmospheric turbulence and the concentration fluctuations. In decaying grid turbulence, vector and scalar fluctuations originate at the same point in space, and therefore have the same 'age'; for this special case, Gibson and Schwarz (1963) have shown that $t_o = 0$ and $T_d = 2/3t$. Csanady supposes that for an individual plume cross-section, the 'age' of S is constant, so that t_o and t_d are independant of y and z.

These assumptions are tested here in the following way: first, equations (5.29) and (5.31) are combined and rearranged so that T_d is expressed in terms of the ratio of concentration variance to time derivative variance,

$$T_d = \frac{U^2}{6D} S / \overline{\left(\frac{\partial c'}{\partial t}\right)^2} \,.$$

(5.32)

Hinze (1975) has applied the concept of a Taylor microscale to

concentration fluctuations, and shows that the dissipation rate may be written as

$$\phi_c = \frac{12 \, D}{\lambda_c^2} \, S \, .$$
(5.33)

Thus the Taylor concentration microscale and the decay-time scale are related by

$$\lambda_c^2 = 12 \, DT_d = 2 \, U^2 \, S/\overline{\left(\frac{\partial c'}{\partial t}\right)^2} \, .$$
(5.34)

The time derivative variance was measured in the wind tunnel (see Ch. III for details) along with S and U, and vertical profiles of the derived values of concentration microscale are shown in Fig. 5.24. There is some small variation with height above surface, but it is not systematic and is probably due to experimental error. Scatter in the lateral profiles (not shown) was about the same. For each of the five plume cross-sections a laterally and vertically averaged value of T_d was calculated. The results are presented in Table 5.2. The values of T_d (in ms) have a best-fit linear dependance on x (in cm) of

$$T_d = 38.5 + 1.65 \, x \, ,$$
(5.35)

with a coefficient of determination $r^2 = 0.995$.

TABLE 5.2

VARIATION OF DECAY TIME SCALE WITH DOWNWIND DISTANCE

x(cm)	T_d(ms)
13.0	57.7 ± 4.5
19.0	71.0 ± 3.0
27.5	86.7 ± 5.8
37.5	99.2 ± 5.3
57.5	133.2 ± 7.8

This experimental data is in agreement with Csanady's suppositions that:

• the dissipation rate of concentration fluctuations downwind of an elevated point source in an atmospheric boundary layer is proportional to the local concentration variance;

• the proportionality factor is independant of y and z, and varies inversely with T_d, a decay time scale which increases with downwind distance.

The values of t_o and t_d must depend on the level of atmospheric turbulence, although other factors may also be important; the question of how to determine a priori the values of t_o and t_d is still unanswered. However, for the simulated plume the need to know these constants is not important,

because the dissipated Gaussian model, which provides a satisfactory description of the concentration variance field, is shown in the next section to imply a specific dependance of T_d on x.

5.7 Theoretical Derivation of the Dissipated Gaussian Model

There is an excellent agreement between $\overline{c'^2}$ calculated from the dissipated Gaussian model proposed in Section 5.3.2 and the values of $\overline{c'^2}$ measured in the simulated plume. Furthermore, the mathematical form of the model is very similar to the classic reflected Gaussian model for mean concentration $\overline{c}$. This suggests that the diffusion equation (5.8) for $\overline{c}$ and the variance balance equation (5.9) may have somewhat similar solutions.

The analysis which follows uses the approach of Csanady (1967, 1973). First, the diffusion and variance equations are rewritten for cylindrical coordinates, implying a plume symmetric about its centerline, far above the ground. A similarity solution to the equations is sought, in which the wind field is uniform and the x-dependant plume growth is incorporated in the empirical variation of the plume standard deviation σ. Thus, the mean concentration is assumed to have the form

$$\overline{c} = c_0\, f(\eta), \qquad (5.36)$$

where the dimensionless radial coordinate is

$$\eta = r/\sigma \qquad (5.37)$$

and the x-dependant centerline variation of $\bar{c}$ is

$$C_0 = \frac{Q}{2\pi U_0 \sigma^2 \cdot \int_0^\infty \eta f(\eta) d\eta} \qquad (5.38)$$

For radially constant $K_y = K_z = K = U_0 \sigma \frac{d\sigma}{dx}$, the diffusion equation (5.8) can be written (with $f' = \frac{df}{d\eta}$, $f'' = \frac{d^2 f}{d\eta^2}$) as

$$f'' + (\frac{1}{\eta} + \eta) \ f' + 2f = 0, \qquad (5.39)$$

which is a homogeneous ordinary linear second order differential equation with variable coefficients. The boundary conditions of axial symmetry and decay to zero at large distances are:

$$f(\infty) = 0,$$

$$\qquad (5.40)$$

$$f'(0) = 0.$$

It is easy to show by substitution that one solution of (5.39) satisfying all the boundary conditions is the simple Gaussian distribution

$$f(\eta) = \exp (- \frac{\eta^2}{2}), \qquad (5.41)$$

for which $\int_0^\infty \eta f(\eta) d\eta = 1$. This gives the well known expression

for mean concentration in an axisymmetric plume,

$$\bar{c} = \left(\frac{Q}{2\pi U_0 \sigma^2}\right) \exp\left(-\frac{r^2}{2\sigma^2}\right).$$ (5.42)

These steps are now repeated for the variance field, with the similarity assumption

$$S = s_0 c_0^2\, g(\eta)$$ (5.43)

and the dissipation ϕ_c given in terms of S by use of Eq. (5.31). Eq. (5.43) for S is different from the form used by Csanady (1967, 1973) only in the use of a source variance strength constant s_0. The balance equation (5.9) for $\overline{c'^2}$ can now be written as

$$\underbrace{-4g - \eta g'}_{\text{advection}} = \underbrace{g'' + \frac{1}{\eta} g'}_{\text{gradient flux}} + \underbrace{2f'^2}_{\text{production}} - \underbrace{\alpha g}_{\text{dissipation}}.$$

Introducing the solution (5.41) for f and collecting terms yields the form given by Csanady (1967, 1973),

$$g'' + \left(\frac{1}{\eta} + \eta\right)g' + (4-\alpha)g = -2\eta^2 \exp(-\eta^2),$$ (5.44)

which is a <u>nonhomogeneous</u> ordinary linear second order differential equation with variable coefficients. The parameter α,

given by

$$\alpha = \frac{\sigma^2}{KT_d}, \qquad (5.45)$$

results from dissipation of $\overline{c'^2}$, and is assumed constant throughout the plume. The nonhomogeneous term on the right hand side of (5.44) is due to production of $\overline{c'^2}$.

The boundary conditions on (5.44) are, in this case, the same as for the mean field: a decay to zero at large distances, and an axisymmetric plume,

$$g(\infty) = 0,$$

$$\qquad (5.46)$$

$$g'(0) = 0.$$

Csanady (1967) has obtained a closed form solution to (5.44) subject to boundary conditions (5.46). What is sought here is an approximate solution to (5.44) that can be generalized to the more complicated case of an asymmetric plume near a solid boundary.

A considerable simplification of (5.44) results if the nonhomogeneous production term is omitted. The figures of Section 5.5 show that production does in fact become negligible as the simulated plume moves downwind. For the assumption of zero production, (5.44) becomes homogeneous,

$$g'' + (\frac{1}{\eta} + \eta)g' + (4-\alpha)g = 0 \qquad (5.47)$$

which is substantially closer to the form of the mean equation (5.39). Only one small step is needed to make the two equations identical, and that is to specify

$$\alpha = 2.$$

Then

$$g'' + (\frac{1}{\eta} + \eta)g' + 2g = 0, \qquad (5.48)$$

one solution of which is

$$g(\eta) = \exp(-\frac{\eta^2}{2}) = \exp(-\frac{r^2}{2\sigma^2}). \qquad (5.49)$$

In cartesian coordinates, the variance becomes

$$S = s_o(\frac{Q}{2\pi U_o \sigma^2})^2 \exp(\frac{-y^2}{2\sigma^2}) \exp(\frac{-z^2}{2\sigma^2}), \qquad (5.50)$$

which is very close in form to the dissipated Gaussian model proposed for S earlier in this chapter. As before, s_o is a source variance strength parameter to be determined from experiment.

By analogy with the known mean field solution for an asymmetric plume, Eq. (5.50) can be generalized for $\sigma_y \neq \sigma_z$,

$$S = s_0 \left(\frac{Q}{2\pi U_0 \sigma_y \sigma_z} \right)^2 \exp\left(\frac{-y^2}{2\sigma_y^2} \right) \exp\left(\frac{-z^2}{2\sigma_z^2} \right),$$

or, shifting the z-coordinate by a constant amount, so the plume centerline is at z = H,

$$S = s_0 \left(\frac{Q}{2\pi U_0 \sigma_y \sigma_z} \right)^2 \exp\left(\frac{-y^2}{2\sigma_y^2} \right) \exp\left[\frac{-(z-H)^2}{2\sigma_z^2} \right]. \quad (5.51)$$

Note that the linearity of Eq. (5.48) permits the solution of a complicated problem to be written as a super-position of solutions to less difficult problems. Eq. (5.48) remains linear when written in cartesian coordinates, so that the process of superposition lends itself to the difficult problem of solving (5.48) (in cartesian coordinates) subject to the boundary condition of complete dissipation of fluctuations at a solid boundary located at z = 0, a distance H below the plume centerline:

$$g(0) = 0.$$

A solution to this problem is obtained by introducing a negative image source a distance H on the opposite side of the solid boundary. This procedure is the same as that used to derive the reflected Gaussian model for mean concentration.

The S-field is then given by a superposition of the fields from both the positive (real) and negative (image) sources,

$$S = s_o \left(\frac{Q}{2\pi U_o \sigma_y \sigma_z}\right)^2 \exp\left(\frac{-y^2}{2\sigma_y^2}\right)\left\{\exp\left[\frac{-(z-H)^2}{2\sigma_z^2}\right] - \exp\left[\frac{-(z+H)^2}{2\sigma_z^2}\right]\right\}. \tag{5.52}$$

The dissipated Gaussian model, originally proposed for S on the basis of empirical arguments, has now been derived as a solution of the variance balance equation (5.9) for the special case of

- Negligible variance production,

- Dissipation parameter $\alpha = 2$.

- Constant diffusivities $K_y' = K_y = U_o \sigma_y \dfrac{d\sigma_y}{dx}$ and $K_z' = K_z = U_o \sigma_z \dfrac{d\sigma_z}{dx}$.

The physical significance of setting the dissipation parameter $\alpha = 2$ must be determined. As was mentioned in Section 5.6, Gibson and Schwarz (1963) have shown that the decay time scale of fluctuations in isotropic grid turbulence is related to distance from the grid by the expression

$$T_d = \frac{2x}{3U} . \tag{5.53}$$

Csanady (1973) has related the dissipation parameter $\alpha = \sigma^2/KT_d$ to downwind distance by considering the asymptotic stage of diffusion in which $\sigma^2 \sim x$, and obtains

$$T_d = \frac{2(x - x_o)}{\alpha U} . \qquad (5.54)$$

Obviously, $\alpha = 3$ corresponds to dissipation of scalar fluctuations in decaying isotropic grid turbulence described by Eq. (5.53). Values of $\alpha < 3$ can be expected in turbulent flows which decay more slowly than grid-type turbulence. Thus, $\alpha = 2$ means that the decay time scale is exactly equal to the travel time of fluctuations from their effective origin $x = x_o$.

Eq. (5.54) can be written as

$$T_d = a + bx_s , \qquad (5.55)$$

where x_s is distance from the plume source. Combining (5.54) and (5.55),

$$x_o = -\frac{a}{b} , \qquad (5.56)$$

from which

$$T_d = \frac{2a}{\alpha U b} + \frac{2}{\alpha U} x_s \qquad (5.57)$$

relative to the plume source. Comparing (5.55) and (5.57), the dissipation parameter α is given by

$$\alpha = \frac{2}{Ub} . \qquad (5.58)$$

Measured values of T_d (in ms) obtained during the present study fit the linear relation

$$T_d = 38.5 + 1.65 \ x_s \ . \qquad (5.59)$$

Taking a typical velocity in the tunnel as U = 800 cm/sec, (5.57) and (5.59) may be combined to give

$$\alpha = 1.5 \ . \qquad (5.60)$$

This shows that helium fluctuations in the wind tunnel were dissipated at only half the rate that would occur in isotropic grid turbulence, for which $\alpha = 3$. More importantly, the wind tunnel tracer fluctuations died away 25% slower than the Gaussian solution ($\alpha = 2$) requires. However, the favorable comparision of measured S-profiles (Figs. 5.1 through 5.7) and measured profiles of the fluctuation intensity $i_c = \sqrt{S}/\bar{c}$ (Figs. 5.8 through 5.13) with the Gaussian model prediction shows not much sensitivity to variations in α. The profile shapes are accurately predicted, and the axial variation (Fig. 5.1) is also well reproduced. This remains true even close to the source, where the assumption of negligible production is certainly violated (Fig. 5.19). The conclusion drawn is that the dissipated Gaussian model, a true solution of the variance equation only for the special case of zero production and decay time scale T_d equal to effective travel time, is in general a

good engineering approximation to the spatial distribution of
concentration variance in plumes.

5.8 Summary

The most important results from the measurements and
analysis presented in this chapter are summarized here:

- For steady flow situations where the parameters Q,
  U_H, σ_y and σ_z are accurately known, the reflected
  Gaussian model (5.12) for mean concentration fits
  observations with relative error less than 10% of the
  local concentration except at the plume edges and near
  the ground, where errors of 20-40% can be observed;

- In flows for which the reflected Gaussian model for
  mean concentration $\bar{c}$ can be used, the concentration
  variance $\overline{c'^2}$ can be calculated from the dissipated
  Gaussian model given by Eq. (5.13). This model in-
  cludes a source variance term s_o which is constant
  through the plume, and which probably depends on
  atmospheric turbulence level at source height;

- The local production and dissipation rates of $\overline{c'^2}$ in
  a plume are not equal. In fact, as the plume moves
  downwind, production becomes negligible in comparison
  with the variance dissipation. This leads to a balance
  equation for $\overline{c'^2}$ which has the same form as the diffusion
  equation for $\bar{c}$;

- The dissipated Gaussian model for $\overline{c'^2}$ is a true solution of the variance equation for the special case of zero in-plume variance production and fluctuations which decay at two-thirds the rate of those in isotropic grid turbulence;

- Measurements of the local dissipation rate of concentration fluctuations support Csanady's (1967) supposition that this rate is _proportional_ to the local concentration variance;

- The measurements confirm Csanady's (1967) assumption that the reciprocal of this proportionality factor is a decay time scale T_d which is constant at a given section and which increases linearly with distance from the source.
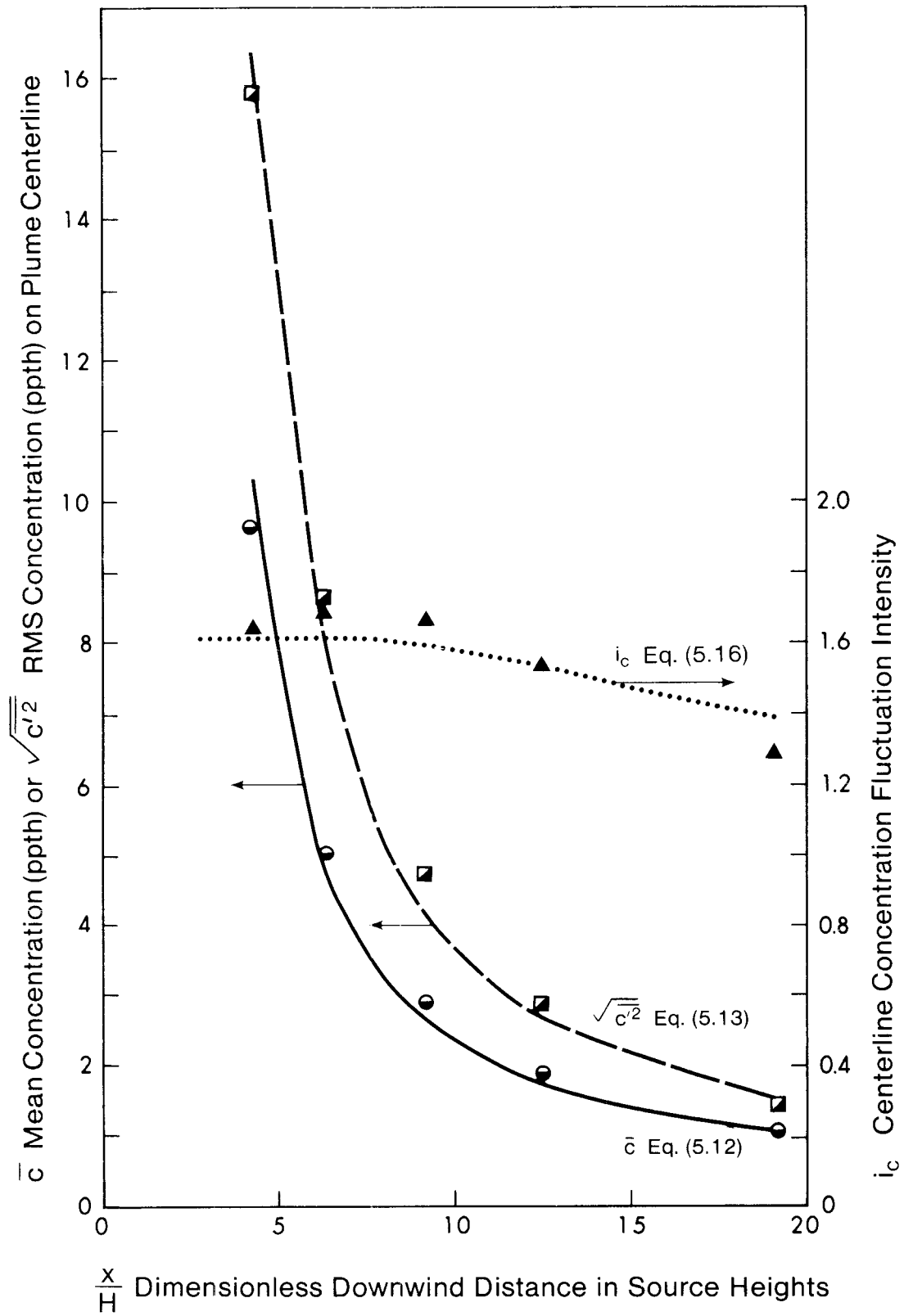
FIG. 5.1 Centerline Variation of Mean and
RMS Concentration
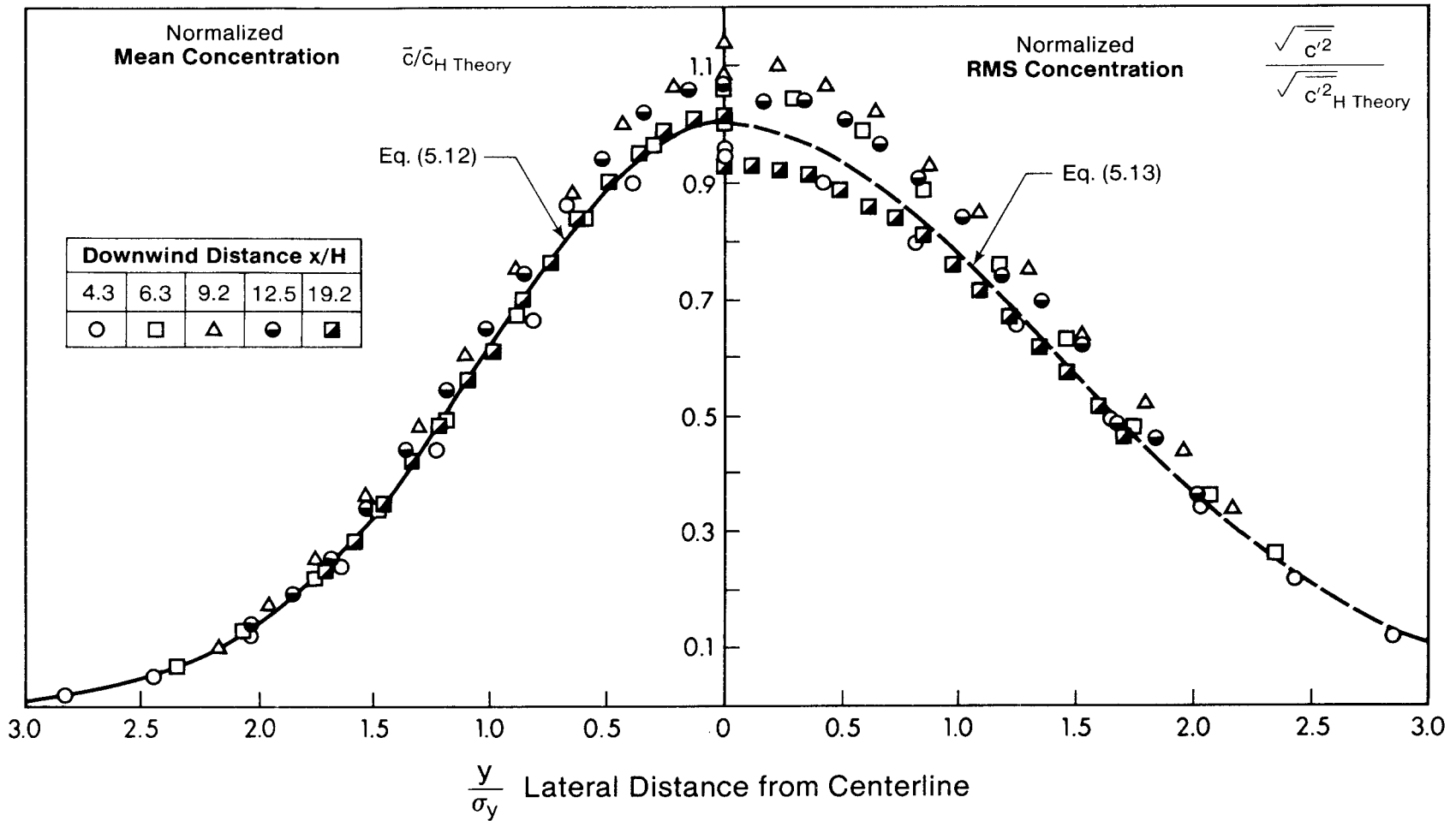
FIG. 5.2   Lateral Distribution of Mean and RMS Concentration

The figure shows normalized mean concentration ($\bar{c}/\bar{c}_{H\ Theory}$) on the left and normalized RMS concentration ($\sqrt{\overline{c'^2}}/\sqrt{\overline{c'^2}}_{H\ Theory}$) on the right, plotted against $\frac{y}{\sigma_y}$ Lateral Distance from Centerline. Eq. (5.12) and Eq. (5.13) are indicated.

Downwind Distance x/H:

4.3	6.3	9.2	12.5	19.2
○	□	△	◐	◪
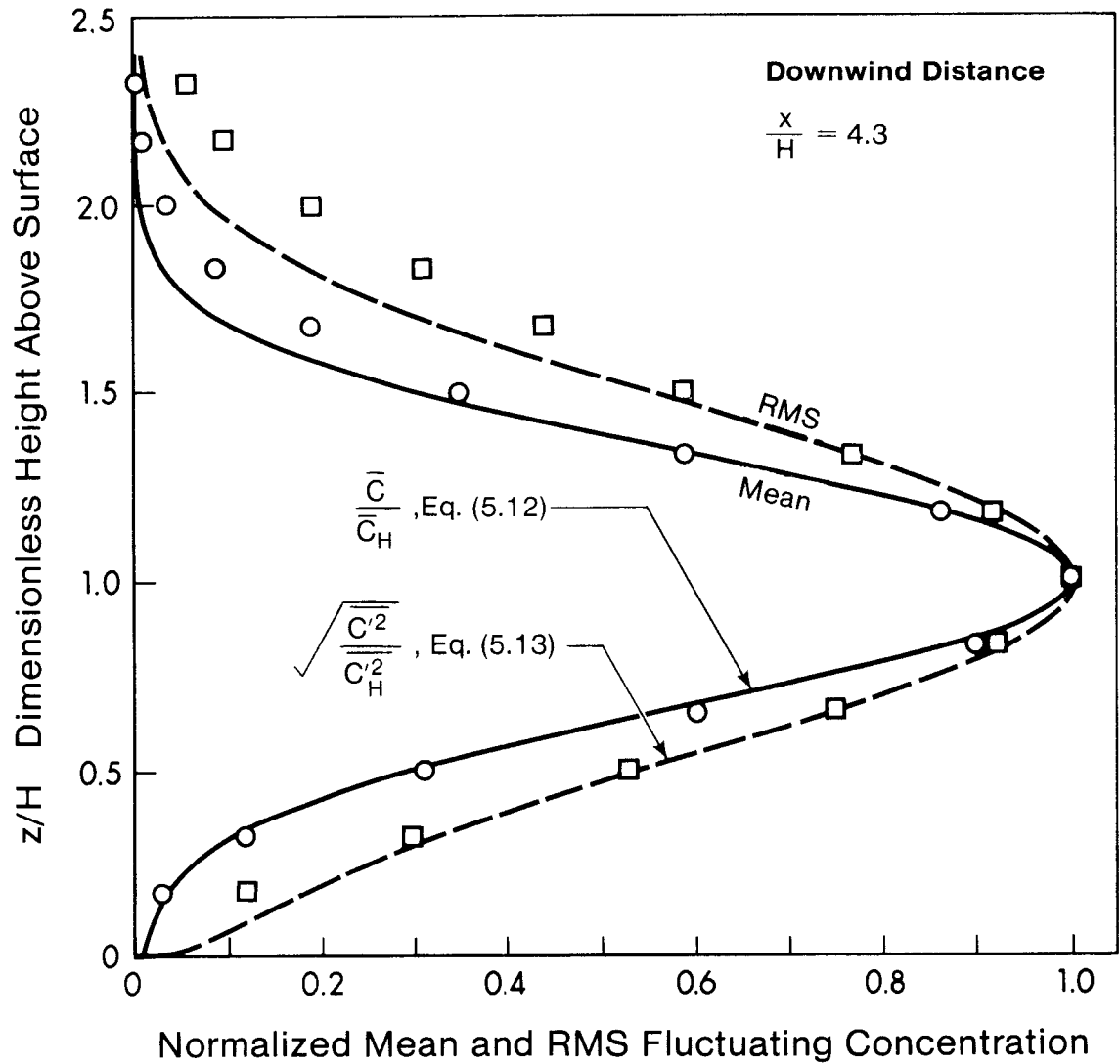
FIG. 5.3 Vertical Variation of Mean and RMS
Concentration at x/H = 4.3
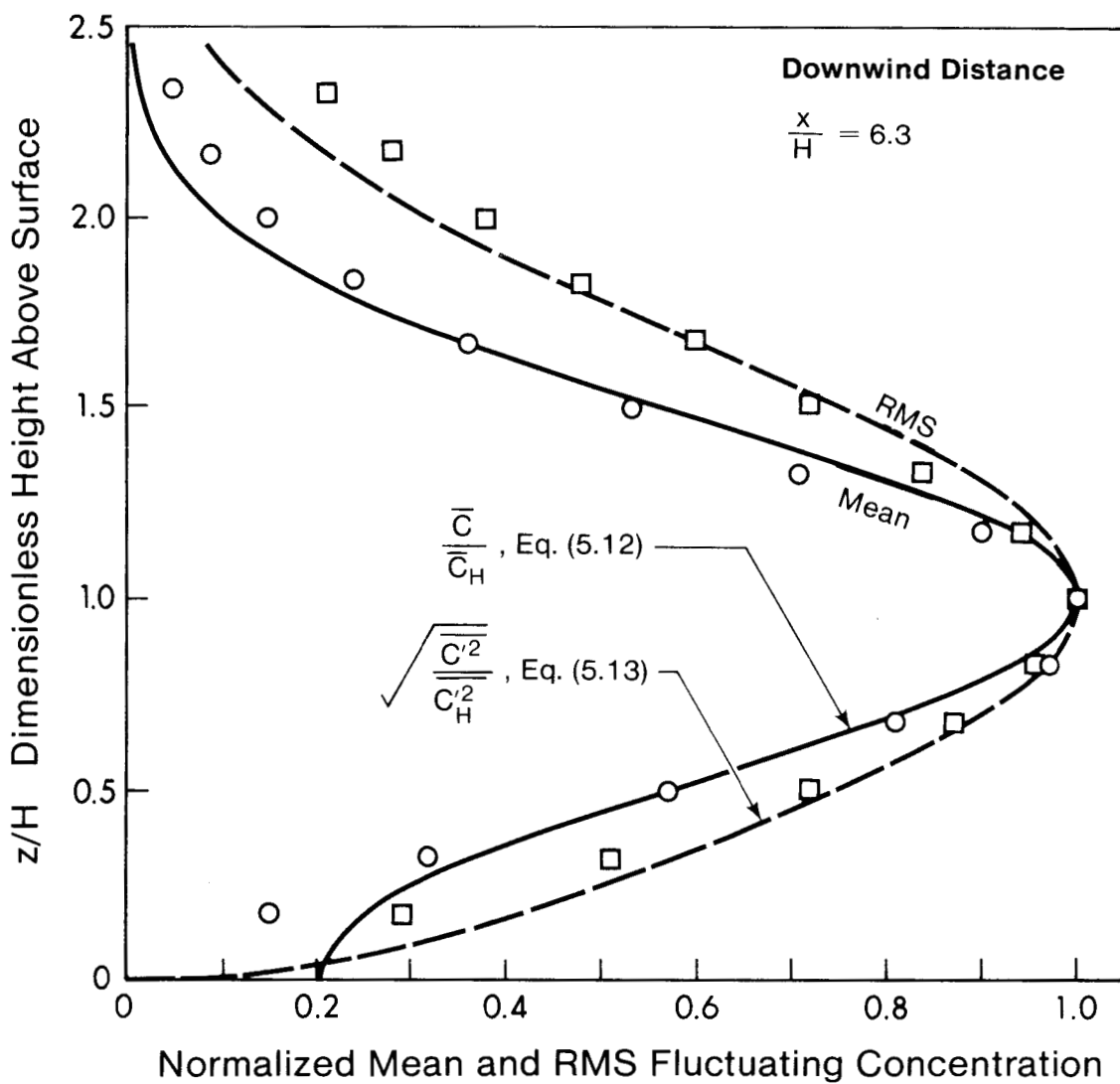
FIG. 5.4   Vertical Variation of Mean and RMS
Concentration at x/H = 6.3
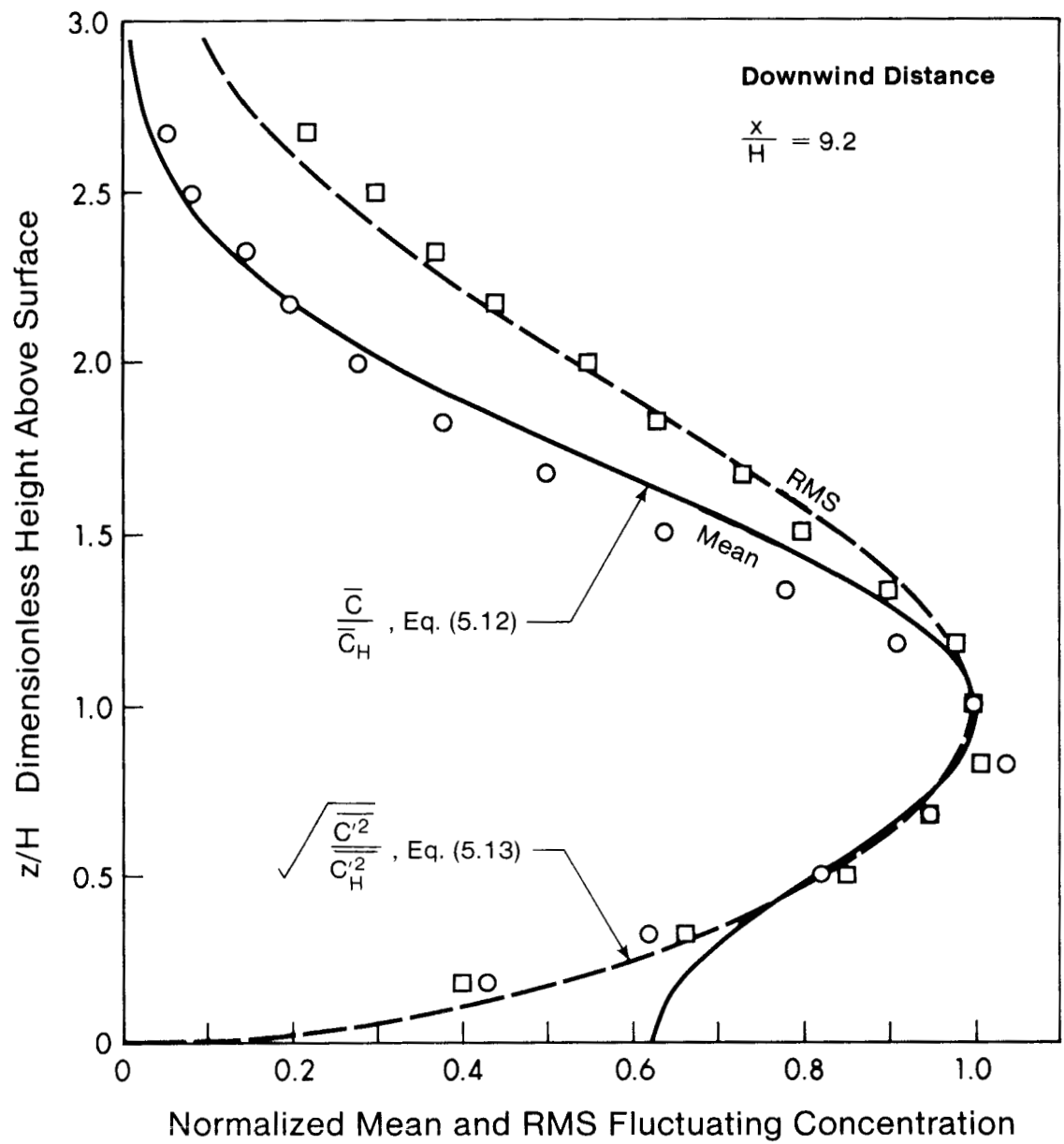
FIG. 5.5   Vertical Variation of Mean and RMS
Concentration at x/H = 9.2
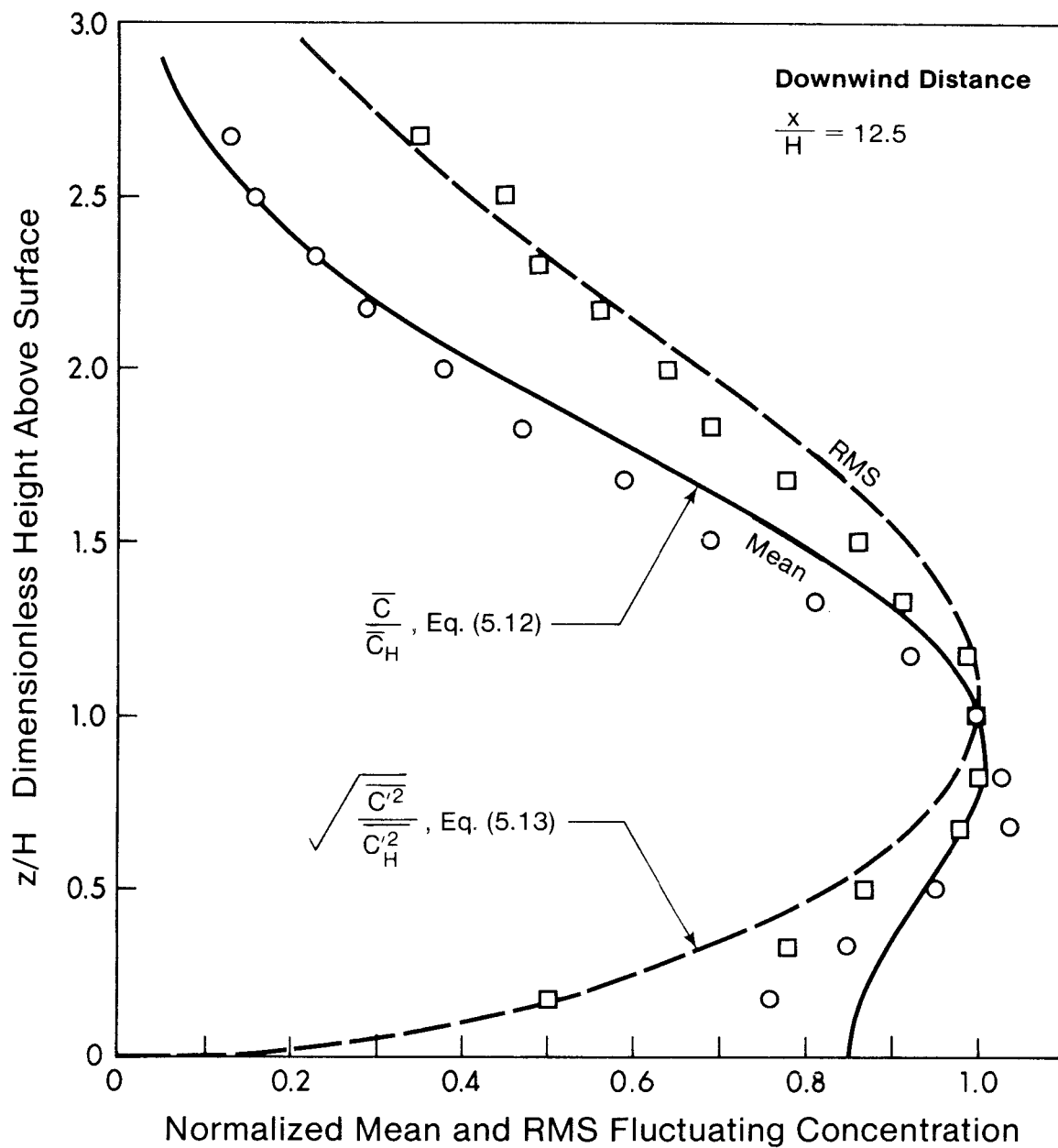
FIG. 5.6 Vertical Variation of Mean and RMS
Concentration at x/H = 12.5
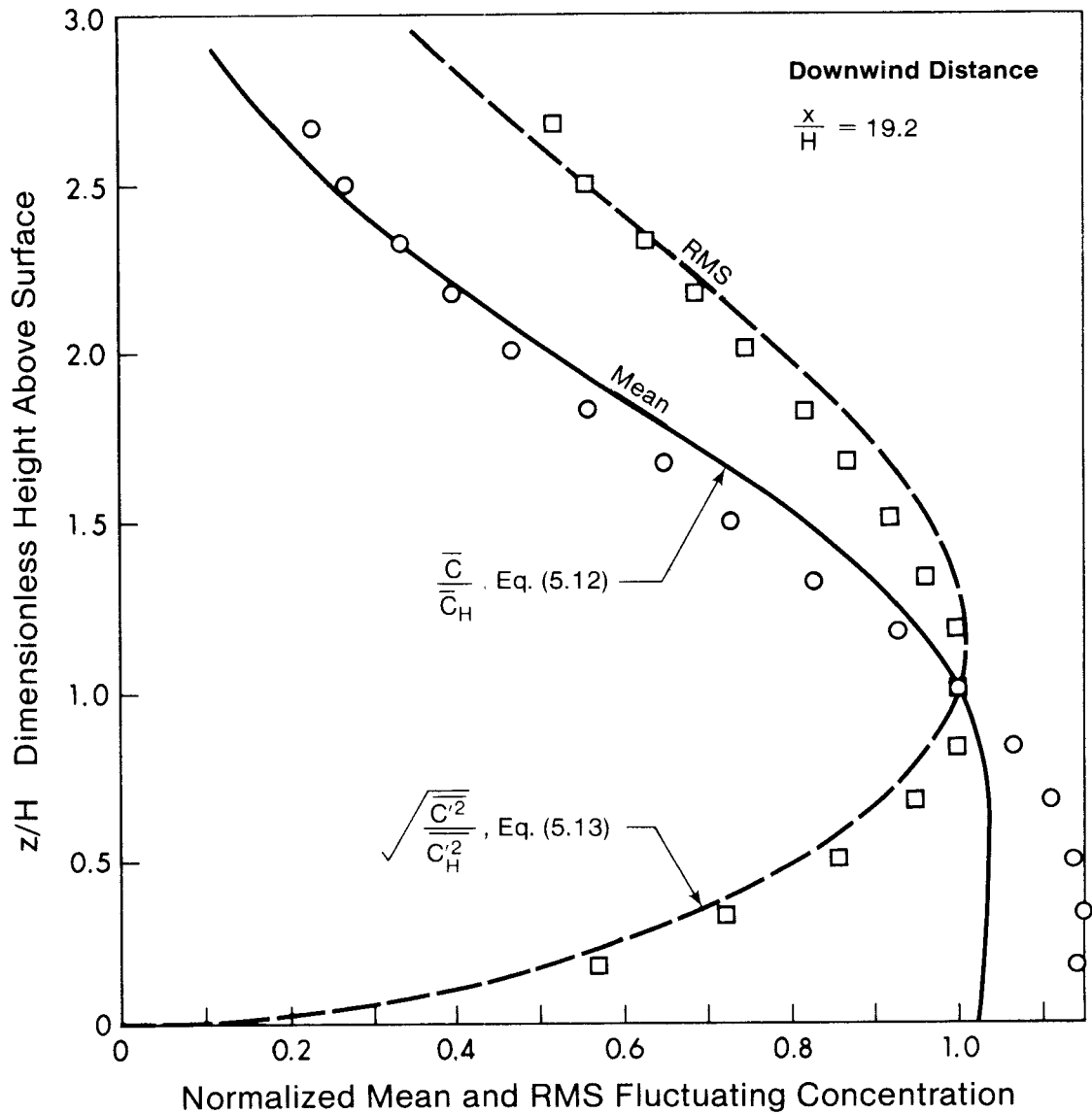
FIG. 5.7 Vertical Variation of Mean and RMS Concentration at x/H = 19.2
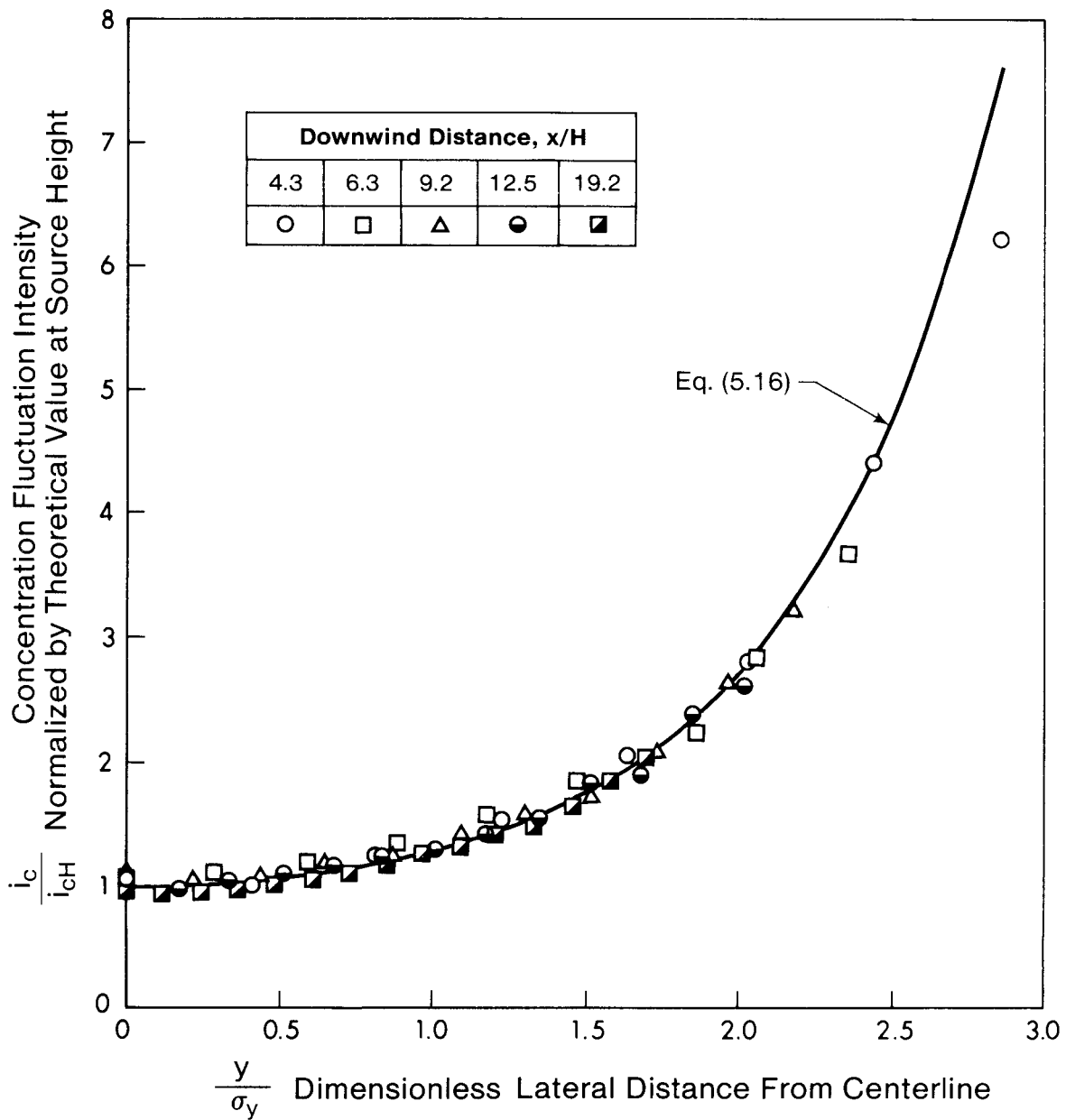
FIG. 5.8 Lateral Distribution of Concentration
Fluctuation Intensity at Plume Height
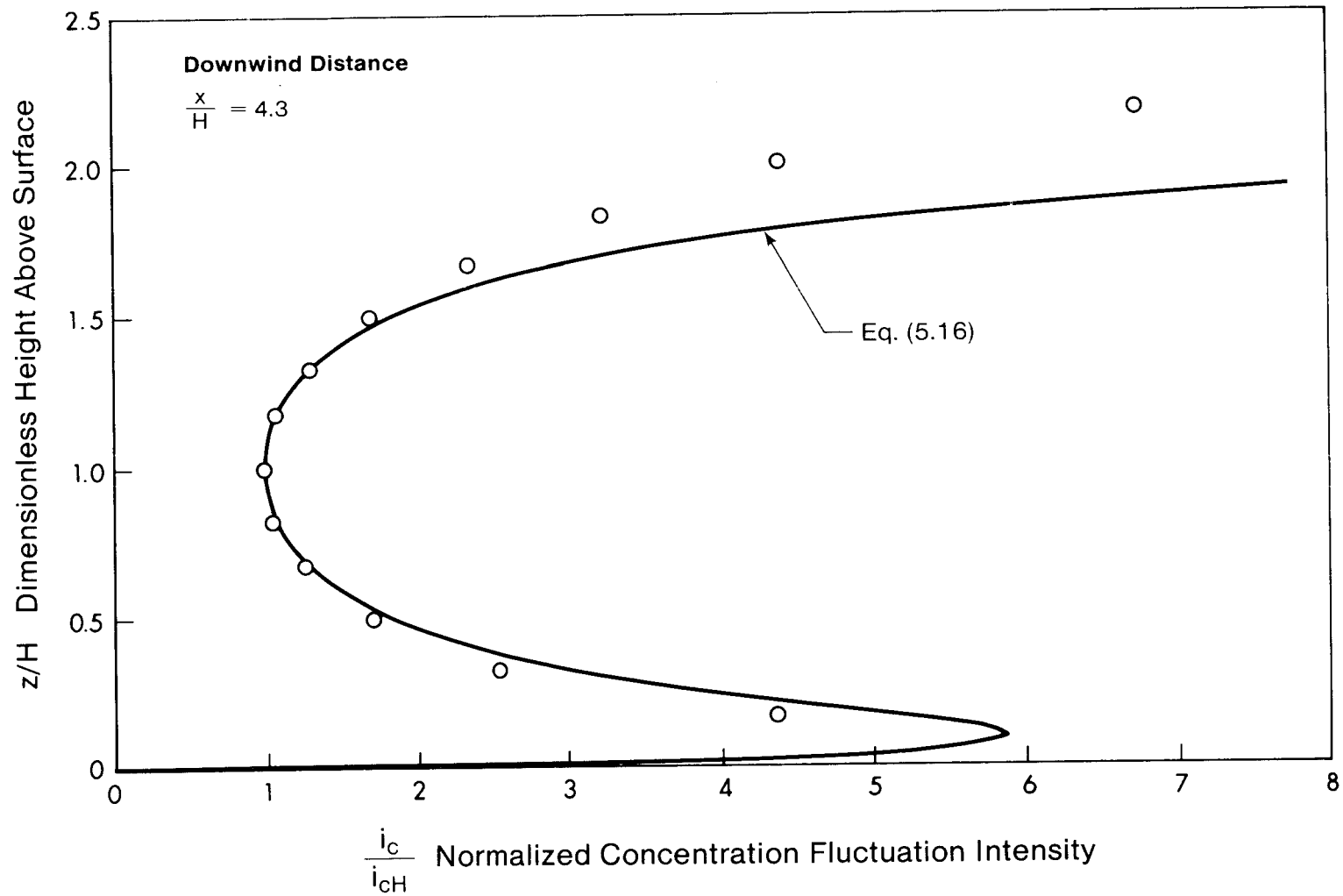
FIG. 5.9 Vertical Distribution of Concentration Fluctuation Intensity at x/H = 4.3
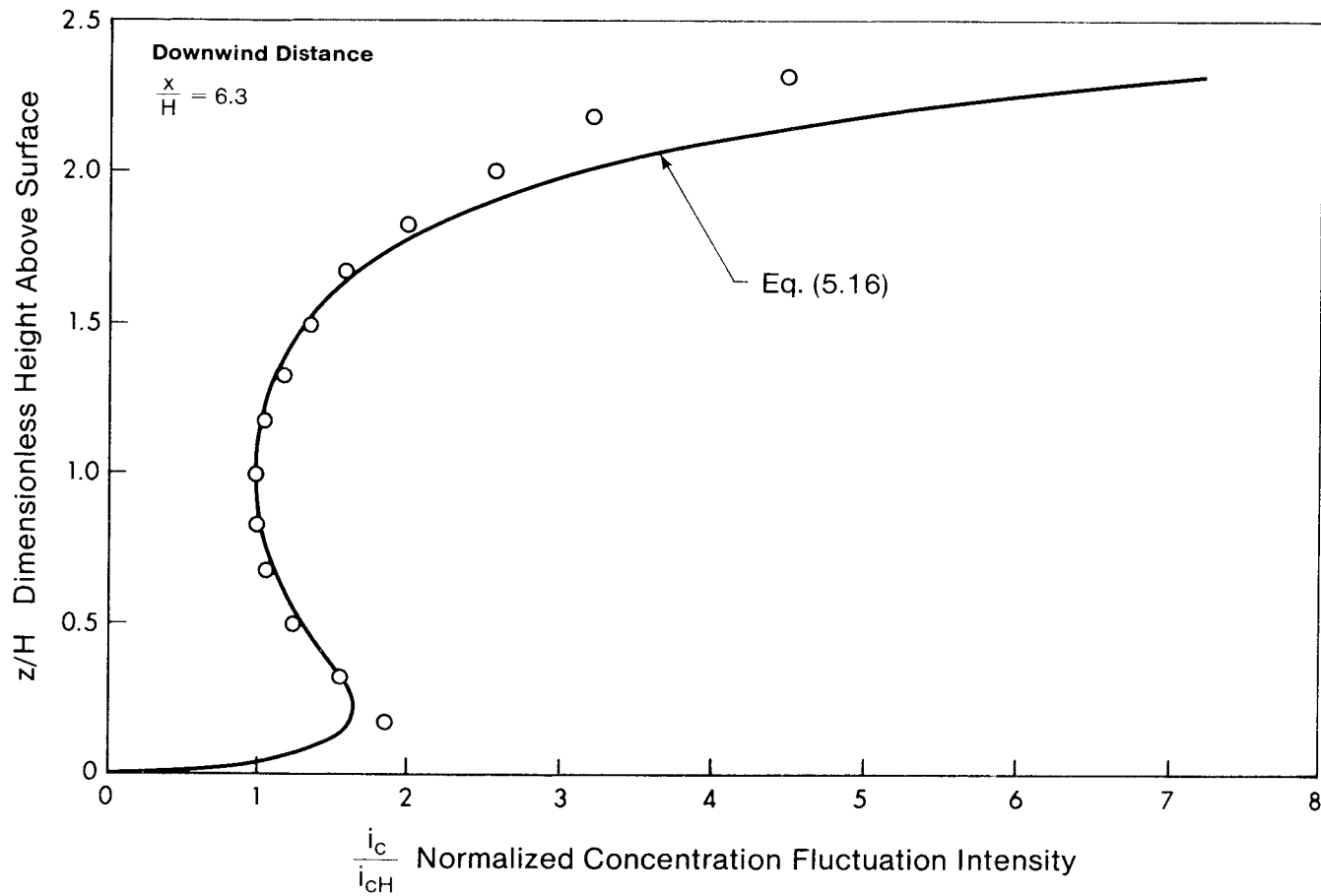
FIG. 5.10 Vertical Distribution of Concentration Fluctuation Intensity at x/H= 6.3
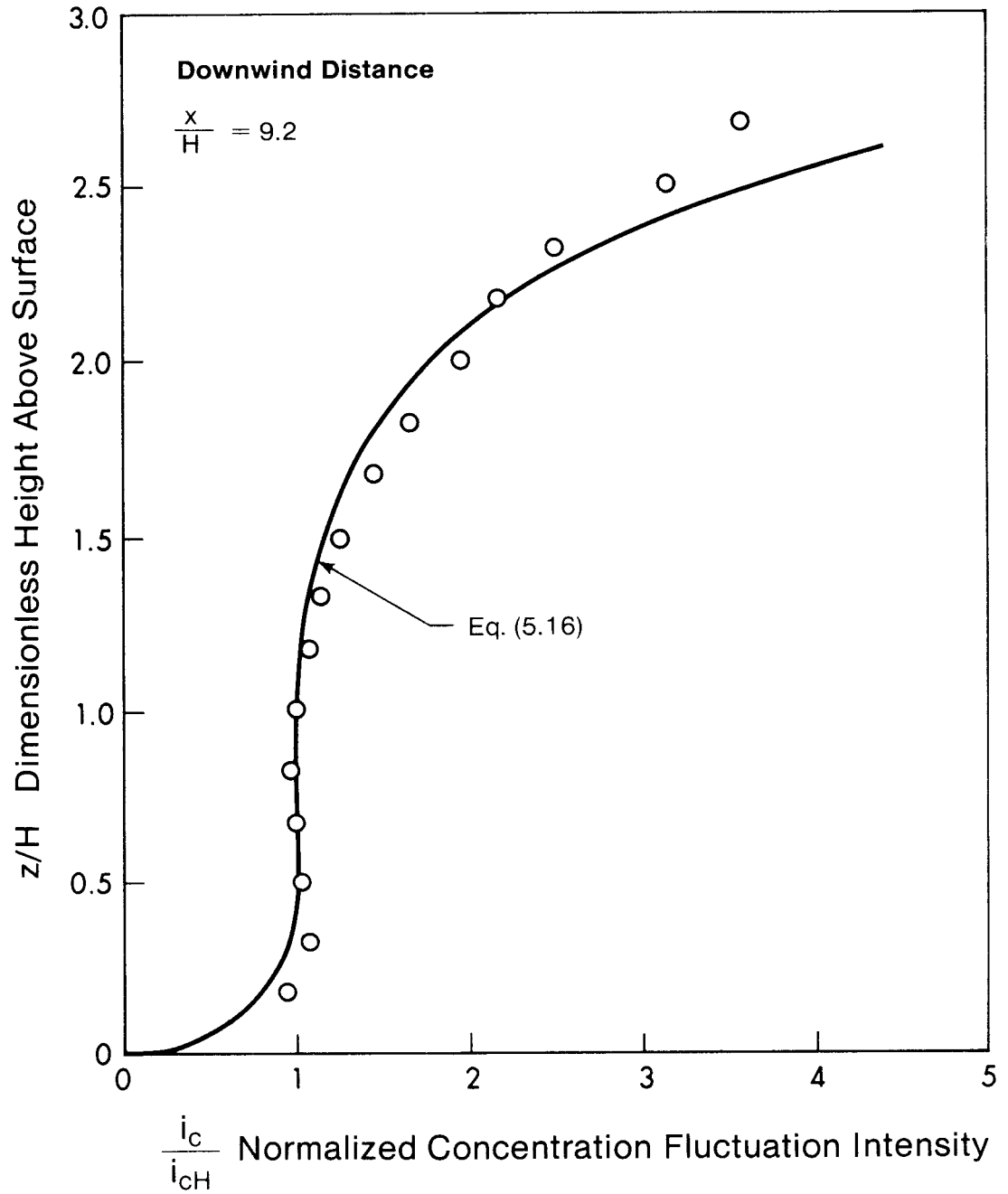
FIG. 5.11 Vertical Distribution of Concentration Fluctuation Intensity at x/H = 9.2
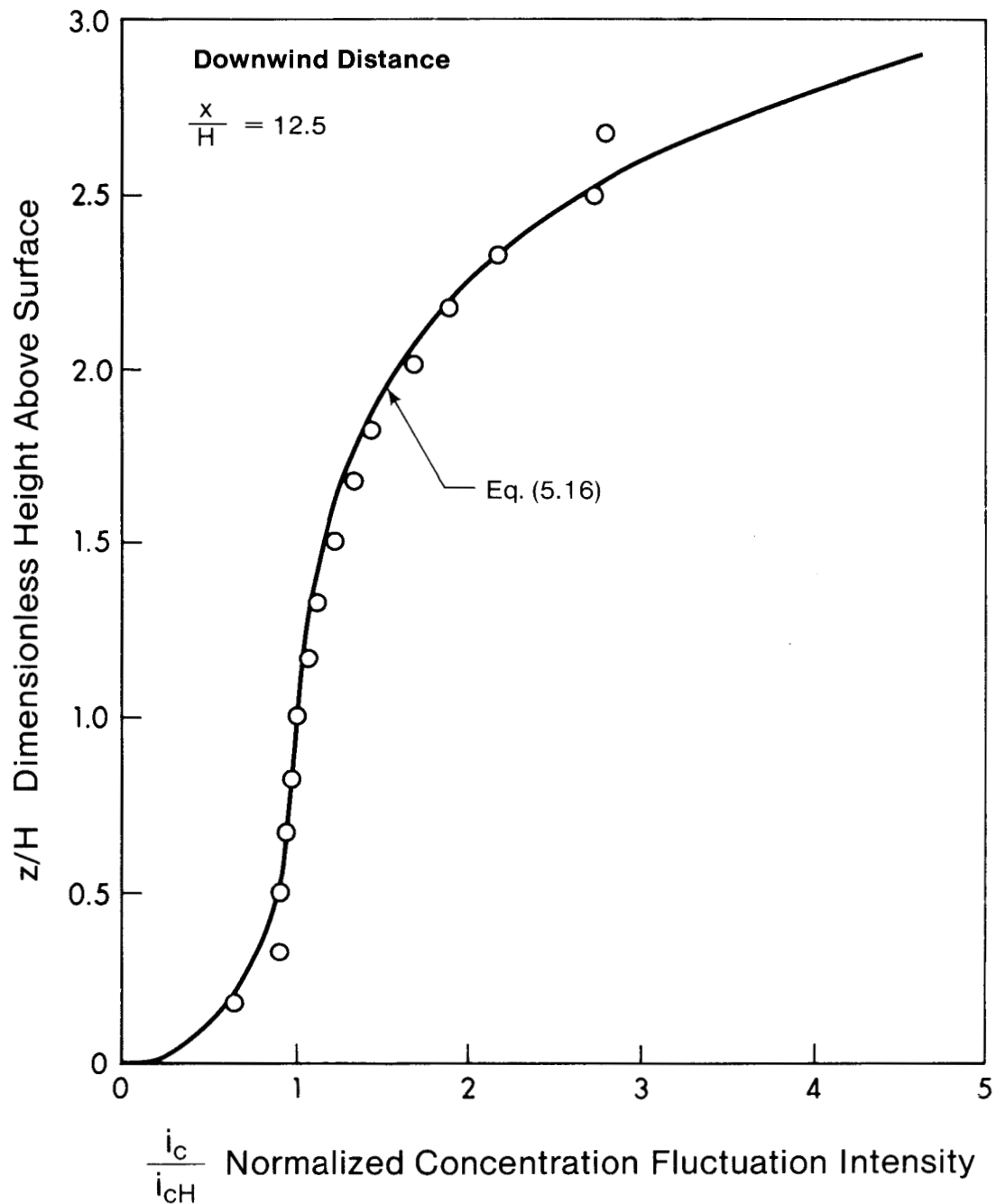
FIG. 5.12 Vertical Distribution of Concentration
Fluctuation Intensity at x/H = 12.5
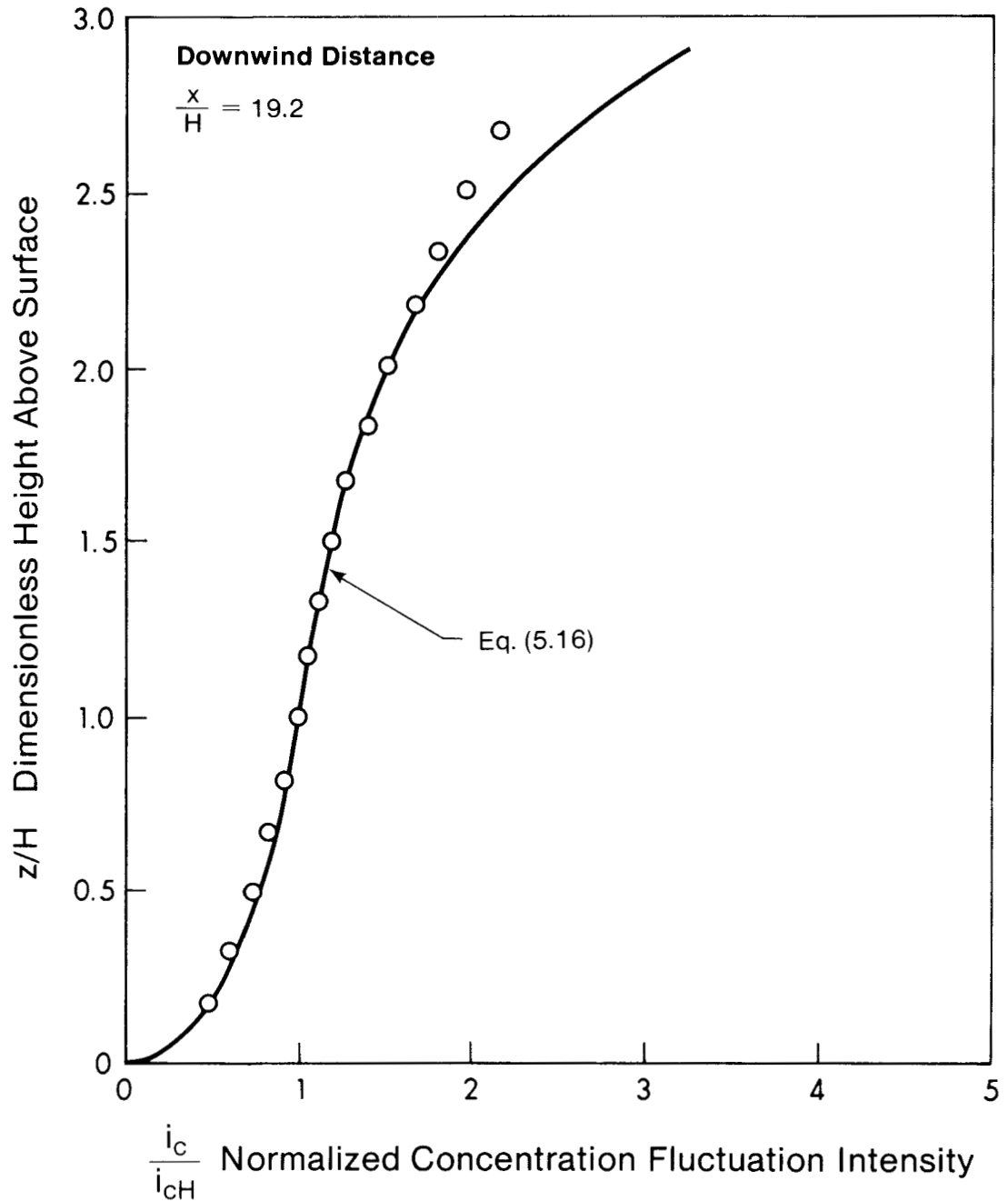
FIG. 5.13   Vertical Distribution of Concentration
Fluctuation Intensity at x/H = 19.2
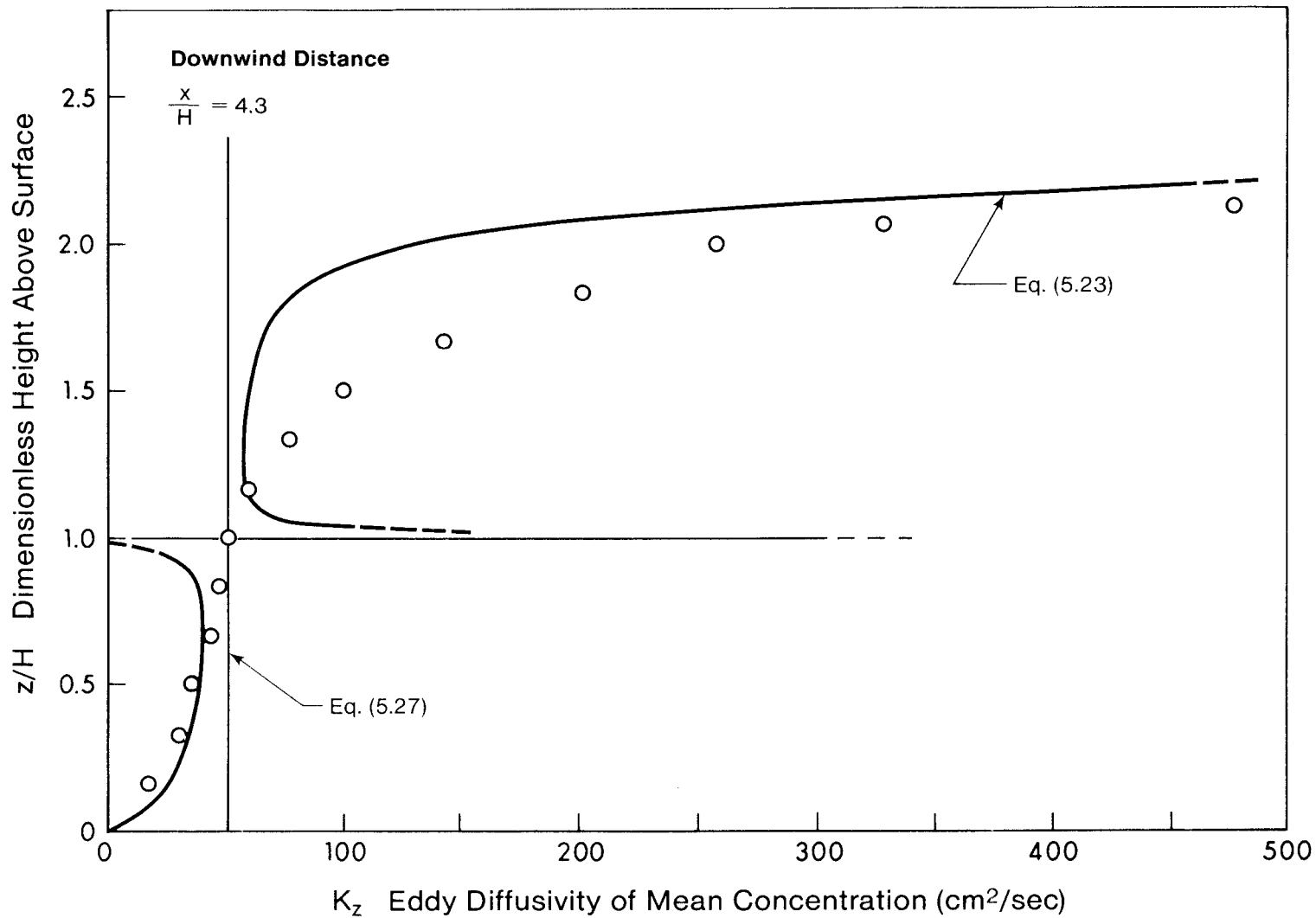
FIG. 5.14 Vertical Distribution of K_z at x/H = 4.3
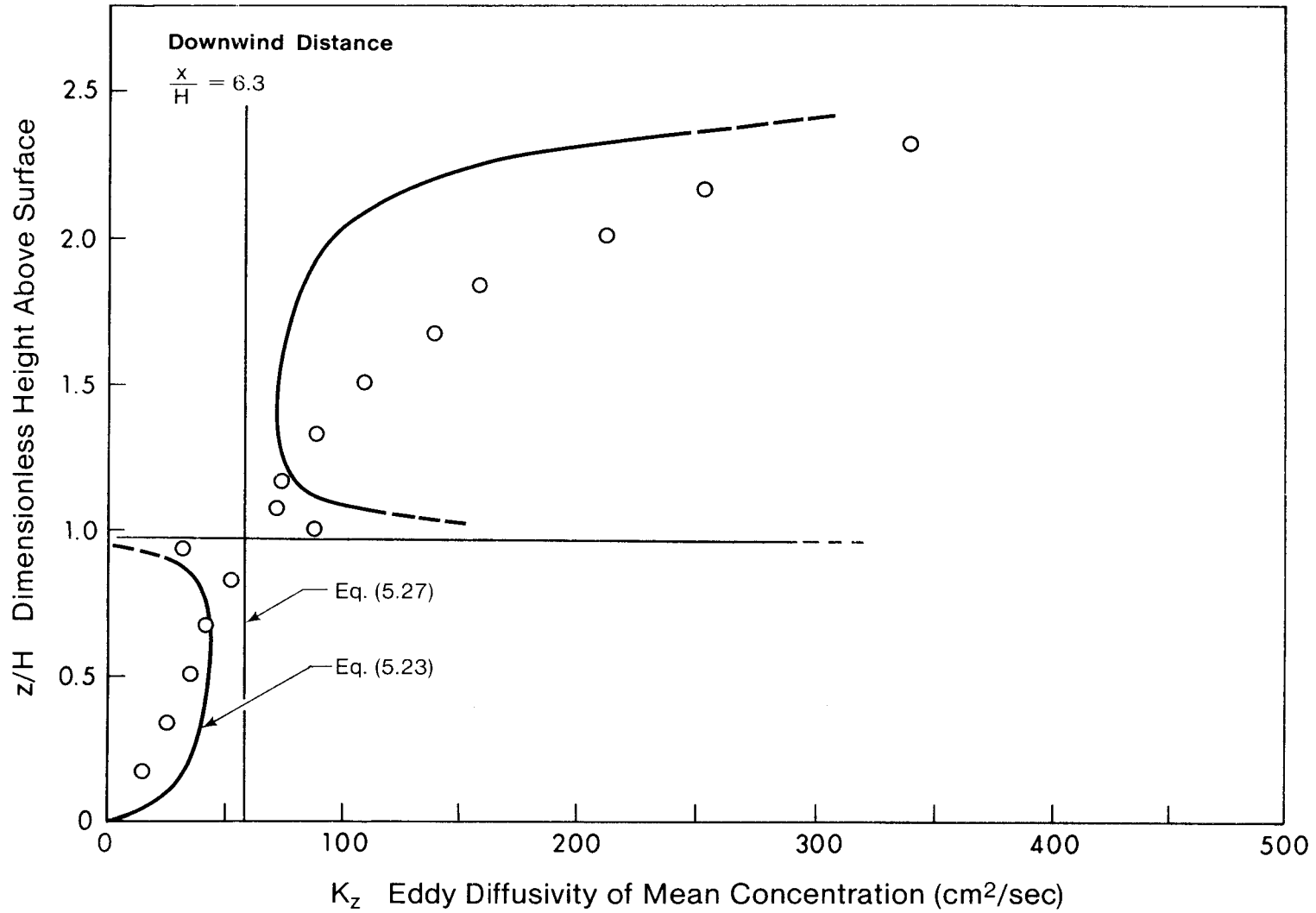
FIG. 5.15 Vertical Distribution of K_z at x/H= 6.3
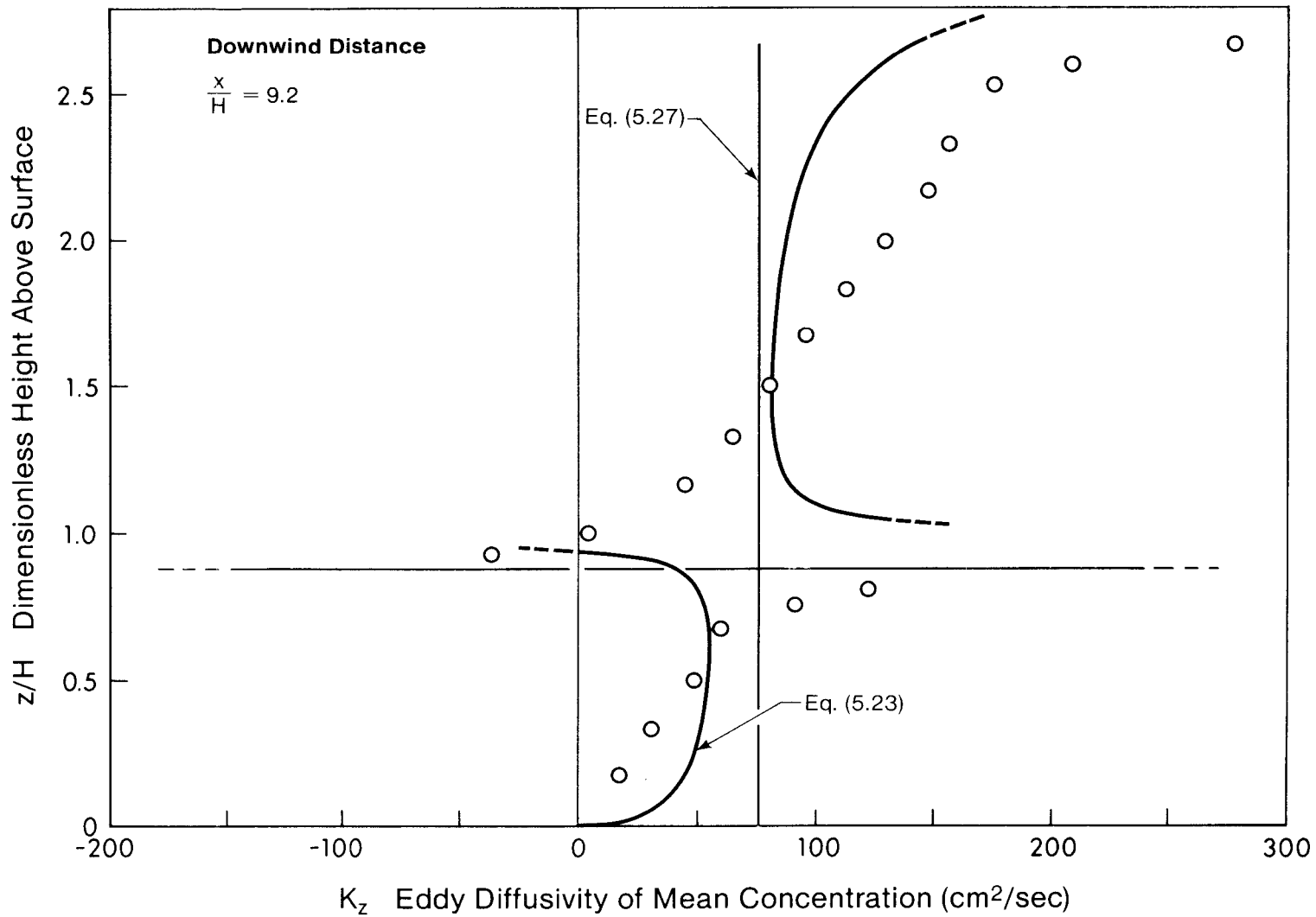
FIG. 5.16 Vertical Distribution of K_z at $x/H = 9.2$
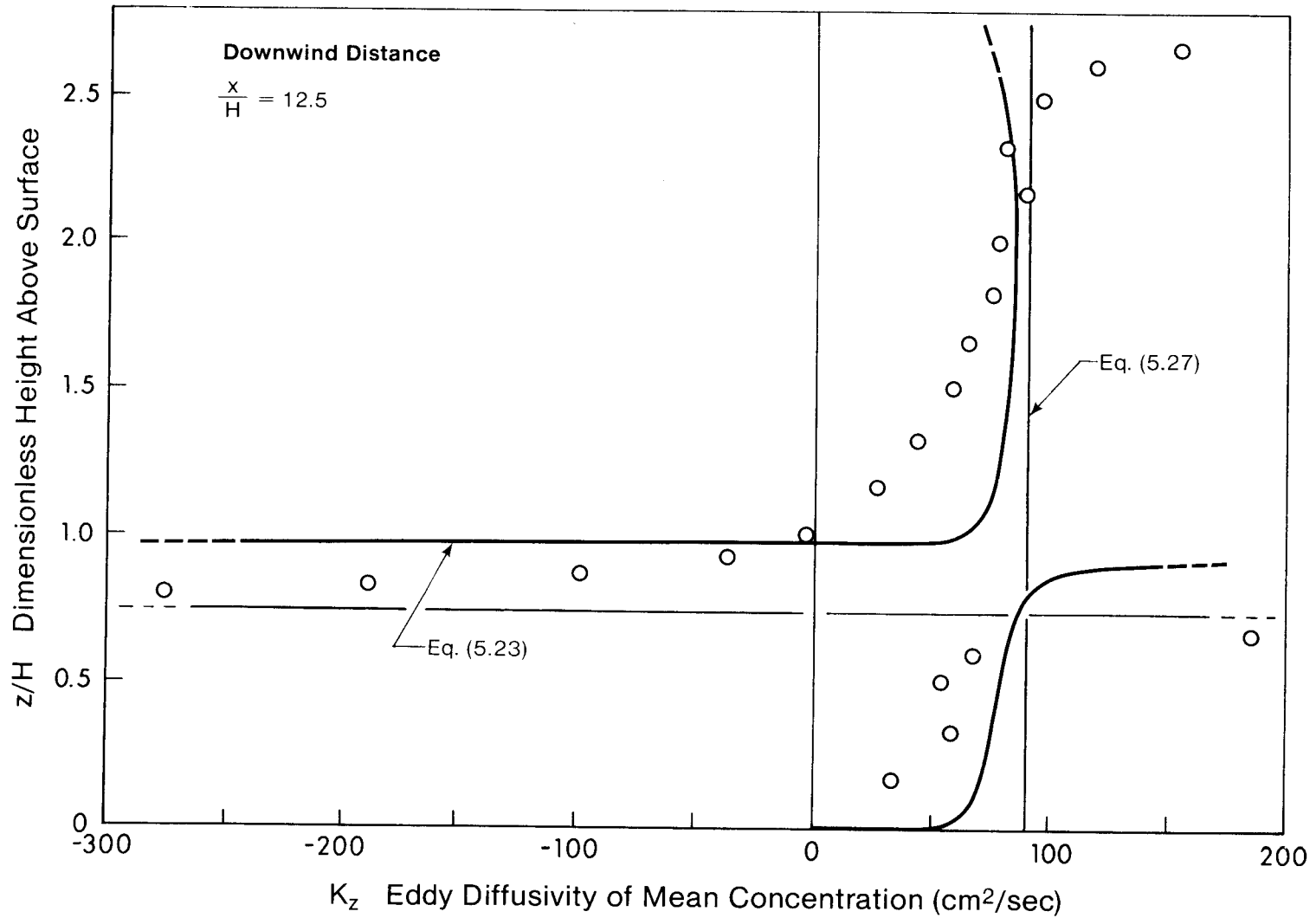
FIG. 5.17 Vertical Distribution of K_z at x/H = 12.5
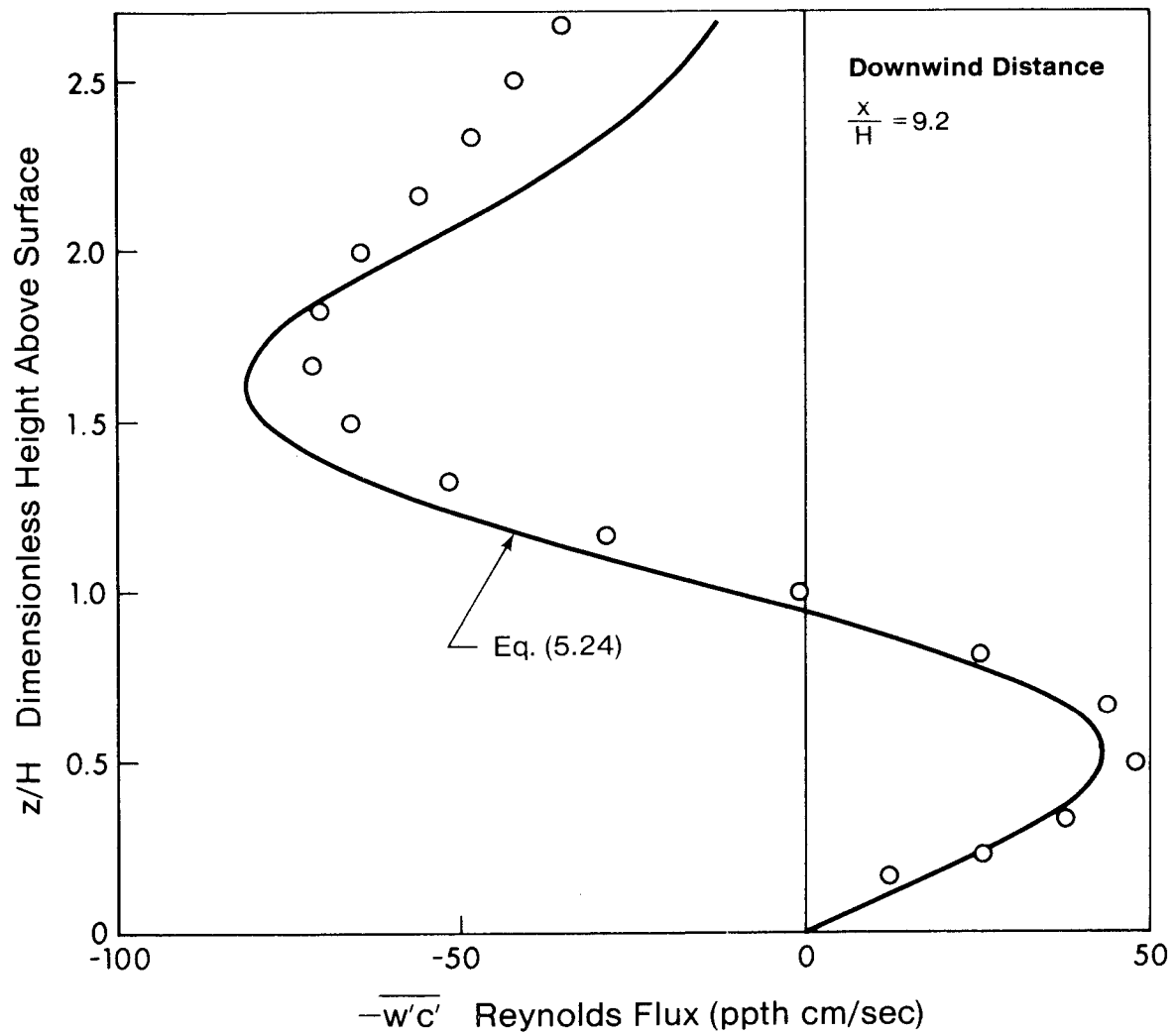
FIG. 5.18 Vertical Profile of Reynolds Flux $-\overline{w'c'}$ at x/H = 9.2

2.5

Production
$2K_z \left(\dfrac{\partial \bar{c}}{\partial z}\right)^2$

Dissipation
$\dfrac{6D}{U^2} \left(\overline{\dfrac{\partial c'}{\partial t}}\right)^2$

2.0

z/H   Dimensionless Height Above Surface

1.5

Net Dissipation

1.0   Source Height

0.5

Downwind Distance
$\dfrac{x}{H} = 4.3$

0

-4000   -2000   0   2000   4000

Dissipation of $\overline{c'^2}$ (ppth²/sec)
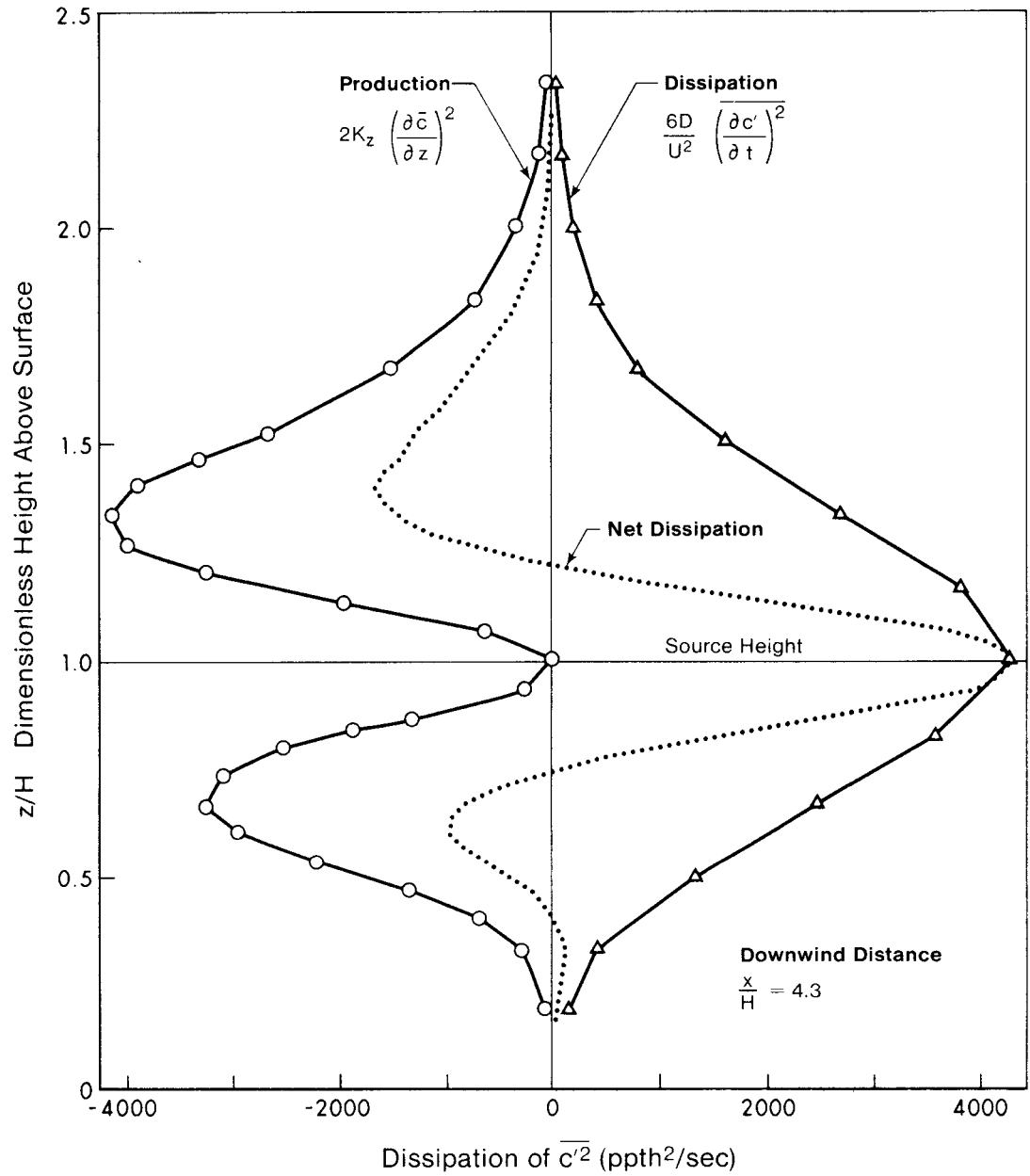
FIG. 5.19   Vertical   Profile   of   Variance   Production   and
Dissipation   on   Plume   Centerline   at   x/H = 4.3
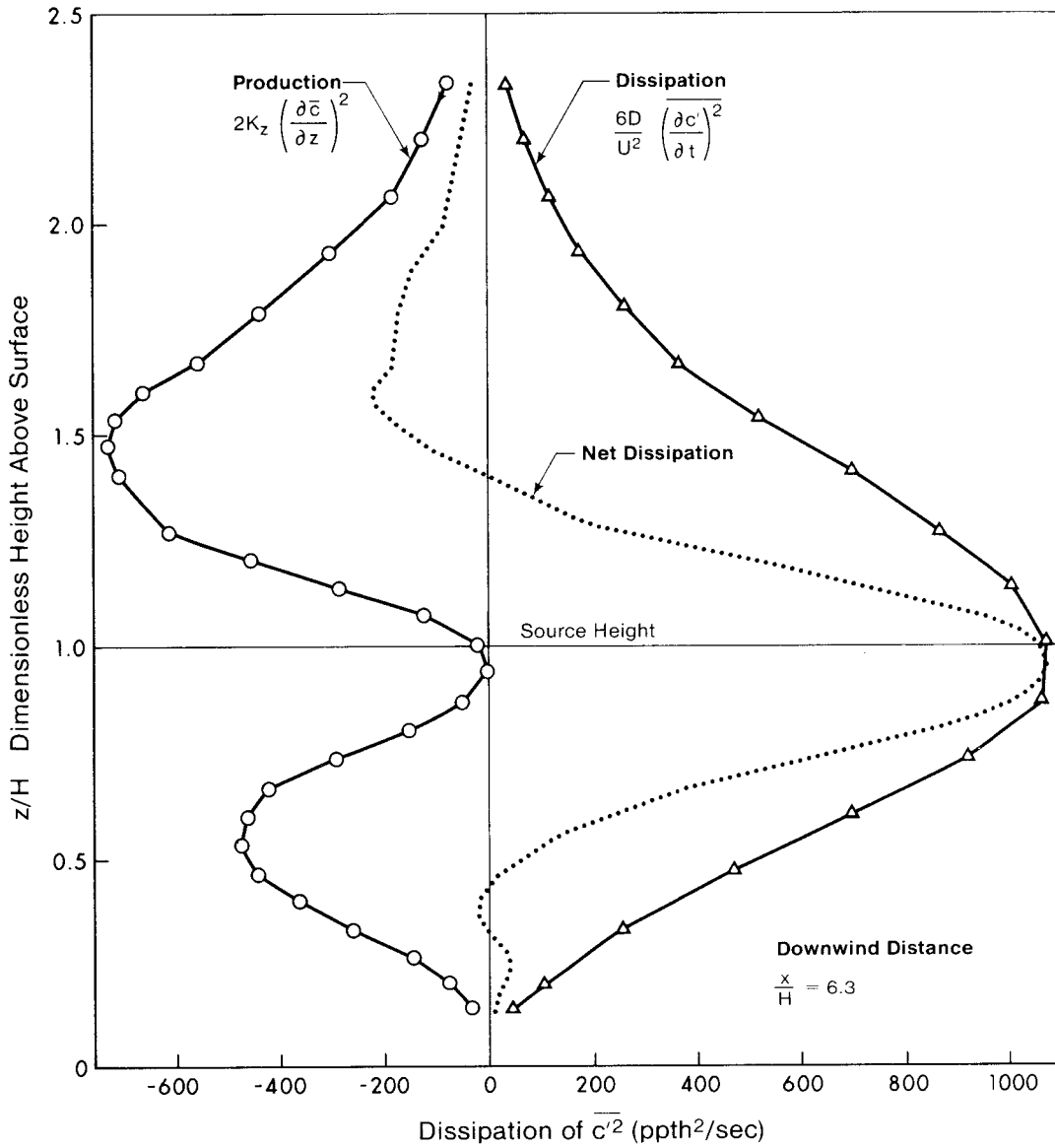
FIG. 5.20 Vertical Profile of Variance Production and

Dissipation on Plume Centerline at x/H= 6.3
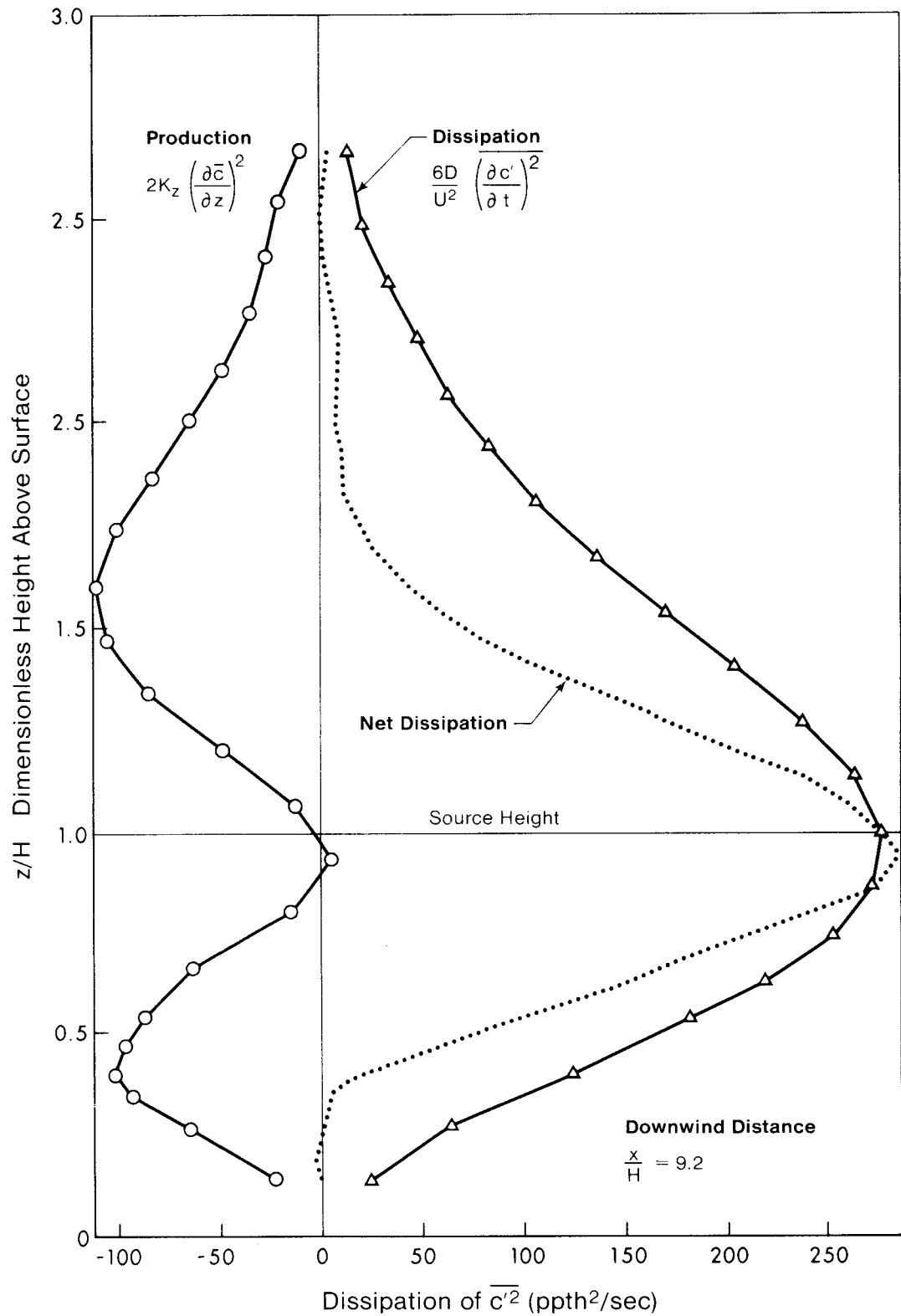
FIG. 5.21 Vertical Profile of Variance Production and
Dissipation on Plume Centerline at x/H = 9.2
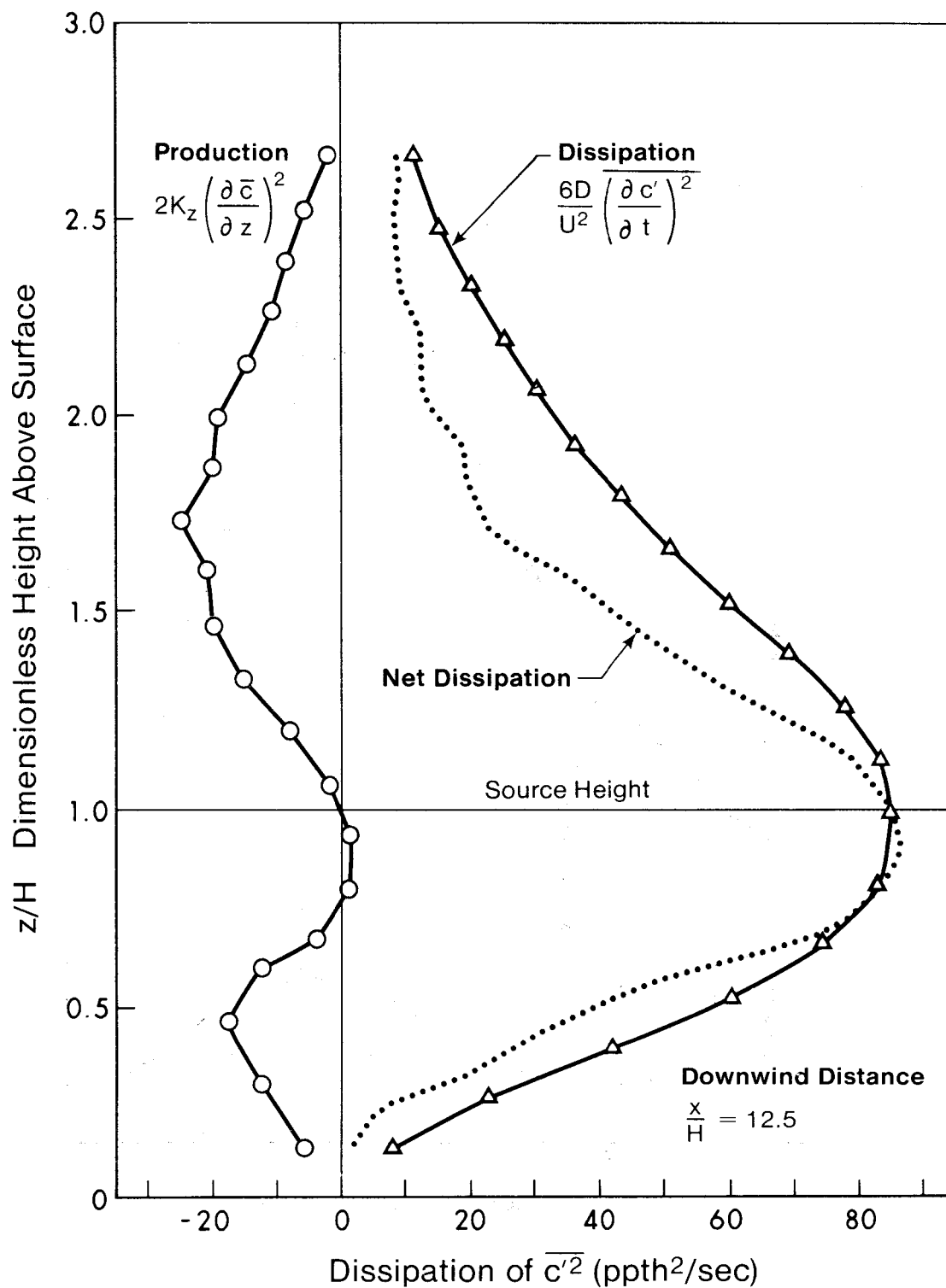
FIG. 5.22 Vertical Profile of Variance Production and Dissipation on Plume Centerline at x/H=12.5
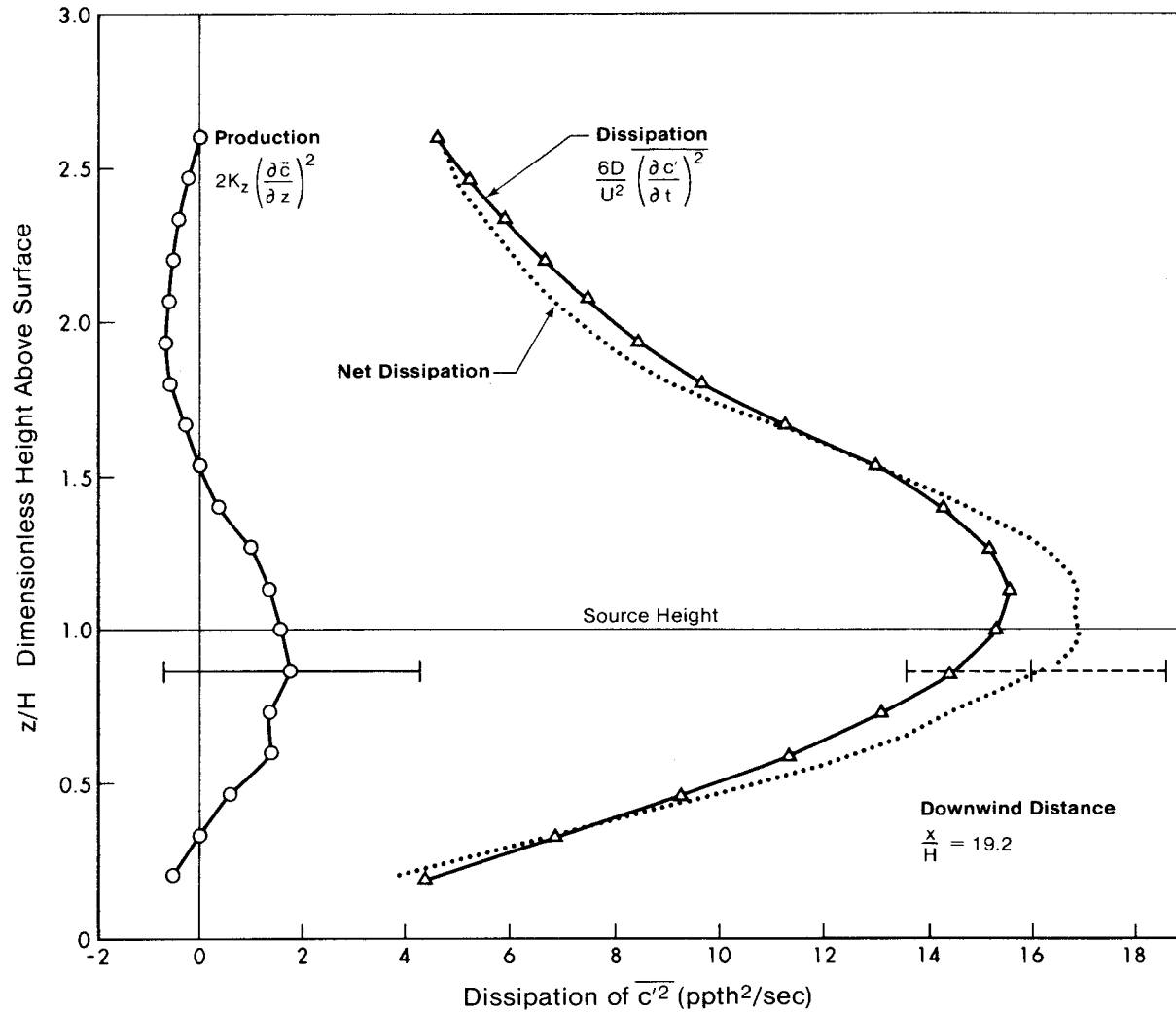
FIG. 5.23 Vertical Profile of Variance Production and Dissipation on Plume Centerline at x/H=19.2
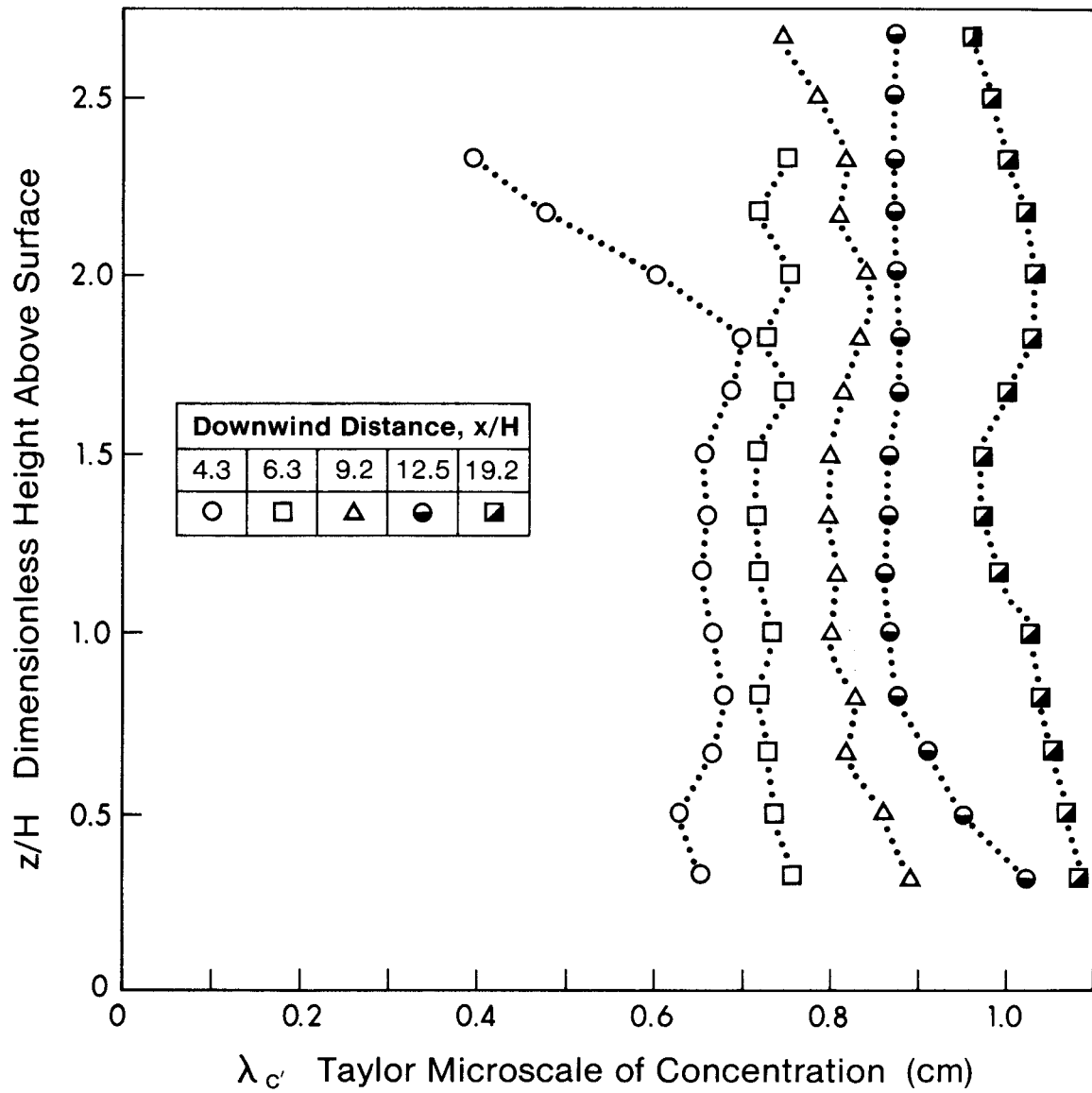
FIG. 5.24   Vertical   Profile   of   Concentration   Microscale
at   Several   Downwind   Locations

CHAPTER VI

STATISTICAL PROPERTIES OF THE

CONCENTRATION FLUCTUATIONS

6.0 Introduction

Most practical applications of atmospheric dispersion
theory focus on identifying the mean concentration expected
at a given point after a specified averaging time. However,
it is well known that the concentration at a receptor varies
with time, and a concentration history which results in
moderate mean concentrations can include short-term peak values
which are much higher than the mean. A measure of this
behavior is the 'peak-to-mean' concentration ratio, where the
'peak' concentration is defined as that value which is not
exceeded more than a fraction P of the time. Knowledge of the
peak concentration at a receptor is necessary when dealing
with pollutants which can have damaging effects at high concen-
trations over short times. Examples are the poisonous gases
hydrogen sulphide and carbon monoxide, the explosive gases
methane and hydrogen, and gases such as sulphur dioxide which
are often vented to atmosphere and to which some vegetation is
sensitive.

Calculation of peak concentrations requires that the
probability of occurrence be known for the entire range of

concentrations. The most compact way to present such data is with the probability density function, or pdf. In this chapter, an intermittent lognormal pdf is proposed as a model for concentration fluctuations downwind of an elevated point source in the atmospheric boundary layer. The model input parameters are mean concentration $\bar{c}$, concentration variance $\overline{c'^2}$ and intermittency γ, and can be computed from mathematical models or measured in the field or laboratory without the need for curve fitting. The pdf model has been compared with wind tunnel measurements, and predicts peak-to-mean concentration ratios within 20% of observed values so long as the dilution parameter D/i_c^2 is greater than 400. Peak concentrations at the ground occur about two thirds of the distance out to the point of maximum mean concentration.

6.1 Eddy Dilution

In experimental studies of atmospheric diffusion one often observes periods of zero concentration directly downwind of the source of emissions. This means that the sampled eddy contains no portion of the diffusing cloud. At the other extreme is observation of an eddy which consists of pure contaminant. In most real situations the atmosphere provides dilutant eddies in such numbers that the contaminant eddies are soon attenuated by the dilution process. In a dispersing plume we find pure contaminant eddies very rarely, pure dilutant eddies more frequently and, most frequent of all, the intermediate eddies

whose concentration fluctuations are the subject of this chapter.

Pure contaminant eddies are restricted mainly to a core region at the stack exit, similar in shape to the non-turbulent core region of a laminar jet in a turbulent cross-flow. These eddies are diluted to the intermediate form so quickly that, except for points a few stack diameters from the source, they can be ignored as a class. Of the remaining two eddy types, the frequency of occurrence of the pure dilutant eddies can be described with a single parameter γ, the concentration intermittency factor discussed in Chapter IV. The non-zero fraction of the concentration readings (from the intermediate eddies) have concentrations of $0 < c < c_{source}$. The probability of observing a concentration which lies in the range c to $c+\Delta c$ is characterized by $p(c)$, the probability density function, or pdf, of eddy concentration. The probability density function $p_I(c)$ for the intermediate eddies has the property that, if it is integrated over all concentrations, it must give a probability of γ. The delta-function pdf $p_D(c)$ for the pure dilutant eddies must integrate to $1-\gamma$, so that the total pdf $p(c)$ will integrate to unity as it should.

The detailed form of the pdf for concentration fluctuations is the subject of much investigation. Csanady (1973, p. 225) has presented a simple physical model to justify a lognormal distribution for the pdf of non-zero concentrations. His

heuristic argument begins with the assumption that eddy con-
centrations are reduced by a random series of independant
diluting steps, so that after N dilutions an eddy's concentra-
tion can be written as c_{source} multiplied by N positive random
numbers less than unity. The logarithms of a multiplicative
series are additive, so the Central Limit Theorem leads to a
normal distribution for the logarithms of eddy concentration
if the number N of diluting steps is large. Thus the concen-
trations themselves are not normally distributed, but have what
is called a 'lognormal' distribution given by

$$p(c) = \frac{1}{\sqrt{2\pi}\ \sigma_L c} \exp[\frac{-\ln^2(c/c_0)}{2\sigma_L^2}] , \qquad (6.1)$$

where c_0 is the median concentration of the lognormal distribu-
tion and σ_L is the logarithmic standard deviation. Csanady
(1973, p. 229) shows that these two parameters are related to
concentration mean $\bar{c}$ and variance $\overline{c'^2}$ by

$$\sigma_L = \sqrt{\ln(1 + i_c^2)} \qquad (6.2)$$

and

$$c_0 = \frac{\bar{c}}{\sqrt{1 + i_c^2}} , \qquad (6.3)$$

where fluctuation intensity i_c has been previously defined as

$i_c \equiv \sqrt{\overline{c'^2}}/\overline{c}$. This two-parameter model requires the mean concentration $\overline{c}$ and concentration variance $\overline{c'^2}$ as input, and does not account for the intermittency of concentration fluctuations. The two-parameter lognormal pdf model is used later in this chapter as the starting point for a more general three-parameter pdf which includes intermittency.

A two-parameter model which does incorporate intermittency is the exponential distribution discussed by Barry (1974). The pdf parameters are mean concentration $\overline{c}$ and intermittency γ, and appear in the cumulative distribution function

$$\mathbb{P}(c) = \int_0^c p(c)dc = 1 - \gamma \exp[\frac{-\gamma c}{\overline{c}}] \, .$$

Barry assumed intermittency to result from two effects, so that

$$\gamma = \gamma_\theta \cdot \gamma_{turb} \, ,$$

where γ_θ is due to large scale fluctuations in horizontal wind direction and γ_{turb} is due to atmospheric turbulence. For wind tunnel experiments the intermittency must be generated solely by turbulence, i.e. $\gamma \simeq \gamma_{turb}$, since $\gamma_\theta = 1$ results from the physical constraint of the tunnel walls. However, actual field measurements of γ are not so constrained. The result is that

short data averaging times ($t_{av} \lesssim$ hours) produce $\gamma \simeq \gamma_{turb}$, and longer averaging times ($t_{av} \gtrsim$ days), $\gamma \simeq \gamma_\theta$. Barry obtained the best fits to $\mathbb{P}(c)$ data from multiple receptor sites with long averaging times, when the model assumption that individual concentration observations were independant was most likely to be valid.

The Weibull three-parameter distribution has been used by Apt (1976) to fit two-week averages of atmospheric radio-activity data taken over periods of one year. The model assumes that $\gamma = 1$, and has the form

$$\mathbb{P}(c) = 1 - \exp[-(c-\delta)^\beta/\alpha] \, ,$$

where α, β and δ are empirically adjusted parameters. The parameter δ can be interpreted either as the background concentration or the lowest observed concentration, in which case its value can be obtained without curvefitting. However, if δ is used as a fitting parameter (as done by Apt) then it must be interpreted as the lowest concentration likely to be observed. The shape parameter β is entirely adjustable. If $\beta=1$ then c has an exponential distribution as described by Barry (1974). If $\beta=2$, the Rayleigh distribution results. For $\beta \simeq 3.25$ the concentration distribution would be close to Gaussian. Usually the scale parameter α is also adjustable. However, for the exponential case of $\beta=1$ and $\delta=0$, the parameter would be $\alpha=\bar{c}$. Such special cases provide the only opportunity to calculate

α without curvefitting.

A 'censored' three-parameter lognormal distribution has been proposed by Ott and Mage (1976) as a model which can incorporate a specified probability of zero concentrations. Although the authors do not say so, the model input parameters can be cast in the form of the mean concentration $\bar{c}$, the concentration variance $\overline{c'^2}$ and the intermittency factor γ. The calculation technique would be first to use the observed values of $\bar{c}$ and $\overline{c'^2}$ to compute the two-parameter lognormal pdf (for which $\gamma=1$). Then the pdf curve is displaced to the left (toward 'negative' concentrations) until the area under the portion to the left of the origin is equal to $1-\gamma$. This probability mass is then lumped as a delta function at the origin, so that negative concentrations do not occur. As a result of this procedure, the most probable concentration, which occurs at the highest point on the pdf curve, is reduced by intermittency, whereas the probability of its occurrence is unchanged. This is not realistic, because the more intermittency is observed, the less probable is observation of a specified non-zero concentration. Also, because the zero and non-zero populations are essentially independant, the magnitude of the most probable non-zero concentration should be unaffected by the presence of intermittency. Mage and Ott did not use the observed mean and variance as input parameters, but iteratively varied their parameters (related to $\bar{c}$ and $\overline{c'^2}$) so as to minimize the least squares error when fitting the observed cdf.

With very few exceptions the accepted procedure for verifying any model for the pdf of concentration fluctuations has been to adjust the model input parameters to obtain the least squares error fit to the observed cumulative distribution function. This method has several disadvantages. First, fitting the observed cdf is not as sensitive an indicator of an incorrect pdf model as is matching the observed pdf itself. Secondly, the curvefitting approach hides errors in the pdf model that might show up if the model parameters were calculated directly from observable variables like $\bar{c}$, $\overline{c'^2}$ and γ. Thirdly, curvefitting is a cumbersome way to determine the pdf parameters in situations where real-time data is being processed, such as the real-time air quality prediction systems used by some industries for supplementary emission control. Whenever the atmospheric or source conditions change, the fitting process must be repeated with a new observed time series which can not begin until steady conditions are established.

The purpose of this chapter is to develop and verify a probability density model for concentration fluctuations which incorporates concentration intermittency in a physically consistent manner and whose parameters can be computed from models or measured in the field or laboratory on a real-time basis.

6.2 The Intermittent Lognormal Distribution

The basic two-parameter lognormal distribution developed by Csanady (1973) is attractive as a model for concentration

fluctuations because:

- the model is based on a plausible heuristic argument;

- the parameters required are concentration mean $\bar{c}$ and variance $\overline{c'^2}$, and can be obtained from mathematical models or from measurements in the field or laboratory.

The disadvantage of the two-parameter lognormal model is that there is no provision for concentration intermittency (a non-zero probability of zero concentrations).

    If the eddy population consists of two groups,

1. contaminated eddies which are diluted in a lognormal manner as described by Csanady (1973, Ch. 7), and

2. uncontaminated eddies whose observed effect is signal intermittency,

then the probability of observing an uncontaminated eddy is $1-\gamma$, and the probability of observing a contaminated eddy is simply γ. It follows that the probability of observing an eddy with a specified degree of contamination must be γ times the lognormal probability function proposed by Csanady for non-zero concentrations. Then the probability density function $p(c)$ for intermittent concentration fluctuations must have the form

$$p(c) = (1-\gamma)\delta(c) + \frac{\gamma}{\sqrt{2\pi}\sigma_L c} \exp\left[\frac{-\ln^2(c/c_0)}{2\sigma_L^2}\right], \quad (6.4)$$

where $\delta(c)$ is a delta function located at the origin $c = 0$. The cumulative probability distribution is obtained by integrating (6.4),

$$\mathbb{P}(c) = \int_0^c p(c)dc = 1 - \frac{\gamma}{2} + \frac{\gamma}{2} \, \mathrm{erf}\left[\frac{\ln(c/c_0)}{\sqrt{2}\,\sigma_L}\right] , \qquad (6.5)$$

which gives $\mathbb{P}(\infty) = 1$ and $\mathbb{P}(0) = 1-\gamma$ as required. An expression similar to Eq. (6.5) has also been derived by Aitchison and Brown (1957, p. 95) in the context of economics data analysis to account for zero observations in an otherwise lognormal population.

In order to plot equation (6.4) for comparison with experiment, all the parameters in $p(c)$ must be known. These parameters are the concentration intermittency γ, and the median concentration c_0 and logarithmic standard deviation σ_L of the concentration fluctuations. The usual method would be to adjust γ, c_0 and σ_L until Eq. (6.4) for $p(c)$ matches the experimental data. However, the three adjustable parameters provide so much flexibility to the shape of $p(c)$ that simply being able to fit Eq. (6.4) to data does not establish the validity of the intermittent lognormal assumption. To test the lognormal hypothesis it is essential to compute these three parameters from directly observable variables. The concentration mean and variance are related to σ_L and c_0 by taking moments of the pdf about the origin $c = 0$. Thus

$$\bar{c} = \int_0^\infty c\; p(c)dc = \gamma c_0 \exp(-\sigma_L^2/2) \tag{6.6}$$

and

$$\overline{c'^2} = \int_0^\infty (c-\bar{c})^2\; p(c)dc = \gamma c_0^2 \exp(\sigma_L^2)[\exp(\sigma_L^2)-\gamma]\,,$$

$$\tag{6.7}$$

which can be combined to give the logarithmic standard deviation

$$\sigma_L = \sqrt{\ln[\gamma\;(1 + i_c^2)]} \tag{6.8}$$

and the median concentration

$$c_0 = \frac{\bar{c}}{\gamma\;\sqrt{\gamma(1 + i_c^2)}} \tag{6.9}$$

of the lognormally-distributed concentrations.

If the intermittency γ is set to unity, these expressions for σ_L and c_0 reduce to the non-intermittent Eqs. (6.2) and (6.3) derived by Csanady (1973). It is also possible to substitute into Eqs. (6.6) and (6.7) the expressions (4.23) and (4.24) developed by Becker, Hottel and Williams (1965) for the mean and variance of non-zero concentrations in an intermittent concentration field. The result is once again a reduction to the non-intermittent Eqs. (6.2) and (6.3) for σ_L and c_0. This is particularly interesting because it means that, in spite of

the explicit appearance of intermittency in Eqs. (6.8) and (6.9), the values of σ_L and c_o are in fact independant of γ. Thus the explicit intermittency in Eqs. (6.8) for σ_L and (6.9) for c_o is exactly cancelled by the implicit effect intermittency has on the values of $\bar{c}$ and $\overline{c'^2}$. It follows that if only the non-zero concentrations were used to calculate $\bar{c}$ and $\overline{c'^2}$, σ_L and c_o could be computed from the non-intermittent expressions (6.2) and (6.3). However, it is more common that $\bar{c}$ and $\overline{c'^2}$ are formed over periods which include instances of zero concentration, in which case the intermittent expressions (6.8) and (6.9) must be used for σ_L and c_o.

By directly computing the parameters c_o, σ_L and γ, we avoid the uncertainties which arise from curvefitting. If the pdf of equation (6.4) is computed using experimental measurements and is found to be a good fit to the observed pdf, the intermittent lognormality of concentration fluctuations would appear to be verified. Another advantage of physically meaningful pdf parameters is that, for simple geometries and boundary conditions, theories exist which describe the $\bar{c}$, $\overline{c'^2}$ and γ fields in plumes, and can provide all input data necessary for a complete probabilistic description of the concentration field. Chapter V discusses the use of a diffusion equation solution for the $\overline{c'^2}$ field, and presents a new theoretical model for the transport and diffusion of $\overline{c'^2}$ which is similar to the classic Gaussian plume model for mean concentrations.

6.2.1 The Effect of Gaussian Noise on Measured PDFs

Concentration observations in the field or laboratory are subject to measurement errors which obscure some of the information contained in the observations. Often the concentration signal is mixed with noise from the signal processing electronics, or the sampling process is subject to small randomly distributed errors. For the present study the noise level in the fast response detection system was measured by simply turning off the helium source. In the field the background noise can be measured whenever the wind is not blowing contaminants from the source to the receptor. If the data and noise are statistically independant, signal subtraction allows easy measurement of the concentration mean and variance. However, a parameter such as the probability density of the concentration fluctuations will be inseparably mixed with the noise, and signal processing can not extract it. The observed signal pdf is a composite of the unknown concentration pdf and the noise pdf. Thus the observed signal is given by

$$s = c + n, \qquad (6.10)$$

where $s = \bar{s} + s'$ is the instantaneous observed signal, $c = \bar{c} + c'$ is the instantaneous concentration and $n = \bar{n} + n'$ is the noise component. If n is independant of c, then

$$\bar{c} = \bar{s} - \bar{n} \tag{6.11}$$

and

$$\overline{c'^2} = \overline{s'^2} - \overline{n'^2}, \tag{6.12}$$

where $\bar{s}$ and $\overline{s'^2}$ are measured when contaminant blows over the receptor, and $\bar{n}$ and $\overline{n'^2}$ when it does not. In this way the pdf of n can also be directly observed.

If $p_1(n)$ is the known noise pdf and $p_2(c)$ is the unknown concentration pdf, then the observed signal pdf $p(s)$ is given by the convolution integral (Spiegel (1975, p. 47)),

$$p(s) = \int_{-\infty}^{\infty} p_1(n)p_2(s-n)dn = \int_{0}^{\infty} p_2(c)p_1(s-c)dc . \tag{6.13}$$

In the experiments, the noise pdf observed with the helium source turned off appeared to have a normal distribution, with mean $\bar{n}$ corresponding to zero ppth helium and standard deviation σ_n equivalent to 0.2 ppth helium. Using a Gaussian pdf for the noise, and assuming the intermittent lognormal model for concentration fluctuations, Eq. (6.13) becomes

$$p(s) = \int_{0}^{\infty} \frac{1}{\sigma_n \sqrt{2\pi}} \exp\left[\frac{-(s-c-\bar{n})}{2\sigma_n^2}\right]\{(1-\gamma)\delta(c) +$$

$$+ \frac{\gamma}{\sqrt{2\pi}\,\sigma_L c} \exp\left[\frac{-\ln^2(c/c_0)}{2\sigma_L^2}\right]\}dc , \tag{6.14}$$

which is partly integrated to yield

$$p(s) = \frac{1-\gamma}{\sigma_n \sqrt{2\pi}} \exp\left[\frac{-(s-\bar{n})^2}{2\sigma_n^2}\right] + \frac{\gamma}{2\pi\sigma_n\sigma_L} \int_0^\infty \frac{1}{c} \exp\left[-\frac{(s-c-\bar{n})^2}{2\sigma_n^2} - \frac{\ln^2(c/c_0)}{2\sigma_L^2}\right] dc .$$

(6.15)

The integral remaining in this expression for p(s) must be evaluated numerically.

The presence of noise in the concentration signal means that the intermittent lognormal model (6.4) cannot be tested directly. However, Eq. (6.15) for the observed signal is based on the intermittent lognormal assumption; if an observed concentration pdf known to contain Gaussian noise is well predicted by this theoretical pdf, then the assumption of intermittent lognormality for concentration fluctuations will be validated.

6.3 Comparison of Theory with Experiment

A number of pdfs were observed in the wind tunnel at the same time that measurements were made for $\bar{n}$, σ_n, c, $\overline{c'^2}$ and γ. The data was used to calculate the theoretical pdf p(s) from the convolution integral according to equation (6.15), which was compared with the pdf obtained by digitizing the concentration signals with an HP 3721A correlator and electronically sorting them into 100 equally spaced bins. An analog signal multiplier and voltage-to-frequency counter were used

to obtain $\bar{n}$, σ_n, $\bar{c}$ and $\overline{c'^2}$. Intermittency γ was measured by triggering a frequency counter whenever the signal was within a few microvolts of zero. Chapter III describes the measurement techniques in detail.

A measure of 'goodness of fit' is the coefficient of determination r^2_{pdf}, which indicates the amount of observed concentration pdf curve 'shape' accounted for by the intermittent lognormal model with Gaussian noise. If $r^2_{pdf} > 0.8$, one may conclude that the theory successfully reproduces a significant portion of the observed variation in the measured pdf. A value of $r^2_{pdf} = 1$ means that all factors affecting the observations are properly included in the theory. The coefficient of determination is calculated from

$$r^2_{pdf} = \frac{[N\Sigma x_i y_i - \Sigma x_i \Sigma y_i]^2}{[N\Sigma x_i^2 - (\Sigma x_i)^2]^2 [N\Sigma y_i^2 - (\Sigma y_i)^2]^2} , \qquad (6.16)$$

where x_i is the value of the observed pdf $p_{obs}(s_i)$ at concentration s_i, and y_i is the corresponding value of the theoretical pdf $p(s_i)$ calculated from Eq. (6.15). Summation is made over all values of s_i for which either $p_{obs}(s_i)$ or $p(s_i)$ is non-zero, with $i_{max}=100$ corresponding to the total number of data points generated for an observed pdf.

The comparison of Eq. (6.15) to data yields values of r^2_{pdf} which are tabulated against distance from source, height

above ground and lateral distance from plume centerline in Table 6.1 From this data it is apparent that:

- as one moves out along the plume centerline, there is a definite improvement in the ability of the intermittent lognormal model to describe the observed concentration fluctuations, and

- there is a tendency for the theory to fit observations better at the plume edges than on the plume centerline.

A direct graphical comparison of the observed and theoretical pdfs is made in Figs. 6.1 through 6.6; independant measurements of $\bar{c}$, $\overline{c'^2}$ and γ were used to compute the theoretical pdf shape parameters σ_L and c_o. The figures show that, in general,

- for the locations where measurements were made ($\frac{1}{2} < x/\Lambda_{Lu} < 4$), the most probable concentrations are about half as large and occur 50% more frequently than those predicted by the intermittent lognormal theory.

- small concentrations ($< \bar{c}/4$) occur more frequently than accounted for by the theory,

- midsize concentrations ($> \bar{c}/4$ and $< 2\bar{c}$) occur less frequently than expected from the theory, and

TABLE 6.1

SPATIAL DISTRIBUTION OF THE COEFFICIENT OF DETERMINATION r^2_{pdf}

Distance From Source (x/Λ_{Lu})	r^2_{pdf} Along Plume Centerline	Height Above Ground (z/H)	r^2_{pdf} at $x/\Lambda_{Lu} = 2.3$	Lateral Distance From Centerline (y/σ_y)	r^2_{pdf} at $x/\Lambda_{Lu} = 2.3$
0.8	0.422	0.2	0.824	0.0	0.755
1.2	0.509	0.5	0.902	0.5	0.728
1.7	0.623	1.0	0.755	1.0	0.855
2.3	0.755	1.5	0.787	-	-
3.6	0.964	2.0	0.889	-	-

- the frequency of occurrence of large concentrations
  (> $2\bar{c}$) is well predicted by the intermittent lognormal
  model.

It must be emphasized that these results apply only for down-
wind distances at which measurements were made. Some other
points to note are:

- a small error in measured intermittency can produce a
  large error in the calculated pdf of low concentrations;

- if the intermittency factor is close to unity, the inter-
  mittent lognormal model is a good fit to concentration
  fluctuations at ground level.

6.4 The Approach to Lognormality

The most important result of the comparisons in Figs.
6.1 to 6.6 is the uncovering of systematic differences between
theory and observations. The flow passing through the sensor
contains more low concentrations than can be explained by the
intermittent lognormal theory. This could be evidence of
probe induced flow distortion causing rapid diffusion inside
the probe. However, probe induced distortion of the pdf does
not explain the strong improvement in coefficient of determin-
ation with distance along the plume centerline. The observed
improvement is consistent with the fact that the opportunity
for plume eddy dilutions increases with travel time. The log-
normal assumption requires that the number of eddy dilutions

be large, and therefore the validity of the theory (and the magnitude of r^2_{pdf}) should improve with downwind distance, as was observed.

Another possible explanation for the difference between theory and experiment is that the independance of dilution steps assumed by the lognormal model may not prevail until the diffusion time becomes large compared to the Lagrangian time scale T_{Lc}. From Chapter IV, the observed Eulerian time scale T_{Ec} of concentration fluctuations was about 1.5 ms, so that for $T_{Lc} = \beta T_{Ec}$ where $\beta \simeq 4$, the Lagrangian time scale was about 6 ms. With an eddy convection velocity just over 8 m/s, the Lagrangian length scale Λ_{Lc} was 5 cm. The requirement that diffusion time be large compared to T_{Lc} is therefore satisfied for downwind distances greater than about 10 Λ_{Lc} = 50 cm $(x/\Lambda_{Lu} \simeq 3)$. This means that most of the pdf measurements were made relatively close to the source, where the diffusion time was not much larger than the Lagrangian integral time scale of eddy diffusion. This would help to explain the observed increase of r^2_{pdf} with distance along the plume centerline.

It is useful to have a parameter which indicates when the intermittent lognormal distribution can be expected to fit a set of concentration fluctuations. One possibility is to consider the degree of plume dilution D. The Gaussian relation for pollutant concentration along the centerline of an axi-symmetric plume is

$$\frac{\overline{c}}{c_s} = \frac{Q}{2\pi U \sigma^2} \, , \qquad (6.17)$$

or, in terms of a dilution factor D,

$$\frac{\bar{c}}{c_s} = \frac{Q/UA_s}{D} \quad , \tag{6.18}$$

where D is proportional to σ^2 and is computed from

$$D = \frac{Q/A_s}{U} \cdot \frac{c_s}{\bar{c}} \quad . \tag{6.19}$$

The coefficient of determination r^2_{pdf} between the observed pdfs and the intermittent lognormal theory has been plotted against dilution factor D in Figure 6.7. There is a strong trend for large dilution factors to be associated with a high degree of correlation between theory and experiment. This reflects the fact that the approach to lognormality requires many dilution steps, in which case the dilution factor must be large.

It is important to note that care must be taken in choosing an eddy convection velocity $U = x/t$ for calculating D from Eq. (6.19), especially when flow patterns are complex, such as in the neighborhood of hills and buildings. Fortunately, the eddy travel time t is frequently underestimated in complex flows. This can produce an underestimation of D, and possibly a decision not to use the intermittent lognormal theory when in fact it could be used. An overestimation of D can have the more serious consequence of providing encouragement to use the

lognormal theory in regions where it poorly fits the concentration pdf.

The coefficient of determination r^2_{pdf} gives only a qualitative measure of the accuracy to be expected from the intermittent lognormal model for concentration fluctuations. In practice the coefficient of determination r^2_{pdf} alone tells very little. For example, what r^2_{pdf} (or equivalently, D) is needed to give calculated peak-to-means that are within 20% of the observed values? A practical answer to this question is given in the next section, where it is shown that a lower limit to the ratio D/i^2_c must be exceeded in order to ensure accurate peak-to-mean calculations.

6.5 Peak-to-Mean Concentration Ratios

The 'peak' concentration at a receptor is defined as that value which is exceeded less than a fraction P of the time. The probability density function for concentration fluctuations may be used to calculate the peak-to-mean concentration ratios at various receptor locations. If c_p is such a peak, then, from Eq. (6.5),

$$\mathbb{P}(c_p) = (1 - P) = 1 - \frac{\gamma}{2} + \frac{\gamma}{2} \cdot \mathrm{erf}[\frac{\ln(c_p/c_o)}{\sqrt{2}\ \sigma_L}] . \quad (6.20)$$

Solving for $c_p/\bar{c}$ gives the peak-to-mean ratio

$$\frac{c_p}{\overline{c}} = \frac{1}{\gamma} \cdot \exp\{\frac{\sigma_L}{2}[2\sqrt{2}\, \mathrm{erf}^{-1}(1-\frac{2P}{\gamma})-\sigma_L]\} , \qquad (6.21)$$

where σ_L is computed from Eq. (6.8). Csanady (1973, p. 232) has developed similar equations for the case where $\gamma = 1$.

The peak-to-mean ratios which would be exceeded 10% of the time (P = .10) along the plume centerline were calculated using Eq. (6.21), and then compared with the values obtained by numerically integrating the observed pdfs.

The ratio of theoretical to observed peak-to-means increased towards unity as dilution factor D became larger, but decreased with distance off the plume centerline. This is evidence that some other parameter besides D plays a role in the approach to lognormality. Inspection of Eqs. (6.8) and (6.21) suggests that the square of concentration fluctuation intensity, i_c^2, has a suitably strong influence on computed peak-to-means, and Ch. V shows that i_c^2 increases rapidly with distance off plume centerline. These observations prompted the plot of theoretical to observed peak-to-mean ratio against the composite dilution parameter D/i_c^2, presented in Fig. 6.8. The data falls approximately on a straight line against this parameter, and indicates that calculated peak-to-mean ratios should be accurate to within 20% at any downwind locations for which D/i_c^2 is greater than 400. For elevated point sources in the atmospheric boundary layer, the reflected Gaussian plume model is a good choice for estimating D; the value of i_c^2 can be

obtained from measurements, or from the dissipated Gaussian model proposed for $\overline{c'^2}$ in Chapter V.

The intermittent lognormal pdf fits the data fairly well close to the ground (see Fig. 6.6), and Eq. (6.21) with σ_L derived from measurements has been used to calculate the peak-to-mean ratios exceeded 10% of the time (i.e. P = .10) along the ground under the plume centerline. Fig. 6.9 shows that the peak-to-mean concentration ratio for P = .1 is maximum at a distance of 0.6 x_{max}, where x_{max} is the distance to the point of maximum mean concentration. However, the largest actual peak concentrations occur farther out, at a distance of $x_{peak} = 0.8 x_{max}$ if P = .1. This distance becomes less as P is reduced. For example, if P = .01 then the largest short-term concentrations are about nine times larger than $\bar{c}$ and occur near 0.5 x_{max}. Since c_{peak} changes slowly near x_{peak}, a simple rule of thumb is to assume that peak concentrations occur at two thirds of the distance out to the point of maximum mean concentration, or

$$\frac{x_{peak}}{x_{max}} \simeq \frac{2}{3} \tag{6.22}$$

for values of P between 0.01 and 0.1.

The source height was not varied during these experiments, so no data is available to check if relation (6.22) applies to a range of source heights. It is possible to vary

the source height in the Gaussian model for $\overline{c'^2}$ presented in Chapter V. The results could then be used in Eq. (6.21) to establish the dependance of x_{peak} on source height.
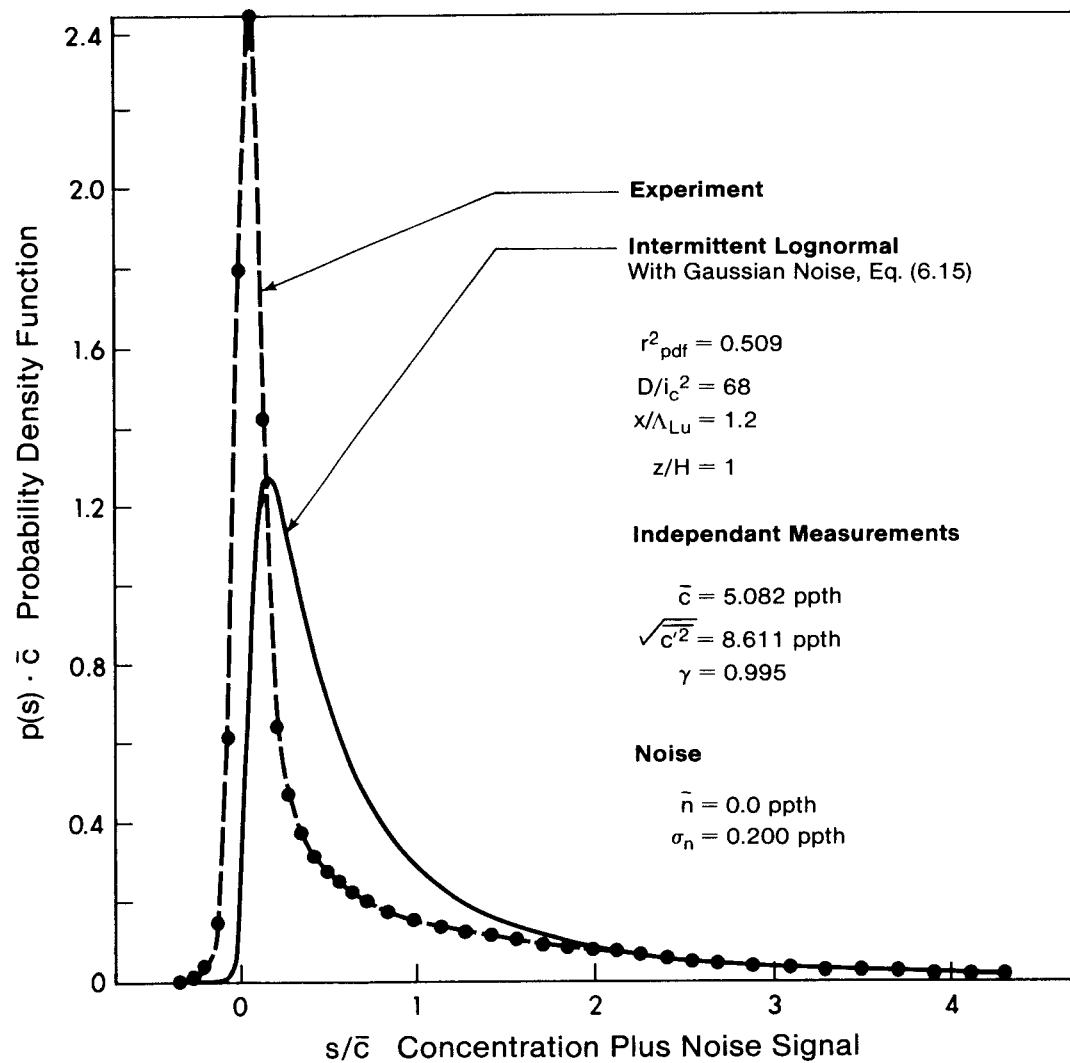
FIG. 6.1 PDF on Plume Centerline at $x/\Lambda_{Lu} = 1.2$

The figure contains the following labels and values:

y-axis: $p(s) \cdot \bar{c}$ Probability Density Function

x-axis: $s/\bar{c}$ Concentration Plus Noise Signal

Experiment

Intermittent Lognormal
With Gaussian Noise, Eq. (6.15)

$r^2{}_{pdf} = 0.509$

$D/i_c{}^2 = 68$

$x/\Lambda_{Lu} = 1.2$

$z/H = 1$

Independant Measurements

$\bar{c} = 5.082$ ppth

$\sqrt{\overline{c'^2}} = 8.611$ ppth

$\gamma = 0.995$

Noise

$\bar{n} = 0.0$ ppth

$\sigma_n = 0.200$ ppth

Experiment

Intermittent Lognormal
With Gaussian Noise
Eq. (6.15)

$r^2_{pdf} = 0.623$

$D/i_c^2 = 126$

$x/\Lambda_{Lu} = 1.7$

$z/H = 1$

Independant Measurement

$\bar{c} = 2.860$ ppth

$\sqrt{\overline{c'^2}} = 4.768$ ppth

$\gamma = 0.979$

Noise

$\bar{n} = 0.0$ ppth

$\sigma_n = 0.200$ ppth

FIG. 6.2 PDF on Plume Centerline at $x/\Lambda_{Lu} = 1.7$

FIG. 6.3 PDF on Plume Centerline at $x/\Lambda_{Lu} = 2.3$

Experiment

Intermittent Lognormal
With Gaussian Noise
Eq. (6.15)

$r^2_{pdf} = 0.964$

$D/i_c^2 = 542$

$x/\Lambda_{Lu} = 3.6$

$z/H = 1$

Independant Measurements

$\bar{c} = 1.118$ ppth

$\sqrt{\overline{c'^2}} = 1.436$ ppth

$\gamma = 0.891$

Noise

$\bar{n} = 0.0$ ppth

$\sigma_n = 0.149$ ppth
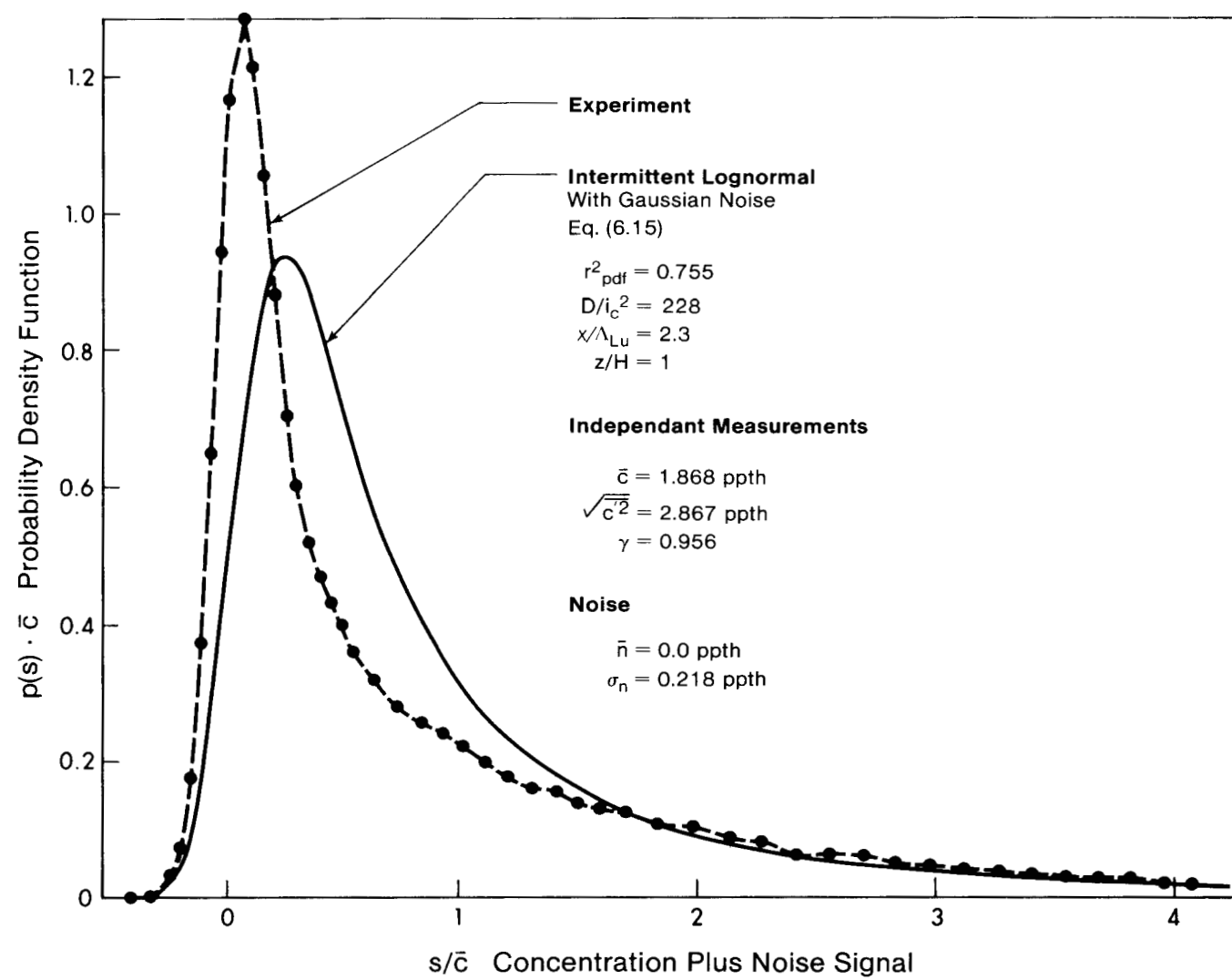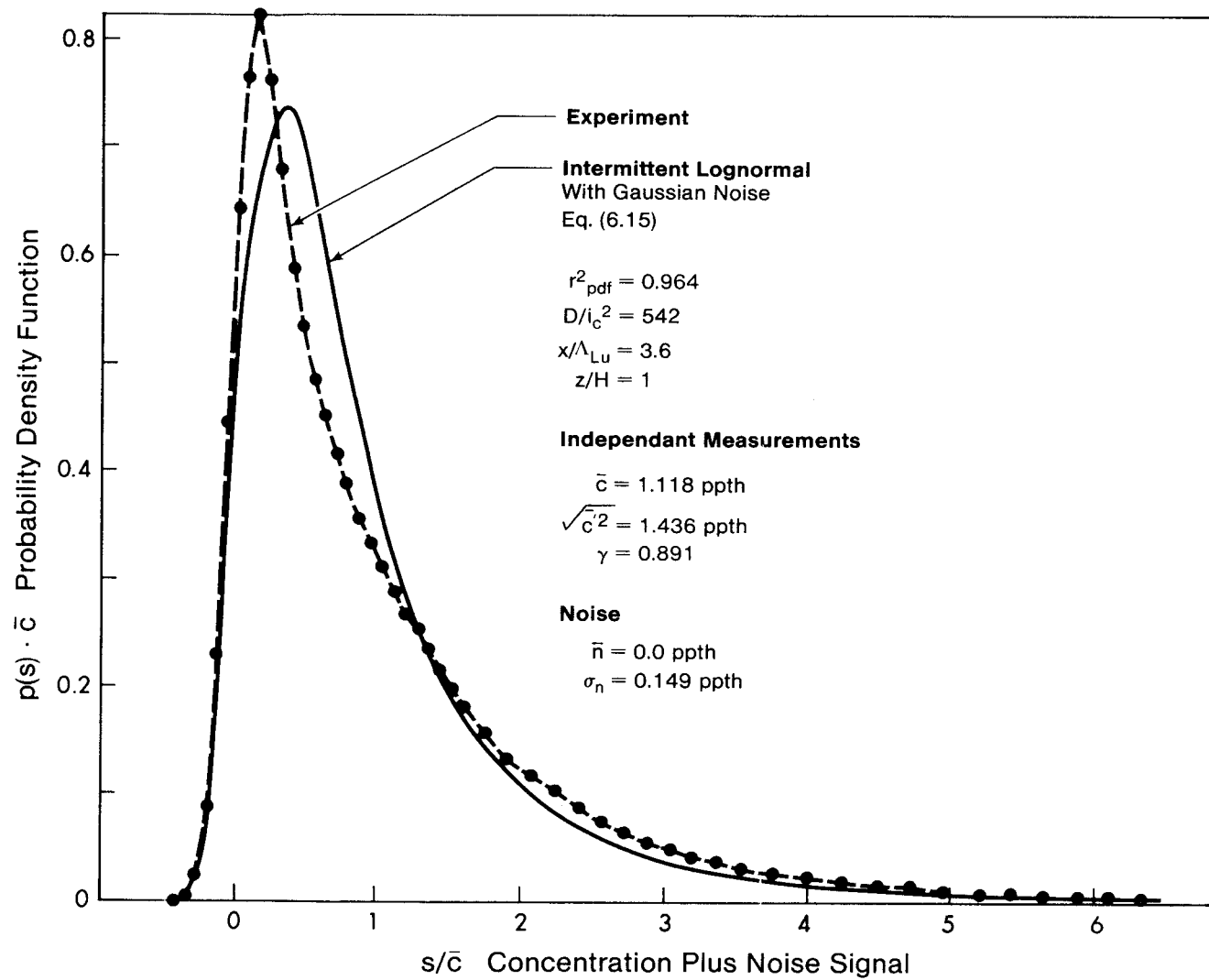
FIG. 6.4 PDF on Plume Centerline at $x/\Lambda_{Lu} = 3.6$
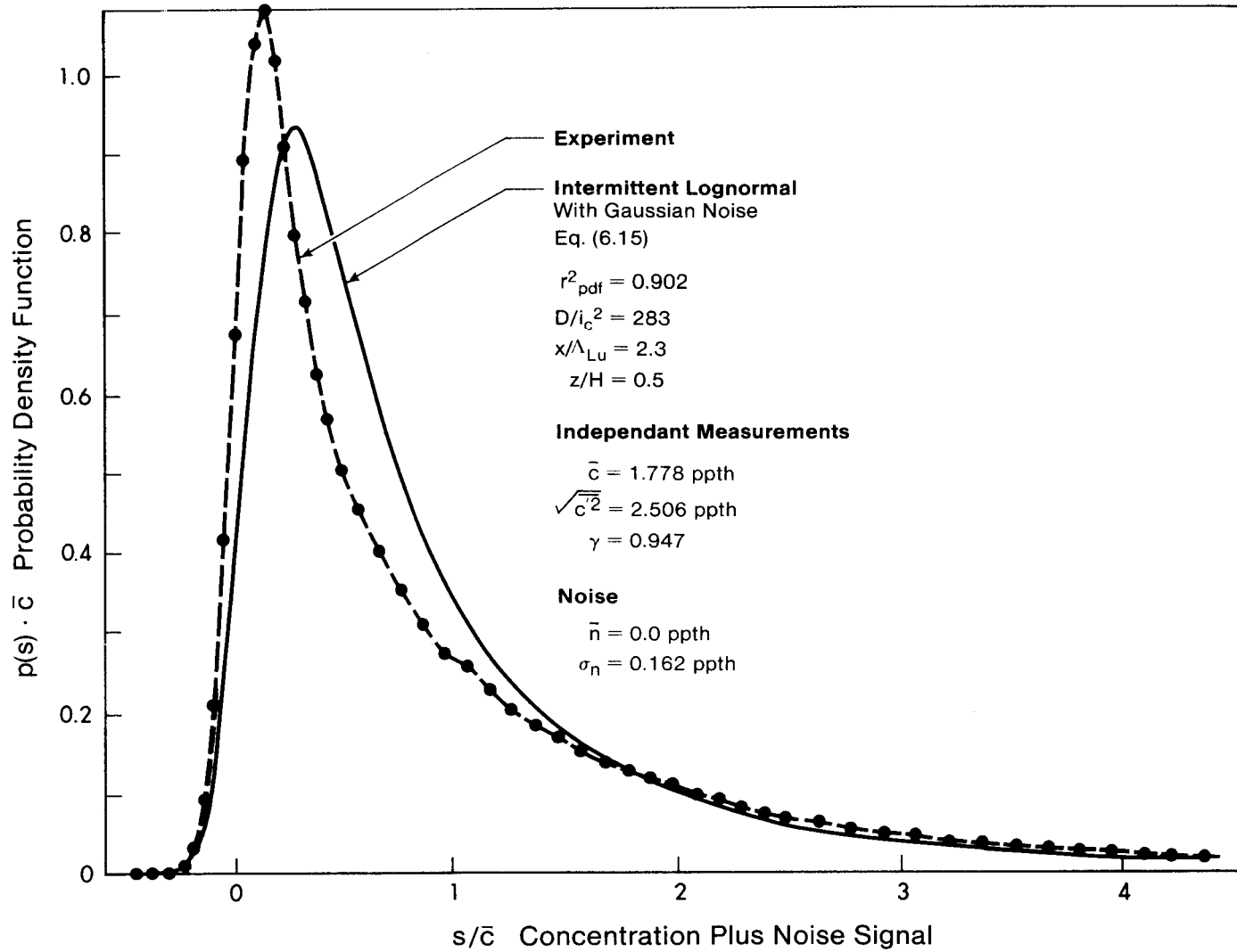
FIG. 6.5 PDF Below Plume Centerline at $x/\Lambda_{Lu} = 2.3$ and $z/H = 0.5$
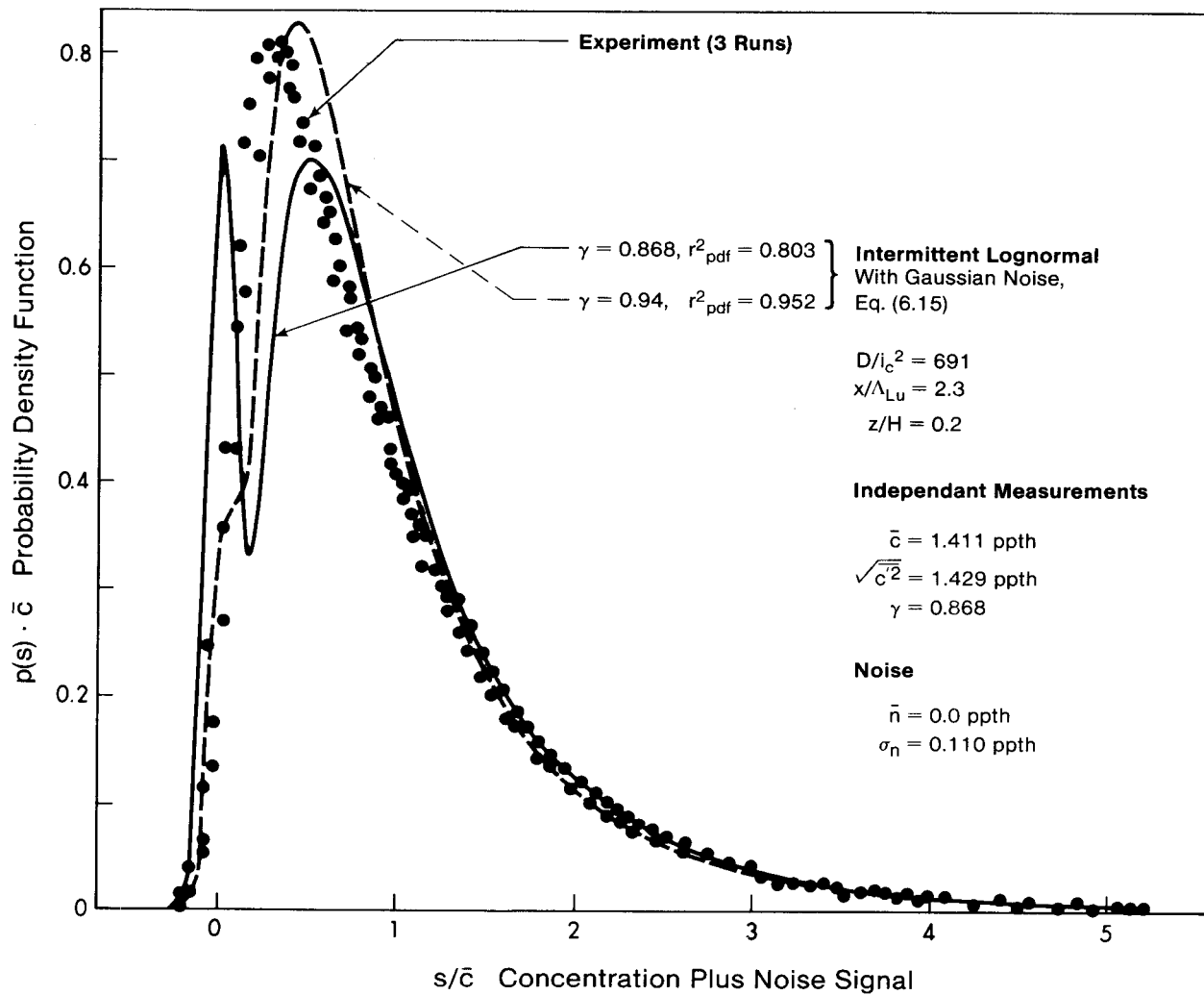
FIG. 6.6 PDF Below Plume Centerline at $x/\Lambda_{Lu} = 2.3$ and $z/H = 0.2$
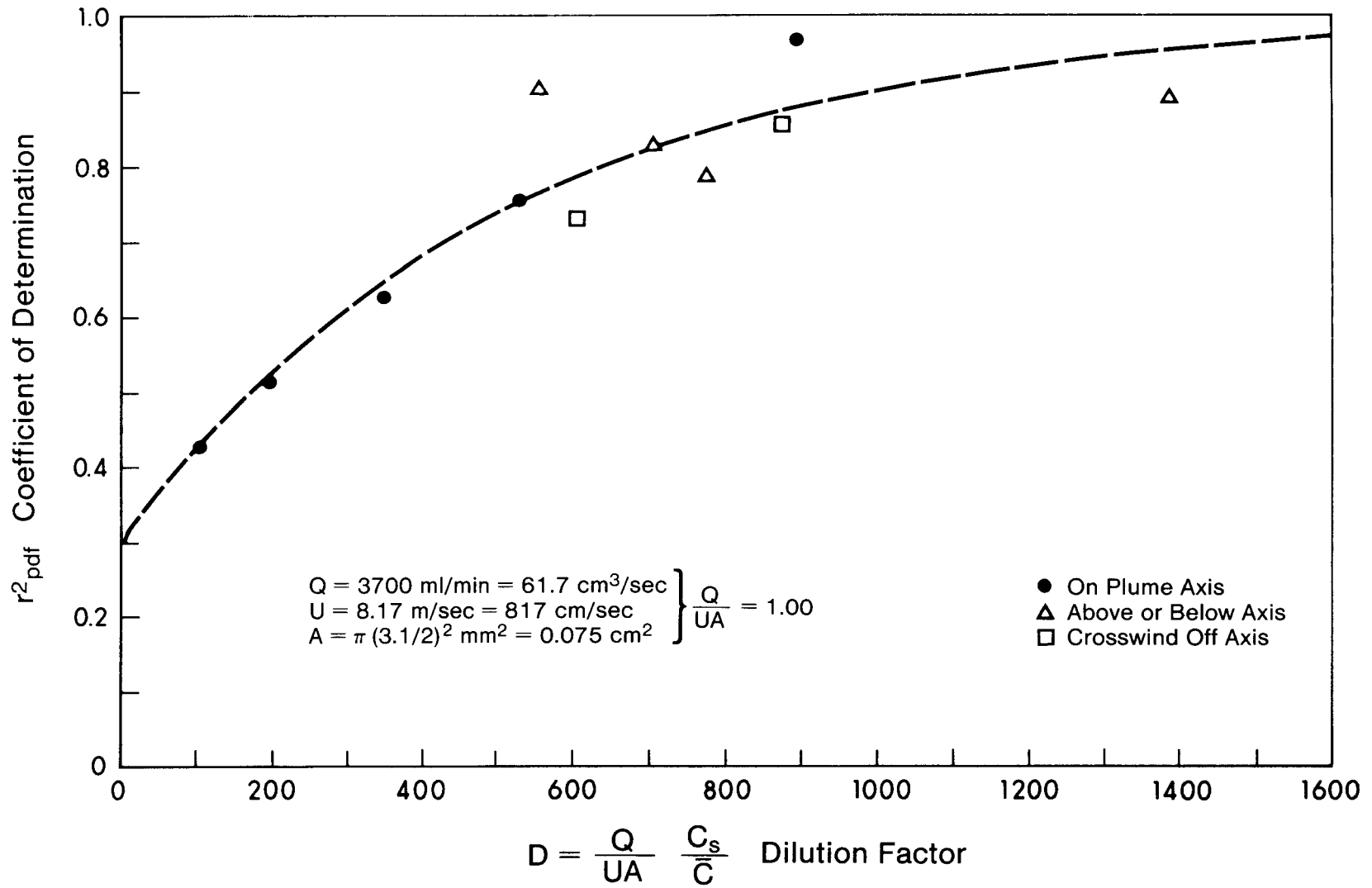
FIG. 6.7 Fit of Intermittent Lognormal PDF Theory vs. Dilution Factor D
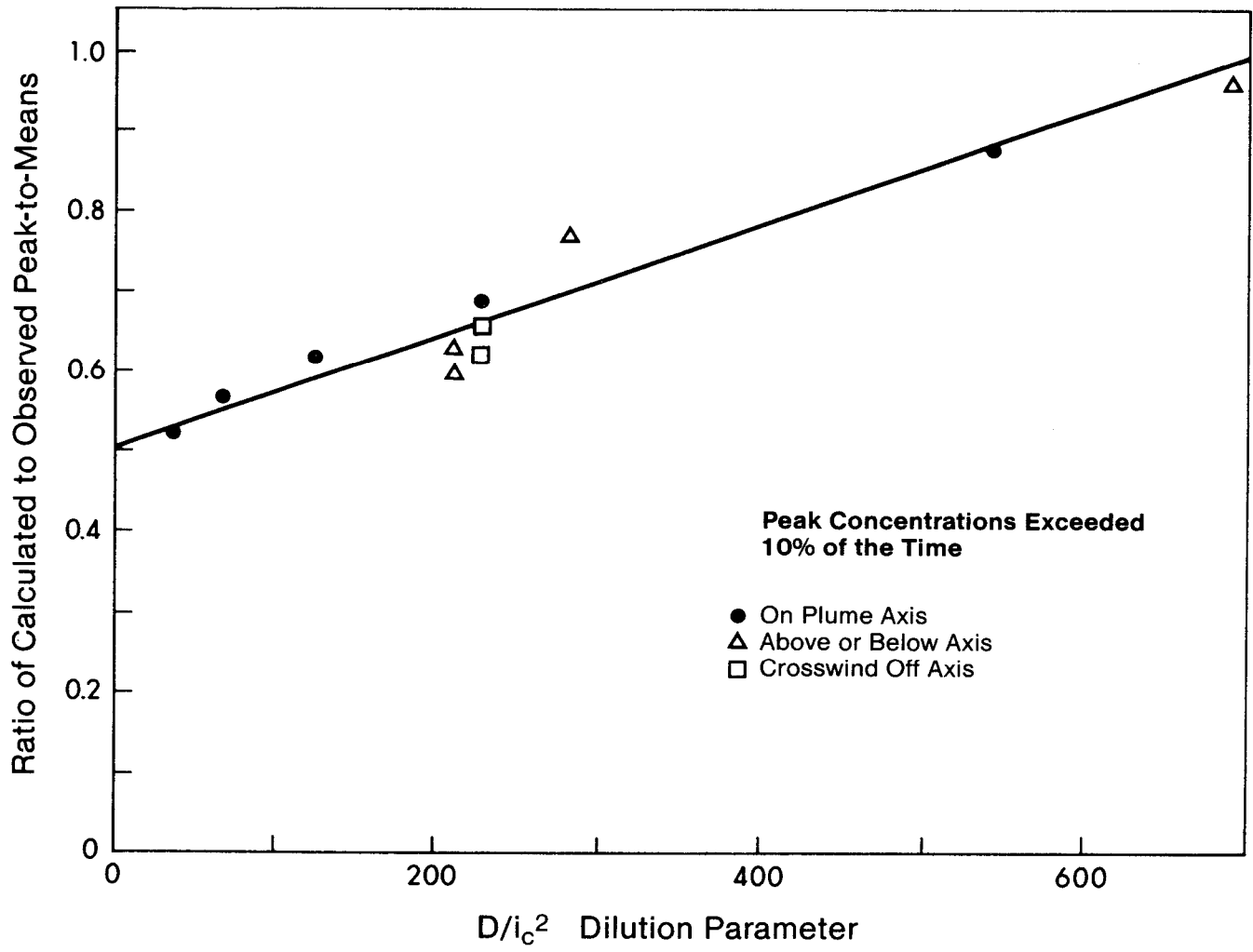
FIG. 6.8 Ratio of Calculated to Observed Peak-to-Means (for P=.1) vs. Dilution Parameter D/i_c^2
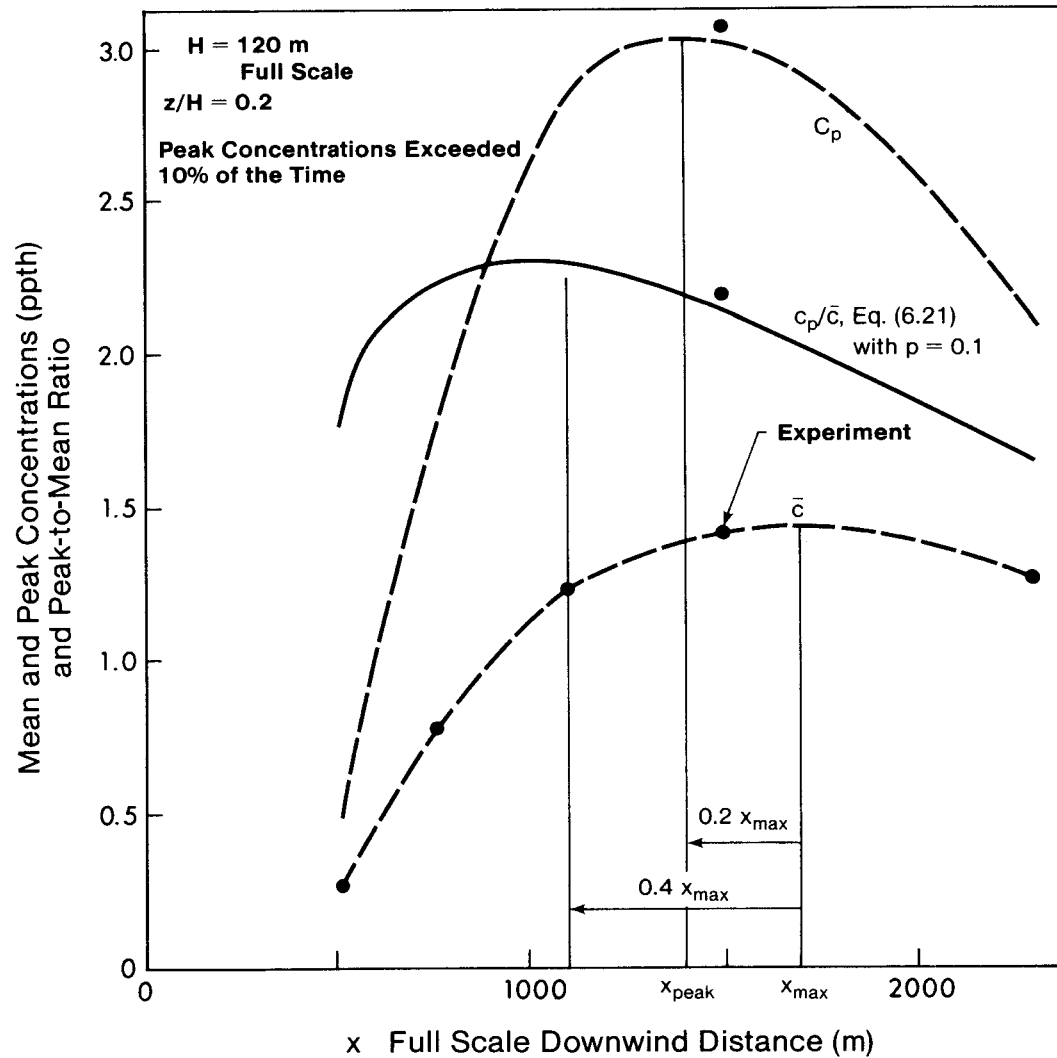
FIG. 6.9 Location of Highest Mean and Fluctuating Concentrations Near Ground Level for 4000:1 Model Scale Factor

CHAPTER VII

SUMMARY AND CONCLUSIONS

7.0 Summary of Results

Knowledge of the statistical and spatial distributions of fluctuating concentration in elevated plumes is necessary before the frequency of pollution incidents can be quantitatively established for the purpose of hazard assessment. This study uses a wind tunnel simulation of dispersion in the atmospheric boundary layer to provide new information on concentration fluctuations in plumes.

An aspirated single hot-film sensor, driven by a constant temperature anemometer, was developed to observe high-frequency fluctuations of helium tracer concentration in an atmospheric boundary layer wind tunnel. This fast-response probe produced about 1 mv output signal for a 2 ppth helium-air mixture, and could follow helium fluctuations up to 530 Hz, at which point the probe output was 3 db down. The noise level in the probe signal corresponded to an rms concentration fluctuation of 0.2 ppth about a mean of zero ppth. Undistorted measurements of concentration variance, probability density function, autocorrelations and spectra were obtained with the aspirated probe; measured values of concentration time derivative required correction for probe-induced dissipation

of the high-frequency signal components. Mean concentration
was measured with an existing high accuracy slow response
detector, since zero-drift problems required removal of the
mean component from the fast response probe signal by capaci-
tive AC coupling of the probe output.

Standard modeling techniques were used to stimulate
the rapid growth of a thick turbulent boundary layer within
the confines of a short wind tunnel. A passive, non-bouyant
plume of helium tracer gas was released above the tunnel floor
at the entrance to the test section. The wind tunnel boundary
layer simulated a neutrally stratified atmospheric boundary
layer with a model scale factor of 4000:1, which was verified
by comparison of measured tracer plume spreading rates with
those reported for the full scale. With this model scale
factor, the helium tracer represented a chimney plume which
had leveled off at a height of 120 m.

Vertical, lateral and alongwind profiles of concentra-
tion intermittency were measured in the tracer plume. The
profile shapes were well described by the Gaussian error
function model originally suggested by Corrsin and Kistler (1954)
for turbulence intermittency in round free jets. This inter-
mittency model worked well everywhere in the plume except near
the ground, which acted to constrain the Gaussian plume boundary
movements upon which the model is based.

Vertical and lateral profiles of mean tracer concen-
tration were fitted to the classic reflected Gaussian equation

often used to describe the mean concentration field. This model reproduced the present measurements with relative error less than 10% of the local concentration except at the plume edges and near the ground, where errors of 20-40% could be observed.

Profiles of concentration variance were measured in the tracer plume, and were well described by a new 'dissipated Gaussian' model developed during this study. In addition to providing a good fit to data, the model is easy to use because its shape parameters are the familiar plume spreads σ_y and σ_z which appear in the reflected Gaussian model for mean concentration. However, the dissipated Gaussian model for fluctuations has two disadvantages. First, it contains a 'source variance' term s_o about which not much is known; s_o is constant through the plume, but probably varies with atmospheric turbulence levels. Second, the model assumes complete dissipation of concentration flucutations at the ground. Total dissipation is unlikely to occur in practice, so it may be necessary to introduce an empirical 'dissipation coefficient' in the model. The present measurements lack sufficient detail to resolve this question.

The reflected Gaussian model has been used in the diffusion equation for $\bar{c}$ to derive an expression for the vertical eddy diffusivity under non-uniform wind conditions. This eddy diffusivity, which relates Reynolds flux $-\overline{w'c'}$ to the vertical gradient of mean concentration, was compared with

the vertical eddy diffusivity obtained by using measured data in the diffusion equation. The experimentally-derived vertical profiles of eddy diffusivity were complicated, having a discontinuity near the source height. Nevertheless, for non-uniform winds the Gaussian mean concentration model was able to successfully predict these diffusivity shapes.

An examination of terms in the variance conservation equation led to the observation that measured values of variance production and dissipation were not in local balance. As the plume moved downwind, production became negligible compared with the local dissipation of concentration variance $\overline{c'^2}$. This in turn led to an approximate balance equation for concentration variance which has the same form as the diffusion equation for mean concentration. The dissipated Gaussian variance model was shown to be a solution to this approximate conservation equation.

The measured variance dissipation term was found to be proportional to the local concentration variance, which confirmed Csanady's (1967) supposition that this should be so. In addition, the measurements supported Csanady's (1967) assumpttion that this proportionality factor is the reciprocal of a decay-time scale which is constant across a given plume section and which increases linearly with distance from the source.

Using the concept of independant zero and non-zero concentration eddy populations, an existing lognormal concentration probability model was modified to include intermittent

concentrations. Measured or calculated values of concentra-
tion mean, variance and intermittency can be used to compute
the shape parameters of this intermittent lognormal model
for the concentration probability density function. The
model was compared with wind tunnel measurements of the pdf
at several points within the plume, and predicted peak-to-mean
concentration ratios within 20% of observed values so long as
a dilution parameter D/i_c^2 was greater than 400. The highest
concentration peaks were observed to occur about two thirds
of the distance out to the point of maximum concentration.

7.1 Recommendations for Further Study

There are several aspects of the fluctuation model
that require further investigation. These can be listed by
model component as follows:

1. Plume Intermittency

- Additional work is necessary to provide an under-
  standing of the relationship between inter-
  mittency profile parameters $y_{1/2}$, $z_{1/2}$ and the
  plume spreads σ_y, σ_z.

- The intermittency model should be refined to
  account for the constraining influence of
  the ground. A truncated Gaussian model of
  plume motion near the ground may be useful
  in this regard.

- More measurements are needed to determine how the centerline intermittency depends on atmospheric turbulence and source/sensor characteristics.

2. Concentration Variance

- The manner in which the source variance parameter s_0 depends on atmospheric turbulence must be established before the dissipated Gaussian model can provide quantitative estimates of fluctuation intensity in full-scale dispersion situations.

- Detailed measurements of concentration variance at and near the ground are needed in order to assess the importance of incomplete surface dissipation of concentration fluctuations.

3. Intermittent Lognormality

- Full scale concentration data should be used to test the statistical model.

- The region of model applicability within the plume should be thoroughly investigated.

- For full-scale measurements, long-term average pdfs seem to be exponential, while short-term average pdfs appear log-normal. This apparent difference of form requires more study.

The measurements needed to guide model refinements for improved performance near the ground can be obtained only if the fast response probe is modified. Specifically, the probe must be redesigned for sampling near and flush to solid boundaries. Also, an alternative to the filter technique used to remove pressure fluctuations should be found, in order to avoid probe-induced dissipation of the high-frequency concentration fluctuations important to measurements of natural dissipation rates.

7.2 Concluding Remarks

This study has developed and tested a model for concentration fluctuations in plumes, which can be used to predict the fraction of time that a specified pollutant concentration is exceeded downwind of an industrial plant. This model can aid legislators in the formulation of more realistic constraints on the emission of waste gases by industry. Until such new regulations are put in effect, government and industry will continue to be faced with unavoidable violations of air quality standards which ignore the inherently random variability of pollutant concentrations dispersed by the turbulent atmosphere.

REFERENCES

Aitchison, J. and Brown, J.A.C., (1957);
The Lognormal Distribution, Cambridge University Press, London.

American Society of Mechanical Engineers (1968);
Recommended Guide for the Prediction of the Dispersion of Airborne Effluents, Smith, M.E., (ed.).

Apt, K. E., (1976);
"Applicability of the Weibull Distribution Function to Atmospheric Radioactivity Data", Atmos. Env., V10, pp. 777-781.

Barry, P. J., (1971);
"Use of Argon-41 to Study the Dispersion of Stack Effluents; Nuclear Techniques in Environmental Pollution; International Atomic Energy Agency", Vienna, Austria; pp. 241-255.

Barry, P. J., (1974);
"Stochastic Properties of Atmospheric Diffusivity", Atomic Energy of Canada Ltd., Chalk River Nuclear Laboratories, Chalk River, Ontario; to be published in "The Effects of Sulfur in Canada" by NRC of Canada, Ottawa, Ontario.

Batchelor, G. K., (1949);
"Diffusion in a Field of Homogeneous Turbulence", Australian J. Sci. Res., 2: pp. 437-450.

Batchelor, G. K., Townsend, A. A. and Howells, I. D., (1959);
"Small Scale Variation of Convected Quantities Like Temperature in Turbulent Fluid", J. Fluid Mech., V5, pp. 113-134.

Becker, H. A. and Booth, B. D., (1975);
"Mixing in the Interaction Zone of Two Free Jets", Report to the Chem. Eng. Dept., Queens University, Kingston, Ontario.

Becker, H. A., Hottel, H. C. and Williams, G. C., (1965);
"Concentration Intermittency in Jets, Tenth Symposium (International) on Combustion", pp. 1253-1263.

Becker, H. A., Hottel, H. C. and Williams, G. C., (1967a); "The Nozzle-Fluid Concentration Field of the Round Turbulent, Free Jet", J. Fluid Mech., V30, pp. 285-303.

Becker, H. A., Hottel, H. C. and Williams, G. C., (1967b); "On the Light-Scatter Technique for the Study of Turbulence and Mixing", J. Fluid Mech., V30, pp. 259-284.

Becker, H. A., Rosensweig, R. E. and Gwozdz, J. R., (1966); "Turbulent Dispersion in a Pipe Flow", A.I. Ch. E. Journal, V12, pp. 964-972.

Blackshear, P.L. and Fingerson, L. (1962); "Rapid-Response Heat Flux Probe for High Temperature Gases", ARS Journal, November, pp. 1709-1715.

Corrsin, S. and Kistler, A. L. (1955); "Free Stream Boundaries of Turbulent Flows", NACA Report 1244.

Counihan, J. (1969); "An Improved Method of Simulating an Atmospheric Boundary Layer in a Wind Tunnel", Atmos. Env., V3, pp. 197-214.

Counihan, J., (1970); "Further Measurements in a Simulated Atmospheric Boundary Layer", Atmos. Env., V4, pp. 259-275.

Counihan, J., (1975); "Adiabatic Atmospheric Boundary Layers: A Review and Analysis of Data from the Period 1880-1972", Atmos. Env., V9, pp. 871-905.

Crum, G. F. and Hanratty, T. J., (1965); "Dissipation of a Sheet of Heated Air in a Turbulent Flow", Appl. Sci. Res., A, V15, pp. 177-195.

Csanady, G. T., (1967); "Concentration Fluctuations in Turbulent Diffusion", J. Atmos. Sci., V24, pp. 21-28.

Csanady, G. T., (1969); "Dosage Probabilities and Area Coverage from Instantaneous Point Sources on Ground Level", Atmos. Env., V3, pp. 25-46.

Csanady, G. T. (1973); Turbulent Diffusion in the Environment, D. Reidel Publishing Co., Boston.

Fackrell, J. E., (1976);
"A Review of Methods of Measuring Fluctuating Concentration Levels in Turbulent Flow", Central Electricity Generating Board, Research Dept., R/M/M177, Job No. TL212.

Fiedler, H. E., (1974);
"Transport of Heat Across a Plane Turbulent Mixing Layer", Adv. in Geophys., V18A, pp. 93-109.

Gibson, C. H. and Schwarz, W. H., (1963a);
"The Universal Equilibrium Spectra of Turbulent Velocity and Scalar Fields", JFM, V16, pp. 365-384.

Gibson, C. H., and Schwarz, W. H., (1963b);
"Detection of Conductivity Fluctuations in a Turbulent Flow Field", JFM, V16, pp. 357-364.

Gifford, F. A., (1959);
"Statistical Properties of a Fluctuating Plume Dispersion Model", Adv. in Geophys., V6, pp. 117-138.

Hay, J. S. and Pasquill, F., (1959);
"Diffusion from a Continuous Source in Relation to the Spectrum and Scale of Turbulent", Adv. in Geophys., V6, pp. 345-365.

Hinze, J. O., (1975);
Turbulence, McGraw-Hill Series in Mech. Eng., McGraw-Hill Book Co., Toronto.

Holman, J. P., (1968);
Heat Transfer, McGraw-Hill Book Co., Toronto.

Kewley, D. J., (1978);
"Atmospheric Dispersion of a Chemically Reacting Plume", Atmos. Env., V12, pp. 1895-1900.

Kumar, A., (1978);
"Pollutant Dispersion in the Planetary Boundary Layer", Syncrude Canada Ltd. Professional Paper 1978-1.

Kuretsky, W.H. (1975);
"On the Use of an Aspirating Hot-Film Anemometer for the Instantaneous Measurement of Temperature", M.Sc. Thesis. Mech. Eng. Dept., U. of Minnesota.

Liu, H. T. and Karaki, S., (1972);
"An Optical System for Measurement of Mean and Fluctuating Concentration in a Turbulent Air Stream", J. Scient. Inst., V5, pp. 1165-1168.

208

Motycka, H. and Leutheusser, H. J., (1972);
   "Concentration Meter for Wind Tunnel Studies of Gaseous
   Dispersion", Atmos. Env., V6, pp. 911-916.

Nappo, C. J. Jr., (1979);
   "Relative and Single Particle Diffusion Estimates Deter-
   mined From Smoke Plume Photographs", Fourth Symposium on
   Turbulence, Diffusion and Air Pollution; Am. Met. Soc.,
   Jan. 1979, Reno, Nevada.

Ott, W. R. and Mage, D. T., (1976);
   "A General Purpose Univariate Probability Model for
   Environmental Data Analysis", Comput. & Ops. Res.,
   V3, pp. 209-216.

Pasquill, F. A., (1975);
   Atmospheric Diffusion, D. Van Nostrand Co. Ltd., London.

Robins, A.G. and Fackrell, J.E. (1979);
   "Continuous Plumes - Their Structure and Prediction",
   CEGB Memorandum MM/Mech/TF148, Research Division,
   Marchwood Engineering Laboratories, Marchwood, South-
   hampton, England.

Rosensweig, R. E., (1959);
   "Measurement and Characterization of Turbulent Mixing",
   Sc. D. Thesis, Chem. Eng. Dept., MIT, Cambridge, Mass.

Rosensweig, R. E., Hottel, H. C. and Williams, G. C., (1961);
   "Smoke-Scattered Light Measurement of Turbulent Con-
   centration Fluctuations", Chem. Eng. Sci., V15, p. 111.

Shruaikar, V. V. and Patel, P. R., (1977);
   "Long Term Statistics of Peak/Mean Concentrations From
   a Point Source", Atmos. Env., V11, pp. 387-389.

Smith, M. E. and Singer, I. A., (1965);
   "An Improved Method of Estimating Concentrations and
   Related Phenomena from a Point Source Emission", USAEC
   Report BNL-9700, Brookhaven National Laboratory.

Spiegel, M. R., (1975);
   Probability and Statistics, Schaum's Outline Series,
   McGraw-Hill Book Co., Toronto.

Taylor, G. I., (1922);
   "Diffusion by Continuous Movements", Proc. London
   Math. Soc., [2]20, pp. 196-202.

Taylor, G. I., (1953);
   "Dispersion of Soluble Matter in Solvent Flowing Slowly
   Through a Tube", Proc. Roy. Soc. London, A219, pp. 186-203.

Tombach, I. H., (1969);
"Velocity Measurements With a New Probe in Inhomogeneous
Turbulent Jets", Ph.D. Thesis, Cal. Inst. Tech.,
Pasedena, Calif.

Veigele, W. J. and Head, J. H., (1978);
"Derivation of the Gaussian Plume Model", J. Air Poll.
Control Assoc., V28, pp. 1139-1141.

Way, J. and Libby, P. A., (1970);
"Hot-Wire Probes for Measuring Velocity and Concentration
in Helium-Air Mixtures", AIAA Journal, V8, pp. 976-978.

Way, J. and Libby, P. A., (1971);
"Application of Hot-Wire Anemometry and Digital Techniques
to Measurements in a Turbulent Helium Jet", AIAA Journal,
V9, pp. 1567-1573.

Weil, J. C. and Jepsen, A. F., (1977);
"Evaluation of the Gaussian Plume Model at the Dickerson
Power Plant:, Atmos. Env., V11, pp. 901-910.

Wilson, D. J., (1977);
"Plume Diffusion Over Downwind Two-Dimensional Hills:
A Wind Tunnel Study", Alberta Environment Research
Project #75-8.

Wilson, D. J. and Netterville, D.D.J., (1979);
"Concentration Fluctuations Around Buildings", to
be published.

Yang, B. T. and Meroney, R. N., (1974);
"A Portable Laser Light-Scattering Probe for Turbulent
Diffusion", Rev. Sci. Inst., V45, No. 2, Feb.

Yang, B.T. and Meroney, R.N. (1975);
"On Diffusion from an Instantaneous Point Source in a
Neutrally Stratified Turbulent Boundary Layer with a
Laser Light Scattering Probe", Project Themis, Tech.
Rep. 20, Fluid Mechanics and Diffusion Laboratory,
Colorado State University, Ft. Collins, Colorado.

APPENDIX A

MEASUREMENT OF TURBULENT SCALAR FLUCTUATIONS

Introduction

The laboratory measurement of high-frequency scalar fluctuations in turbulent flows has attracted little attention during the last several decades. Scalar properties of interest have usually been the fluid temperature or species concentration. The lack of data is due in large part to the experimental difficulties encountered in making the measurements.

Experimental problems encountered generally include: detector sensitivity to extraneous noise sources (environmental or electronic), insufficient frequency response, inability to obtain a dynamic calibration, cumbersome or expensive designs, and toxic, explosive or messy tracer materials. Of this short list, sensitivity to extraneous noise sources is probably the most often encountered. Environmental noise refers to factors in the sensor's environment which produce an output signal, but which are not of immediate interest. Depending on what is being measured and what detection system is being used, disturbing environmental factors can include fluctuations in laboratory air temperature, moisture content, acoustic noise level, tobacco smoke content, air turbulence, air velocity, lighting systems and the nearby operation of high voltage electronic equipment.

Because of the random nature of turbulent fluctuations, random electronic noise from the signal generation or processing equipment can sometimes obscure the information contained in the signal. Even when the signal-to-noise ratio is adequate for some parts of an experiment, there can often be large regions of the turbulent flow field which are closed to investigation because the associated data signal is too weak to appear through the noise.

Light-Scattering Techniques

In spite of these problems, which are after all not unique to the measurement of turbulent scalar fluctuations, several measuring systems have been developed which can give satisfactory results. Rosensweig (1959, 1961) developed a scattered-light technique for studying the concentration field of suspended colloidal particles marking one of the fluid streams entering a mixing field. A linear response was obtained to both the time-mean and the time-variant components of material concentration at a point, in a sheet, or in a volume, according to the modes of illumination and observation. The capabilities and limitations of the method were reviewed by Becker, Hottel & Williams (1967). The technique gives excellent results in the convection region of the turbulence spectrum but fails where molecular diffusion is important. This is because the tracer particles have a Schmidt number $Sc \equiv \nu/D$ of almost 4×10^4 and therefore diffuse much more

slowly than the molecules of the stream into which they are introduced. A Schmidt number of 0.74 is appropriate for diffusion of air into air. The bulky nature of the optical system prevented extensive use, even in large wind tunnels. This problem was overcome when Liu and Karaki (1972) introduced fibre optics as flexible light transmitters for the high-intensity multichromatic light used.

Yang and Meroney (1974, 1975) have further refined the light-scattering technique by employing a 5 mW, He-Ne gas laser as the incident light source. The great advantage of using a laser beam over an incandescent light source is that the monochromatic characteristics of a laser beam permit doppler techniques to be applied to the scattered light. From such analysis the instantaneous velocity fluctuation components can be abstracted, while the total scattered energy yields the concentration fluctuations. Thus, there is the possibility of combining the two signals in order to measure the three unknown correlation terms $\overline{u'c'}$, $\overline{v'c'}$ and $\overline{w'c'}$, where u', v' and w' are the fluctuating velocity components and c' is the concentration fluctuation.

Yang and Meroney's probe was about 20 cm long, 8 cm high and about 2 cm thick, whereas the volume sampled was on the order of only 1 mm^3. In spite of the small sample volume, a probe this size is too large for use in small wind tunnels or for measurements near a finely detailed wind tunnel model. Reductions in probe size would result if a smaller laser and photomultiplier tube were used. The sample volume has a lower

size limited by the signal-to-noise ratio which decreases with sample volume.

Motycka and Leutheusser (1972) have constructed a very small light scattering probe which is only 1 cm long and which samples the average concentration within a volume of 40 mm^3. The probe contains a miniature solid-state infrared light source and a silicon photo-detector; the time constant for the system is stated to be about 2 ms, which is not particularly fast. Presumably the dynamic calibration was done by suddenly exposing the photo-detector to the light from the IR source, and examining the output signal on an oscilloscope. If such was the case, the response of the probe is probably limited by the response characteristics of the photo-receptor. A faster response time and a smaller sample volume should be possible with further development.

The advantages of a light-scattering system are powerful. With proper design, the measurements are obtained entirely remotely from an undisturbed flow field. The frequency response of most systems is for all practical purposes limited only by the inertia of the aerosol particles. Measurements can be obtained from sample points, sheets or volumes, and dual systems allow spatial correlations of concentration fluctuation to be measured. The size of the probe limits the space into which the probe can be inserted, and as noted above, the system cannot observe the dissipation of fluid concentration fluctuations by molecular diffusion. Finally, as

mentioned previously, a laser-doppler system operated simultaneously will permit calculation of the unknown velocity-concentration correlation terms, required for the study of turbulent diffusivity.

Temperature Fluctuations

The measurement of turbulent temperature fluctuations has met with some success, and has provided useful data on turbulent scalar fluctuations. Crum and Hanratty (1965) used hot-wire anemometers run at low probe current (5 ma) to detect only temperature fluctuations and not velocity fluctuations. These probes responded fully to frequencies in excess of 7 kHz. For flow regions having low signal-to-noise ratios, a 0.25 mm bead thermistor was used in place of the hot-wire. Fiedler (1974) used a DISA 55 F05 resistor probe which responded to temperature fluctuations up to 2 kHz. The main advantage of measuring temperature fluctuations rather than species concentration is that fairly standard anemometer technology (i.e. sensors and electronic equipment) and techniques can be used. Because of the high frequency response and small spatial resolution available, it is possible to extend the measurements well into the dissipative range of eddy sizes. However, there are several disadvantages which must also be considered. Acceptable signal-to-noise ratios require either a sensitive probe or a powerful heat source. A probe with sufficient sensitivity may also have unwanted sensitivity to velocity

fluctuations, or poor frequency response. Sufficiently
powerful heat sources may be impossible to provide without
creating undue flow disturbance. Also, because of surface
heat transfer, any solid boundaries in the flow will act as
sinks for the diffusing scalar, and for a large group of
dispersion experiments this is undesireable.

Hot-Wire Anemometers

Becker and Booth (1975) have stated that hot-wire
anemometry is the only proven technique presently available
for studying dissipation in systems of laboratory scale. They
state further that the only scalar quantity which is easy to
detect by this means is temperature. There is no doubt about
the truth of this statement, as demonstrated by the efforts
of Tombach (1969) to apply hot-wires to the measurement of
velocity fluctuations in a turbulent concentration field.
He encountered difficulty with the hot-wire technique because
of a "historical" effect somewhat akin to hysteresis, which
occurred after the sensor had been exposed to high concentra-
tions of helium. This phenomenon was not a problem for Way
and Libby (1970, 1971) in their work using a dual-probe combin-
ation of hot-wire and hot-film sensors. They attributed
success to a mode of calibration and data collection which did
not require exposure of the probe to high helium concentrations
for long periods of time.

As mentioned previously, a disadvantage of hot-wires or films is their sensitivity to environmental factors such as air velocity, temperature and species concentration. There are several ways around this problem: the sensitivity to unwanted fluctuations must be eliminated, the unwanted fluctuations must somehow be removed prior to reaching the sensor, or the effect of the different fluctuations must be explicitly accounted for. This last method has the advantage of yielding the most information about the turbulent flow field, and was the choice of Way and Libby. Their dual-sensor probe separated velocity fluctuations from concentration fluctuations by taking advantage of the different response characteristics of hot-films and hot-wires. Briefly, the method requires calibration curves for each sensor, with first velocity and then concentration being held constant. With proper probe geometry, an observed voltage pair from the two sensors will correspond to a unique combination of velocity and concentration; a set of probe calibration equations is used to calculate velocity and concentration. Because the equations for probe response hold only approximately, and because sensor interactions strongly affected sensitivity, determining optimum probe geometry is a major problem.

The main advantage of the dual-sensor probe is its ability to measure the fluctuating velocity and concentration simultaneously, with a frequency response and spatial resolution sufficient to observe the dissipative eddies. It is then

possible to directly measure and study the velocity-concentration correlation terms $\overline{u'c'}$, $\overline{v'c'}$ and $\overline{w'c'}$ for all eddy sizes of interest. A triple-sensor configuration using an X-wire and hot film would permit measurement of two instantaneous velocity components rather than one.

The most noticeable disadvantage of the system is the large amount of digital data reduction required to extract the velocity and concentration fluctuations from the observed probe voltages. Way and Libby found continuous on-line data analysis was not possible because it took six seconds of computer time to process one second of raw data. Advances in micro-processor technology are such that real-time data analysis should be possible in the near future. A disadvantage of more permanency is the extreme care required during calibration, testing and data reduction in order to ensure satisfactory accuracy in the results.

Measurements in Liquids

The turbulence fluctuation sensors described so far were operated only in gaseous mediums. Turbulent scalar fluctuations exist in liquid systems also, and have been the subject of laboratory investigations. Gibson and Schwartz (1963a, 1963b) describe the design, construction, calibration and use of a single-electrode conductivity sensor which detects very small amplitude fluctuations of concentration or temperature in aqueous electrolytic solutions. The spatial

resolution of the probe is on a par with that available from hot-wires or films, and is superior to that of a light-scatter probe. The detector is capable of following fluctuations at frequencies of several thousand Hertz. The conductivity sensor is insensitive to velocity fluctuations, but is sensitive to fluctuations of both temperature and scalar concentration. It is simple to statically calibrate the detector for scalars, and to design experiments where first temperature and then concentration is the scalar being observed. This easily controlled dual sensitivity makes the sensor very versatile.

Gibson and Schwartz do not describe their calibration procedure, but steady-state calibration is likely to be straightforward. A dynamic calibration of the conductivity probe appears to be much more difficult; the theoretical response of a spherical electrode to a sinusoidal concentration fluctuation was used to estimate performance of the actual hemispherical probe.

Salt concentration fluctuations ($Sc \simeq 700$) diffuse much more slowly than temperature fluctuations ($Sc \simeq 7$). Thus the conductivity sensor has some of the limitations of the light-scattering probe in that the salt tracer (like the oil fog) sustains eddy sizes much smaller than could exist if the tracer had properties more like those of the medium. This problem is particularly important when trying to measure the modelled fluctuations of air pollutants.

Summary

Five techniques for laboratory measurement of turbulent scalar fluctuations have been described. None of the detectors are perfect: their relative strengths and weaknesses often make one system perform better than others in a given experiment. The advantages and disadvantages of the available detectors are compared in Table 1.1. Chapter II describes the design, construction and calibration of a fast response helium concentration detector developed as part of the present work.

APPENDIX B

CONSTRUCTING THE HOT-FILM CONCENTRATION DETECTOR

One of the objectives of this study was to construct a fast response concentration detector that would be small enough for use in a wind tunnel of cross-section 30 cm x 30 cm. A hot-wire or hot-film was proposed for the sensing element, since their frequency response was known to be good. In order to detect species concentration, the user must exploit the sensitivity of a hot-film or wire to the heat conductance of the gas flowing past the element. Helium was chosen as the tracer material because it conducts heat seven times faster than air, and was therefore easily detected. Also, it has the desireable attributes of being clean, safe, inexpensive and easy to use. Helium's natural bouyancy is expected to be an advantage for the modelling of bouyant chimney plumes.

The temperature of a hot-wire is sensitive to local velocity fluctuations in addition to fluctuations in the composition of the surrounding gas. For this reason an aspirated probe was proposed, in which velocity over the sensor would be held constant regardless of the turbulence around the probe. Choked flow through either an orifice, needle valve or capillary tube would provide the necessary constant flow rate. The adjustability of a needle valve makes isokinetic

sampling possible, so it was the candidate of first choice.
The selection of position for the choking device, either
upstream or downstream of the sensing element, is critical.
If the flow is choked before it reaches the sensor (upstream-
sonic), there is a risk that concentration fluctuations will
be distorted or diffused as they pass through the shock wave
at the sonic region. The alternative of choking the flow
after it passes over the sensor (downstream-sonic) means that
only the mean flow over the sensor is held constant; turbulence
external to the probe may still find its way inside and affect
the probe output signal. It was felt that sensitivity to
external turbulence was the lesser of two evils, so the
downstream-sonic probe configuration was chosen.

A brass prototype was built with a DISA miniature
hot-wire as the sensing element. Wind tunnel tests immediately
revealed a serious problem: with a choked capillary downstream
from the hot-wire, the background noise level from the sensor
was much too large. Further investigation showed the noise
to have three components: high frequency electronic noise
generated in the anemometer circuitry, acoustic noise produced
inside the probe due to internal roughness and sharp corners,
and wind tunnel turbulence which found its way into the probe.
A battery-powered model 3342 Krohn-Hite variable low-pass active
filter was used to eliminate the high frequency electronic
noise (above 1500 Hz). Removal of turbulence noise was more
difficult. It was found that a short fibre plug (cut from a

cigarette filter) inserted into the probe inlet caused an immediate reduction in sensitivity to wind tunnel turbulence. Because the filter material was expected to distort or smear the smallest concentration eddies, a trial-and-error procedure was used to obtain the shortest length and loosest packing of filter material which would adequately remove the wind tunnel turbulence. Chapter III presents a method for empirically correcting the probe signal to compensate for probe-induced dissipation of the high-frequency concentration fluctuations. The last source of noise was internally generated turbulence, and its reduction required smoothing of the internal flow passages in the probe.

Along with excessive background noise, the first prototype probe had other problems. It was slow to build, difficult to repair (i.e. replacement of burnt-out hot-wires), and it was too large. These problems were mainly overcome with the second prototype, which was of modular construction, composed of concentric aluminum and brass tubes inside a 1/8" ID plastic "T". The sensing element was changed to a TSI 1276-10A hot-film because of its superior sturdiness and more suitable length. The sensor was held firmly in the probe by a machined brass plug which fitted snugly into the plastic T. This probe design was very satisfactory from many points of view. It was low cost ($75 hot-film + $5 materials + $10 machine shop labor), easy to put together or repair (5 hours to build from scratch, 2 hours to replace a burnt-out hot-film),

and it was small (6 mm OD, 40 mm long). However, initial calibration attempts showed there were still some problems. Up to this point, the probe aspiration velocity was controlled by choking a capillary tube of length chosen to obtain the desired velocity. This was a temporary configuration used only for initial simplicity; the final setup was expected to use choked flow through an adjustable needle valve. However, steady state calibration showed a "step" effect in the output signal when the probe was exposed to a step-change in helium concentration:

OUTPUT VOLTAGE

E_2

STEP

E_1

E_0

t_1 - Helium reaches hot-film

t_2 - Helium reaches capillary

t_1 t_2 TIME
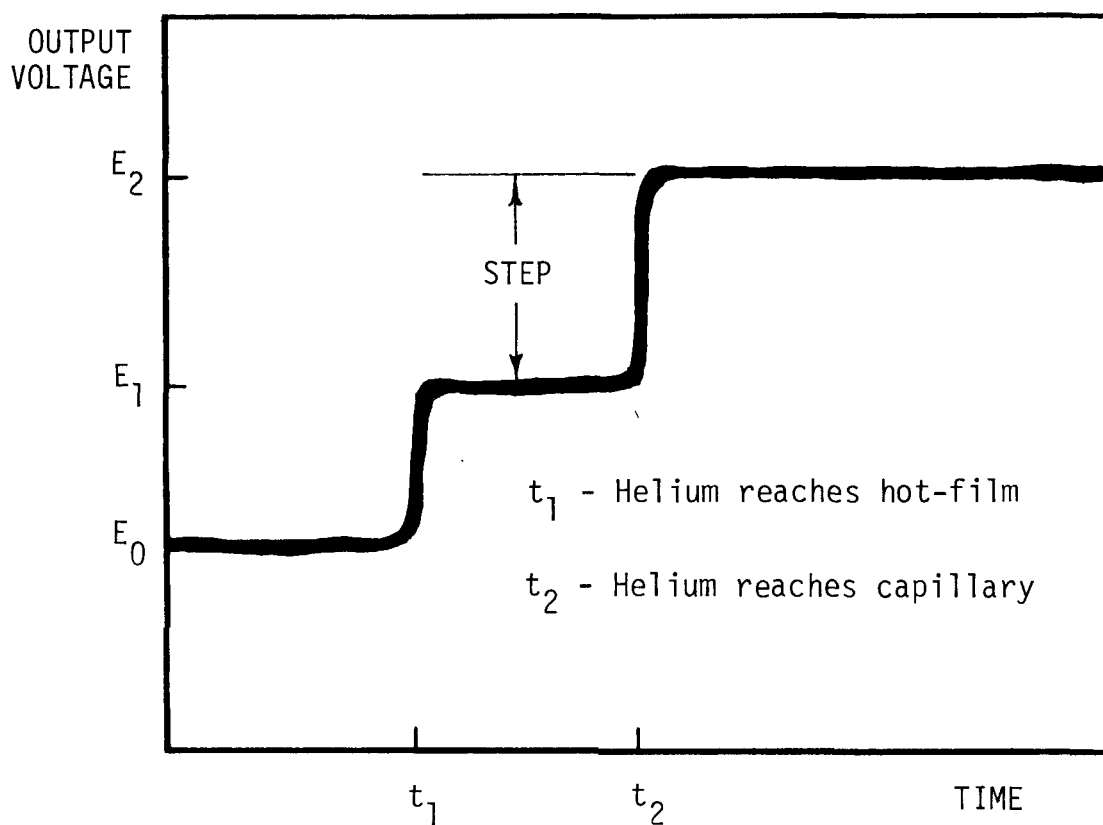
The first voltage change from E_0 to E_1 was expected, and is caused by probe response to the helium-air mixture as it is drawn over the hot-film. The unexpected second voltage change from E_1 to E_2 should have been foreseen, but wasn't. It occurs when the helium-air mixture reaches the choked capillary tube located about 1 m away from the probe itself. The speed of sound in the helium-air mixture is higher than in air, and the mixture passes through the choked capillary tube more quickly. This velocity change is propagated back upstream to the probe and enclosed hot-film, where it is detected as an abrupt increase in probe output voltage. If the capillary is thought of as part of the probe, then probe response to the step change in concentration is $E_2 - E_0$. However, the transient response of the probe is then governed by the time required for the helium-containing eddies to travel from the probe to the capillary tube.

For the prototype configuration, the lag time of several seconds was much too long for the probe to accurately follow high frequency concentration fluctuations. One solution is to place the sensor and capillary tube so close together that the two voltage effects merge into one, and probe response is assumed to be a single step change of $E_2 - E_0$. The alternative is to place the capillary tube so far from the probe that a complete set of measurements can be made before the capillary tube sees any fluctuating concentrations. A large volume container placed between the probe and the

capillary tube would act as a concentration fluctuation damper, so that the capillary would at worst see only a slowly changing helium concentration. The correspondingly slow velocity change could then be ignored or if necessary removed from the probe signal by high-pass filtering.

The method of separating the choking device from the probe itself was rejected because it limited the length of time the probe could be used without flushing the system. The only choice left was to incorporate the flow choker in the probe itself, which meant that a capillary tube could not be used because of its undesireable length. The adjustable needle valve was also rejected because of size restrictions; this eliminated the possibility of isokinetic sampling. The final choice for a velocity limiting device was a choked orifice formed by drilling a fine hole through a thin brass plug cemented into the probe body as close as possible to the hot-film sensor. This procedure re-awoke the old spectre of internally generated turbulence noise - basically a microscopic "roaring" sound as the flow passed over the sensor at about 14 m/s and turned a 90° corner while rapidly accelerating to the speed of sound, all in a length of about 5 mm. This noise was minimized by using a tapered slot brass sensor mount which gently turned the flow 90° toward the sonic orifice. Care was taken to eliminate sharp edges or abrupt cross-sectional area changes inside the probe. The orifice diameter was varied by trial and error to give an ingestion velocity of about 7 m/s,

which was close to the wind tunnel velocity used in the
experiments. The final probe design is shown as Figure 2.1
of Chapter II, which deals with the methods used to calibrate
the sensor for steady and fluctuating concentration levels.
The two figures at the end of this Appendix describe electric
circuits used with the fast response concentration sensor,
and are discussed in Chapter II.

To Vacuum Pump

Probe Support

Probe

5 m Probe Cable

Digital Ohmmeter

R_Y (shorted)

R_{cable} (shorted)

R_{total}

R_{cp} = cold probe resistance

R_{hp} = hot probe resistance

R_{op} = operating resistance

R_{ext} = external resistance

OHR = overheat ratio

$$R_{cp} = R_{total} - R_{cable}$$

$$R_{hp} = OHR \times R_{cp}$$

$$R_{op} = R_{hp} + (R_{cable} - R_Y)$$

$$R_{ext} = 10R_{op} + R_Y$$
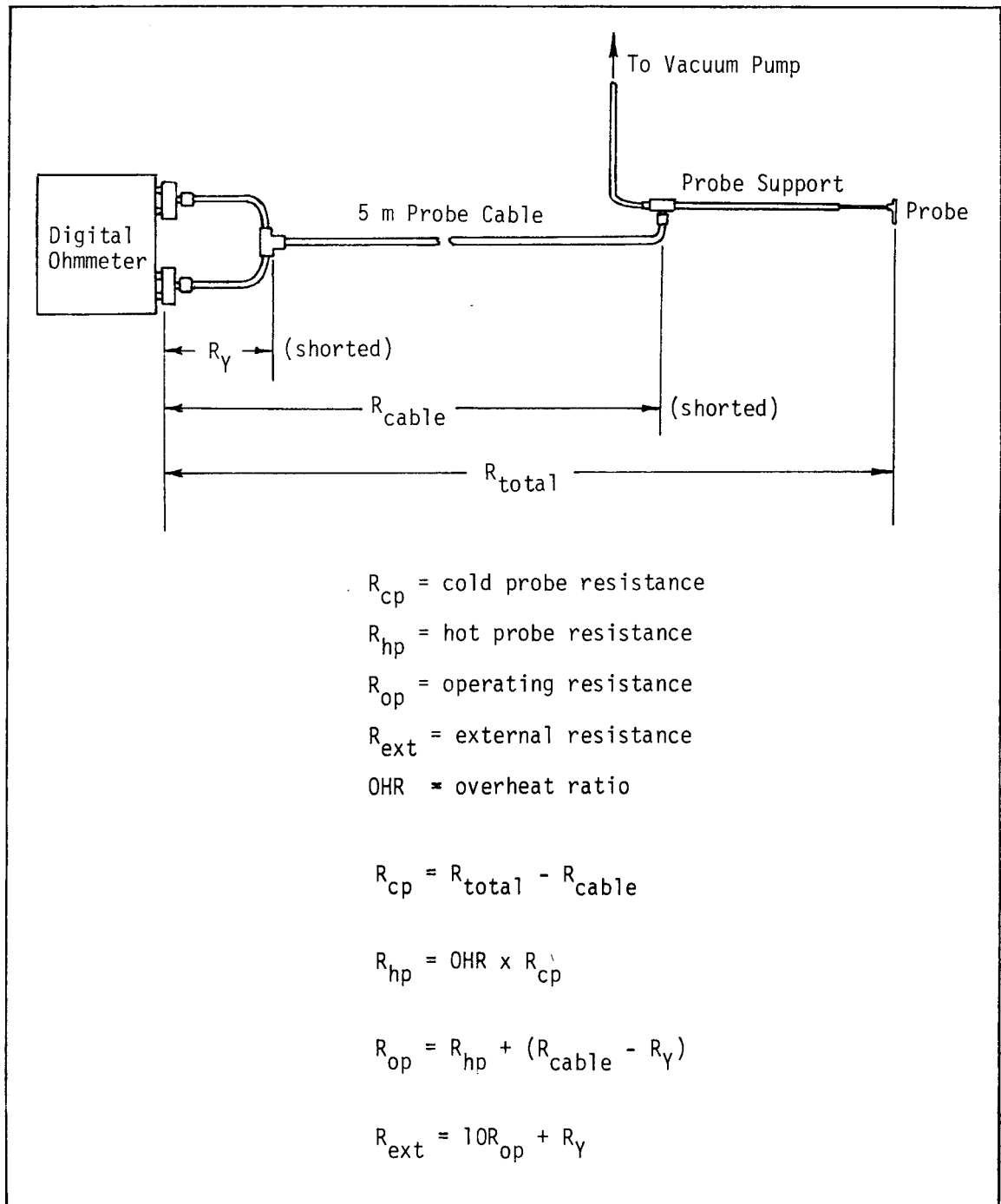
FIG. B.I   Probe Resistance Measurements
for Setting Overheat Ratio

a) Offset Voltage Supply

From External DC Power Supply

BNC Input (optional)

100 Ω ballast resistor

9 volt battery

Triple Pole Double Throw Switch

6.8 volt Zener Diodes

1000 Ω 10T Pot   100 Ω 10T Pot

BNC Output

to voltage offset box

b) Voltage Offset Box

Offset Voltage Input

BNC

Signal Input   BNC

Signal Output   BNC
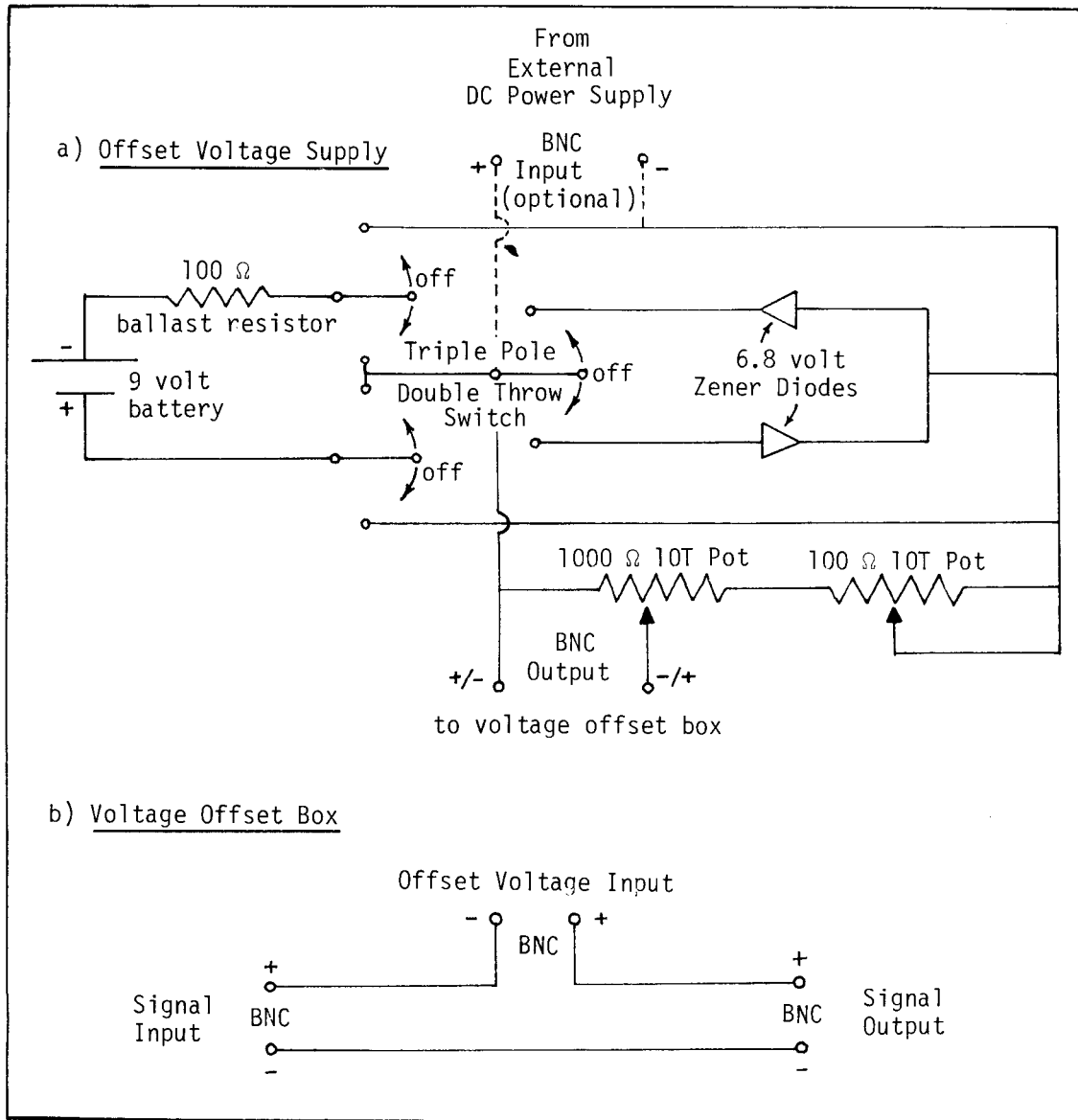
FIG. B.2   Voltage Offset Circuits

Conditions of Use

Netterville, D.D.J., 1979. Concentration fluctuations in plumes. Syncrude Canada Ltd.,
Edmonton, Alberta. Environmental Research Monograph 1979-4. 228 pp.